International
Progress Report

IPR-04-39

Äspö Hard Rock Laboratory

Äspö Task Force

Modelling of Task 6A and Task 6B2

Johan Holmén
Jonas Forsman

Golder Associates AB

October 2004

Svensk Kärnbränslehantering AB
Swedish Nuclear Fuel
and Waste Management Co
Box 5864
SE-102 40 Stockholm Sweden
Tel 08-459 84 00
+46 8 459 84 00
Fax 08-661 57 19
+46 8 661 57 19

Äspö Hard Rock
Laboratory

Report no.	No.
IPR-04-39	F65K
Author	Date
Johan Holmén Jonas Forsman	October 2004
Checked by	Date
Hakim Benabderrahmane	October 2004
Approved	Date
Christer Svemar	October 2004

Äspö Hard Rock Laboratory

Äspö Task Force

Modelling of Task 6A and Task 6B2

Johan Holmén
Jonas Forsman

Golder Associates AB

October 2004

Keywords: Transport modelling, Inverse modelling, Fractured media, Tracer test, Performance assessment, Retention, Matrix diffusion

ANDRA

NATURE DU DOCUMENT : *NATURE OF DOCUMENT*: RAPPORT	Identification / *Identification*: G RP 0GOL 03. ? ? ?

ANDRA.002.E - 1/2

Émetteur *Originator*: DIRECTION SCIENTIFIQUE Service Milieux Géologique	Repère support/Secrétaire : *Support ref./Secretary:* GRP0GOL03- ? ? ? ? .doc	Date d'origine : *Original date*: ? ? ?	Page *Page*: 1/

ÄSPÖ MODELLING TASK FORCE

MODELLING OF TASK 6A AND TASK 6B2

Documents associés / *Associated documents*:

Titulaire / *Supplier*:	N° du marché : *ANDRA contract or order number:* N° 021569	
GOLDER ASSOCIATES Oy	Référence du titulaire : *Supplier's identification:* ?????	Visa ANDRA pour diffusion *OK Andra for distribution* Nom / *Name* : H. Benabderrahmane Visa / *Signature*:

Ind. *Ind.*:	Date : *Date:*	Nom et visa Rédacteur : *Written by (1):*	Nom et visa Vérificateur : *Reviewed by(1):*	Nom et visa Approbateur : *Approved by (1):*
A	? ? ?	Johan Holmén Jonas Forsman	Ian Miller	Yrjo Lintu

(1) : Name and signature.

Abstract

Introduction and general objectives of Task 6A and Task 6B2

The general objective of Task 6 is to provide an understanding of the link between: (i) the characterisation of the properties and the processes which govern the flow and the solute transport in a fractured crystalline formation, and (ii) the performance assessment of a repository site hosted in such a formation. Solute transport over a single geological feature is studied in Task 6A and 6B2. The feature studied was identified in the Äspö TRUE Block Scale experiments. (Solute transport over longer distances is studied in Task 6D and 6E.)

Flow model and Transport model – Methodology and computer codes

Both in Task 6A and in Task 6B2, the modelling work was separated into flow modelling and transport modelling. Flow modelling was done by use of a continuum approach (stochastic continuum) and by means of the Geoan computer code. The established transport models represent the part of the studied rock block (part of flow model) within which the simulated plume of contaminated water moved. The transport modelling was carried out by use of the GoldSim computer code. The transport modelling was based on one dimensional pipes placed in a series (Task 6A) or in parallel (Task 6B2). The length and the width of the pipes were determined based on the results of particle tracking in the flow model. Several different retention processes (e.g. sorption and matrix diffusion) were included in the transport model. The transport modelling was carried out by applying a stochastic approach in which the transport properties were defined by use of probability distributions. In this study we have analysed two tracers: a non-sorbing tracer (HTO) and the slightly sorbing strontium tracer.

Task 6A

The purpose of Task 6A is to model and reproduce selected TRUE-1 tracer tests and thereby assess the constraining power of these tracer tests, i.e. the capability to quantify the basic characteristics of the parameters and processes affecting the radionuclide transport in the fractured rock. For the analyses of the constraining power of the tracer tests, the unknown rock mass properties were initially defined by ranges of plausible values within which the rock mass properties may vary. The results of the analyses of constraining power are constrained distributions of rock mass properties.

Considering the complex and non-linear system that we are studying, the approach we have used in this study recognises that it would not be possible to extract conventional probability distributions for individual parameters and their correlations by use of simple tracer tests. By generating random realisations, based on a set of plausible (given) parameter distributions, and keeping only the realisations that produce an acceptable match to the measured breakthrough curves (the tracer tests), we have carried out an informal Bayesian approach to map the entire joint probability density space and convert the parameter distributions from prior to corrected (posterior) probabilities. In this way we have derived the constrained parameter distributions. We also derived constrained coupled parameter distributions, which consist of the ensemble of coupled parameter values as defined by the accepted realisations. The difference compared to the constrained (uncoupled) parameter distributions is that in the constrained coupled parameter distributions the individual parameter values are combined, according to the parameter combinations that resulted in the accepted realisations.

The total time scale of the tracer tests studied was within 200 hours. Recovery of 50% of injected mass took place after 11 hours for HTO; and after 24 hours for strontium. In the established flow model of Task 6A, the length of flow paths from source to sink varies between 5 m and 8 m.

A general conclusion, based on the assessment of the constraining power of the HTO and strontium tracer tests, is that the tracer tests will not produce a strong constraining power as regards any of the parameters studied. This observation reveals that a good match to measured breakthrough curves can be obtained for a very large spectrum of parameter values. Consequently, the key to finding a good match and to obtain constraining power from a tracer test, is the understanding of how the parameter values should be combined, and how these combinations may be propagated to other simulations. Therefore, the constrained coupled parameter distributions constitute an important result of Task 6A.

Task 6B2

The purpose of Task 6B2 is to model selected flow and transport cases at the TRUE-1 site with performance assessment relevant (long-term) boundary conditions and temporal scales (natural hydraulic gradient, i.e. no pump test). The constraining power of the tracer test evaluated in Task 6A was included in the Task 6B2 transport modelling; this was done as the parameter values of Task 6B2 was defined by the parameter distributions derived in Task 6A.

After steady state conditions were reached in the flow model, a tracer was injected along a release line, and recovered along an interception line. The length of the release line was set to 2 m and the distance between the release line and the interception line was 10 m. Two types of tracer injection boundary condition were used: A constant injection rate of 1MBq/year and A Dirac pulse injection (a unit input = 1MBq). Examples of results are given below:

Amount of recovered mass	Time for recovery of mass considering different parameter distributions. Considering a Dirac pulse and a non-sorbing tracer (HTO) With a probability of 90% the mass will be recovered within [Years]:		
	GIVEN Parameters (prior distributions)	CONSTRAINED Parameters (posterior distributions)	CONSTRAINED COUPLED Parameters (posterior distributions)
5%	0.44	0.17	0.14
50%	0.92	0.59	0.52
95%	2.32	3.80	3.60

Amount of recovered mass	Time for recovery of mass considering different parameter distributions. Considering a Dirac pulse and a slightly sorbing tracer (STRONTIUM) With a probability of 90% the mass will be recovered within [Years]:		
	GIVEN Parameters (prior distributions)	CONSTRAINED Parameters (posterior distributions)	CONSTRAINED COUPLED Parameters (posterior distributions)
5%	36.5	9.2	3.9
50%	72.7	29.2	20.7
95%	174.6	205.2	145.3

The given parameter distributions represent reasonable ranges of parameter values, but these distributions are not constrained by the results of the Task 6A tracer test, and as seen above, the given distributions will generally produce a much later arrival of the mass (except for recovery of 95% of injected HTO mass) than the results produced with the constrained coupled parameter distributions..

Implications of the applied methodology, considering performance assessment modelling based on site characterisation data

The use of the constrained coupled parameter distributions for the performance assessment modelling will produce better predictions with smaller uncertainties than the use of the constrained parameter distribution, because the constrained coupled parameter distributions will include the correct correlation between the parameters studied; and this is an important improvement compared to an assumption of independent parameters or the inclusion of some uncertain and limited correlation between a few parameters.

This might have important implications for how performance assessments analyses should be carried out. The approach, in which one tries to establish independent distributions for each parameter, possibly with some correlations, is not necessarily the best approach. It is a better approach to derive and apply constrained coupled parameter distributions

Sammanfattning

Introduktion och övergripande syfte förTask 6A och Task 6B2

Det övergripande syftet för Task 6 är att öka förståelsen av länken mellan. (i) mätning och karakterisering av egenskaper och processer som styr grundvattenflöde och föroreningstransport i ett sprickigt kristallint berg (Site Characterisation), och (ii) säkerhets- och funktionsanalys av ett förvar placerat i ett sådant berg (Performance assessment). Föroreningstransport över en ensam geologisk struktur (spricka) studeras i Task 6A och 6B2. Den studerade strukturen har identifierats vid Äspö berglaboratorium, som en del av undersökningarna i TRUE Block Scale Experiments. (Föroreningstransport över längre avstånd studeras i Task 6D och Task 6E).

Modeller för flöde och transport – Metodik och datorkoder

Både i Task 6A och i Task 6B2 delades modellarbetet upp i två separata delar: flödesmodellering och transportmodellering. Flödesmodellering baserades på en kontinuum modell (stokastiskt kontinuum) och arbetet utfördes med datorkoden Geoan. Den simulerade plymen av förorenat vatten strömmar bara i en del av det studerade bergblocket, det är bara denna del av flödesmodellen som representeras i transportmodellen. Transportmodelleringen utfördes med datorkoden GoldSim. Transportmodellen baseras på endimensionella strukturer placerade i serie (Task 6A) eller parallellt placerade (Task 6B2). Längden och vidden på strukturerna bestämdes baserat på resultatet av partikelspårning i flödesmodellen. Flera olika fördröjande och kvarhållande mekanismer inkluderades i transportmodellen (tex sorption och matrisdiffusion). Transportmodelleringen utfördes som en stokastisk modellering i vilken transportegenskaperna definierades med sannolikhetsfördelningar. I denna studie har vi analyserat två spårämnen: ett icke sorberande (HTO) och en svagt sorberande (strontium).

Task 6A

Syftet med Task 6A är att reproducera utvalda TRUE-1 spårämnesförsök och därigenom uppskatta den bestämmande förmågan hos dessa spåämnesförsök. Med bestämmande förmåga menar vi hur väl man kan beskriva och bestämma det sprickiga bergets transportegenskaper baserat på de analyserade spårämnesförsöken. I analyserna av spårämnesförsökens bestämmande förmåga definierades först de okända transportparametrarna med hjälp av fördelningar av rimliga parametervärden. Resultaten av analyserna av spårämnesförsökens bestämmande förmåga är en uppsättning bestämda sannolikhetsfördelningar av transportparametrarna.

Metoden som vi har använt i denna studie bejakar att det är omöjligt att ur enkla spårämnesförsök extrahera konventionella sannolikhetsfördelningar för enskilda flödes- och transportparametrar och ej heller deras korrelationer. Detta följer av det studerade systemets komplexa och icke linjära egenskaper. Genom att generera slumpmässiga realiseringar baserade på rimliga initiala parameterfördelningar (prior distributions) och genom att endast spara de realiseringar som producerar en acceptabel överensstämmelse med uppmätta genombrottskurvor (spårämnesförsöken) utför vi en Bayesiansk statistisk analys för att bestämma hela den gemensamma sannolikhetsrymden för det studerade systemet av parametrar. Egenskaperna hos de accepterade realiseringarna representerar de studerade parametrarnas korrigerade sannolikhetsfördelningar (posterior distributions), som

vi kallar bestämda parameterfördelningar. Vi har också tagit fram bestämda och kopplade parameterfördelningar. Skillnaden jämfört med de bestämda fördelningarna (icke kopplade) är att i de kopplade fördelningarna är varje parametervärde länkat till de övriga parametervärden som tillsammans (i en realisering) producerade en accepterad realisering.

Den totala tidsskalan för det studerade spårämnesförsöket var 200 timmar. Återhämtning av 50% av injicerad massa skedde inom 11 timmar för HTO och inom 24 timmar för strontium. I den upprättade modellen för Task 6A varierar längden på flödesvägarna från injiceringspunkt till återhämtningspunkten mellan 5 m och 8 m.

De studerade spårämnesförsökens har endast en ringa bestämmande förmåga med avseende på de studerade parametrarna. Task 6A kan sammanfattas med slutsatsen att en rimlig överensstämmelse mot uppmätta genombrottskurvor kan erhållas för ett stort spektrum av parametervärden. Av detta följer att nyckeln till att erhålla en bra överensstämmelse mot uppmätta genombrottskurvor och för att erhålla en bestämmande förmåga hos spårämnesförsöken, ligger i att förstå hur parametervärden kan kombineras och hur dessa kombinationer kan propageras till andra simuleringar. Därför är de bestämda och kopplade parameterfördelningarna ett viktigt resultat av Task 6A.

Task 6B2

Syftet med Task 6B2 är att modellera olika utvalda flödes- och transportfall definierade med randvillkor och tidsskalor vilka är relevanta för en säkerhets- och funktionsanalys av ett förvar (naturliga gradienter, ingen pump test). Den bestämmande förmågan som utvärderats i Task 6A inkluderades i transport modelleringen i Task 6B2 genom att parametervärdena i Task 6B2 definierades av de parameterfördelningarna som härletts i Task 6A.

Efter det att stationära förhållanden hade uppnåtts i flödesmodellen, injicerades ett spårämne längs med en injiceringslinjelinje (längd 2 m, vinkelrät mot flödesriktningen), spårämnet återhämtades längs med en återhämtningslinje (vinkelrät mot flödesriktningen). Avståndet mellan linjerna var 10 m. Två olika typer av injicering i tiden studerades: en konstant injicering av 1MBq/år och en Dirac-pulsinjicering (1 MBq). Exempel på resultat ges nedan:

Mängd återhämtad massa	Tid för återhämtning av injicerad massa för olika parameterfördelningar Avseende en Dirac-puls och ett icke sorberande spårämne (**HTO**) Med en sannolikhet på 90% kommer massan att återhämtas inom en viss tid (ÅR)		
	Initiala parameterfördelningar (prior distributions)	Bestämda parameterfördelningar (posterior distributions)	Bestämda och Kopplade parameterfördelningar (posterior distributions)
5%	0.44	0.17	0.14
50%	0.92	0.59	0.52
95%	2.32	3.80	3.60

Mängd återhämtad massa	Tid för återhämtning av injicerad massa för olika parameterfördelningar Avseende en Dirac-puls och ett svagt sorberande spårämne (**STRONTIUM**) Med en sannolikhet på 90% kommer massan att återhämtas inom en viss tid (ÅR)		
	Initiala parameterfördelningar (prior distributions)	Bestämda parameterfördelningar (posterior distributions)	Bestämda och kopplade parameterfördelningar (posterior distributions)
5%	36.5	9.2	3.9
50%	72.7	29.2	20.7
95%	174.6	205.2	145.3

De initiala parameterfördelningarna representerar troliga värden, men dessa fördelningar är inte korrigerade med avseende på resultaten av spårämnesanalysen i Task 6A. Tabellerna ovan demonstrerar att de icke korrigerade fördelningarna producerar återhämtningstider som ofta är mycket större än de tider som produceras av de bestämda och kopplade fördelningarna (undantag är återhämtning av 95% av injicerad HTO)

Innebörd av den tillämpade metodiken med avseende på en säkerhets- och funktionsanalys

Användandet av bestämda och kopplade parameterfördelningar vid en säkerhets- och funktionsanalysmodellering kommer att producera bättre uppskattningar med mindre osäkerheter än en analys baserad på endast rimliga eller bestämda parameterfördelningar. Skälet är att de bestämda och kopplade parameterfördelningarna inkluderar en experimentellt bestämd korrelation mellan enskilda parametervärden. Detta är en betydelsefull förbättring i jämförelse med antagandet om oberoende parametervärden, eller introduktionen av en osäker och begränsad korrelation mellan ett fåtal parametrar. Denna slutsats kan ha en viktig betydelse för hur man bör utföra en säkerhets- och funktionsanalysmodellering. Säkerhets- och funktionsanalysmodellering baserad på oberoende parameterfördelningar är inte nödvändigtvis det bästa sättet. En bättre metod synes vara att applicera bestämda kopplade parameterfördelningar.

Executive summary

This study may be characterised as a probabilistic performance assessment modelling, exercise based on site characterisation data. Task 6A is a site characterisation (SC) modelling, and Task 6B2 is a performance assessment (PA) modelling.

TASK 6A

The purpose of Task 6A is to model and reproduce selected TRUE-1 tracer tests and thereby assess the constraining power of these tracer tests, i. e. the capability to quantify the basic characteristics of the parameters and processes affecting the radionuclide transport in fractured rock.

The tracer test was conducted by a simultaneous injection of several radioactive tracers with different characteristics. The monitored tracers consisted of HTO, Strontium, Iodine and Cobalt. The HTO tracer is considered to be a conservative tracer, i.e. it does not adsorb onto the rock surface. Strontium, Iodine and Cobalt are non-conservative tracers (reactive), of which strontium has the weakest reactive characteristics. This study concerns an evaluation of the transport of HTO and Strontium

The result of an experimental evaluation is model dependent. To obtain a framework where model bias may be compared and discussed, the Task Force group apply several different model concepts. For Task 6A, the common platform for the modelling teams consists of data sets including experimental breakthrough curves (breakthrough curve = temporal distribution of tracer concentration) for several tracers, as well as independent material properties evaluated by various tests. The observed experimental (measured) breakthrough curves for a conservative tracer (HTO) and a reactive tracer (Strontium) are given in Figure 3-1.

A large number of different rock mass properties may influence the tracer tests, e.g. porosity, flow wetted surface, amount of stagnant water, Kd-values, dispersivity, matrix diffusion etc, etc, and theoretically there is an infinite number of combinations of the unknown rock mass properties that will produce approximately the same breakthrough curve. However, based on information derived from observations, other hydraulic test, and laboratory experiments, it is possible to establish plausible ranges within which the unknown rock mass properties may vary. The purpose of Task 6A is to analyse the constraining power of the tracer tests with regard to the given plausible ranges within which the unknown rock mass properties may vary.

A summary of the methodology that we have used for Task 6A and 6B2 is presented in flow charts in Figure 1-1 through Figure 1-4.

The tracer tests studied took place in a fractured rock mass, the part of the rock mass in which the tracers moved with the groundwater and interacted with the rock mass is called Feature A. Feature A could be a single fracture or a system of fractures. We have assumed that Feature A is a single fracture that can be represented by a fracture plane with varying flow properties inside the fracture plane.

A continuum approach was used for calculation of the groundwater flow field inside the fracture plane that represented Feature A. For flow modelling we used the GEOAN computer code (finite differences). The flow model included the heterogeneity of the permeability field, as a two dimensional stochastic continuum approach was used for description of the permeability field. The well test was simulated in a large number of different realisations of the permeability field. The calculated flow fields of the different realisations were analysed; as a part of these analyses we calculated the flow through the point/cell were the tracers were released. The realisations that produced a flow that was close to the measured flow were identified. The flow field of these identified realisations were further analysed by the use of particle tracking. Based on the results of the particle tracking of the identified realisations, the shape of the plume of contaminated water (contaminated by the tracers) was derived as a probabilistic distribution of the size and shape of the flow wetted surface area. The distribution of the flow wetted surface area was propagated to the transport model.

For the transport modelling we used the GoldSim computer code. The transport processes that are represented by the transport model are: (i) advection, (ii) dispersion, (iii) retardation, (iv) decay and ingrowth [not used in this study], and (v) exchanges with immobile storage zones (e.g. matrix diffusion). The retardation processes are represented by equilibrium partitioning between: (i) the fluid in the pathway and a user defined infill medium, and (ii) the fluid in the pathway and a user specified coating medium as well as a skin zone (around the perimeter of the pathway/fracture), and (iii) the diffusing fluid and the rock matrix. The hydraulic interchanges with immobile storage zones along the main transport pathway are governed by (i) matrix diffusion into immobile zones in which the transfer rate into and out of the zone is proportional to the concentration gradient and the diffusive properties of the zone, and (ii) a "stagnant" dispersive zone, in which the interchange is proportional to the concentration difference and a transfer rate. As defined in the task specifications, *radioactive decay and ingrowth are not considered in the modelling*. The layout of the transport model is given in Figure 3-2, Figure 3-3 and in Figure 3-4.

The following parameters were studied.

- Altered Diorite Rock: Amount along plume, Thickness, Porosity and Kd-value.
- Mylonite Rock: Amount along plume, Thickness, Porosity and Kd-value.
- Fault Gouge: Thickness, Porosity and Kd-value.
- Infill (fracture filling): Porosity and Kd-value.
- Stagnant zones: Amount along plume and exchange Rate.
- Dispersivity.
- Flow wetted surface area.
- Combined parameters: F-parameter and retardation factor.

The transport modelling was carried out as a probabilistic sensitivity analysis. Hence, the uncertainties in the parameters of the system studied were included in the analysis as the transport parameters were defined with probability distributions (statistical distributions). The *given parameter distributions* reflect the assumed likely ranges of parameter values. These specified distributions are given as input to the transport model.

A large number of different realisations of the parameters were created (i.e. 300 000 different realisations of a transport model with different properties). For each realisation (transport model), the measured concentration distribution at the point of injection was used as an upper boundary condition (at the injection well). In this way the transport models reproduce the injection of tracers. The resulting simulated breakthrough curves of tracers at the lower boundary (at the extraction well) are compared to the measured breakthrough curves. The realisations that produced the best fit to the measured breakthrough curves were identified (accepted) and moved to a new ensemble of realisations–the accepted realisations. The methodology and criteria for acceptance of a realisation is discussed in Section 3.7. The properties (parameter values) of the accepted realisations were analysed separately.

Considering all realisations established with the given parameter distributions, together these realisations demonstrate a large variation in simulated breakthrough curves. The lower envelope of all simulated breakthrough curves is very close to zero and the upper envelope is much higher than that of the measured breakthrough. The median (50^{th} percentile) breakthrough curve is very low and has a much later arrival time of the peak, than the measured breakthrough. This indicates that only a small fraction of all the simulated breakthrough curves will match the measured breakthroughs. The given parameter distributions (see Section 5.1), are based on data that is considered as reasonable, however these distributions will, with a very large probability, produce breakthrough curves that are far from the measured breakthroughs.

As stated above, the *given parameter distributions* reflect the assumed likely ranges of parameter values based on data available prior to the tracer test. The distributions of parameter values that are found within the ensemble of accepted realisations are the results of the sensitivity analysis, and these distributions are called the *constrained distributions*. The differences between: (i) the given parameter distributions and, (ii) the constrained distributions, demonstrate the constraining power of the tracer test; as simulated by the applied modelling approach. A large difference between a given and a constrained distributions demonstrates a large constraining power and a small difference demonstrates a small constraining power. If the distribution of a parameter of the accepted realisations is identical to, or very close to, the given distribution of all realisations, for such a situation the tracer test studied has no constraining power as regards the parameter studied.

It is important to note that the calculated constraining power of a parameter needs to be evaluated together with the given properties of the probability distribution of the parameter studied (the input data), and the given parameter distribution needs to be defined with reasonable values.

The tracer tests were analysed separately and combined:

- First analysis. The HTO tracer test was analysed separately. For acceptance of a realisation only the HTO breakthrough curve was considered.
- Second analysis. The Strontium test was analysed separately. For acceptance of a realisation only the Strontium breakthrough curve was considered.
- Third analysis. The HTO test and the Strontium tests were analysed together. For acceptance of a realisation both the HTO and the Strontium breakthrough curves were considered. An accepted realisation had to produce acceptable results for both tracers.

The tracer tests, with HTO and Strontium were evaluated separately and combined. The analyses demonstrated that the derived constraining powers where not the same for the three different analyses. The separate HTO analysis demonstrated less constraining power than the separate Strontium analysis. This is also partly reflected by the number of accepted realisations produced by the different tests. Using the same relative criteria for the acceptance of a realisation, the numbers of accepted realisations produced by the different analysis varied substantially. Considering the first analysis i.e. the HTO tracer test, 0.40% of the realisations were accepted. Considering the second analysis i.e. the Strontium tracer test, only 0.03% of the realisations were accepted. Hence, the Strontium test is more discriminating. For the third analysis, i.e. the combined test, the criteria for acceptance were relaxed compared to the separate tests, nevertheless only 0.01% of the realisations were accepted. The results of the third analysis (the combined test) were very close to the results of the separate Strontium analysis. Hence, it is the Strontium tracer that determines the results of the combined test.

It is important to note that even if the constraining powers demonstrated by the evaluation of the different tracers tests differ, there is not necessarily a contradiction between the results. The results reflect different properties of the system studied. The differences occur because the Strontium test is more discriminating; which is demonstrated by the results of the combined test that is very close to the results of the Strontium test.

The constraining power of the Strontium tracer test is presented in Figure 5-3 through Figure 5-11. A summary of the constraining power of the HTO tests is given in Yable 4-4 and for the Strontium test in Table 5-5.

The analyses of constraining power demonstrates three different types of results:

- The constrained distributions are identical to the given distributions. For such a situation no constraining power is demonstrated considering the parameter studied.
- The constrained distributions have the same range as the given distribution, but demonstrate another probability density function. This is an indication of some constraining power. Because a probabilistic simulation is dependent on both the range and type of probability density function characterising a parameter. (Even if the range is the same for the constrained and given distributions, there is still constraining power; because, if the probabilistic approach is continued to predictive simulations, and if the constrained distributions are used as input data for such simulations, the resulting predictions will depend not only on the range of the input data but on the probability density function of the input data.)
- The constrained distribution has a different range than the given distribution, and demonstrates a different probability density function. This is an indication of genuine constraining power.

A general conclusion, based on the assessment of the constraining power of the HTO and Strontium tracer tests, is that the tracer tests will not produce a large constraining power as regards any of the parameters studied.

The Diorite and the Mylonite rock is located behind the Fault Gouge, and not in direct contact with the flowing water. No constraining power is demonstrated considering the properties of these two rock types (amount, thickness and porosity). It is likely that this result is given by the relatively short time-scale of the experiments. The mass exchange with the inner zones is insignificant during such short time.

The Fault Gouge is located on the surface of the fracture planes and in direct contact with the flowing water. In the Strontium test no constraining power, was demonstrated as regards the porosity of this material, in comparison the HTO test demonstrated some very weak constraining power regarding the porosity. More constraining power was demonstrated as regards the thickness of the Fault Gouge. For the Fault Gouge thickness, the ranges of the constrained distributions were the same as in the given distributions, but the constrained distributions demonstrated very different probability density functions. The range of the Fault Gouge Kd values was defined as very large in the given distribution. The Strontium test demonstrated a distribution with a smaller range.

A filling material (the Infill) is specified inside the open space of the fracture studied, this material is in direct contact with the flowing water. For the HTO tracer a constraining power was demonstrated for the porosity of the Infill, but primarily as regards the probability density function and not as regards the range of accepted values. In contrast, the Strontium test demonstrates no constraining power for the Infill porosity. The range of the Infill Kd values was defined as very large in the given distribution. The Strontium test demonstrated a distribution with a smaller range. The constrained distribution of Kd-values were approximately the same for both the infill and the Fault Gouge.

Zones of stagnant water are specified inside the fracture. The amount of such stagnant water (fraction) and the rate with which this water interacts with the flowing water is also analysed. Constraining power was demonstrated as regards the Stagnant Zone Fraction and Stagnant Zone Rate. For both the Fraction and the Rate, the ranges of the constrained distributions were the same as in the given distributions, but the constrained distributions demonstrated a different probability density function. Hence, some constraining power was demonstrated for these properties.

- Considering the Strontium test and the Stagnant Zone Fraction, 80% of the accepted realisations demonstrated a Fraction larger than 0.77. Hence, most of the accepted simulations had a large amount of stagnant zones, but a few simulations with very small amount of stagnant zone were also accepted. These results are different compared to the results of the HTO tracer test; the HTO tracer demonstrated a large amount of accepted realisations with a small stagnant zone.

- Considering the Strontium test and the Stagnant Zone Rate, 90% of the accepted realisations had a Rate less than 0.15 m^{-1}. Hence, most of the accepted simulations had small values of the Rate, but a few simulations with large values of Rate were also accepted. These results are different to the results of the HTO tracer test, for the HTO tracer the constraining power as regards the Rate was much weaker, and most of the accepted realisations had rates larger than those of the accepted Strontium realisations.

Comparing the constrained and given parameter distributions, the differences in the probability density functions of the stagnant zone parameters are larger than for any other parameters, and this is an indication of some constraining power. But, the ranges of the constrained parameter distributions for the stagnant zones are identical to the ranges of the given distributions; hence acceptable fits to measured values were found for all different values of the stagnant zone parameters (but not for all combinations). In addition, the probability density functions derived with the HTO tracer are very different (close to a mirror image) from the probability density functions derived with the Strontium tracer. Together this indicates that the concept of a stagnant zone is a very

useful concept when modelling and matching breakthrough curves, but its ability to represent the actual processes and properties that occur along the fracture plane should be considered with care.

The dispersivity of the flow domain was also analysed and the results demonstrated a weak constraining power for this parameter. The accepted realisations of the Strontium test demonstrate results that are a mirror image of the results derived from the HTO test.

The flow wetted surface area (or the wet area) is the area on the fracture plane, along which the transport takes place. The area is defined as the sum of the areas on the upper and the lower planes. A distribution of possible areas was derived from the modelling of the flow field (flow modelling); this distribution was transferred to the transport model and defined as the given distribution of the flow wetted surface. The transport model reduces the size of the cross-sectional area where the flow takes place, by introducing the stagnant zones. Hence, there are two different concept of flow wetted surface area: (i) Flow wetted surface area including the stagnant zones and (ii) Flow wetted surface area without the stagnant zones. We have studied both concepts. Considering the first concept (including stagnant zones in the flow wetted surface area), the transport modelling demonstrated no constraining power by use of the Strontium tracer. However, for the second concept (excluding the stagnant zones from the flow wetted surface area), the transport modelling demonstrates a significant constraining power for this parameter.

The F-parameter is a parameter characterising some aspects of the flow, it is defined as the product of several different parameters (see Equ. 4-2). The transport modelling demonstrated significant constraining power as regards the F-parameter.

The retardation factor is a parameter that represents the retardation of the front of a migrating contaminant, relative the movement of the bulk mass of water, assuming that the retardation is caused by a fast reversible adsorption with a linear isotherm (see Equ 5-3). The transport modelling demonstrated a significant constraining power considering the retardation factors of the materials in direct contact with the flowing water (Infill and Fault Gouge), but no constraining power for the materials not in direct contact with the flowing water (Mylonite and Diorite).

Considering all realisations established with the given parameter distributions, together these realisations demonstrate a large variation in simulated breakthrough curves. The lower envelope of all simulated breakthrough curves is very close to zero (extremely retarded realisations) and the upper envelope is much higher than that of the measured breakthrough. The median (50^{th} percentile) breakthrough curve is very low and has a much later arrival time of the peak, than the measured breakthrough. This indicates that only a small fraction of all the simulated breakthrough curves will match the measured breakthroughs. The given parameter distributions (see Sections 4.1 and 5.1), are based on data that is considered as reasonable, however these distributions will, with a very large probability, produce breakthrough curves that are far from the measured breakthroughs.

Compared to all simulated breakthrough curves, the accepted breakthrough curves are characterized by earlier arrival times and a higher peak (mass flow). More than 99.9% of the simulated breakthrough curves have a slower breakthrough and a smaller peak (compared to the accepted curves). By studying the properties of the constrained distributions it is possible to see how the match to the measured breakthrough curves was obtained (i.e. faster breakthroughs, higher peaks as well as the shape of the tail).

In the constrained parameter distributions for Strontium, the stagnant zone fraction is preferred as large and the stagnant zone rate is preferred as small. Fraction is the cross sectional area occupied by stagnant zones, and rate is the exchange velocity from mobile zone to the stagnant zone. The stagnant zones will: (i) cause a delay of the breakthrough (of mass and peak in mass flow) as they will accumulate and release tracer mass, but (ii) a large stagnant zone will also produce a small cross sectional area available for the main advective transport (the mobile water), which caused a larger advective flow velocity and a faster tracer transport and earlier breakthrough.

In the constrained distributions for Strontium, the thickness of the Fault Gouge is preferred as small. The flowing tracer mass will interact with the Fault Gouge volume (thickness and porosity) by means of diffusion. A small thickness implies a small storage capacity, which will result in a rapid saturation of the storage volume and a faster breakthrough than would have been the case for large values of thickness.

In the constrained parameter distributions for Strontium, the distribution of Kd-values of Fault Gouge and Infill are smaller (smaller range and higher probability of small Kd-values) than in the corresponding given parameter distributions. Two types of linear retardation processes will take place in the model. (i) Equilibrium partitioning between the fluid in the pathway and an infilll material; and (ii) equilibrium partitioning between the fluid in the pathway and a coating medium, i.e. the Fault Gouge. The partitioning processes are (in the model) simulated by means of the equilibrium-partitioning concept. Small Kd-values will produce a breakthrough curve with a higher peak and less emphasised tail, than a breakthrough curve produced with larger Kd-values. As mentioned in Section 5.6, there is an interesting relationship between the Stagnant zone fraction and the Infill Kd-value (also between the Stagnant zone fraction and the Fault Gouge Kd), in the constrained parameter distributions.

In the constrained parameter distributions for Strontium, the distribution of Dispersivity values is somewhat larger (smaller range and higher probability of larger values) than in the corresponding given parameter distributions. Dispersion is the tendency for a solute (tracer), dissolved in the groundwater, to spread out from the path that it would be expected to follow according to the advective hydraulics of the flow system. Diffusion and mechanical mixing during fluid advection cause dispersion. In the transport model the effect of mechanical mixing during fluid advection is controlled by a parameter called dispersivity. A large value of dispersivity will produce an early breakthrough, a wide breakthrough curve and a lower peak, compared to a breakthrough curve produced with a small value of dispersivity.

The weak constraining power of the tracer tests studied (as demonstrated by the presented analyses), and the good match to measured values that was obtained with the parameter distributions studied, this situation reveals that a good match to measured values can be obtained for a very large spectrum of parameter values, and that the key to finding the good match is to understand how the parameter values should be combined.

We have divided the parameter distributions into three different sets that will be used in the Task 6B2 modelling.

- The given parameter distributions are the input data for the Task 6A modelling. The distributions are based on data given Task 6A and 6B specifications, by Selroos and Elert (2001) and Elert and Selroos (2001). In the given parameter distributions we presume that all parameters are independent.

- The constrained parameter distributions are the results of Task 6A. Based on the analyses of breakthrough curves, as produced by use of the Strontium tracer, we have derived the constrained parameter distributions. The constrained parameter distributions are based on the 89 realisations that produced breakthrough curves for Strontium with an acceptable match to the measured breakthrough (of Strontium). In the constrained parameter distributions we presume that all parameters are independent.
- The constrained coupled parameter distributions are also results of Task 6A, they consists of the ensemble of coupled parameter values as defined by the 89 accepted realisations. The difference compared to the constrained parameter distributions is that in the constrained coupled parameter distributions the individual parameter values are combined according to the combinations of parameter values that resulted in the 89 accepted realisations. In the constrained coupled parameter distributions the parameters are combined in accordance to the accepted realisations and are not considered as independent. The probability distribution of the parameter values that takes place within the 89 accepted realisations are the same in: (i) the constrained parameter distributions and in (ii) the constrained coupled parameter distributions; the difference is in the way these values are combined.

TASK 6B2

The purpose of Task 6B2 is to model selected flow and transport cases at the TRUE-1 site with Performance Assessment (PA) relevant (long-term) boundary conditions and temporal scales. Compared to Task 6A, the temporal scale of Task 6B2 is much larger and reflects a PA-situation and not the flow of a standard tracer test, as used in Site Characterisation (SC). It is primarily the longer time scale that makes Task 6B2 into a PA case, as the spatial scale is approximately the same in Task 6A and Task 6B2. Normally a PA case involves both a long time period and a large spatial domain. Such PA cases will be studied in Tasks 6D and 6E.

A summary of the methodology that we have used for Task 6A and 6B2 is presented in flow charts in Figure 1-1 through Figure 1-4.

For the simulation of tracers in Task 6B2, the same type of flow medium as in Task 6A was used. Feature A was modelled as a single fracture that can be represented by a fracture plane with varying flow properties inside the fracture plane. The fracture was defined as a two dimensional plane. The heterogeneity in the flow properties along the fracture plane (the variation in flow properties) was represented by use of the stochastic continuum approach, as in Task 6A. For flow modelling we used the GEOAN computer code (finite differences).

The fracture was defined as a rectangle of size 15 x 15 m, in line with the description given in the modelling specification. The finite difference grid along the fracture plane was defined with the same properties as in Task 6A; hence, with a cell size of 0.2 m x 0.2 m and with a heterogeneous conductivity. The heterogeneity in the flow properties along the fracture plane was defined as in Task6A. For the established model we have used specified head boundary conditions along two opposing sides and the no-flow boundary condition along the other two sides. The gradient between the upper and lower specified head boundaries was set to 0.001 (as specified defined in the modelling specifications). The simulation of the flow field was continued until steady state conditions were reached.

After steady state conditions were reached in the simulations, a tracer was injected along a release line, and recovered along an interception line. The length of the release line is 2 m and the distance between the release line and the interception line is 10 m. In Task 6A we studied a radial flow towards an extraction well, in Task 6B2 the flow is not radial, but on the average uniform, and the area of the plume is much larger in Task 6B2 than in Task 6A.

A large number of different realisations of the conductivity field were created. Flow paths were released in the flow fields of the different realisations. The paths released along the release line create a plume that describes the flow between the release line and the interception line. In the first part of the analysis of the flow fields of the different realisations, the entire plumes (of the different realisations) were analysed as single units.

In the second part of the analysis of the flow fields and the plumes, a plume studied is divided into 10 sections (sub-plumes) that starts along the release line. At the release line, each section (sub-plume) has the same width (equal to 0.2 m) that is given by the cell size of the stochastic continuum mesh. Because of the heterogeneous properties of the flow medium, the width and size of these sub-plumes varies a lot along the flow direction from the release line and to the interception line. The reason for dividing the plume into 10 sub-plumes is that we want to include, in the transport model, the flow and velocity distribution inside the plume.

For the transport modelling we used the GoldSim computer code. The shapes and flows of the plumes (from release line to interception line) were transferred from the flow model to the to the transport model. In the GoldSim transport model, a GoldSim pipe represents each one of the 10 sub-plumes.

The properties that are transferred to the pipes of the transport model are the following: (i) flow in a sub-plume, (ii) length of a sub-plume and (iii) flow wetted surface area of a sub-plume. These properties are coupled to each other in a complicated way, e.g. it is likely that a sub-plume with a large flow also has a large flow wetted surface area. Therefore, we have used a bootstrapping method in which the properties of the GoldSim pipes of different realisation of the transport model are directly given by the properties of the sub-plumes of the different realisations of the flow model. By use of this method the correlation between the flow, length and flow wetted surface area, is preserved in the transport modelling.

As in Task 6A, the transport modelling for Task 6B2 is based on the GoldSim Transport Module. The modelling was carried out as a probabilistic analysis. Hence, the uncertainties in the parameters of the system studied were described with ranges within which the parameters may vary (the parameters were defined by statistical distributions). A large number of different realisations of the parameters was created, i.e. 10 000 different realisations of a transport model, for each case studied.

The modelled transport processes were the same as in Task 6A, and as in Task 6A radioactive decay and ingrowth were not considered in the modelling.

The solute transport model consists of ten “GoldSim pipes” in parallel, representing 10 parallel sections along the plume from the injection line (release line) to the interception line. The pipes represent the part of the fracture studied (Feature A) that is affected by the plume, between the injection line and the interception line. The defined flow as well as length and width of the pipes (flow wetted surface area) were based on the results of

the stochastic continuum modelling of the flow field and of the sub-plume as discussed above. For each of the ten GodSim pipes that together represent the plume, a vertical cross section of the flow domain (along the flow path) is identical to that of Task 6A. The cross sectional lay out of the materials, as used in Task 6B2, were the same as in Task 6A (e.g. Mylonite and Diorite behind the Fault Gouge, and an Infill material within the fracture opening). The layout of the transport model is given in Figuer 9-1, Figure 9-2 and in Figure 9-3.

We have generated approximately 700 plumes by use of the flow model. For each realisation of the transport model one of these plumes is randomly selected, the flow properties of the GoldSim pipes are given by the properties of the sub-plumes of the selected plume. For a single realisation of the transport model, the flow properties are different for all 10 pipes of the transport model. The transport properties are however stochastically generated by GoldSim and are the same for all ten pipes of a single realisation of the transport model, but vary between different realisations.

We have studied two tracers, HTO and Strontium. The HTO tracer is considered to be a conservative tracer, i.e. it does not adsorb onto the rock surface. Strontium is a non-conservative tracer (reactive) with relative weak reactive characteristics.

As defined in the modelling task specification, two types of tracer injection boundary condition were used:

(i) A constant injection rate of 1MBq/year.

(ii) A Dirac pulse injection (a unit input = 1MBq).

In the transport model at the injection line, an equal amount of activity (tracer mass) was injected in each GoldSim pipe, regardless of flow in pipe.

Considering a conservative tracer (HTO), the recovery of 95% of the injected mass took 77 hours in the Task 6A tracer test, but may take 3 years in the flow field of Task 6B2. Hence, the temporal scale of Task 6B2 is several hundreds of times larger. Because of the relatively long period studied in Task 6B2, transport processes that are of importance in the longer time perspective of a PA analysis e.g. matrix diffusion, will have an important influence on the transport modelled in Task 6B2.

We have modelled the transport processes based on the three different parameter distributions, discussed above in the Task 6A section. (i) Given parameter distributions. (ii) Constrained parameter distributions and (iii) Constrained coupled parameter distributions.

Examples of breakthrough curves are given in:

For constant injection rate:

Figure 10-1 through Figure 10-6

For a Dirac pulse injection:

Figure 11-1 through Figure 11-8.

The parameter distributions that produce the most representative results for the TRUE-1 site is the Constrained coupled parameter distributions; the parameter properties of this distribution were constrained by the evaluation of the tracer test studied in Task 6A, and these distributions also include the correct combinations of parameter values.

Considering the Given parameter distributions and the HTO tracer:

- For a Dirac pulse the peak in mass flow will take place,
  Within 4.8 months regarding the median (50% probability).
  Within 8.7 months with a probability of 90%.
- For a Dirac pulse, and with a probability of 90%,
  5% of the mass will be recovered within 0.44 years.
  50% of the mass will be recovered within 0.9 years.
  95% of the mass will be recovered within 2.3 years.

Considering the Given parameter distributions and the STRONTIUM tracer:

- For a Dirac pulse the peak in mass flow will take place,
  Within 32 years regarding the median (50% probability).
  Within 58 years with a probability of 90%.
- For a Dirac pulse, and with a probability of 90%,
  5% of the mass will be recovered within 36 years.
  50% of the mass will be recovered within 73 years.
  95% of the mass will be recovered within 175 years.

Considering the Constrained coupled parameter distributions and the HTO tracer:

- For a Dirac pulse the peak in mass flow will take place,
  Within 0.6 months regarding the median (50% probability).
  Within 2,6 months with a probability of 90%.
- For a Dirac pulse, and with a probability of 90%,
  5% of the mass will be recovered within 0.14 years.
  50% of the mass will be recovered within 0.5 years.
  95% of the mass will be recovered within 3.6 years.

Considering the Constrained coupled parameter distributions and the STRONTIUM tracer:

- For a Dirac pulse the peak in mass flow will take place,
  Within 1.8 years regarding the median (50% probability).
  Within 5.5 years with a probability of 90%.
- For a Dirac pulse, and with a probability of 90%,
  5% of the mass will be recovered within 4 years.
  50% of the mass will be recovered within 21 years.
  95% of the mass will be recovered within 145 years.

The Given parameter distributions represent reasonable ranges of parameter values, but these distributions are not constrained by the results of the abovementioned tracer test. And as seen above, the given distributions will generally produce a much later arrival of the mass (except for recovery of 95% of injected HTO mass) than the results produced with the constrained coupled parameter distributions.

The uncertainty in the breakthrough curves of tracer mass can be described by the length of the period between the arrival times with 90% and 10% probability, for a given condition of mass flow e.g. the peak in mass flow or recovery of a certain amount of injected mass. Considering uncertainty expressed in this way, for HTO as well as for Strontium, the smallest uncertainty in prediction was obtained by utilising the Constrained coupled parameter distributions, when simulating: peak arrival time, as well as recovery of 5%, 50% and d95% of injected mass. The only exception is for HTO and recovery of 95% of injected mass, for this situation the smallest uncertainty was obtained with the given distributions.

Considering the Strontium tracer and magnitude of uncertainty in prediction of breakthrough curves (as defined above), the smallest magnitude of uncertainty is produced by us of the constrained coupled distributions. However, compared to the magnitude of uncertainty produced by the other parameter distributions, the difference in magnitude of uncertainty is largest at the first part of the breakthrough curves. When 95% of the injected mass is recovered, the magnitude of uncertainty produced by the constrained coupled parameter distributions is smaller, but not much smaller, than the magnitude of uncertainty produced by the given parameter distributions.

The reason for this is that when considering the last part of the breakthrough curves in Task 6B2 (e.g. recovery of 95% of the injected mass), the time scale is much larger than the time scale studied in the Task 6A tracer test. Transport processes that had no large influence on the tracer test studied in Task 6A, for example interaction (e.g. matrix diffusion and adsorption) with materials (Diorite and Mylonite) that are not in direct contact with the flowing water, may be very important at the time scales of the recovery of 95% of injected mass in Task 6B2. It follows that because the tracer test studied and analysed in Task 6A demonstrated no constraining power for these transport properties (e.g. matrix diffusion), the uncertainty in the result produced by the constrained coupled parameter distributions is not necessarily much smaller than the uncertainty produced with the given parameter distributions, at these large time scales (large time scales in comparison to the time scale of the tracer test).

An interesting result is that the uncertainty discussed above, as described by the length of a time period, is approximately the same for the constant injection of tracer and for the Dirac pulse injection. Except for the constrained coupled parameter distribution and 95% of recovered mass, for this situation the uncertainty is smaller for the Dirac pulse than for the Constant injection rate. Hence, considering the constrained coupled parameter distributions (which produce the best predictions) and the first 50% of recovered mass, the uncertainty is approximately the same when considering a constant injection of mass or a Dirac pulse.

The measured (and reproduced) breakthrough curves of the tracer test studied in Task 6A, demonstrated that the peak in mass flow of HTO occurred approximately 7 hours after the start of injection, while the peak in mass flow of Strontium occurred after approximately 12 hours. Hence, in Task 6A, the peak arrival time of Strontium was 1.7 times longer than that of HTO. HTO is considered to be a conservative tracer, i.e. it does not adsorb onto the rock surface, but it will interact with stagnant zones etc. A delay factor may be defined (see Equ. 11-1) by means of the difference in breakthrough time between HTO and Strontium. The delay factor is a measure of the effects (retardation) of reactive transport processes. Considering the arrival time of the Strontium peak, the delay factor observed in the tracer test of Task 6A is 1.7. Considering the recovery of 5%, 50% and 95% of injected mass, the delay factor for Strontium in Task 6A (the STT-1b experiment) is, 1.5, 2.1 and 2.2, respectively.

In Task 6B2, the flow and flow velocities are relatively small (compared to those of Task 6A) and the effects of the delaying transport processes will be larger than in Task 6A, even for a relative weakly interacting tracer as Strontium. Considering Task 6B2, a Dirac pulse and the constrained coupled parameter distributions, we summarise the following results:

- The simulated arrival times of the peaks in HTO and Strontium mass flow give rise to a delay factor for Strontium equal to approximately 27.
- The simulated breakthrough times of the recovery of 5%, 50% and 95% of injected HTO and Strontium mass will produce a delay factor for Strontium close to 36, for all three amounts of recovered mass, when considering the median breakthrough time (50% probability).

As demonstrated above, the delay factor is much larger in Task 6B2 than in Task 6A. In Task 6B2, considering the constrained coupled parameter distribution (which produce the best estimate) and the peak arrival time, the delay factor is 29 (for the median of the peak arrival time), which is 17 times larger than the corresponding delay factor of Task 6A

In Task 6B2, considering the constrained coupled parameter distribution and the recovery of 5%, 50% and 95% of injected mass, the delay factor is close to 36 for all three amounts of recovered mass, when considering the median of the breakthrough times. A delay factor of 36 is 17 times larger than the corresponding delay factor of Task 6A.

The retardation factor (see Equ 5-3) represents the retardation of the front of a migrating contaminant, relative the movement of the bulk mass of water, assuming that the retardation is caused by a fast reversible adsorption with a linear isotherm. This concept of retardation factor, calculated separately for each material along the flow route, is not necessarily directly comparable to the delay factor (as defined in Equ 11-1). Nevertheless, for the modelled transport of Task 6B2 a comparison of the two concepts demonstrated that the difference between the calculated (and estimated) retardation factors and the calculated delay factors is not very large. Considering the Strontium tracer and the constrained coupled parameter distributions, a rough estimate of a median retardation value representing the retardation of the whole system of different materials is approximately equal to 50 (see Section 11.7.1). We have calculated a delay factor, considering the Strontium tracer and the breakthrough time for recovery of 50% of injected mass. For the constrained coupled parameter distribution and the 50^{th} percentile, the delay factor is equal to 37, for the 90^{th} percentile the delay factor is equal to 40.

Considering Task 6A, a comparison of: (i) the estimated median value of the retardation factors, and (ii) the measured delay factors directly obtained from the tracer test studied in Task 6A (measured data), will not produce a good agreement. The measured delay factor for the breakthrough time of the recovery of 50% of injected mass is equal to 2.2 (see Table 11-1); the estimated median retardation factor is equal to 50. The main reason why the estimated delay caused by the reactive transport processes is overestimated, is because the total time scale of the experiment of Task 6A is small.

The interaction of the tracers with rock masses not in direct contact with the flowing water is an important process at PA-time scales, e.g. reactive processes and matrix diffusion. And the properties that control these processes are not well constrained by a standard tracer test. Disregarding these processes at PA time scales will cause substantial underestimations of transport times.

Implications of the applied methodology, considering performance assessment modelling based on site characterisation data.

Traditionally when using SC data for deriving plausible ranges of parameter values, the objective is to derive probability distributions of the parameters studied. It is also often assumed that these distributions are independent and not correlated to each other, or some uncertain correlation is introduced between a few parameters.

The basic problem is that flow and transport models incorporate a large number of parameters, and credible fits to test results can be achieved with many different combinations of those parameters. Thus, testing can not be expected to produce definitive values of the parameters, or even useful probability distributions for them. The probability distributions are not very useful because it is the specific *combinations* of parameter values that succeed or fail to match tests. In other words, the analysis of the tests will result in extremely complex joint probability functions for the entire suite of parameters.

The approach we have used in this study recognises that it would not be possible to extract conventional probability distributions for individual parameters, and their correlations, for the complex non-linear system that we are studying.

By generating random realisations, based on a set of plausible (given) parameter distributions, and keeping only the realisations that produce an acceptable match to the field-test data set (the tracer test), we have done an informal Bayesian approach to map the entire joint probability density space and convert from prior to updated probabilities. In this way we have derived the constrained parameter distributions. The individual constrained distributions are, however, not necessarily very useful (as discussed above). Therefore we have established the constrained coupled parameter distributions.

The constrained coupled parameter distributions consist of the ensemble of coupled parameter values as defined by the accepted realisations. The difference compared to the constrained (uncoupled) parameter distributions is that in the constrained coupled parameter distributions the individual parameter values are combined, according to the parameter combinations that resulted in the accepted realisations.

The use of the constrained coupled parameter distributions for the PA modelling will produce better predictions with smaller uncertainties than the use of the constrained parameter distribution, because the constrained coupled parameter distributions will include the correct correlation between the parameters studied; and this is an important improvement compared to an assumption of independent parameters or the inclusion of some uncertain and limited correlation between a few parameters.

This might have important implications for how PA analyses should be carried out. The approach, in which one tries to establish independent distributions for each parameter, possibly with some correlations, is not necessarily the best approach, as it may be nearly impossible to integrate the knowledge gained from different field-tests into such distributions.

Instead, we propose the following approach, which is an approach used in this study:

I. Use as much general data as possible to develop the given (prior) parameter distributions (with possible correlations).

II. Use the given parameter distributions as input data for SC modelling. Only realisations that produce an acceptable match to field-test data sets, considering one or several tests, will be propagated to the PA-modelling. To improve the efficiency of the process of finding the acceptable realisations, constrained parameter distributions can be derived and these distributions can be used instead of the given distributions, as input data for the SC modelling. In a wider perspective, a more complex modelling can be carried out; and the field-test data, against which the modelling results are matched, may not only come from tracer tests, but could also be taken from other tests and analyses, e.g. pump tests, laboratory analyses of chemical properties etc.

III. PA modelling for the specific combinations of parameter values that passed all tests against field data (the constrained coupled parameter distributions).

Contents

List of figures

1 Introduction, objectives and general methodology

1.1 Introduction and general objectives of Task 6

The general objective of Task 6 is to provide an understanding of the link between the characterisation of the properties and the processes which govern the flow and the solute transport in a fractured crystalline formation, and the performance assessment of a repository site hosted in such a formation Task 6 seeks to provide a bridge between Site Characterisation (SC) and Performance Assessment (PA) approaches to the study of transport of solutes in fractured rock. In Task 6 both PA-type and SC-type models will be applied, considering both the experimental boundary conditions and boundary conditions for the PA scale. There is no formal difference between PA and SC models, however typically the description of the groundwater flow is more detailed in a SC models than in a model used for PA. Task 6 combines the use of PA and SC models, using both PA and SC type boundary conditions. The geometric scale of the transport studied in Task 6 is within 200 m. (The smallest transport distances takes place for Task 6A and the largest transport distances takes place for Task 6E.)

1.2 Objectives of Task 6A

Task 6A is the first component of Task 6. The purpose of Task 6A is to model and reproduce selected TRUE-1 trace tests and thereby assess the constraining power of these tracer tests, i.e. the capability to quantify the basic characteristics of the parameters and processes affecting the radionuclide transport in the fractured rock.

Solute transport over a single geological feature is studied in Task 6A and 6B2. The feature studied was identified in the Äspö TRUE Block Scale experiments. (Solute transport over longer distances is studied in Task 6D and 6E.)

The result of an experimental evaluation is model dependent. To obtain a framework where model bias may be compared and discussed, the Task Force group apply several different model concepts. For Task 6A, the common platform for the modelling teams consists of data sets including experimental breakthrough curves for several tracers, as well as independent material properties evaluated by various tests.

A large number of different rock mass properties may influence the tracer tests, e.g. porosity, flow wetted surface, amount of stagnant water, Kd-values, dispersion, matrix diffusion etc, etc, and theoretically there is an infinite number of combinations of the unknown rock mass properties that will produce approximately the same breakthrough curve. However, based on information derived from observations, other hydraulic test, as well as laboratory experiments, it is possible to establish plausible ranges within which the unknown rock mass properties may vary. The purpose of Task 6A is to analyse the constraining power of the tracer tests with regard to the given plausible ranges within which the unknown rock mass properties may vary.

1.3 Objectives of Task 6B2

The objectives of Task 6B2 are to model selected PA cases at the TRUE-1 site with PA relevant (long term) boundary conditions and temporal scales (i.e. natural gradients, no pump test).

Solute transport over a single geological feature is studied in Task 6A and 6B2. The feature studied was identified in the Äspö TRUE Block Scale experiments. (Solute transport over longer distances is studied in Task 6D and 6E.)

Compared to Task 6A the temporal scale of Task 6B2 is much longer. Considering a conservative tracer, the recovery of 95% of the injected mass took 77 hours in the Task 6A tracer test, but may take 3 years in the flow field of Task 6B2. Hence, the temporal scale of Task 6B2 is several hundreds of times larger. Because of the relative long period studied in Task 6B2, transport processes that are of importance in the longer time perspective of a PA analysis e.g. matrix diffusion, will have a significant influence on the transport modelled in Task 6B2. A comparison with the results obtained from Task 6A will demonstrate the importance of these processes.

1.4 Documents specifying the modelling work of Task 6

The specification of Task 6 is presented in the following documents:

- "Task 6: Performance Assesement Modelling Using Site Characterisation Data" by Benabderrahmane *et al* (2000).

- "Task 6A & 6B. Modelling task specification. Ver 1.0" (T6ABMS) by Selroos and Elert (2001).

- "Task 6B2. Modelling task specification. Ver 1.0" (T6B2MS) by Elert and Selroos (2001).

- "General Technical Specification, Äspö Modelling Task Force Task 6, 2002-2004" by ANDRA (2001).

- "Task 6C – A semi-synthetic model of block scale conductive structures at the Äspö HRL" (description of the T6C block scale semi.synthetic hydrostructural model) by Dershowitz et al., 2003. (SKB IPR-03-13).

- "Task 6D. Modelling task specification. Ver 1.0" (T6DMS) by Elert and Selroos (2002).

- Task 6E. Modelling task specification. Version 3.0 (T6EMS) by Elert and Selroos (2004)

1.5 Terminology and concept of transport processes

1.5.1 Groundwater, solute and tracers

This study is about groundwater and about transport of contaminants in groundwater. By a solute we mean a constituent of the groundwater that is not water, but a dissolved substance that may occur at small concentrations in the water. If the concentration of the substance is very small we may call the constituent a tracer. The tracer is the solute and the water is the solvent.

1.5.2 Advection

Dissolved substances (solutes) are carried along with the flowing groundwater. This transport process is called advection, or advective transport. The amount of solute that is being transported follows from the concentration of the solute and amount of groundwater flowing.

1.5.3 Hydrodynamic Dispersion

Hydrodynamic dispersion is the tendency for a solute, dissolved in the groundwater, to spread out from the path that it would be expected to follow according to the advective hydraulics of the flow system. Dispersion is caused by molecular diffusion and mechanical mixing during fluid advection. Molecular diffusion is the process of spreading of a solute of higher concentration to a region of lower concentration, as a result of thermal movement of the molecules of the solute. The mechanical mixing, often called mechanical dispersion, is caused by the heterogeneous properties of a flow medium. Mechanical dispersion is scale dependent and will occur both at a microscopic scale and at a macroscopic scale.

1.5.4 Retardation

Solutes dissolved in the groundwater are subjected to different processes through which they can be removed from the groundwater and transformed. For example: Solutes can be sorbed onto the surfaces of minerals, sorbed by organic carbon that may occur in the groundwater, undergo chemical precipitation, be subject to biodegradation, participate in oxidation-reduction reactions, etc, and in addition radioactive compounds will decay. As a result of delaying processes (such as sorption etc) some solutes, or amounts of solutes, will move slower through the flow system studied than the bulk motion of the flowing groundwater; this effect is called retardation.

1.5.5 Fractured crystalline rock, retardation and matrix diffusion

The established models represent a fractured crystalline rock mass. Groundwater flow in such a rock occurs in fractures and in fracture zones of different size and significance. These fractures and fracture zones determine the heterogeneous and anisotropical hydraulic properties of the rock mass.

All the transport processes described above may influence the transport of a solute in a fractured rock mass. A fractured rock mass has however certain geometric and hydraulic properties and from these special properties follows the concept of matrix diffusion.

In a fractured crystalline rock mass the groundwater will flow along a system of permeable and connected fractures, in addition to these "flowing" fractures there are:

- Fractures of significant size that are connected to the system of fractures with flowing groundwater, but very little advective flow takes place in these fractures; because these fractures are either dead-end fractures or have a very small permeability.

- Micro-fractures or micro fissures that were created during the cooling of the crystalline rock mass. Such micro fissures are very small but occur in very large numbers. The micro-fissures occur in the crystalline rock mass between larger fractures, the micro-fissures surrounds the crystals of the crystalline rock mass.

The micro fissures and the larger dead-end fractures will together produce a certain small porosity that is an importante attribute of the crystalline rock mass between the larger flowing fractures. This porosity, even if it is small, is a significant component of the studied system, especially when considering the transport of solutes by groundwater that moves under natural (small) gradients.

The micro fissures and the larger dead-end fractures are important because of a transport process called matrix diffusion. Matrix diffusion is the process by which solutes diffuse from a fracture with flowing water (mobile zone) into: (i) surrounding micro fissures, (ii) larger dead-end fractures and (iii) a possible porous matrix material. In mathematical models, the domain that surrounds a flowing fracture is often simplified into one or several matrix diffusion zones, which are defined by values of thicknesses, porosities and values of effective diffusivity.

Matrix diffusion will influence the transport of all solutes.

Matrix diffusion is a key-element of a mathematical model for calculation of transport and retardation of solutes in a fractured rock mass, especially if the groundwater flow takes place under natural hydraulic gradients. When analysing a tracer test, for which the hydraulic gradients is artificially large (due to pumping at a recovery well), matrix diffusion may be of less importance, because of the short time scale of the test.

1.6 Applied general methodology

This study may be characterised as a probabilistic performance assessment modelling exercise, based on site characterisation data. Task 6A is a site characterisation (SC) modelling exercise, and Task 6B2 is a performance assessment (PA) modelling exersice. It is primarily the longer time scale that makes Task 6B2 into a PA case, as the spatial scale is approximately the same in Task 6A and Task 6B2. Normally a PA case involves both a long time period and a large spatial domain. Such PA cases will be studied in Task 6D and 6E.

In this study, the site characterisation data is information about the properties of the fracture plane studied. This information is given by the results of different pump tests and tracer tests. This site characterisation data is included in the Task 6A modelling. The next step is the Task 6B2 modelling, which is based on the results of the Task 6A modelling.

Both the Task 6A and Task 6B2 modelling are separated into:

(i) Modelling of the flow field.

(ii) Transport modelling.

We have used an extensive probabilistic approach, in which uncertainties of the properties of the fracture plane studied are propagated to the Performance assessment modelling.

The methodology applied in this study is presented in a number of flow charts, given below.

METHODOLOGY OF PROBABILISTIC PERFORMANCE ASSESSMENT MODELLING.

- DIRECT APPROACH -

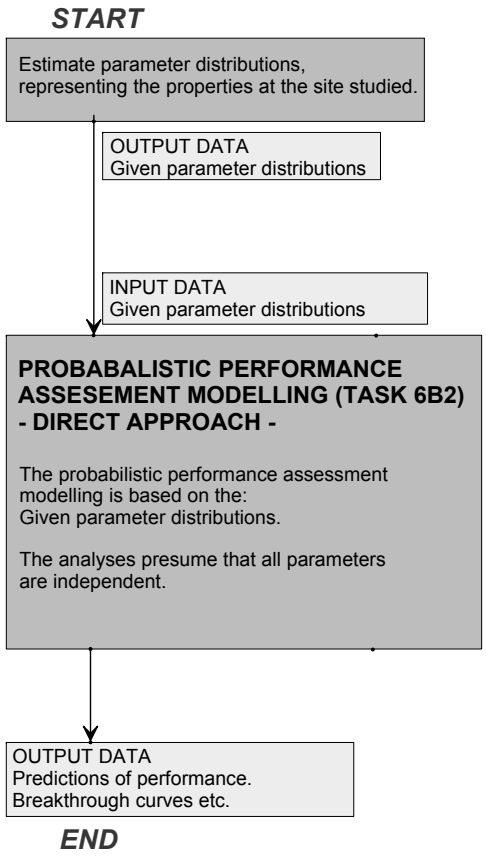

Figure 1-1 *TASK 6A and TASK 6B2. Methodology of probabilistic performance assessment modelling based on site characterisation data.*

METHODOLOGY OF PROBABILISTIC PERFORMANCE ASSESSMENT MODELLING, BASED ON SITE CHARACTERIZATION DATA.

- STANDARD AND IMPROVED APPROACH -

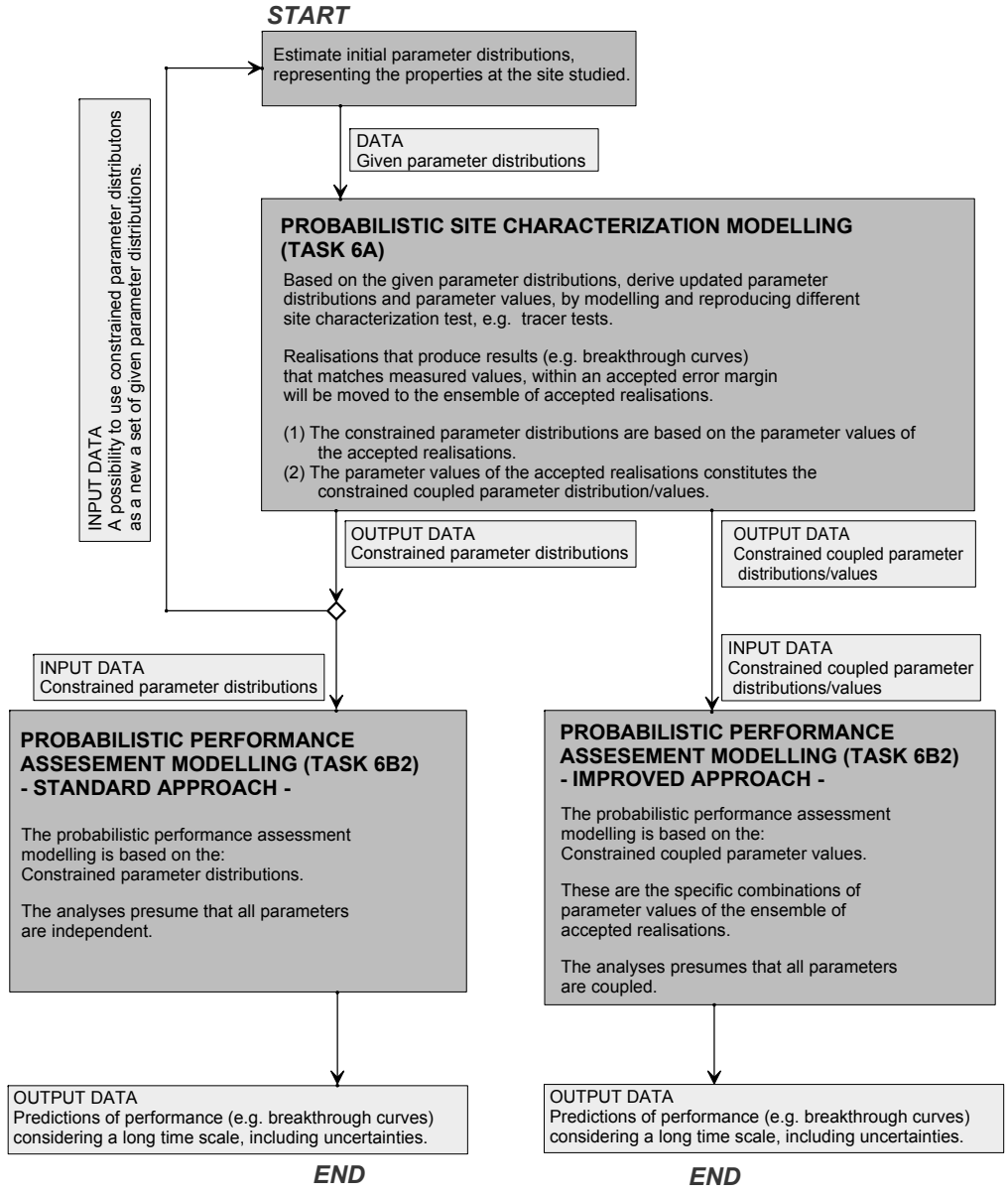

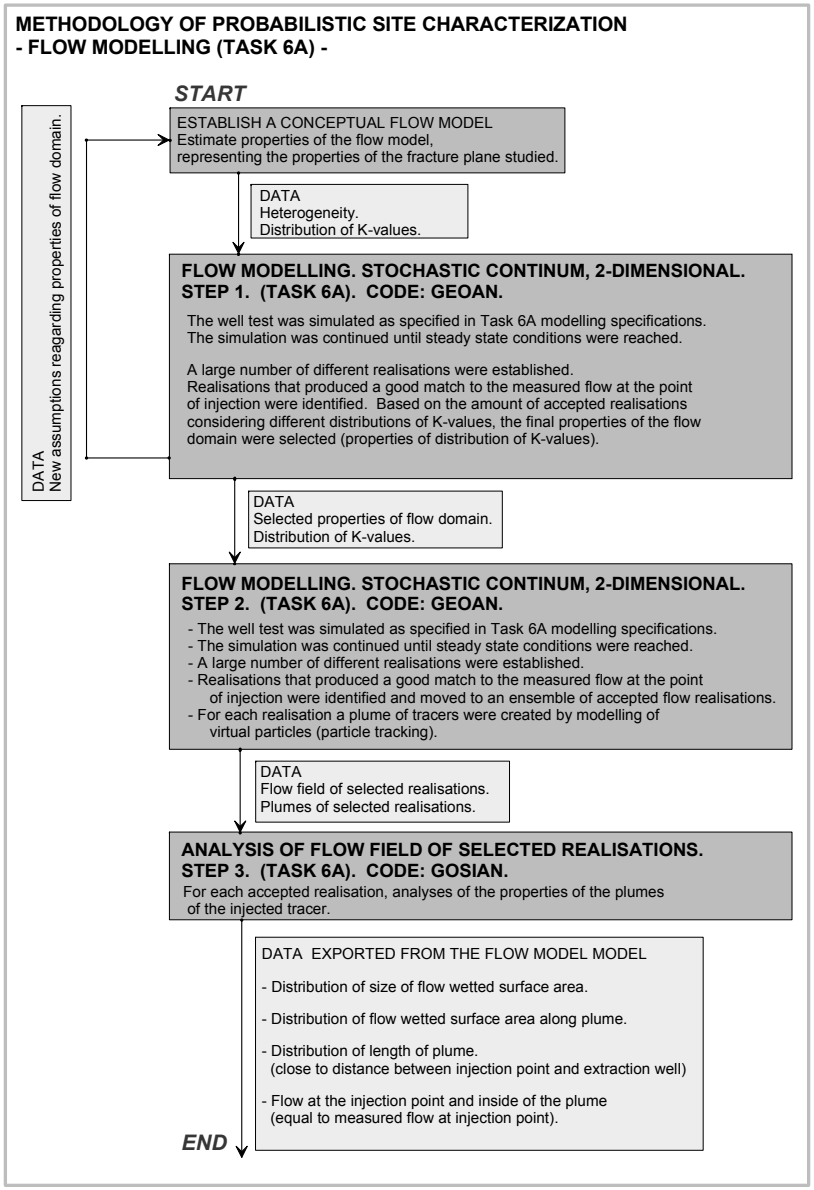

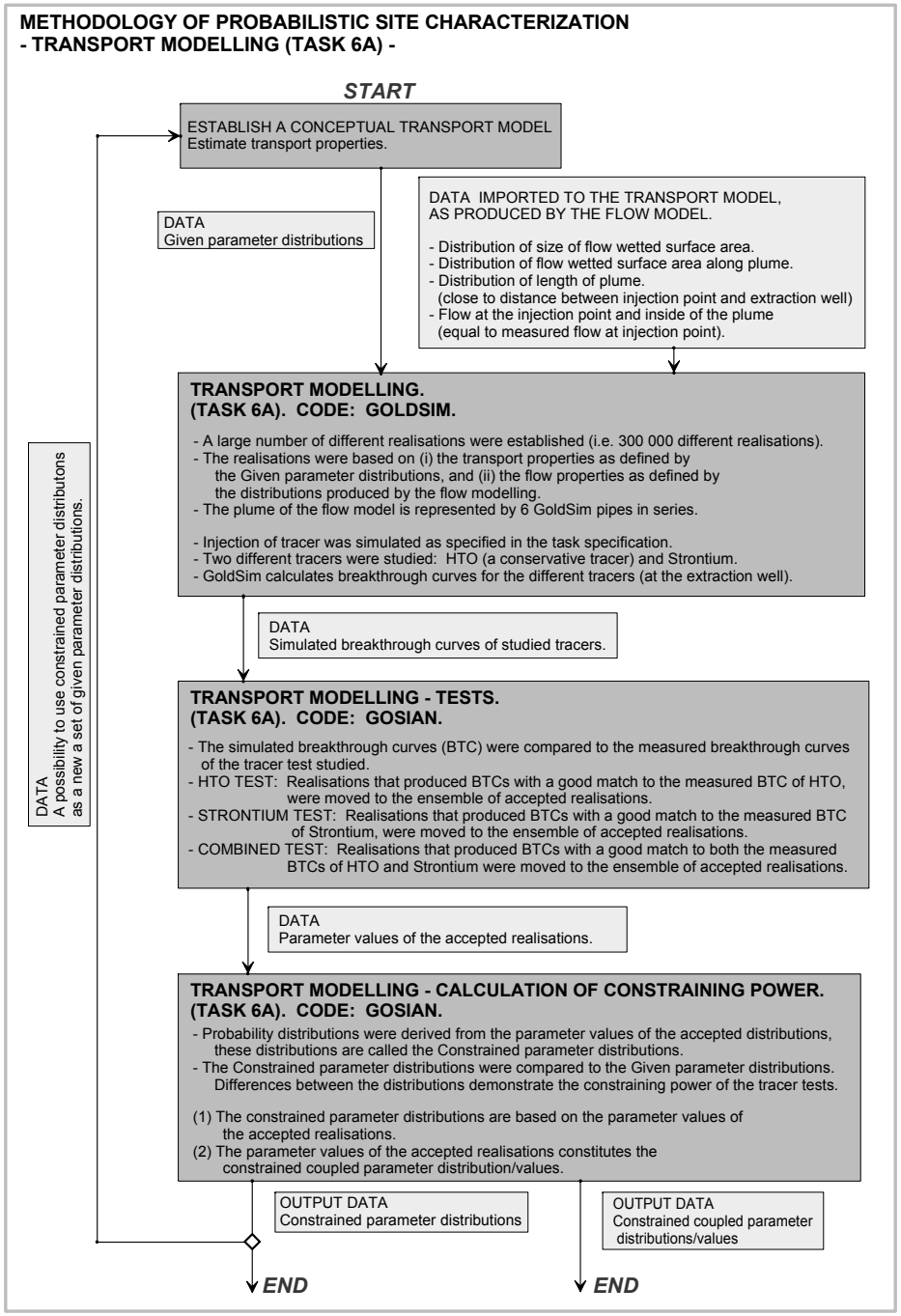

Figure 1-2 *TASK 6A - Methodology of flow and transport modelling.*

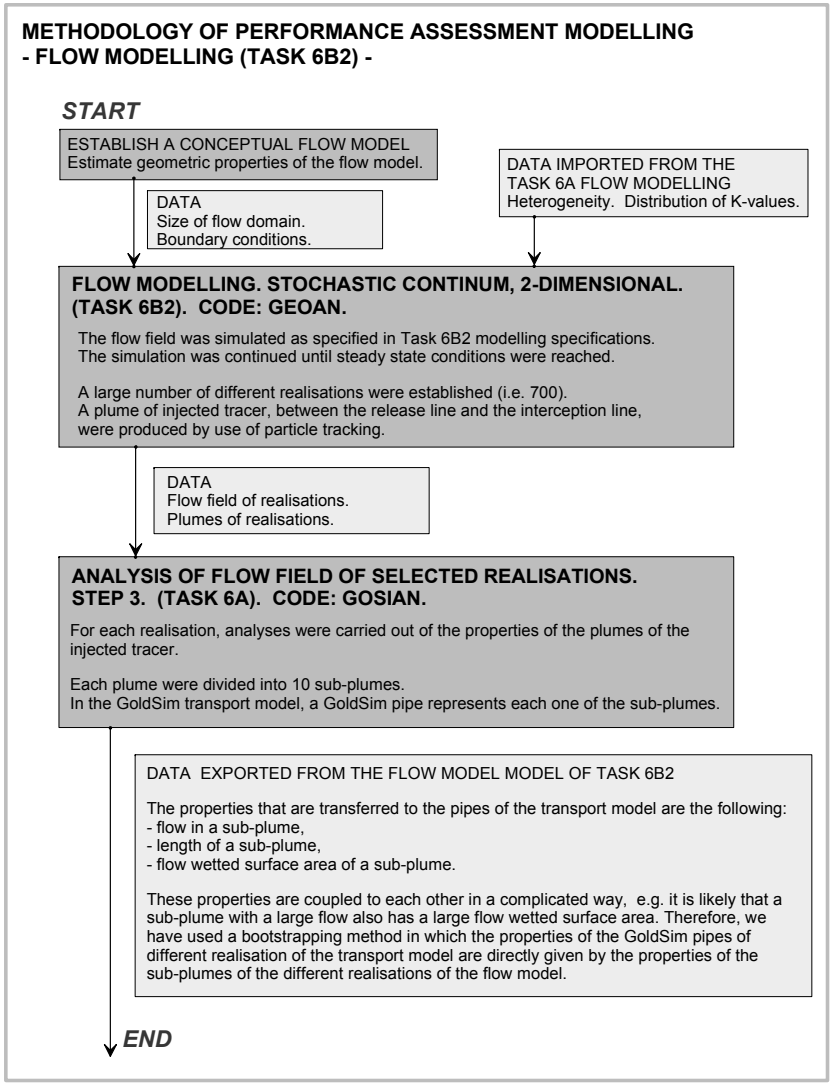

Figure 1-3 *TASK 6B2 - Methodology of flow modelling.*

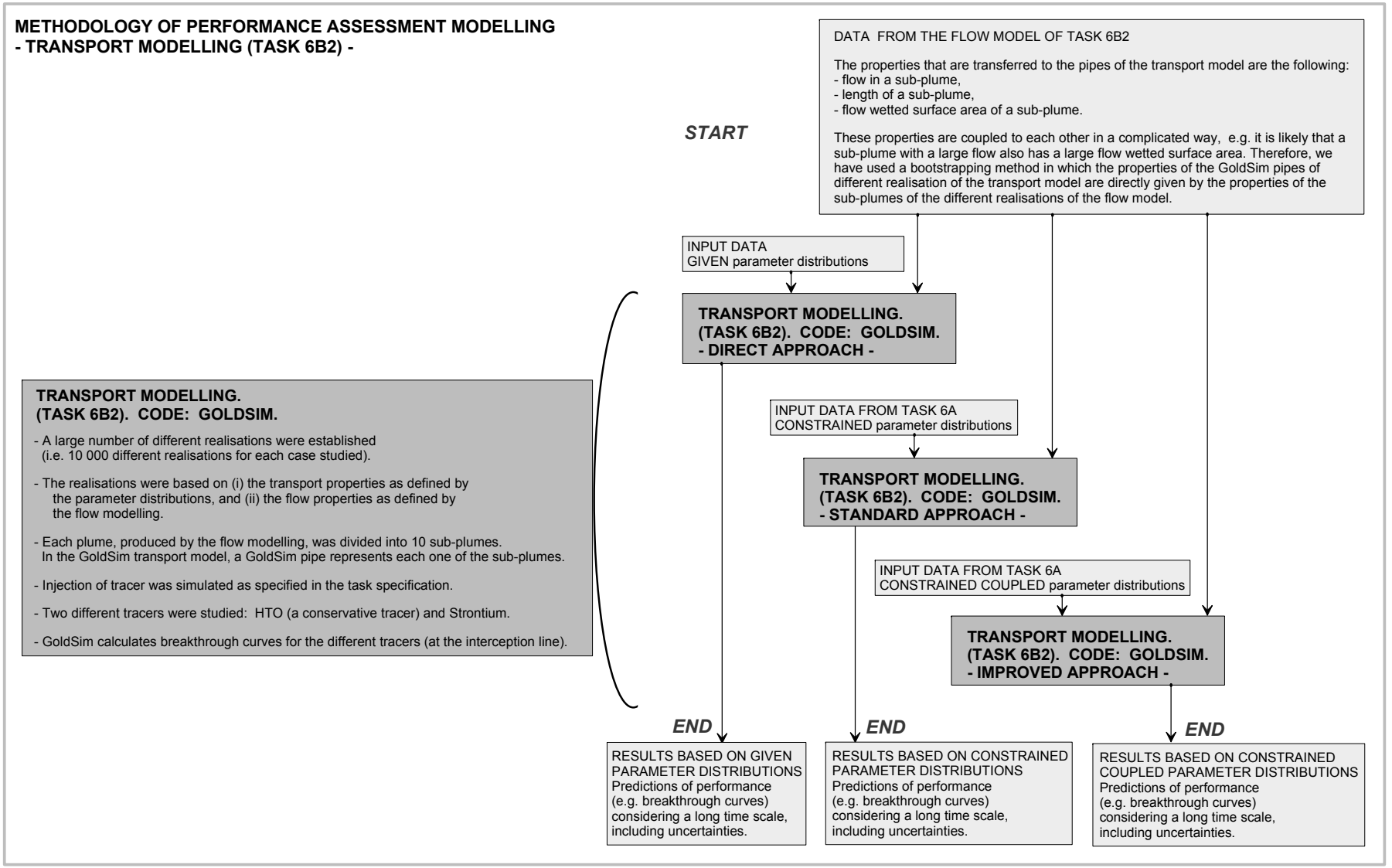

Figure 1-4 *TASK 6B2 - Methodology of transport modelling.*

2 TASK 6A – Modelling of flow field and flow paths

2.1 Purpose

This chapter presents the simulation of the flow field and of flow paths (flow modelling) inside Feature A. The flow modelling is based on several assumptions regarding the properties of the system studied, these assumptions are presented below. Based on the results of the flow modelling, we have derived a probabilistic description of the shape of the plume of contaminated water (tracers) inside Feature A. The shape of the plume will be propagated to the transport modelling.

2.2 Conceptual model

The tracer tests studied took place in a fractured rock mass, the part of the rock mass in which the tracers moved with the groundwater and interacted with the rock mass is called Feature A. Feature A could be a single fracture or a system of fractures. We have assumed that Feature A is a single fracture that can be represented by a fracture plane with varying flow properties inside the fracture plane. The fracture is defined as a two dimensional plane. The heterogeneity in the flow properties along the fracture plane (the variation in flow properties) was represented by use of the stochastic continuum approach.

2.3 Computer code used

We have modelled the flow in Feature A by use of the GEOAN computer program. GEOAN is a computer program for simulation of groundwater flow and transport; the code is based on the finite difference approach, see Holmén (1992) and Holmén (1997).

2.4 Boundary conditions

For the established model, the initial situation was defined in line with the description given by: (i) Task 6 modelling specification (T6MS) by Selroos and Elert (2001), see Section 7.1, and (ii) "Äspö HRL Final report of the first stage of the tracer retention understanding experiments" (TR-00-07), by Winberg *et al*, 2000.

A number of observation wells are located inside the Feature A. In the model, the measured heads in the observation wells were extrapolated to the boundaries of the fracture plane studied. Hence, along the boundaries of the modelled fracture plane, the specified head boundary condition was defined; and the applied head values were based on the measured heads in the observation wells.

The purpose of the study is to simulate a tracer test. The tracers were introduced into Feature A at an injection well. The injection of tracers at the injection well was done in a passive way, the injection of tracers had a minimal effect on the flow in Feature A.

A steady outflow of water from the fracture plane was created by the introduction of an extraction well. During the test studied, the groundwater flow in Feature A was dominated by the discharge at the extraction well and consequently the flow in the vicinity of the extraction well was towards the extraction well.

In the model, at the centre of the fracture plane studied, an extraction well is defined with a specified flow boundary condition. No special boundary condition was applied at the injection point, the injection point was defined as a cell with a continuous flow condition. The simulations were continued until steady state conditions were reached.

2.5 Mesh and Conductivity

The fracture was defined as being 20 x 20 m, this is in line with the description given in T6MS by Selroos and Elert (2001). The finite difference grid along the fracture plane was defined with a cell size of 0.2 m x 0.2 m.

The heterogeneity in the flow properties along the fracture plane was represented by a stochastic continuum. The conductivity field was defined as a Log-Normal distribution, with a geometric mean of 2.8E-4 m/s. The hydraulic aperture was set to 1 mm. These assumptions follows from the transmissivity values given in TR-00-07 (Winberg *et al*, 2000), these transmissivity values are estimated based on a large number of hydraulic tests conducted in Feature A. The range of transmissivity values is 8E-9 m^2/s through 4E-7 m^2/s, the range illustrates the uncertainty in permeability of Feature A. For a hydraulic aperture of 1 mm, the transmissivity values produce a range of conductivity values that is 8E-6 m/s - 4E-4 m/s. It is stated in TR-00-07 (Winberg *et al*, 2000) that there are some indications of an underestimation of the transmissivity values, due to hydraulic turbulence close to the extraction wells (the wells used for the hydraulic tests); hence the range of transmissivity values given above might be an underestimation.

It is stated in TR-00-07 (Winberg *et al*, 2000) that the correlation length of the K-field is in the range of 0.3 m and 0.4 m; as this is close to the cell size applied in the model (i.e. 0.2 m), the K-field was defined as not correlated.

The K-values along the fracture plane was, as stated above, defined by a Log-Normal distribution. The standard deviation of the Log-Normal distribution is a measure of the heterogeneity of the K-field. As a part of the modelling a sensitivity analysis has been carried out in which the standard deviation was varied. A standard deviation (STD) of zero produces a homogeneous flow field in which all cells have a K-value equal to the geometric mean (2.8E-4 m/s). Larger values of the STD will create a heterogeneous flow field. The following values of the standard deviation were studied, given in 10Log space: 0.25, 0.5, 1.0 and 2.0. A standard deviation of 2 corresponds approximately to the observed K-values of rock blocks of size: 3 m x 3 m x 3 m, as measured by double packer tests at Äspö. A standard deviation of 1 corresponds approximately to the observed K-values of rock blocks of size 30 m x 30 m x 30 m, as measured by double packer tests at Äspö. A standard deviation of 0.5 corresponds approximately to the observed K-values of rock blocks of size 100 m x 100 m x 100 m, as measured by packer tests at Äspö.

We have also established a homogeneous flow model, presented in several figures e.g. Figure 2-1 and Figure 2-7. It should be noted that the purpose of the homogeneous flow model is to demonstrate the flow field of a homogeneous flow medium. The homogeneous model is not used in the modelling of the transport processes.

2.6 Simulated test

The well test was simulated as specified in T6MS (Selroos and Elert , 2001). The flow at the extraction well was defined as 0.401 Litre/min (T6MS, Selroos and Elert 2001). The extraction well was defined at the centre of the fracture plane studied. The simulation was continued until steady state conditions were reached. The distance between the point of injection and the extraction well is 5 metres.

2.7 Simulation of flow paths

After steady state conditions was reached in the simulations a tracer was injected at a position corresponding to the injection point (Well KXTT1 R2). The tracer was simulated by use of virtual particles that followed the flow field towards the extraction well.

The flow paths were determined by use of an analytic solution (Pollock, 1989). Only advection was simulated, no hydromechanical dispersion and no chemical diffusion etc were included in the simulations of flow paths.

For each realisation of the flow field, 1000 flow paths were released inside the cell that represented the injection point; it follows that the size of the area where the release took place was 0.2 m x 0.2 m (given by the cell size). Examples of the resulting flow paths are given in Figure 2-1 through Figure 2-6.

It should be noted that the homogeneous model, presented in Figure 2-1, is only used to demonstrate the flow field of a homogeneous flow medium, it is not used in the modelling of the transport processes.

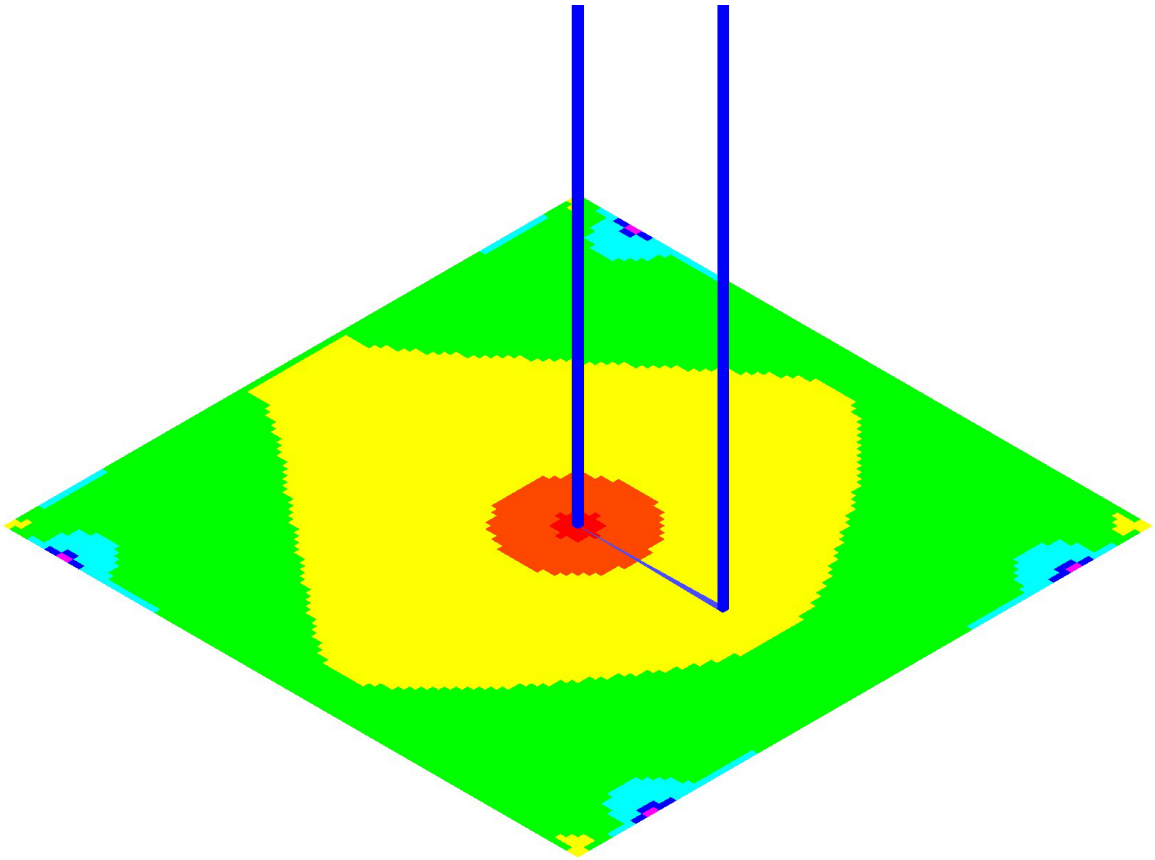

Figure 2-1 *The fracture plane (Feature A) as defined in the model, and an example of a simulated groundwater velocity field inside the fracture. The velocity field represents the tracer test studied. For the presented simulation it was assumed that the conductivity field inside the fracture is perfectly homogeneous.*

The different colours on the fracture plane represent different velocities. The largest velocities are denoted by red colour, the following colours denote the velocity in an order given by decreasing velocity and a logarithmic scale: red, yellow, green and blue (smallest velocity). The colours on the fracture plane illustrate the converging flow field–a flow towards the well from all directions.

The dark blue and triangular plume at the centre of the figure denotes flow paths from the injection well to the extraction well. The wells are denoted with blue pipes. The pipe at the centre of the fracture is the extraction well. The rightmost well is the injection well.

It should be noted that the homogeneous model is only used to demonstrate the flow field of a homogeneous flow medium. The homogeneous model is not used in the modelling of the transport processes.

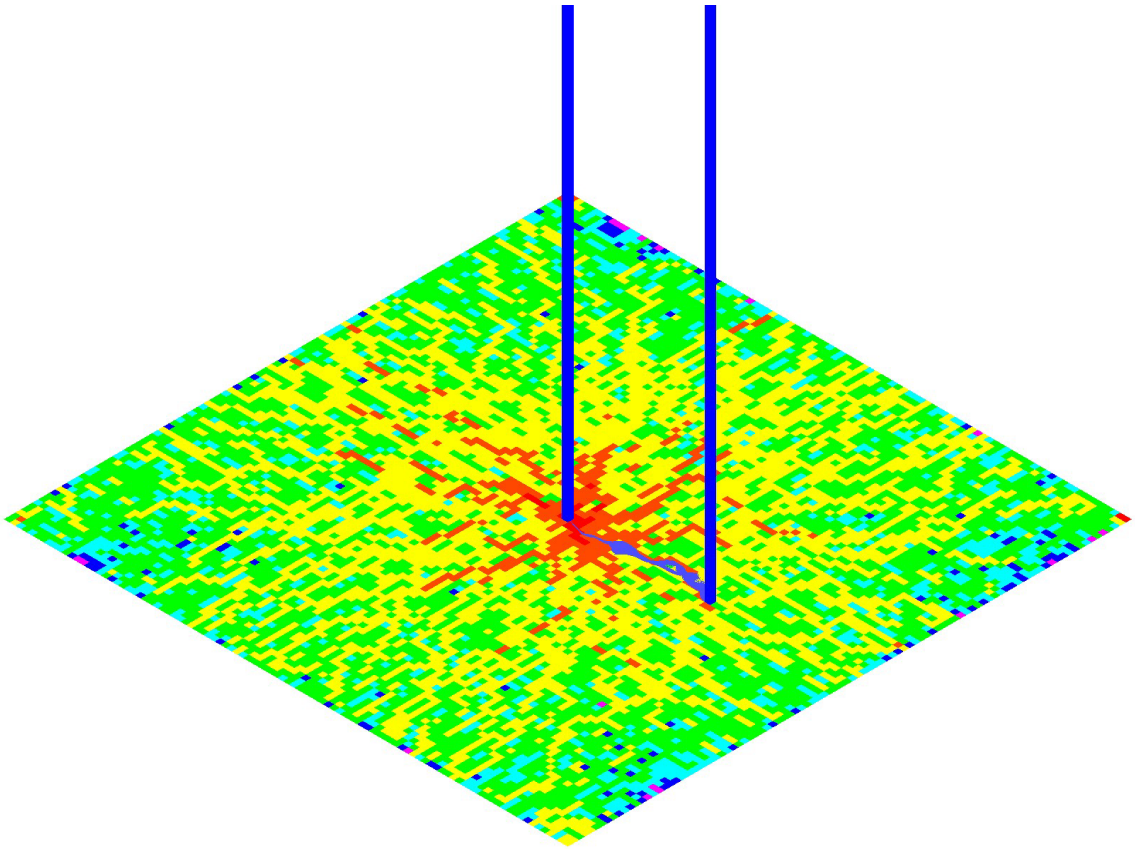

Figure 2-2 *The fracture plane (Feature A) as defined in the model, and an example of a simulated groundwater velocity field inside the fracture. The velocity field represents the tracer test studied. For the presented simulation it was assumed that the conductivity field inside the fracture is heterogeneous, as modelled by use of the stochastic continuum approach.*

The conductivity values of the realisation were given by a Log-Normal distribution with a standard deviation of 1.0 in 10Log space.

The figure presents one realisation of the velocity field. The different colours on the fracture plane represent the different velocities. The largest velocities are denoted by red colour, the following colours denote the velocity in an order given by decreasing velocity and a logarithmic scale: red, yellow, green and blue (smallest velocity). The colours on the fracture plane illustrate the converging flow field–a flow towards the well from all directions. The colour scale used in this figure is not exactly the same as in the previous.

The dark blue plume at the centre of the figure denotes flow paths from the injection well to the extraction well. The wells are denoted with blue pipes. The pipe at the centre of the fracture is the extraction well. The rightmost well is the injection well.

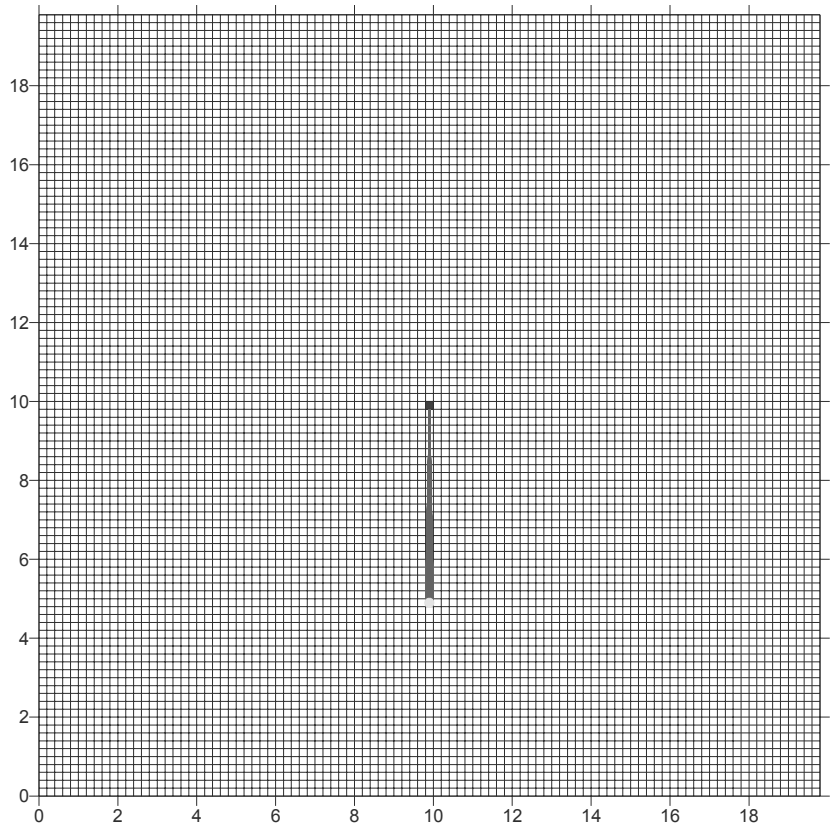

Figure 2-3 *Flow paths from injection point to well. Homogeneous K-field.*

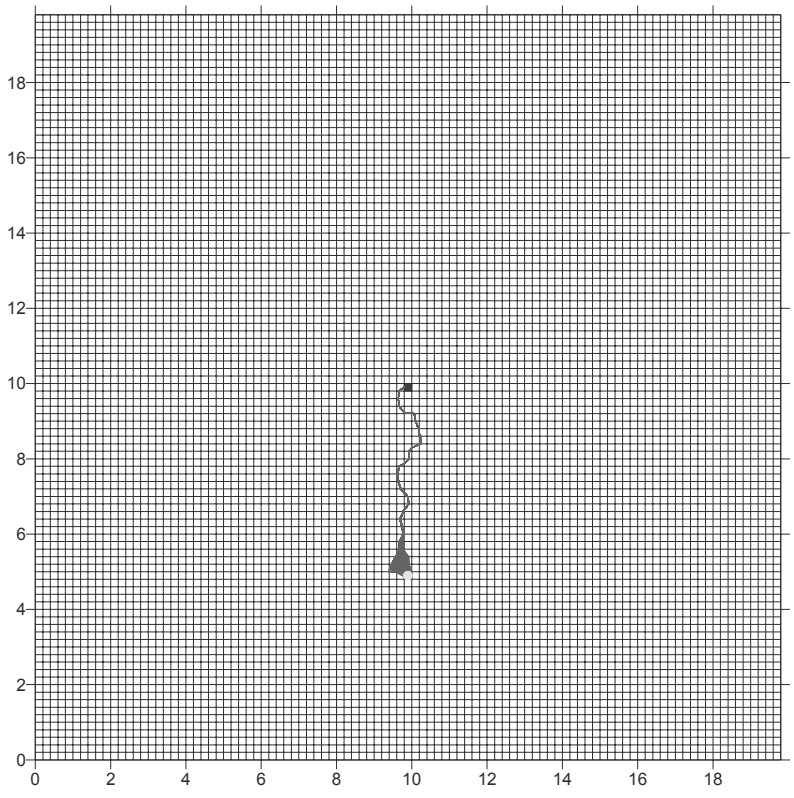

Figure 2-4 *Flow paths from injection point to well. Heterogenous K-field. One realisation. Standard deviation of the K-field = 1 (in 10Log space).*

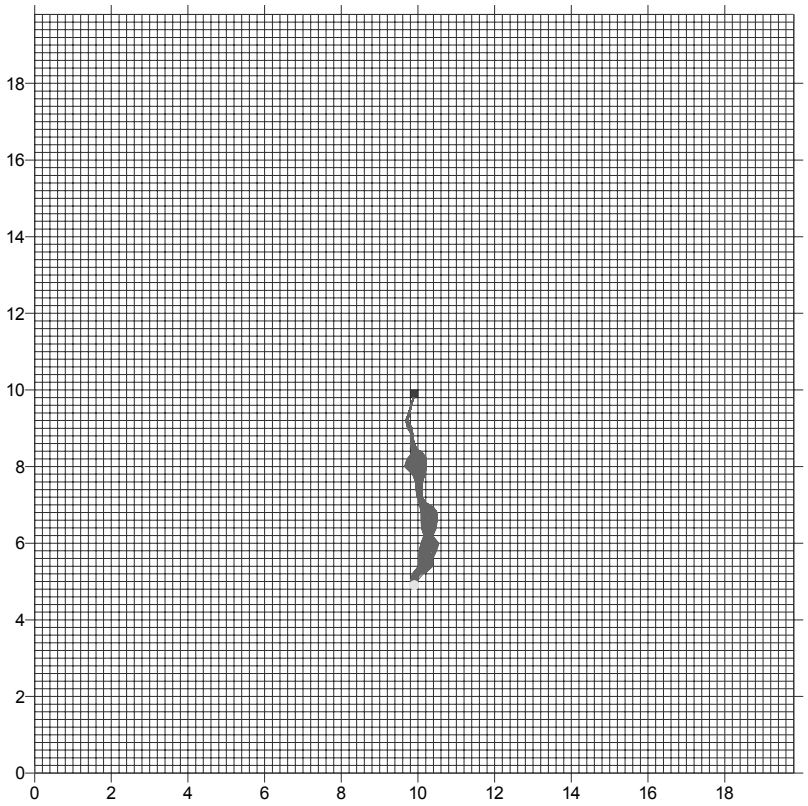

Figure 2-5 *Flow paths from injection point to well. Heterogenous K-field. One realisation. Standard deviation of the K-field = 1 (in 10Log space)*

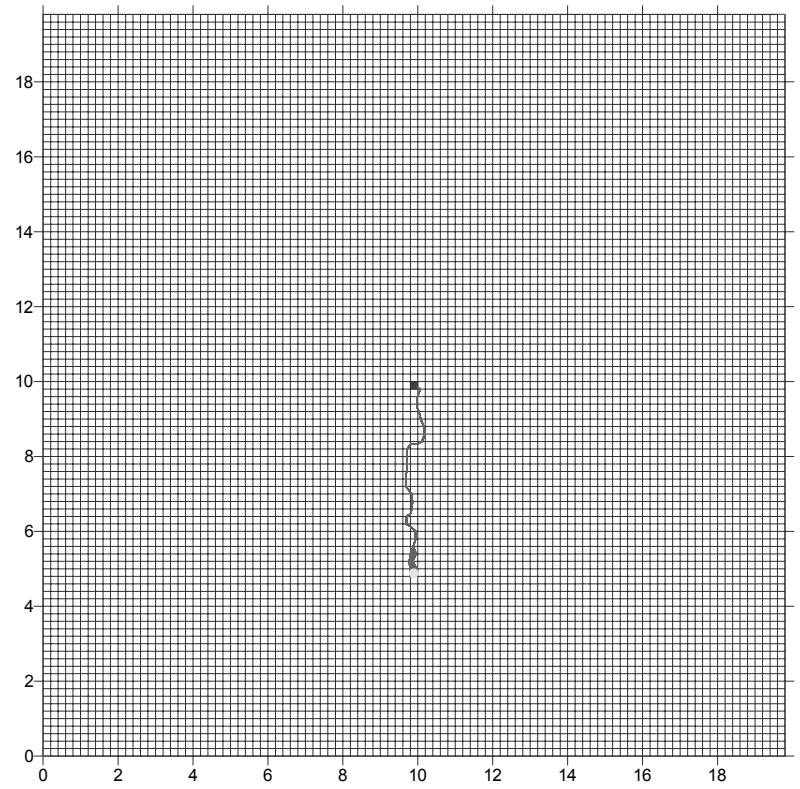

Figure 2-6 *Flow paths from injection point to well. Heterogenous K-field. One realisation. Standard deviation of the K-field = 1 (in 10Log space)*

2.8 Simulated flow path length (all realisations)

By analysing the length of the flow paths it is possible to estimate distributions of flow path lengths. The results are given in Figure 2-7. The figure demonstrates that the minimum length is 5m, as given by the shortest distance from source to sink, and that the flow path length increases as the heterogeneity increases. Also the distribution changes, a more skewed distribution is obtained for large values of heterogeneity. The 50th percentile of flow path lengths increases form 5m at a homogeneous flow field and up to 6.6m for K-field with a standard deviation of 2 (10Log space), the 99th percentile of flow path length is larger than 8m for this K-field.

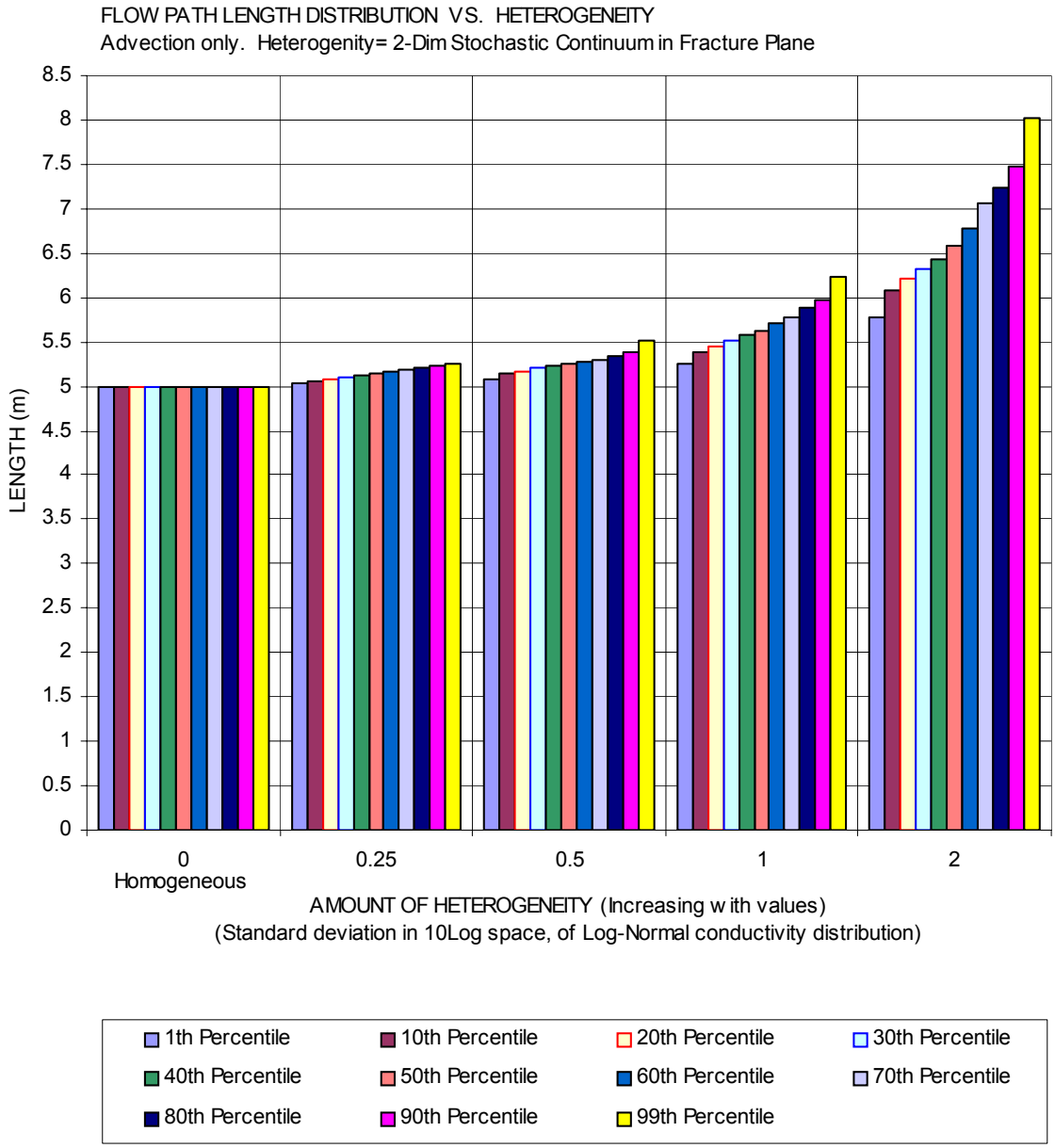

Figure 2-7 *Distribution of flow path lengths, for different values of heterogeneity, considering all realisations.*

2.9 Simulated flow wetted surface area (all realisations)

By analysing the distribution of flow paths from the injection point–the plume–it is possible to estimate the flow wetted surface area (wet area). In this study the flow wetted surface is defined as two times the extension of the plume (the area on the upper fracture plane and the area on the lower fracture plane). The results are given in Figure 2-8. It is well demonstrated by the figure that the size of the flow wetted surface changes substantially between different realisations of the flow field, particulary if the heterogeneity is large.

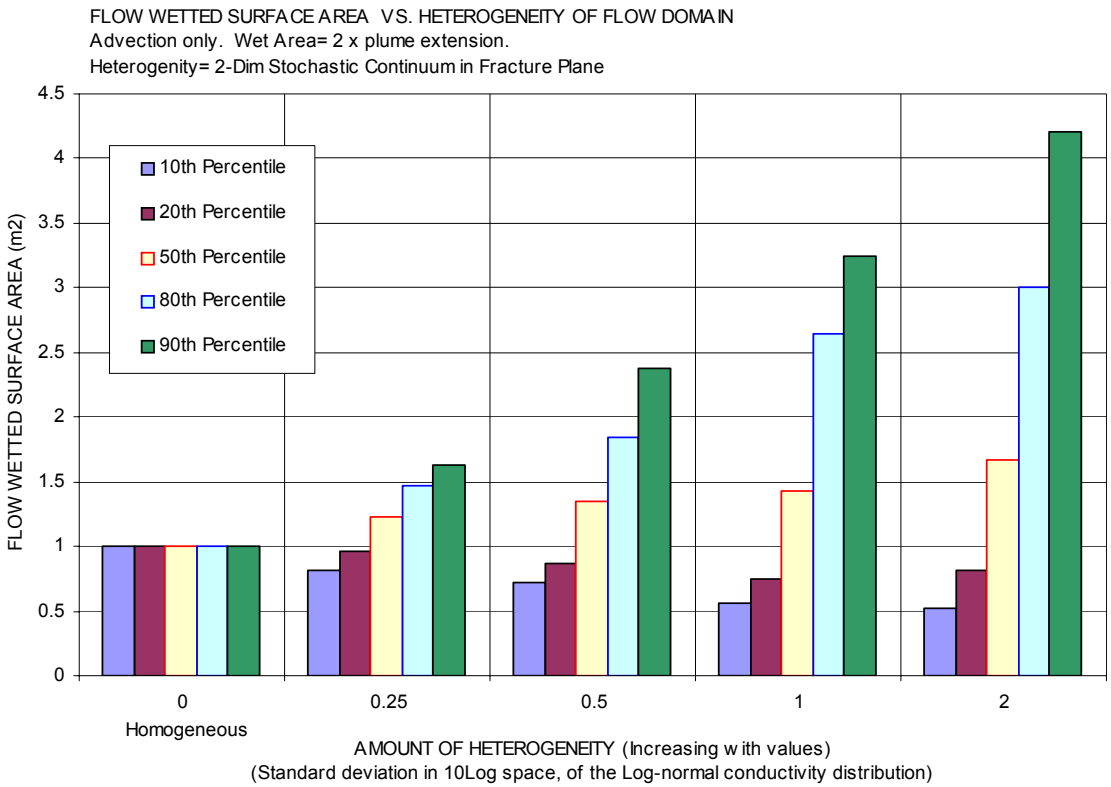

Figure 2-8 *Flow wetted surface area as given by the extension of the flow paths (plume), for different values of heterogeneity of the K-field. All realisations are considered.*

The plume has a non-uniform shape. The shape of the plume varies between different realisations. On the average however, the width of the plume is converging to wards the well, as given by the converging flow field. Separating the plume into six separate sections of equal length demonstrates this. The first section is closest to the injection point; and the last section is closest to the well. The results are given in Figure 2-9. It is demonstrated by Figure 2-9 that on the average the plume gets smaller as it gets closer to the well. Close to the well the velocity of the converging flow field is large, consequently, close to the well the plume is very narrow and the corresponding flow wetted surface is small.

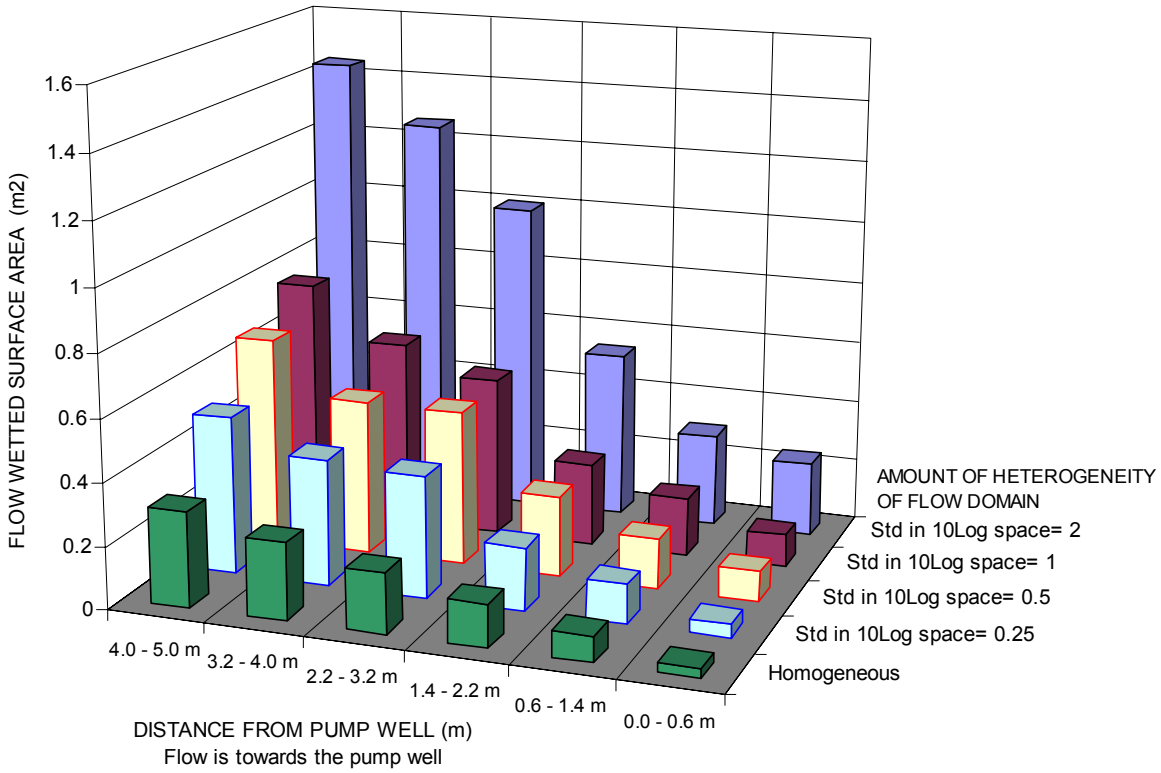

Figure 2-9 *The 80th percentile of the flow wetted surface area, considering six sections along the length of the plume, for different values of heterogeneity of the flow domain (K-field).*

2.10 Flow at injection point (all realisations)

The tracer test studied was test in which the tracers were injected at the release point in a passive way, hence the tracers were not pumped into the fracture with a large injection flow.

- The actual flow, in Feature A, at the injection point during the test studied, was estimated to be an undisturbed flow of approximately 9.7 x 10^{-4} Litre/min (0.509 m^3/year); this is the release flow (TR-00-07, Winberg *et al*, 2000).

- During the test, the flow at the extraction well was set to 0.401 Litre/min (210.8 m^3/year); this is the extraction flow (T6MS, Selroos and Elert, 2001)

In the model, the flow at the extraction well was set to 0.401 Litre/min, as a specified flow boundary condition. We have not in the model defined the flow at the release point (9.5 x 10^{-4} Litre/min) as a specified-flow boundary condition. Instead we have analysed the simulated flow in a large number of different realisations of the heterogeneous flow domain. As a part of the analyses we have for each realisation calculated the flow through the cell that represents the injection point (the release cell), and identified the realisations that produced a simulated release flow close to the true release flow.

Considering all realisations studied, the flow through the release cell varies markedly, because of the heterogeneous permeability of the flow domain, i.e. the different K-values of the cells. The distribution of flow through the release cell considering *all realisations* is given below in Figure 2-10. In the figure different flow distributions are given for different amounts of heterogeneity of the flow domain.

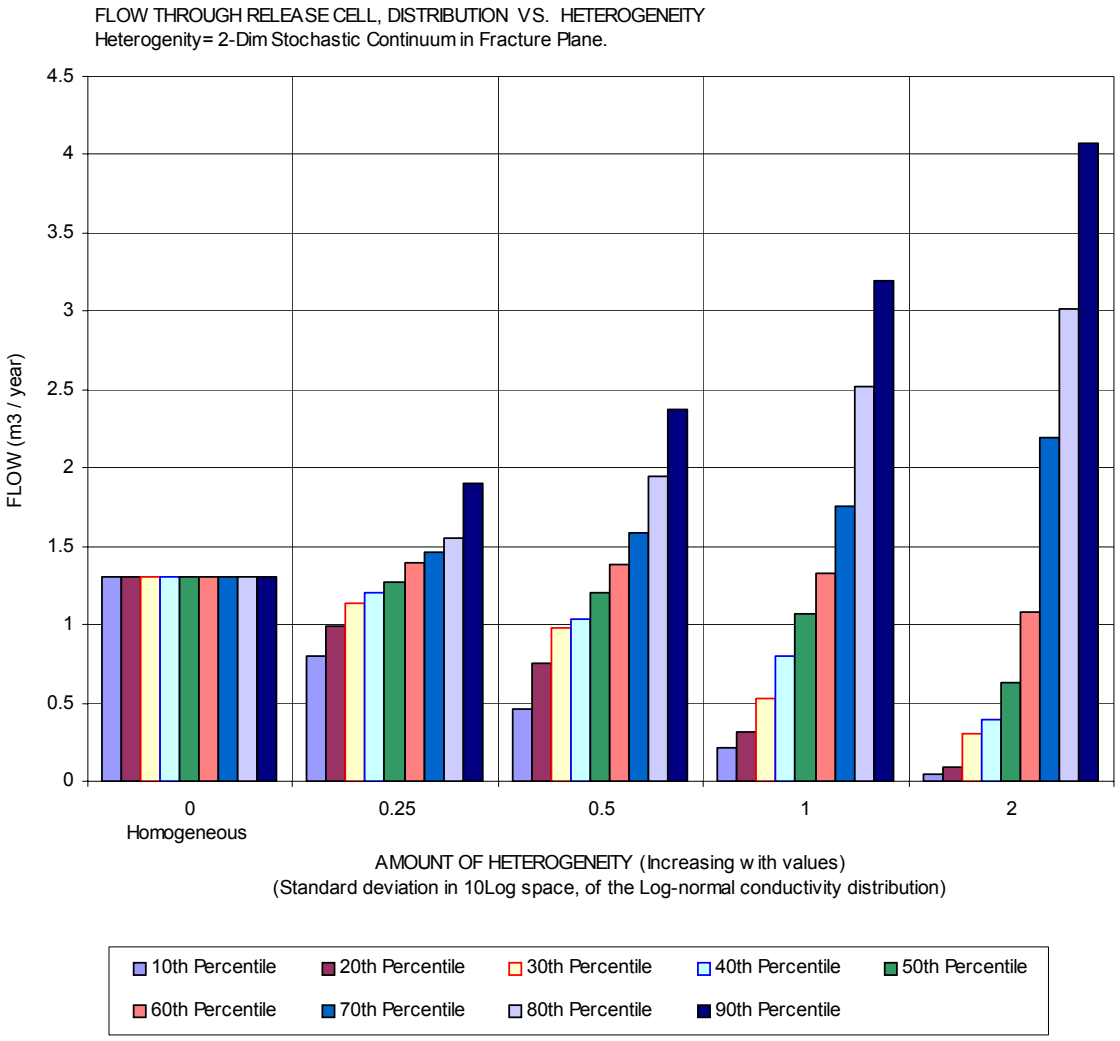

Figure 2-10 *Distribution of flow through the release cell (at the injection point), for different values of heterogeneity, considering all realisations.*

2.11 Flow at injection point for selected realisations

At present there is no detailed knowledge of the actual heterogeneity of Feature A. Consequently, we have simulated the flow in Feature A for flow domains with different amounts of heterogeneity (see previous sections). In the following calculations we have however assumed that a heterogeneity equal to 1.0 (in 10Log space) is a good representation of the actual heterogeneity of Feature A (see Section 2.5).

We have simulated and analysed a large number of realisations of a flow domain with heterogeneity equal to 1.0 (in 10Log space). A certain number of these realisations demonstrated a flow through the release cell that was close to the estimated true release flow, 0.5 m^3/year (9.7 x 10^{-4} Litre/min); these realisations were identified and selected from the ensemble of *all realisations* and formed an ensemble of *selected realisations*. Figure 2-11 given below, demonstrates the selection of realisations. The selected realisations demonstrate a variation in release flow between 0.4 m^3/year through 0.6 m^3/year.

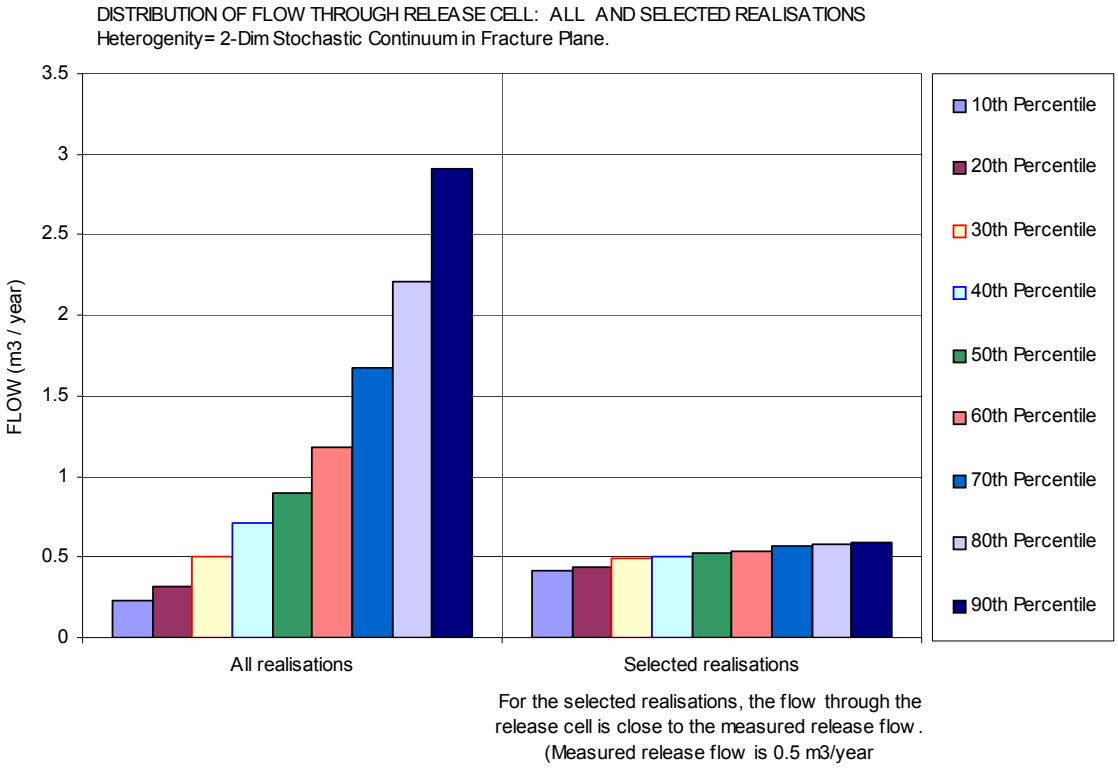

Figure 2-11 *Selection of realisation based on the flow through the release cell (injection point). Heterogeneity of flow domain is 1.0 in 10Log space*

2.12 Flow wetted surface area of the selected realisations

By analysing the distribution of flow paths from the injection point–the plume–it is possible to estimate the flow wetted surface area (the wet area). In this study the flow wetted surface is defined as two times the areal extent of the plume.

The realisations that take place in the ensemble of selected realisations were selected based on a certain flow criterion. Therefore, the distribution of the flow wetted surface area for the ensemble of selected realisations is not identical to the distribution of the flow wetted surface area of all realisations (considering a flow domain with heterogeneity equal to 1.0 in 10Log space). The ensemble of selected realisations demonstrates a distribution of the flow wetted surface area that has a smaller variance than the distribution produced by all realisations. A comparison of the two distributions is given below in Figure 2-12. The distribution of the flow wetted surface area for the ensemble of selected realisations is also given in Table 2-1, below.

A scatter plot is given below in Figure 2-13; the figure presents the correlation between the flow at the release cell and the flow wetted surface area of the plume, for all realisations as well as for the selected realisations. The figure demonstrates that when all realisations are considered, there is a positive correlation between the flow at the release point and flow wetted surface area. The selected realisations demonstrate a large variation in flow wetted surface area when comparing to the variation in release flow.

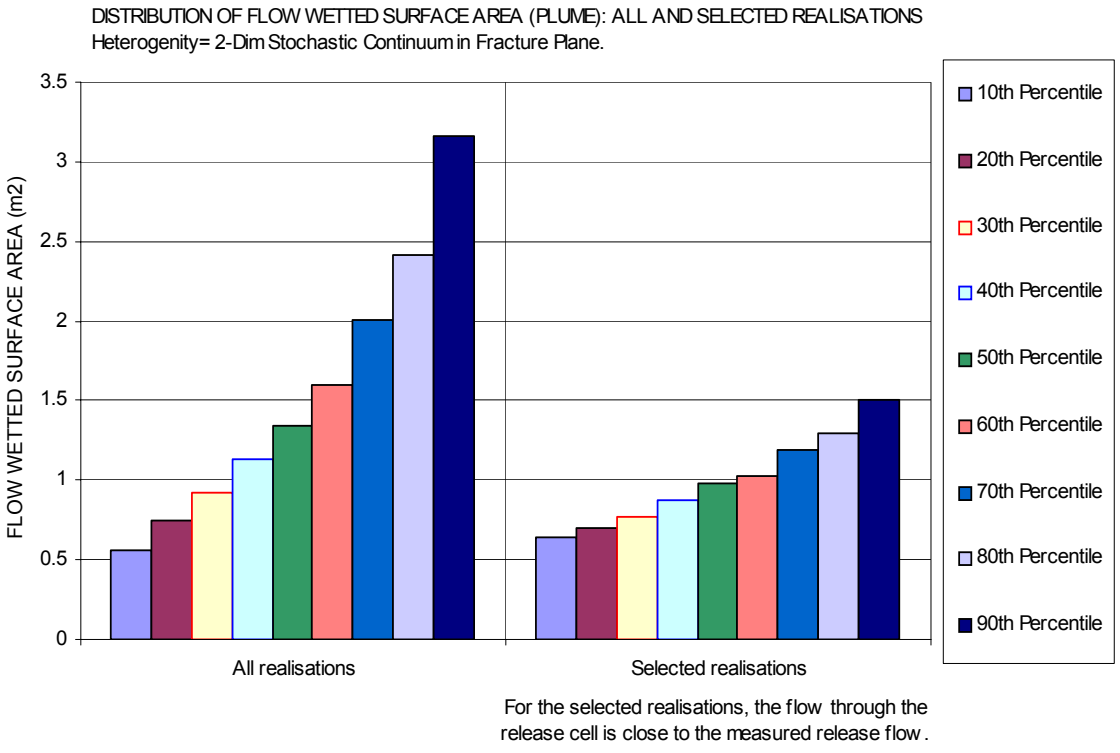

Figure 2-12 *Comparison of the flow wetted surface area (plume area) of the selected realisations and that of all realisations. Heterogeneity of flow domain is 1.0 in 10Log space.*

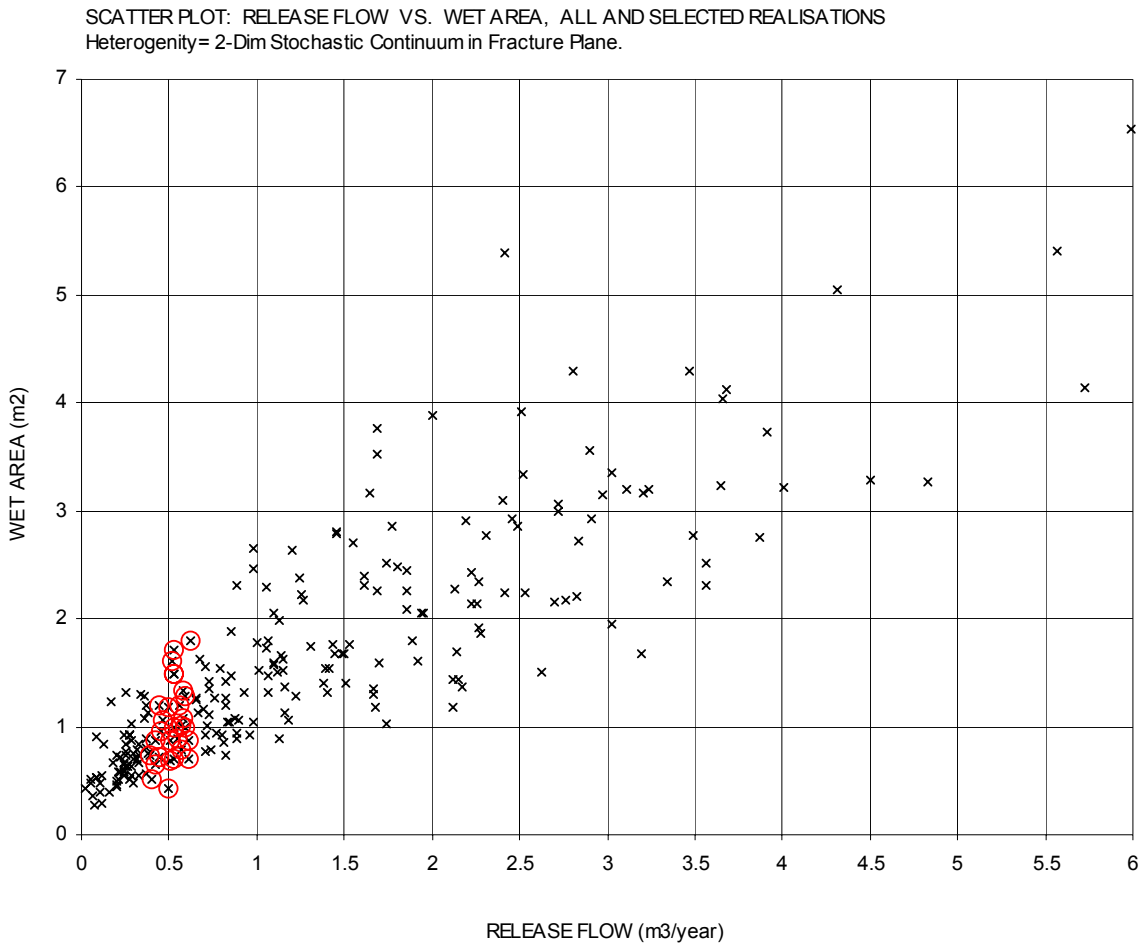

Figure 2-13 *Scatter plot demonstrating the correlation between flow at release cell (injection point) and flow wetted surface area of the plume. For all realisations and for selected realisations. Encircled markers represent examples of selected realisations. The heterogeneity of the flow domain is 1.0 in 10Log space.*

Table 2-1 Percentiles of the flow wetted surface (of the plume), considering the ensemble of selected realisations.

Percentiles	Flow wetted surface area (m2)
10 percentile	0.65
20 percentile	0.70
30 percentile	0.77
40 percentile	0.87
50 percentile	0.98
60 percentile	1.03
70 percentile	1.18
80 percentile	1.30
90 percentile	1.51

2.13 Distribution of flow wetted surface area along the plume, for the selected realisations

As demonstrated in Section 2.9, the plume has not a uniform shape; the shape of the plume is converging to wards the well. As in Section 2.9 (Figure 2-9) we have analysed the shape of the plume by use of six sections of equal length; the first section is closest to the injection point; the last section is closest to the well. We have done the analysis for all realisations and for the ensemble of selected realisations (heterogeneity of flow domain equal to 1.0 in 10Log space).

The results are given in Figure 2-14. It is demonstrated by the figure that on the average the plume gets smaller as it gets closer to the well, for all realisations and for the ensemble of selected realisations.

Considering the ensemble of selected realisations, the distribution of flow wetted surface along the length of the plume is given below in Table 2-2; the distribution is given in percent of the total area of the flow wetted surface of the 50^{th} percentile ($0.98\ m^2$, see Table 2-1).

Table 2-2 Distribution of flow wetted surface of the plume studied, along the length of the plume, considering the ensemble of selected realisations. The distribution is given in percent of the total size of the flow wetted surface (plume) of the 50^{th} percentile.

Length of section	Distance from pump well (m)	Amount of flow wetted surface (%)
1m	4.6	41.0
0.8m	3.8	21.5
1m	2.9	16.5
0.8m	2.1	8.6
0.8m	1.2	8.0
0.6m	0.4	4.4
Total = 5m	-	*Total = 100*

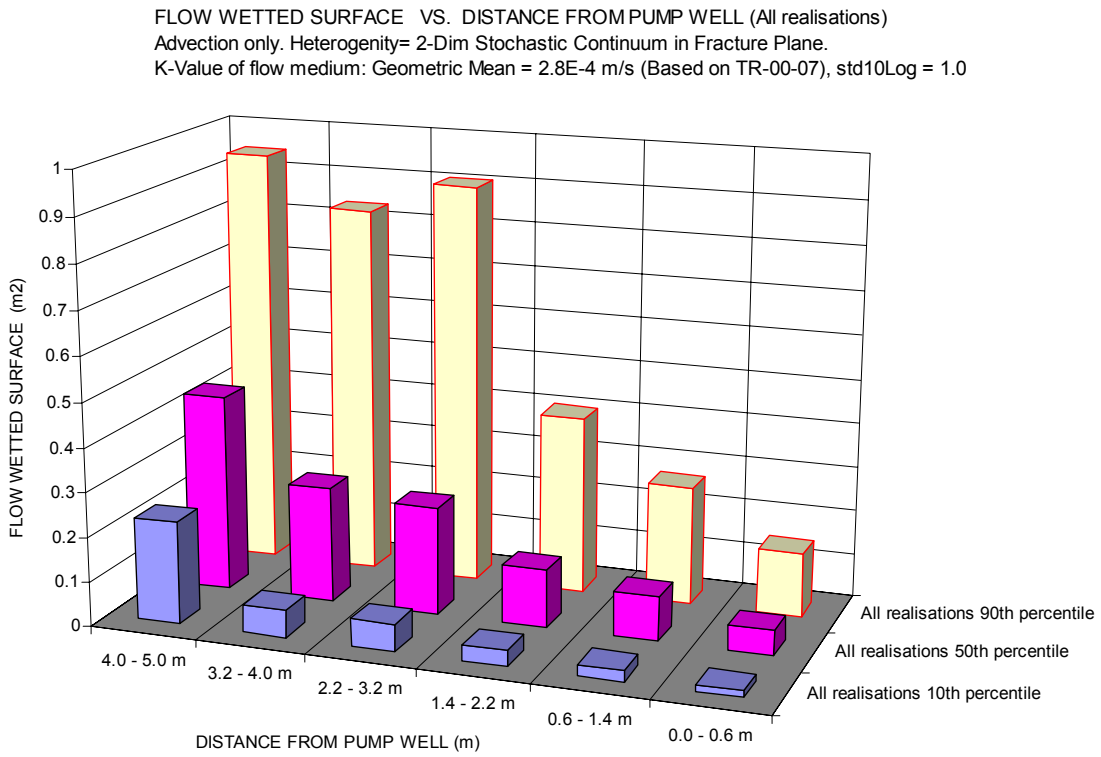

FIGURE (I)

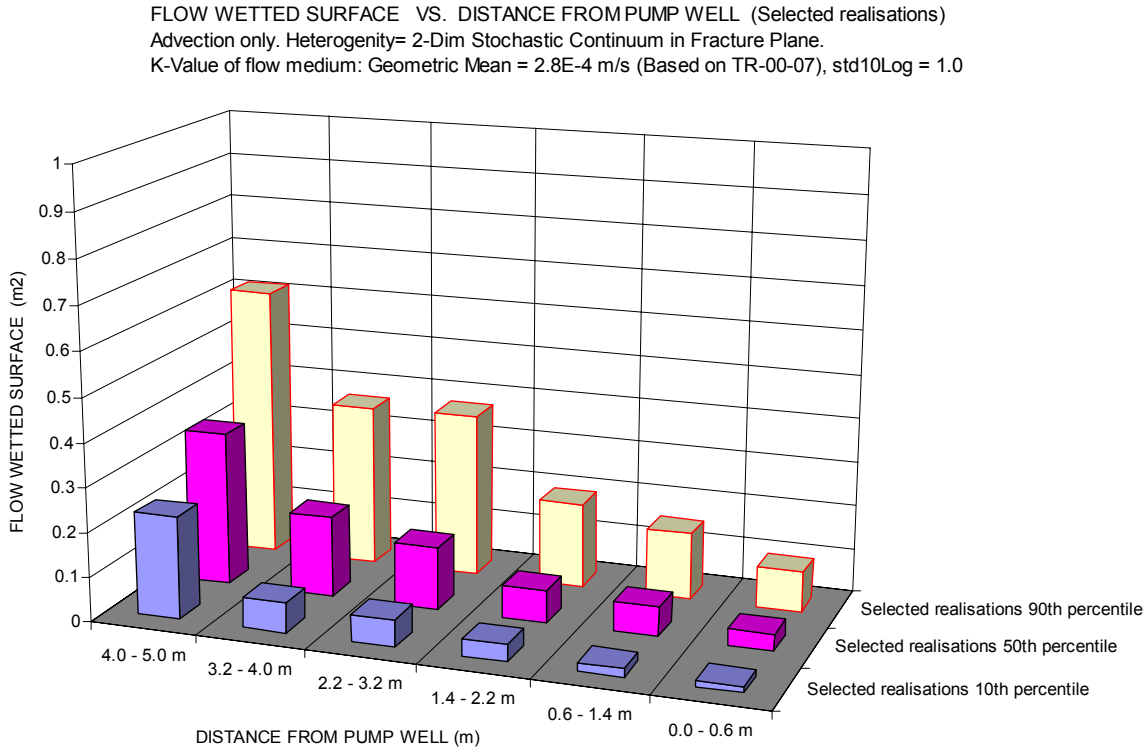

FIGURE (II)

Figure 2-14 *Size of the flow wetted surface, along six sections between the injection point and the well (along the length of the plume), for different percentiles of flow wetted surface. Figure (I) gives the distribution for all realisations and Figure (II) gives the distribution for the selected realisations. Heterogeneity of flow domain is 1.0 in 10Log space.*

2.14 Data transferred to the transport model

Based on the stochastic continuum modelling of the test studied, the shape of the simulated plume of the selected realisations (from injection point to extraction well) was transferred to the transport model. The transferred data, describing the plume, were as follows.

Size of flow wetted surface area

In the transport model, the variation of the total size of the flow wetted surface area of the plume was defined according to the distribution given in Table 2-1.

Distribution of flow wetted surface area along plume

In the transport model, the distribution of the size of the flow wetted surface area along the plume was defined according to the values given in Table 2-2.

Length of plume

The total length of the plume were set to 5.5m, see Figure 2-7.

Flow at the injection point and inside of the plume

The actual flow, in Feature A, at the injection point during the simulated test, was estimated to be approximately 9.7×10^{-4} Litre/min (0.509 m^3/year). This flow was used in the transport model as the flow inside of the plume. One should note that this flow is not equal to the pumping rate at the extraction well of the test studied.

3 TASK 6A – Transport model - Methodology

3.1 Purpose

The purpose of Task 6A is to model and reproduce selected trace tests, and thereby assess the constraining power of these tracer tests. This chapter discusses the methodology of the transport modelling and that of the analyses for constraining power.

3.2 The tracer test and the measured breakthrough curves

The tracer test was conducted by a simultaneous injection of several radioactive tracers with different characteristics. The monitored tracers consisted of HTO, Strontium, Iodine and Cobalt. The HTO tracer is considered to be a conservative tracer, i.e. it does not adsorb onto the rock surface. Strontium, Iodine and Cobalt are non-conservative tracers (reactive), of which strontium has the weakest reactive characteristics. This study concerns an evaluation of the transport of HTO and Strontium. The measured breakthrough curves of these two tracers are shown below in Figure 3-1.

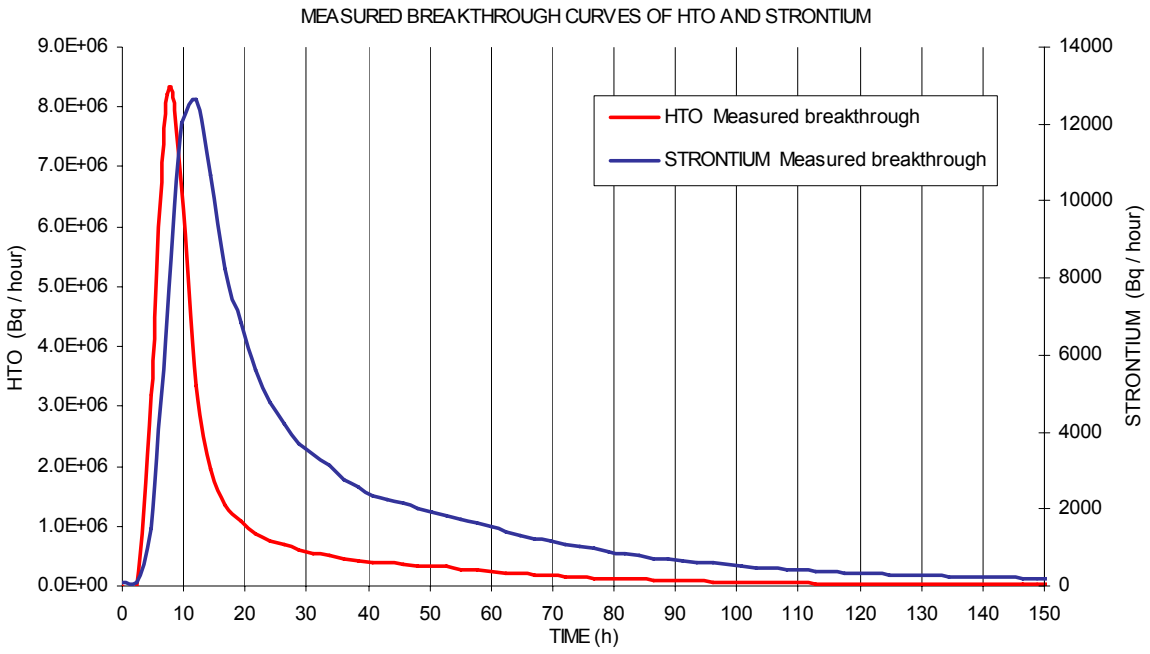

Figure 3-1 *Measured breakthrough curves of the two tracers studied.*

Although Strontium is considered to be a weakly reactive tracer, there are obvious differences between the two breakthrough curves. The breakthrough curve of Strontium has a somewhat slower increase of concentration in the leading edge of the curve, and a substantially larger tail. These effects are primarily considered to be a result of sorption processes.

Considering the HTO tracer the following properties can be observed:

Peak time = 7 hours
5% recovered mass at 5.2 hours
50% recovered mass at 11.1 hours
95% recovered mass at 77.0 hours

Considering the Strontium tracer the following properties can be observed:

Peak time = 12 hour
5% recovered mass at 7.9 hours
50% recovered mass at 24.4 hours
95% recovered mass at 165.6 hours

3.3 Computer code used

Modelling of the solute transport processes was conducted by using the GoldSim computer program. The transport model was constructed by utilising the standard elements of the GoldSim Radionuclide Transport Module.

3.4 Modelling approach – General methodology

The transport modelling for Task 6A is based on the GoldSim Transport Module. The modelling was carried out as a probabilistic sensitivity analysis. Hence, the uncertainties in the parameters of the system studied were included in the analysis as the transport parameters were defined as probability distributions (statistical distributions); within which the parameters may vary. A large number of different realisations of the parameters was created, i.e. 300 000 different realisations of a transport model with different properties. For each realisation (transport model), the measured concentration distribution at the point of injection was used as an upper boundary condition (at the injection well). In this way the transport models reproduce the injection of tracers. The resulting simulated breakthrough curves of tracers at the lower boundary (at the extraction well) are compared to the measured breakthrough curves. The realisations that produced the best fit to the measured breakthrough curves were identified (accepted) and moved to a new ensemble of realisations–the accepted realisations. The methodology and criteria for acceptance of a realisation is discussed in Section 3.7.

Consider the realisations with the best match to the measured breakthrough curves–the accepted realisations–the variation of the parameter values among these realisations indicates to what extent the simulated tracer test constrains the parameters studied. If a parameter has a small variation within the ensemble of accepted realisations, this indicates that the parameter is well estimated by the tracer test (large constraining power); and the opposite takes place if the observed variation is large (small constraining power). If the distribution of a parameter of the accepted realisations is identical to, or very close to, the given distribution of all realisations, the evaluated tracer test has no constraining power with regard to the parameter studied. In this way the probabilistic sensitivity analysis will assess the constraining power of the tracer test studied.

Thus, the *given parameter distributions* reflects the assumed likely ranges of parameter values. These specified distributions are given as input to the transport model. The distributions of parameter values that take place within the ensemble of accepted realisations are the results of the sensitivity analysis, and these distributions are called the *constrained distributions*. And as stated above, the differences between: (i) the given parameter distributions and, (ii) the constrained distributions, demonstrate the constraining power of the tracer test; as simulated by the applied modelling approach. A large difference between a given and a constrained distributions demonstrates a large constraining power and a small difference demonstrates a small constraining power. The tracer tests were analysed separately and combined:

- First analysis. The HTO tracer test was analysed separately. For acceptance of a realisation only the HTO breakthrough curve was considered.
- Second analysis. The Strontium test was analysed separately. For acceptance of a realisation only the Strontium breakthrough curve was considered.
- Third analysis. The HTO test and the Strontium tests were analysed together. For acceptance of a realisation both the HTO and the Strontium breakthrough curves were considered. An accepted realisation had to produce acceptable results for both tracers.

It is important to note that the calculated constraining power of a parameter needs to be evaluated together with the given properties of the probability distribution of the parameter studied (the input data), and the given parameter distribution needs to be defined with reasonable values.

3.5 Represented transport processes

The transport processes that are represented by the GoldSim Transport Module are: (i) advection, (ii) dispersion, (iii) retardation, (iv) decay and ingrowth [not used in this study], and (v) exchanges with immobile storage zones (e.g. matrix diffusion). The retardation processes are represented by equilibrium partitioning between: (i) the fluid in the pathway and a user defined infill medium, and (ii) the fluid in the pathway and a user specified coating medium as well as a skin zone (around the perimeter of the pathway/fracture), and (iii) the diffusing fluid and the rock matrix. The hydraulic interchanges with immobile storage zones along the main transport pathway are governed by (i) matrix diffusion into immobile zones in which the transfer rate into and out of the zone is proportional to the concentration gradient and the diffusive properties of the zone, and (ii) a "stagnant" dispersive zone, in which the interchange is proportional to the concentration difference and a transfer rate. As defined in the task specifications by Selroos and Elert (2001) and Elert and Selroos (2001), radioactive decay and ingrowth is not considered in the modelling.

The geometry and transport processes are illustrated in the cross-section of Figure 3-2.

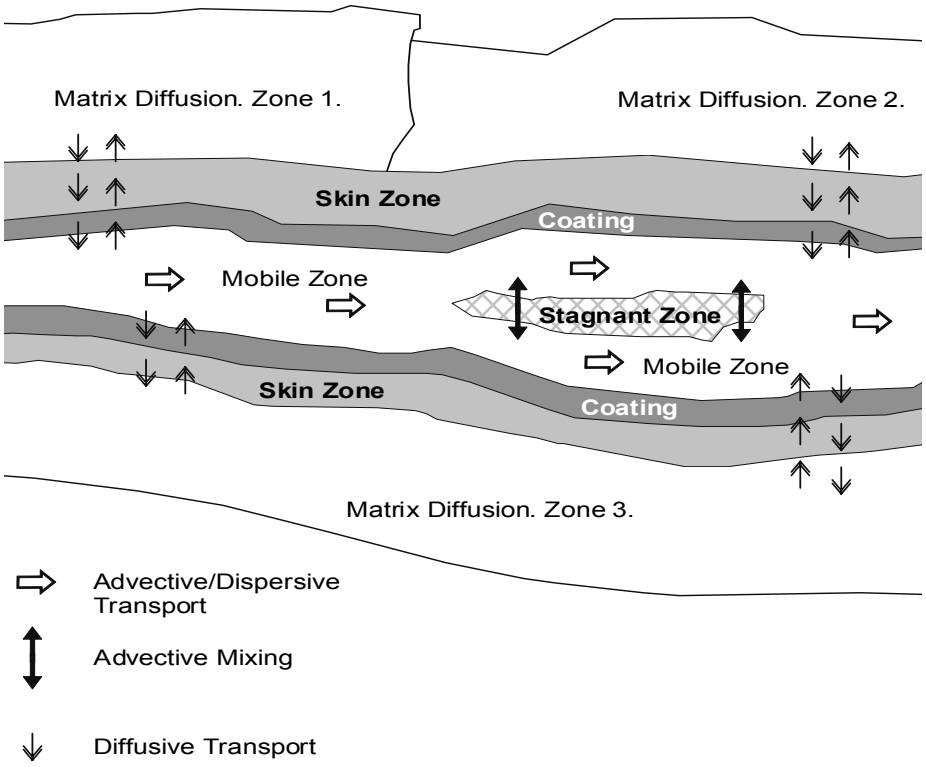

Figure 3-2 *A schematic cross-section along a pathway, showing examples of the features and processes that can be represented in the GoldSim Radioactive Transport Module.*

We have included the concept of stagnant zones in the transport model. In a GoldSim pipe the stagnant zones represents regions where low velocity or "stagnant" water takes place within the represented fracture plane. In a GoldSim pipe, the stagnant zones influence the mass transport in two ways: (i) By direct transfer of mass between zones of mobile water and the stagnant zone (the mass transfer is proportional to the difference in concentration between the mobile and stagnant zones as well as on a constant of proportionality called the transfer rate). (ii) By reducing the cross-sectional area available for the mobile water; hence a large fraction (amount) of stagnant zone will reduce the cross-sectional area available for mobile water and consequently increase the velocity of the mobile water (as the flow is constant).

3.6 Transport model – Geometry and Flow

The idealised geometry of the fracture zone is presented below in Figure 3-3 in terms of a vertical cross section along the transport path. The open fracture and the stagnant zones contain a highly porous infill material with a stochastic porosity in the range 0.1–1, i.e. for some cases these zones are merely filled with streaming water. The fracture wall is covered with a coating (Fault Gouge) along the entire wetted perimeter. Behind the coating, there are two immobile zones in parallel; Altered Diorite and Mylonite.

The solute transport model consists of six "GoldSim pipes" in series, representing six sections along the plume from the injection point to the well. The pipes represent the part of the fracture studied (Feature A) that is affected by the plume, between the injection point and the extraction well. The defined length and width of the pipes were based on the results of the stochastic continuum modelling of the flow field and of the plume (see previous chapters). The largest width is close to the injection point and the smallest width is close to the extraction well (pump well).

A horizontal view of the geometry of the GoldSim pipes is given below in Figure 3-4. The length (L) of each section was set to 0.92m. The widths of the sections (W) were given by:

(i) The total size of the flow wetted surface area of the plume. This value was varied between different realisations of the GoldSim model (see Table 2-1)

(ii) The average shape of the plume. Each of the six pipes of the GoldSim model was defined as having an area given by a percentage (or fraction) of the total flow wetted surface area of the plume. These percentages were the same for all GoldSim realisations (see Table 2-2)

The groundwater flow through the pipes was set equal to the estimated injection flow of the test studied, which is 9.7 x 10^{-4} Litre/min. Note that this flow is not equal to the pumping rate at the extraction well of the test studied. The GoldSim model only represents the plume from the injection point to the extraction well; it does not represent the complete flow domain.

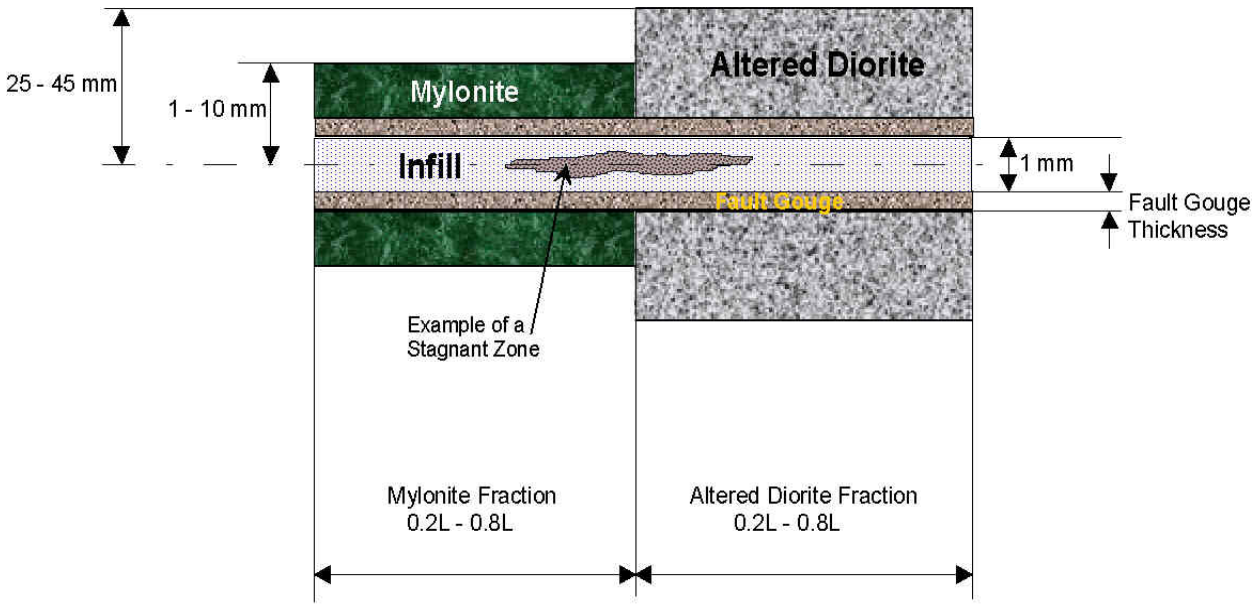

Figure 3-3 *Vertical cross section of an idealised geometry along a GoldSim pipe element. The total length is L. The element thicknesses are not to scale.*

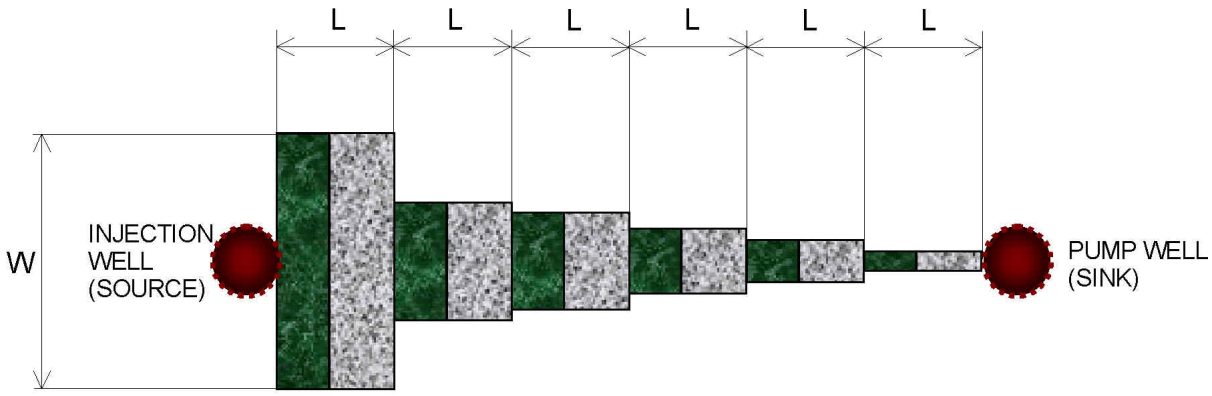

Figure 3-4 *Horisontal view of idealised geometry along the six GoldSim pipe elements. The total length of each element is L=0.92 m and the width of the elements, W, varies according to the results of the modelling of the flow field. The figure gives an approximate illustration of the average geometry of the pipes. The element widths are shown to scale, but the ratio L / W is not to scale. The largest width is close to the injection point and the smallest width is close to the extraction well (pump well).*

3.7 Stochastic approach and criteria for acceptance of a realisation

Based on the given parameter distributions, see Sections 4.1 and 5.1, a large number of different realisations of the transport properties were created. For each realisation, injection of tracers is simulated in the same way as for the tracer tests studied. The resulting simulated breakthrough curves of the tracers were compared to the measured breakthroughs.

The process of finding the realisations with the best fit to measured breakthrough was based on comparison between the measured breakthrough curves and the simulated breakthrough curves. Only realisations that produced breakthrough curves close to the measured breakthrough curves were accepted and moved to the ensemble of accepted realisations.

- Accepted realisations must demonstrate breakthrough curves with a deviation from the measured breakthrough curves that is less than a given maximum acceptable deviation. Two different maximum deviations have been used: (i) plus/minus 25% of the measured values for the separate tests of HTO and Strontium, and (i) plus/minus 50% of the measured values for the combined test of HTO and Strontium.
- The test for maximum deviation is applied in the time interval between 4.8 hours and 70 hours. Hence, the test is applied during a period that covers the peaks of the breakthrough curves as well as a part of the tails of the curves.

The boundaries of the test for maximum deviation forms a "channel". A simulated breakthrough curve must follow this channel (be constrained within) to be accepted. If a simulated breakthrough curve, at any point along the channel, is larger than or smaller than the boundaries of the channel, the simulation (realisation) is rejected.

Two figures below (Figure 3-5 and Figure 3-6) present examples of boundaries used in the tests for maximum deviation. In addition, the figures present the envelope of the 300 000 simulated breakthrough curves, as well as the 99th and 50th percentile of the simulated breakthrough curves. The ensembles of realisations were established with use of the given parameter distributions, see Sections 4.1 and 5.1. Note that the simulated breakthrough curves in Figure 3-5 and Figure 3-6 corresponds to an ensemble of realisations that has **not** been tested for maximum deviation from measured breakthrough. The purpose of the maximum deviation test is to select a number of acceptable realisations from all the simulated breakthrough curves.

As can be seen in the figures, the realisations not tested demonstrate a large variation in simulated breakthrough curves, the lower envelope of the simulated breakthrough curves is very close to zero and the upper envelope is much higher than that of the measured breakthrough. The median (50th percentile) breakthrough curve is very low and has a much later arrival time of the peak, than the measured breakthrough. This indicates that only a small fraction of the simulated breakthrough curves will match the measured breakthroughs. The given parameter distributions (see Sections 4.1 and 5.1), are based on data that is considered as reasonable, however these distributions will, with a very large probability, produce breakthrough curves that are far from the measured breakthroughs.

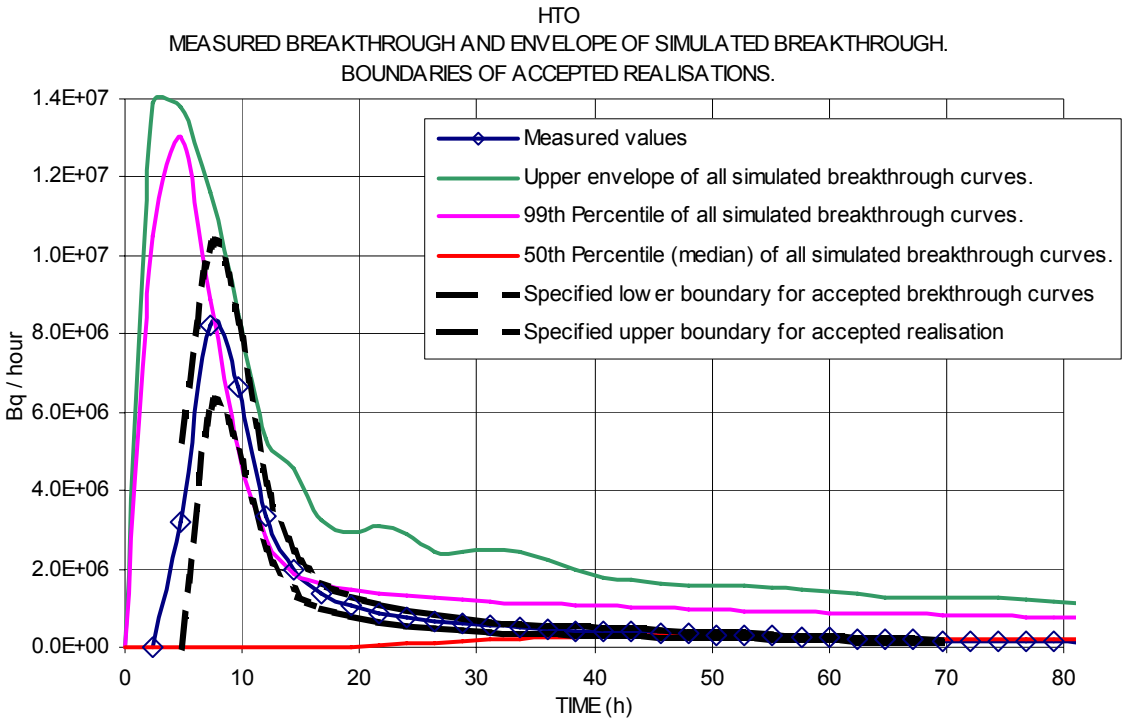

Figure 3-5 *HTO deviation test. The boundaries correspond to a maximum deviation of plus/minus 25% of measured values. The figure also presents the envelope as well as the 99th and the 50th percentile of the breakthrough curves of 100 000 realisations.*

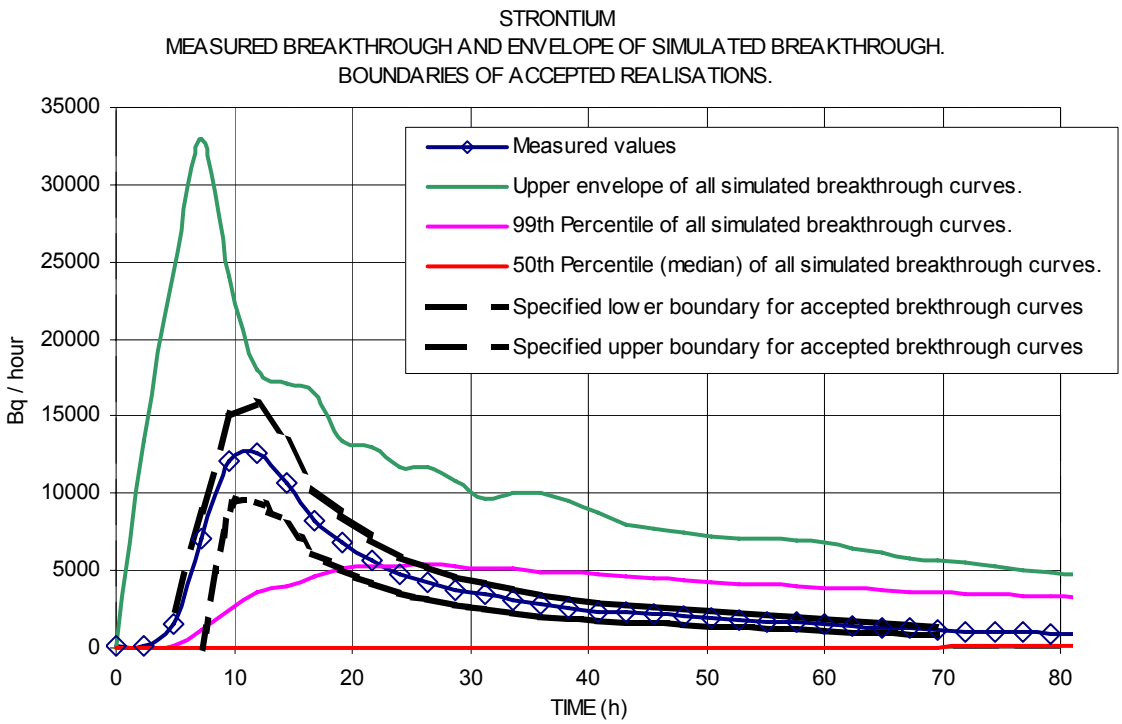

Figure 3-6 *Strontium deviation test. The boundaries corresponds to a maximum deviation of plus/minus 25% of measured values. The figure also presents the envelope as well as the 99th and the 50thpercentiles of the breakthrough curves of 100 000 realisations.*

4 TASK 6A – Simulation and analyses of a conservative tracer (HTO) test

4.1 Given parameter distributions for HTO test

The given parameter distributions for the HTO test are given below. Based on these distributions a large number of different realisations of the transport properties were established. For the HTO test, the Kd-values are set to zero, as the HTO tracer is a non-reactive tracer. The number of independent parameters is 13. The distributions are based on data given in Task 6A and 6B specifications, by Selroos and Elert (2001) and Elert and Selroos (2001).

Table 4-1 Conservative tracer. Material properties (stochastic)

	Min value	Max value	Distribution	Unit
Altered Diorite Poros	1e-3	4e-3	Uniform	-
Altered Diorite Kd	0	0	Discrete	m3/kg
Mylonite Poros	5e-4	5e-3	Uniform	-
Mylonite Kd	0	0	Discrete	m3/kg
Fault Gouge Poros	0.1	0.2	Uniform	-
Fault Gouge Kd	0	0	Discrete	m3/kg
Infill Poros	0.1	1	Uniform	-
Infill Kd	0	0	Discrete	m3/kg

Table 4-2 Conservative tracer. Transport geometry properties (stochastic)

	Range	Distribution	Unit
Altered Diorite Fraction	0.2-0.8	Uniform	-
Altered Diorite Max Thickness	25 – 45	Uniform	mm
Mylonite Fraction	0.2-0.8	Uniform	-
Mylonite Max Thickness	1 – 10	Uniform	mm
Fault Gouge Fraction	1	Discrete	-
Fault Gouge Max Thickness	0 – 0.5	Uniform	mm
Dispersivity	0.01 – 1	Uniform	M
Stagnant Zone Fraction	0 – 1	Uniform	-
SZ Rate	0 – 1	Uniform	1/m
Flow wetted surface	0.44 - 1.7	Special	m^2

In GoldSim, the effective diffusivity (D_e) is defined as

$$D_e = D_0 * p * \tau \qquad \text{Equ. 4-1}$$

In which D_0 is the free water diffusivity for each tracer, p is the matrix porosity and τ is a back-calculated theoretical tortuosity. The effective diffusivity calculated in accordance with Equ. 10-1 is presented in Table 10-3, below.

Table 4-3 Conservative tracer. Material properties (stochastic). Effective diffusivity

	Effective diffusivity		D_0	$p_{, min}$	$p_{, max}$	τ
	Minimum	*Maximum*				
Altered Diorite	3.12E-14	1.25E-13	2.40E-09	1.00E-03	4.00E-03	0.013
Mylonite	1.56E-14	1.56E-13	2.40E-09	5.00E-04	5.00E-03	0.013
Fault Gouge	3.12E-12	6.24E-12	2.40E-09	0.1	0.2	0.013

4.2 Criteria for acceptance of a realisation

Only the realisations that produced a breakthrough curve close to the measured breakthrough were accepted for further analyses. The accepted realisations must demonstrate a deviation from the measured breakthrough that is less than plus/minus 25% of the measured activities; the test is applied in the time interval between 4.8 hours and 70 hours (see Figure 3-5). We have simulated and analysed 300 000 realisations, of which 1172 realisations passed the test defined by the specified boundaries.

4.3 Envelope of accepted realisations

The envelopes of the breakthrough curves of the accepted realisations are given below in Figure 4-1. The green curve is the upper envelope of all accepted realisations; it is not given by a single realisation, but by all accepted realisations; the purple curve is the lower envelope of all accepted realisations.

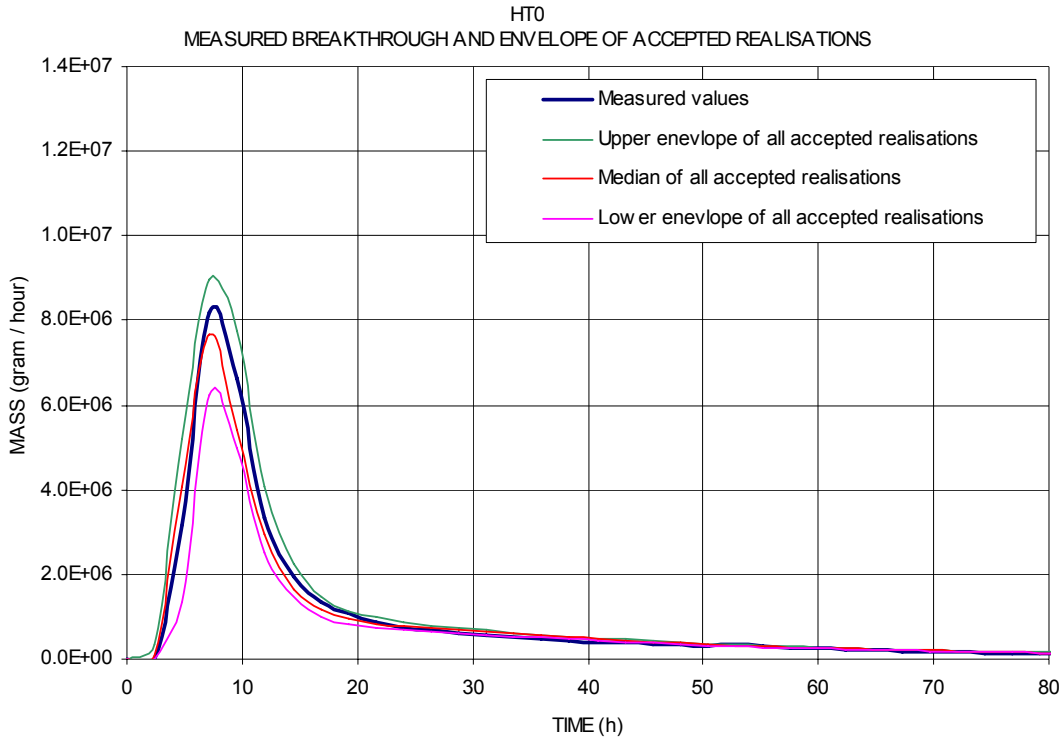

Figure 4-1 *HTO. Measured breakthrough and envelope of the accepted realisations.*

4.4 The best realisations

The three best realisations were found by sorting all accepted realisations, considering deviation from the measured breakthrough. Different sorting criteria have been tested. The best results were obtained when the modelled breakthrough curves were sorted for squared minimum difference. The test were applied for all time steps for which the measured breakthrough is larger than zero. The breakthrough curves for the three best realisations are given below in Figure 4-2.

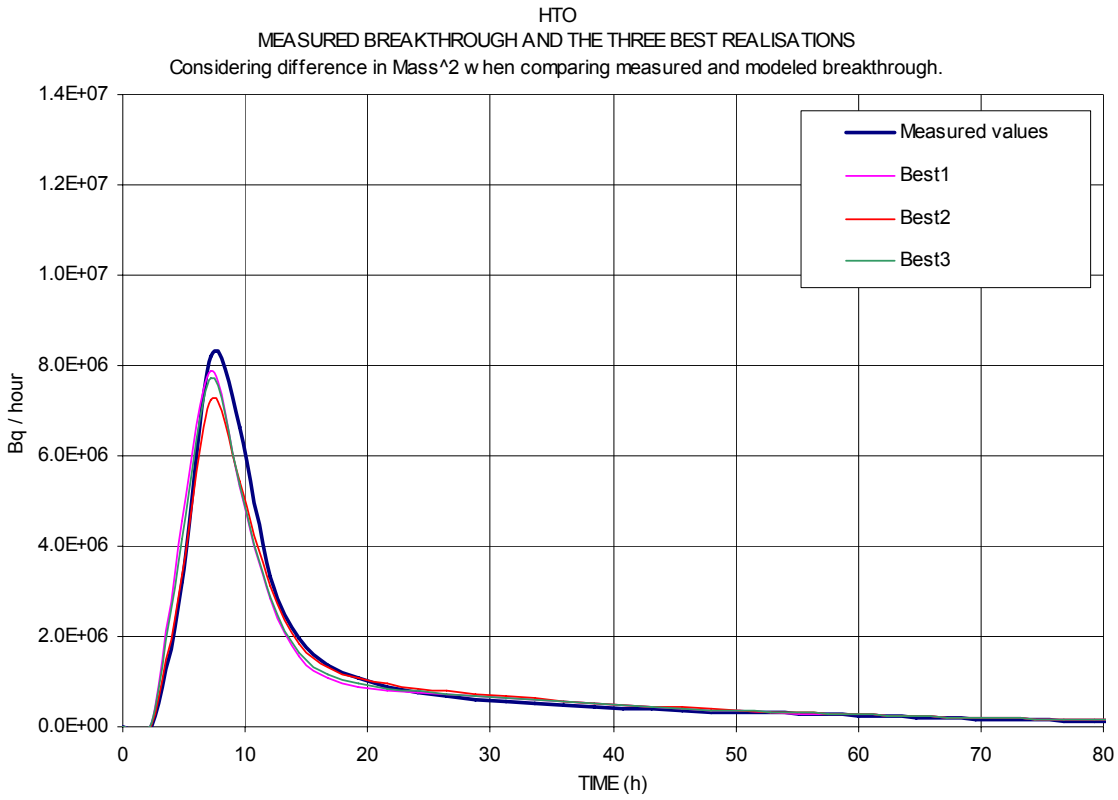

Figure 4-2 *HTO. Measured breakthrough and the modelled breakthrough for the three best realisations.*

4.5 Assessment of the constraining power of the HTO tracer test (conservative tracer)

In the figures below (Figure 4-3 through Figure 4-9) we present the given parameter distributions and the constrained distributions, as produced by the simulated HTO tracer test. The constraining power, or the lack of it, is summarised in Table 4-4, below.

4.5.1 Basic parameters

We conclude:

A general conclusion, based on the assessment of the constraining power of the HTO tracer test, is that a conservative tracer will not produce a large constraining power.

Diorite and the Mylonite rock is located behind the Fault Gouge, and not in direct contact with the flowing water. No constraining power is demonstrated considering the properties of these two rock types (fraction, thickness and porosity). It is likely that this result is given by the relatively short time-scale of the experiments. The mass exchange with the inner zones is insignificant during such short time.

Fault Gouge is located on the surface of the fracture planes and in direct contact with the flowing water. A very weak constraining power, was demonstrated as regards the porosity of this material. Some more constraining power was demonstrated as regards the thickness of this material. For both the Fault Gouge porosity and the Fault Gouge thickness, the ranges of the constrained distributions were the same as in the given distributions, but the constrained distributions demonstrated different probability density functions. Hence, some weak constraining power was demonstrated for this material.

Filling material (the Infill) is specified inside the open space of the fracture studied. This material is in direct contact with the flowing water. A large constraining power was demonstrated for the porosity of the Infill. In 90 percent of the accepted realisations, the Infill porosity was larger than 0.85. In addition, 10 percent of the accepted realisations demonstrated a porosity between 0.25 and 0.85 , and no realisations had a Infill porosity smaller than 0.25.

Zones of stagnant water are specified inside the fracture. The amount of such stagnant water (Fraction) and the Rate with which this water interacts with the flowing water is also analysed. Constraining power was demonstrated both as regards the Fraction and the Rate. For both Fraction and Rate, the ranges of the constrained distributions were the same as in the given distributions, but the constrained distributions demonstrated a different probability density function. Hence, some constraining power were demonstrated for these properties, especially for the Fraction, 90% of the accepted realisations demonstrated a Fraction less than 0.55, while in the given distribution 90% had a Fraction less than 0.9.

Dispersivity of the flow domain was also analysed and the results demonstrated a weak constraining power for this parameter. No accepted realisation had a dispersivity larger than 0.86 mm, while the given distribution had an upper limit at 1.0 mm. The 80^{th} percentile of the constrained distribution is 0.59 mm and in the given distribution the 80^{th} percentile is 0.82 mm. The lower part of the distributions are very similar.

Flow wetted surface area (or the wet area) is the area on the fracture plane, along which the transport takes place. The area is calculated as the sum of the areas on the upper and the lower planes. A distribution of possible areas was derived from the modelling of the flow field, this distribution was transferred to the transport model and defined as the given distribution of the flow wetted surface. The transport model reduces the size of the area where the flow takes place, by introducing the stagnant zones. Hence, there are two different concept of flow wetted surface area: (i) Flow wetted surface area including the stagnant zones and (ii) Flow wetted surface area without the stagnant zones. We have studied both concepts. Considering the first concept (including stagnant zones in the flow wetted surface area), the transport modelling demonstrated no constraining power; the constrained distribution produced is very close to the given distribution. However, for the second concept (excluding the stagnant zones from the flow wetted surface area), the transport modelling demonstrates a constraining power for this parameter. The range of the constrained distribution is approximately the same as that of the given distribution, but the probability density function is different. Considering all realisations, the 10^{th} percentile and the median of the produced values of the flow wetted area were 0.085 m^2 and 0.44 m^2, respectively; but for the accepted realisations the 10^{th} percentile and the median of the produced values of the flow wetted area were 0.34 m^2 and 0.66 m^2, respectively. Hence, the flow wetted surface areas (without stagnant zones) of the accepted realisations are significantly larger than those of all realisations; the large values of flow wetted surface areas follows from the small amounts of stagnant zones among the accepted realisations.

4.5.2 Combined flow parameters

For a situation with a simplified flow geometry e.g. flow through channels of a known size, the parameters controlling matrix diffusion may be expressed as the product of a parameter characterising the flow, generally called the F-parameter, and a group of parameters including the distribution coefficients (Kd-values), diffusion coefficients and matrix porosity. The F-parameter may be expressed in several different ways; we have used the following formulation:

Equ. 4-2

$$F_1 = \frac{\frac{a_w}{\eta_e} L}{q}$$

F_1 = F-parameter [s/m]

a_w =Flow wetted surface area divided by the bulk-volume of the flow medium in which the flow take place [/m] The bulk volume is calculated based on the flow wetted surface area (half of it) and the hydraulic aperture.

η_e =Effective porosity (transport porosity), in this modelling equal to the Infill porosity [-]

L =Length of transport route, in this modelling equal to the total length of the GS-pipes[m]

q =Specific flow [m/s]. In this modelling equal to the flow at the point of injection, divided by a cross-section area. The cross-section area is calculated based on the flow wetted surface area (half of it), the hydraulic aperture and the total length of the GS-pipes.

Considering the HTO test, we have calculated (i) the distribution of the F-parameter for all realisations (given parameter distributions) and (ii) the distribution of the F-parameter for the selected realisations (constrained parameter distributions). We have used both concepts of flow wetted surface area, as discussed above in Sec.10.5.1. For both concepts, the transport modelling demonstrates significant constraining powers, when analysing for the F-parameter and the HTO tracer. The most consistent method is to calculate the F-parameter by use of the second concept–using a flow wetted surface area without the stagnant zones. The results of such calculations are given in Figure 4-10. Considering all realisations, the 90th percentile, the median and the 10th percentile of the produced values of the F-parameter were 179 800 s/m, 52 400 s/m and 9900 s/m, respectively; but for the accepted realisations the 90th percentile, the median and the 10th percentile of the of the produced values of the F-parameter were 79 800 s/m, 45 300 s/m and 23 700 s/m, respectively. Hence, the upper part of the constrained distribution is much smaller than that of the given distribution; the median of the constrained distribution is close to that of the given distribution; and finally the lower part of the constrained distribution is larger than that of the given distribution; in all the constrained distribution demonstrates a smaller variance.

The F-parameter as defined in Equ. 4-2, includes both the flow wetted surface area and the Infill porosity. Considering the HTO-tracer test, constraining power was demonstrated for both these parameters. Combined in Equ. 4-2 they also demonstrate a constraining power.

Another combined parameter, closely related to the F-parameter, or another way of defining the F-parameter, is the flow wetted surface area over flow, as given below.

Equ. 4-3

$$F_2 = \frac{A}{Q}$$

F_2 = *F-parameter [s/m]*

A = *Flow wetted surface area (m^2)*

Q = *Flow at point of injection (m^3/s)*

This formulation does not include the porosity of the Infill material, which is included in Equ. 4-2. We have calculated the probability distributions for this formulation of the F-parameter (Equ. 4-3), for all and for the selected realisations. As the flow (Q,) at the injection point is the same in all realisations, the constraining power will be the same as for the flow wetted surface area (A).

Table 4-4 Summary of the constraining power of the HTO tracer test (a conservative tracer).

CONSTRAINING POWER OF HTO TRACER TEST				
PARAMETER		CONSTRAINING POWER (1)	GIVEN DISTRIBUTION PERCENTILES 20^{th} , 50^{th} , 80^{th}	CONSTRAINED DISTRIBUTION PERCENTILES 20^{th} , 50^{th} , 80^{th}
ALTERED DIORITE	Fraction	No		
	Thickness	No		
	Porosity	No		
	Kd – value	-		
MYLONITE	Fraction	No		
	Thickness	No		
	Porosity	No		
	Kd – value	-		
FAULT GOUGE	Thickness *(mm)*	YES1	0.10 , 0.25 , 0.40	0.20 , 0.34 , 0.44
	Porosity *(-)*	YES1		
	Kd–value*)*	-		
INFILL (fillling material)	Porosity *(-)*	YES2	0.28 , 0.55 , 0.82	0.89 , 0.94 , 0.98
	Kd–value	-		
STAGNANT ZONE	Fraction *(-)*	YES1	0.20 , 0.50 , 0.80	0.09 , 0.26 , 0.46
	Rate *(1/m)*	YES1	0.20 , 0.50 , 0.80	0.32 , 0.63 , 0.86
DISPERSIVITY	*(m)*	YES1	0.28 , 0.55 , 0.82	0.26 , 0.43 , 0.59
FLOW WETTED SURFACE AREA	Excluding stagnant zones *(m2)*	YES1	0.17 , 0.44 , 0.77	0.43 , 0.66 , 0.97
F_1-PARAMETER	*(s/m)*	YES2	19 700 , 52 400 , 114 900	30 000 , 45 300 , 79 800

(1)

No = The constrained distribution is very similar to the given distribution. No constraining power is demonstrated.

YES1 = The range of the constrained distribution is similar to that of the given distribution, but the constrained distribution demonstrates a new probability density function. Hence, some constraining power is demonstrated.

YES2 = The range of the constrained distribution is different from the given distribution. The probability density function is also different. Real constraining power is demonstrated.

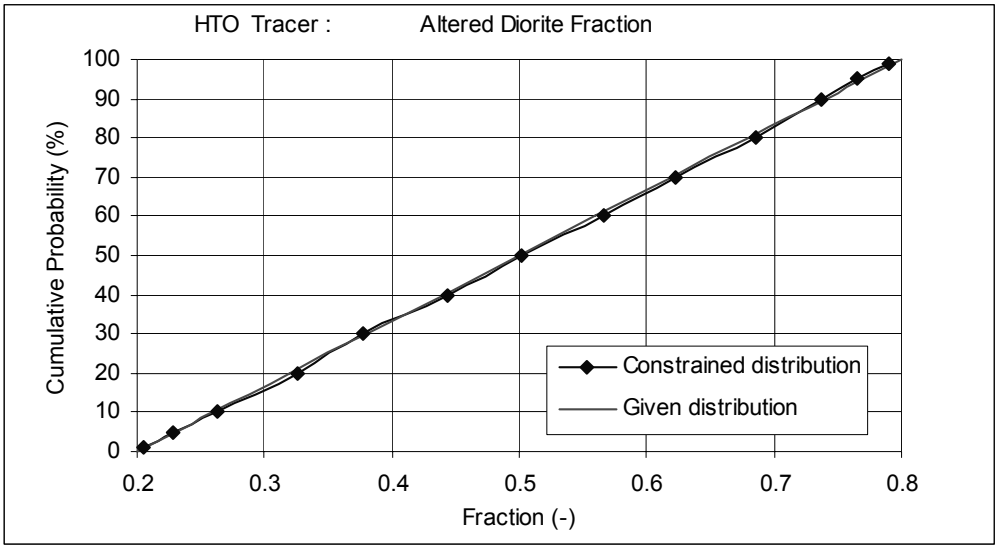

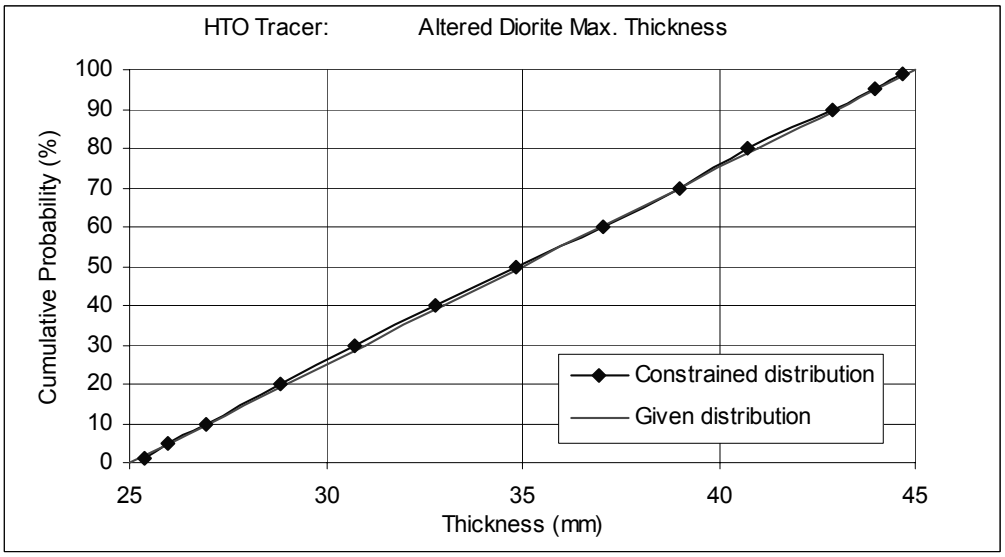

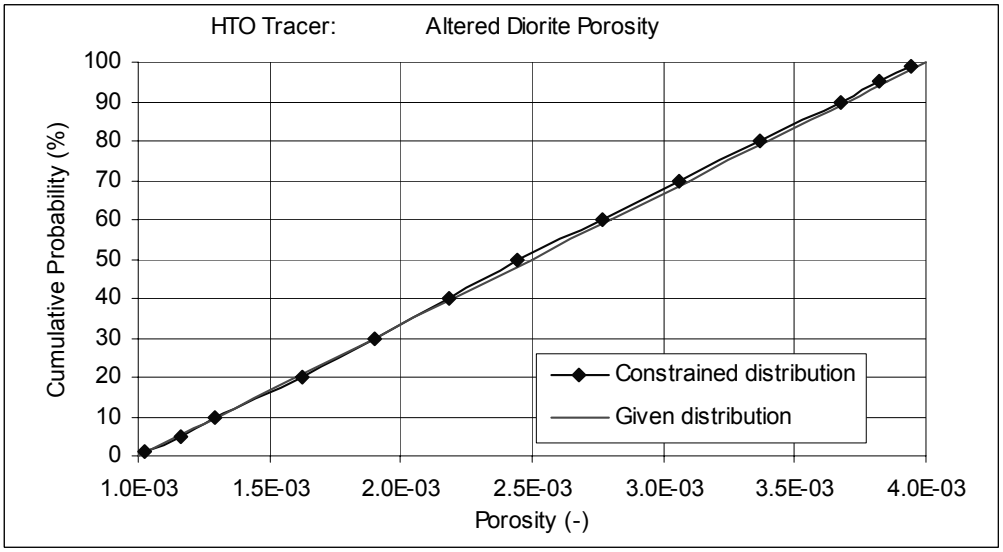

Figure 4-3 *Diorite Parameters*

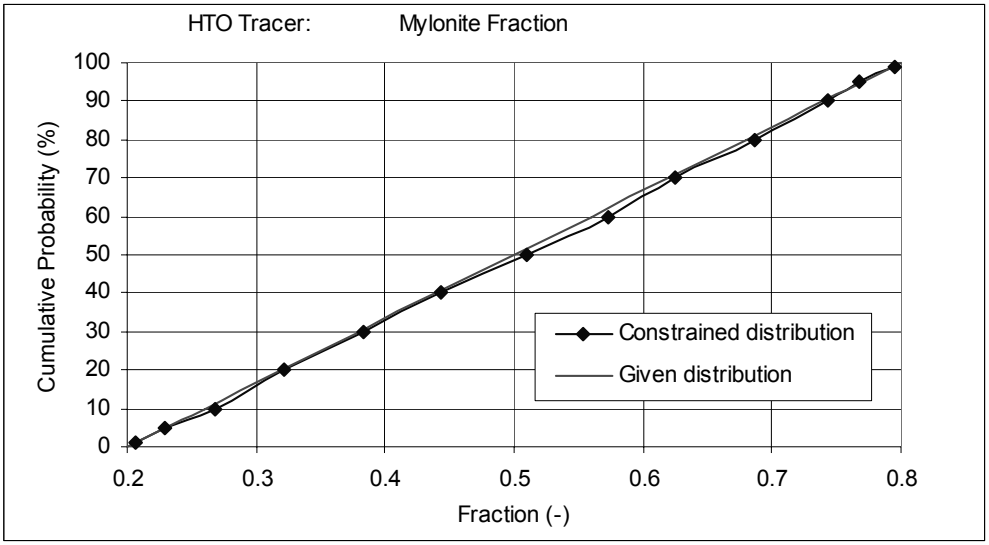

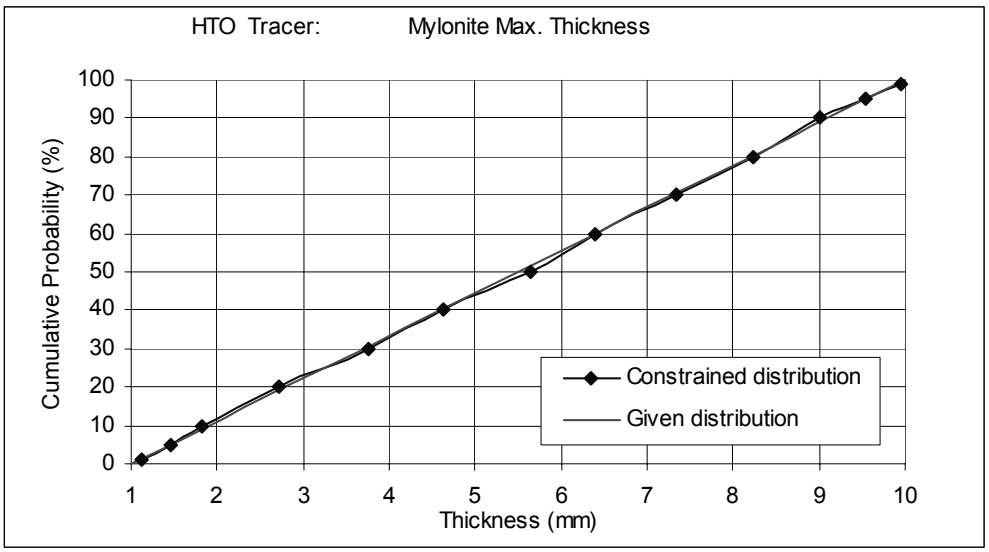

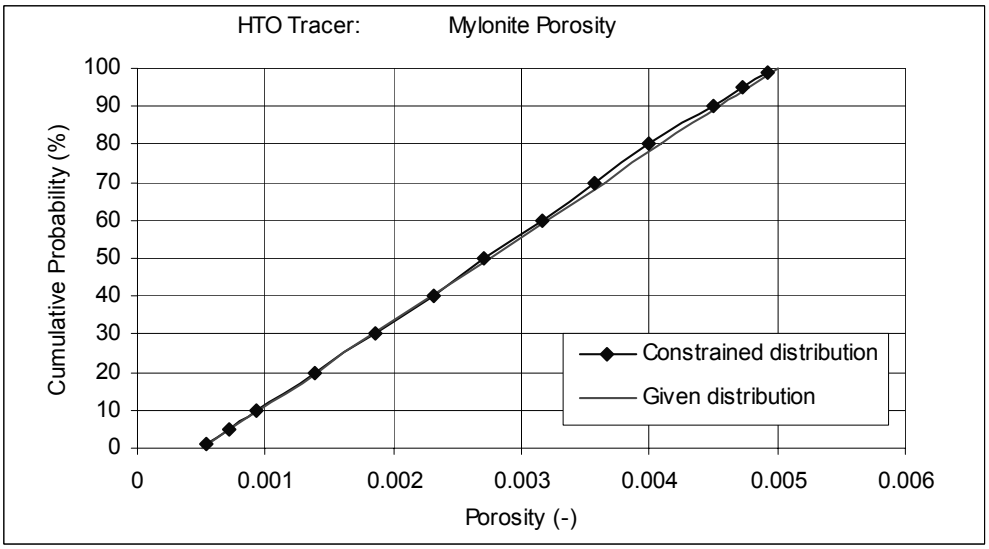

Figure 4-4 *Mylonite parameters*

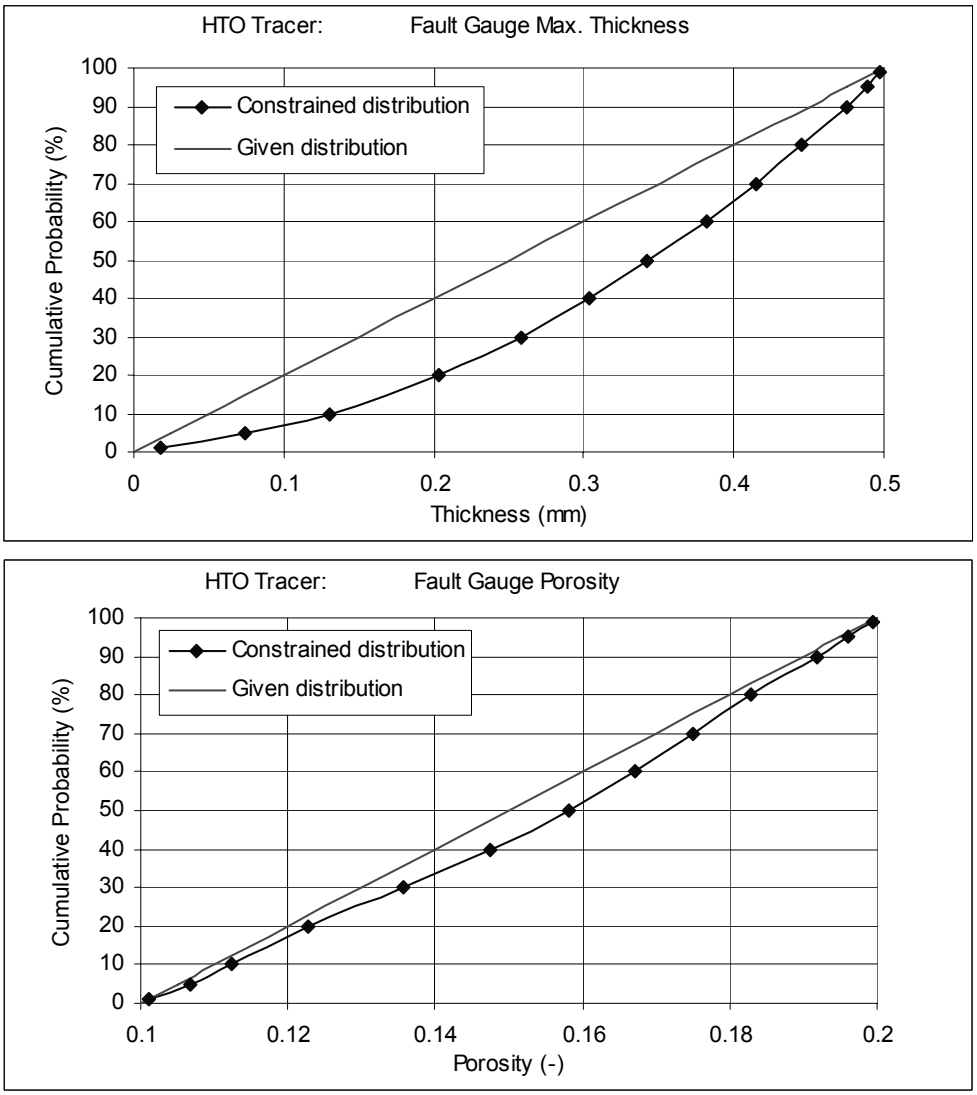

Figure 4-5 *Fault Gouge parameters*

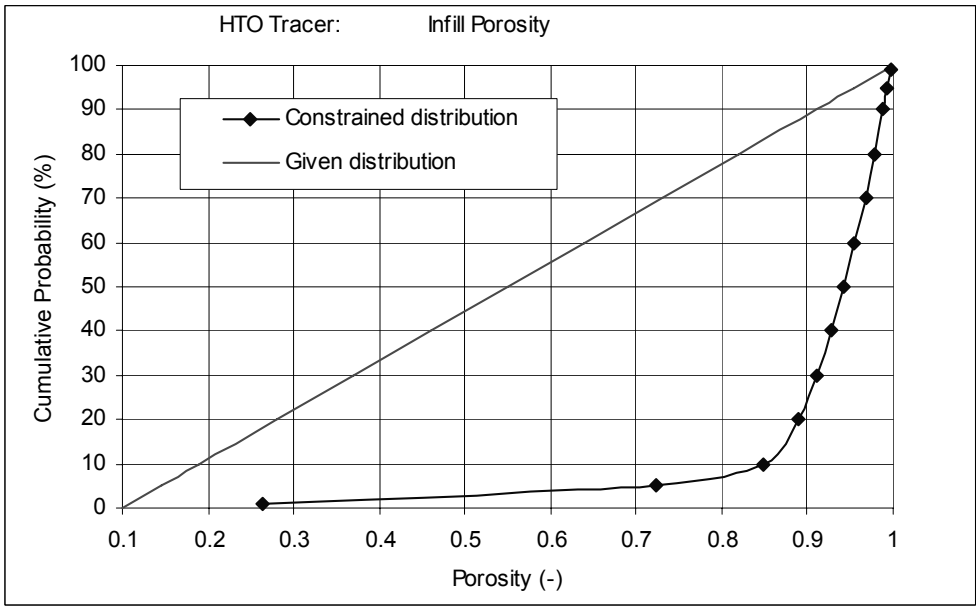

Figure 4-6 *Infill parameter*

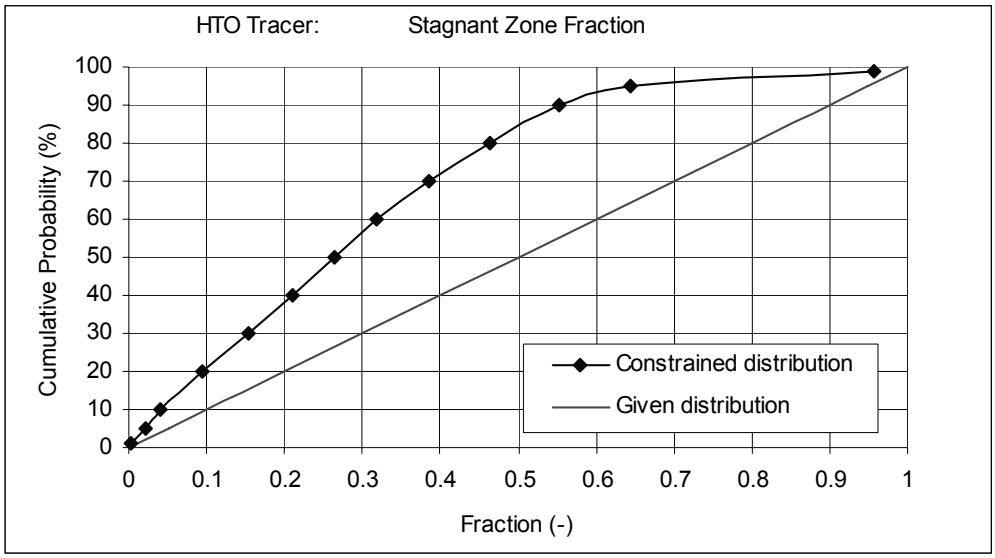

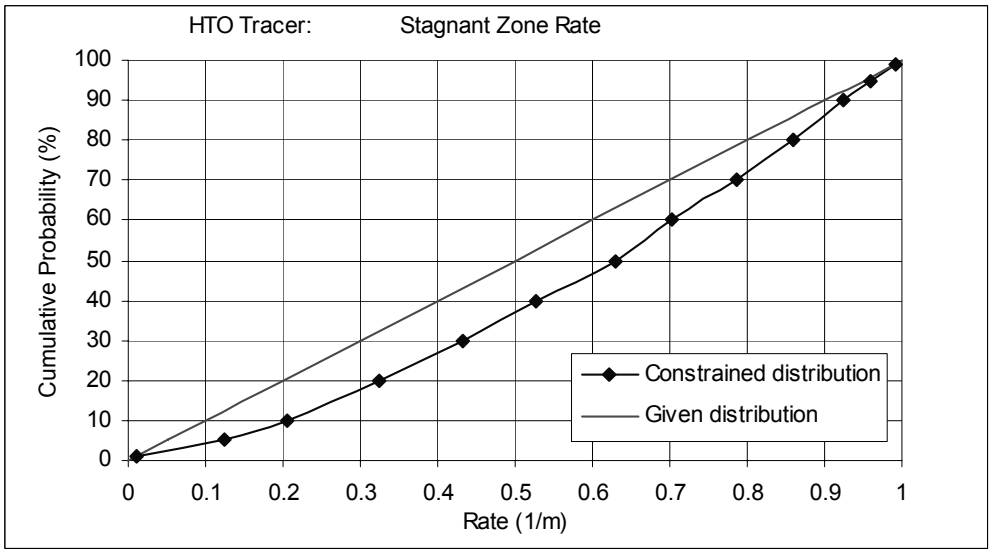

Figure 4-7 *Stagnant zone parameters*

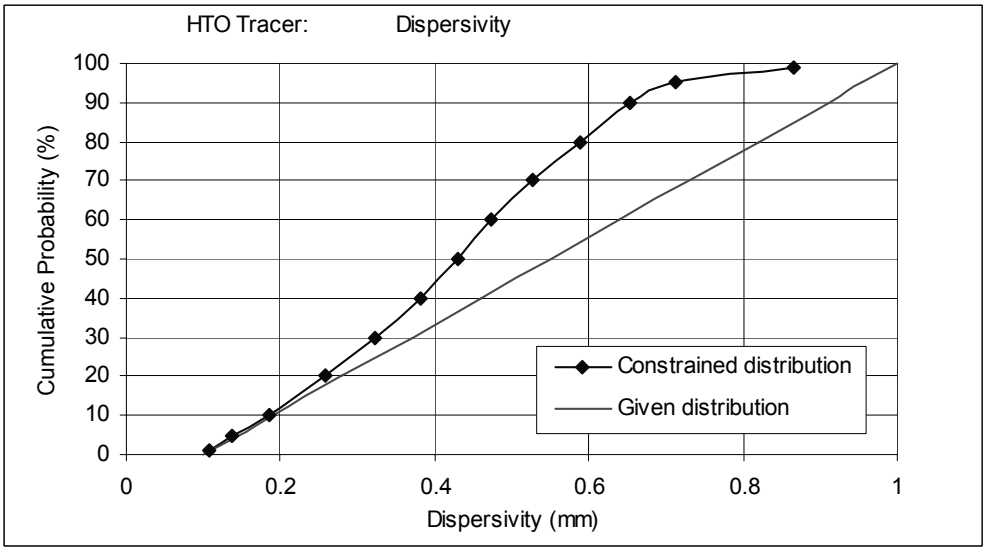

Figure 4-8 *Dispersivity parameter*

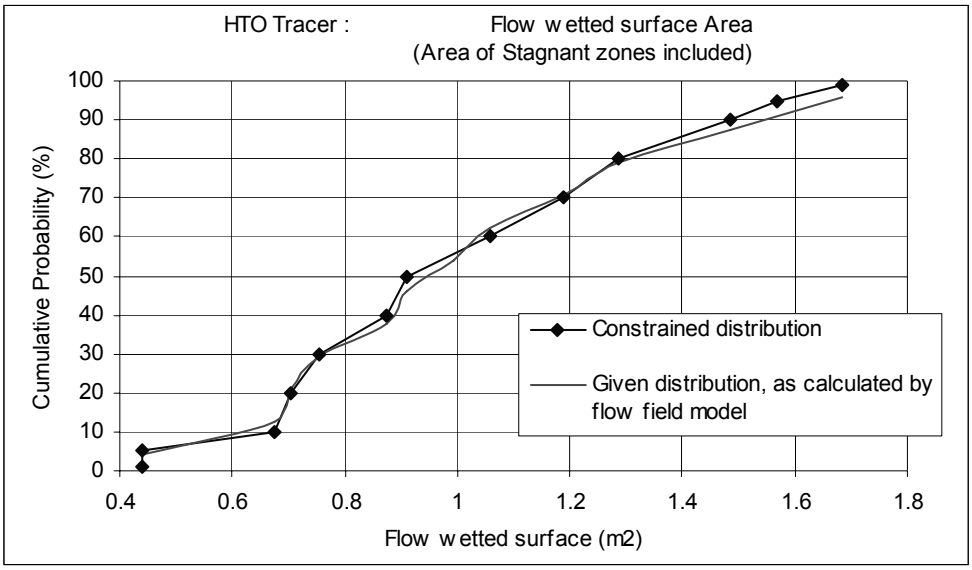

(i)

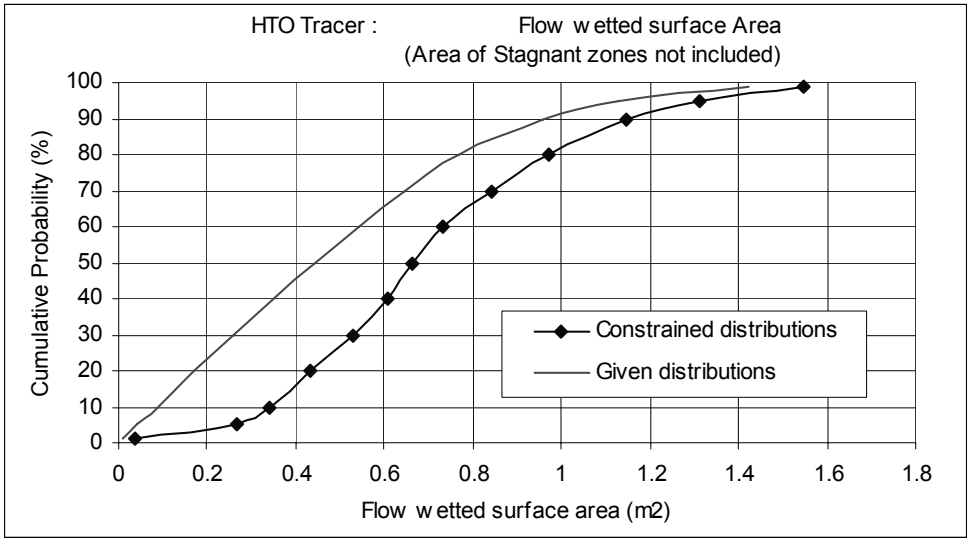

(ii)

Figure 4-9 *Flow wetted surface area, with (i) and without (ii) inclusion of the stagnant zones.*

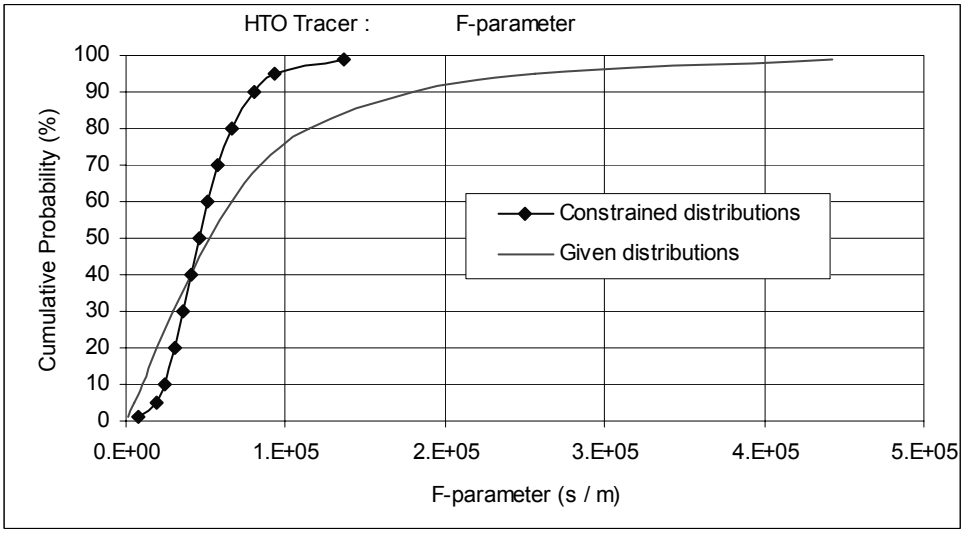

Figure 4-10 *The F-parameter.*

5 TASK 6A – Simulation of a reactive tracer – Strontium

5.1 Given parameter distributions for Strontium test

The given parameter distributions for the Strontium test are given below. Based on these distributions a large number of different realisations of the transport properties were established. For the Strontium test, the Kd-values are not set to zero, as Strontium is reactive tracer. The number of independent parameters is 17. The distributions are based on data given in Task 6A and 6B specifications, by Selroos and Elert (2001) and Elert and Selroos (2001).

Table 5-1 Strontium. Material properties (stochastic)

	Min value	Max value	Distribution	Unit
Altered Diorite Poros	1e-3	4e-3	Uniform	-
Altered Diorite Kd	4.7e-8	9.4e-5	Uniform	m3/kg
Mylonite Poros	5e-4	5e-3	Uniform	-
Mylonite Kd	2.6e-7	2.5e-4	Uniform	m3/kg
Fault Gouge Poros	0.1	0.2	Uniform	-
Fault Gouge Kd	2.6e-10	2.5e-2	Uniform	m3/kg
Infill Poros	0.1	1	Uniform	-
Infill Kd	2.6e-10	2.5e-2	Uniform	m3/kg

Table 5-2 Strontium. Transport geometry properties (stochastic)

	Range	Distribution	Unit
Altered Diorite Fraction	0.2-0.8	Uniform	-
Altered Diorite Max Thickness	25 – 45	Uniform	mm
Mylonite Fraction	0.2-0.8	Uniform	-
Mylonite Max Thickness	1 – 10	Uniform	mm
Fault Gouge Fraction	1	Discrete	-
Fault Gouge Max Thickness	0 – 0.5	Uniform	mm
Dispersivity	0.01 – 1	Uniform	m
Stagnant Zone Fraction	0 – 1	Uniform	-
Stagnant Zone Rate	0 – 1	Uniform	1/m
Flow wetted surface	0.44 - 1.7	Special	m^2

In GoldSim, the effective diffusivity (D_e) is defined as

Equ. 5-1

$$D_e = D_0 * p * \tau$$

In which D_0 is the free water diffusivity for each tracer, p is the matrix porosity and τ is a back-calculated theoretical tortuosity. The effective diffusivity calculated in accordance with Equ. 5-1 is presented in Table 5-3, below.

Table 5-3 Reactive (Strontium) tracer. Matrix properties (stochastic). Effective diffusivity.

	Effective diffusivity					
	Minimum	*Maximum*	D_0	$p_{, min}$	$p_{, max}$	τ
Altered Diorite	1.03E-14	4.11E-14	7.90E-10	1.00E-03	4.00E-03	0.013
Mylonite	5.14E-15	5.14E-14	7.90E-10	5.00E-04	5.00E-03	0.013
Fault Gouge	1.03E-12	2.05E-12	7.90E-10	0.1	0.2	0.013

5.2 Criteria for acceptance of a realisation

Only the realisations that produced a breakthrough curve close to the measured breakthrough were accepted for further analyses. The accepted realisations must demonstrate a deviation from the measured breakthrough that is less than plus/minus 25% of the measured activities; the test is applied in the time interval between 4.8 hours and 70 hours (see Figure 3-5). We have simulated and analysed 300 000 realisations, only 89 of these realisations passed the test defined by the specified boundaries.

5.3 Envelope of accepted realisations

The envelopes of the breakthrough curves of the accepted realisations are given below in Figure 5-1. The green curve is the upper envelope of all accepted realisations; it is not given by a single realisation, but by all accepted realisations; the purple curve is the lower envelope of all accepted realisations.

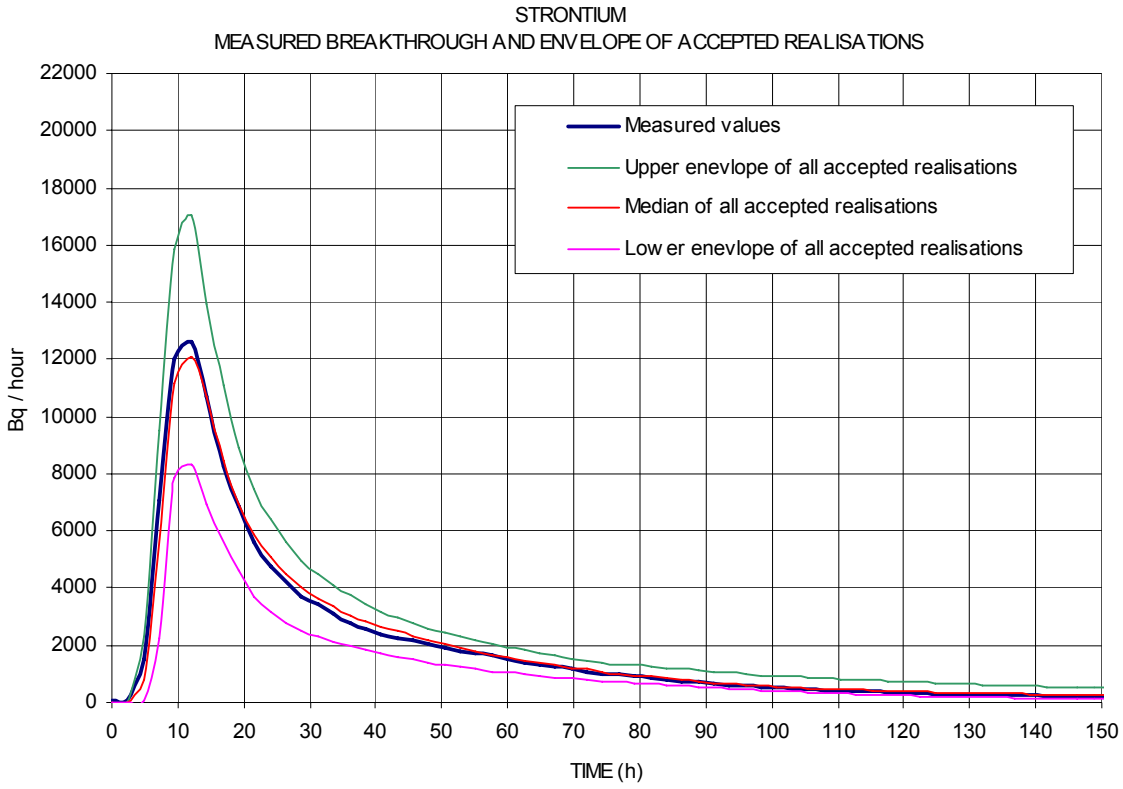

Figure 5-1 *Strontium. Measured breakthrough and envelope of accepted realisations.*

5.4 The best realisations

The three best realisations were found by sorting all accepted realisations, considering deviation from the measured breakthrough. Different sorting criteria have been tested. The best results were obtained when the modelled breakthrough curves were sorted for squared minimum difference. The test was applied for all time steps for which the measured breakthrough is larger than zero. The breakthrough curves for the three best realisations are given below in Figure 5-1

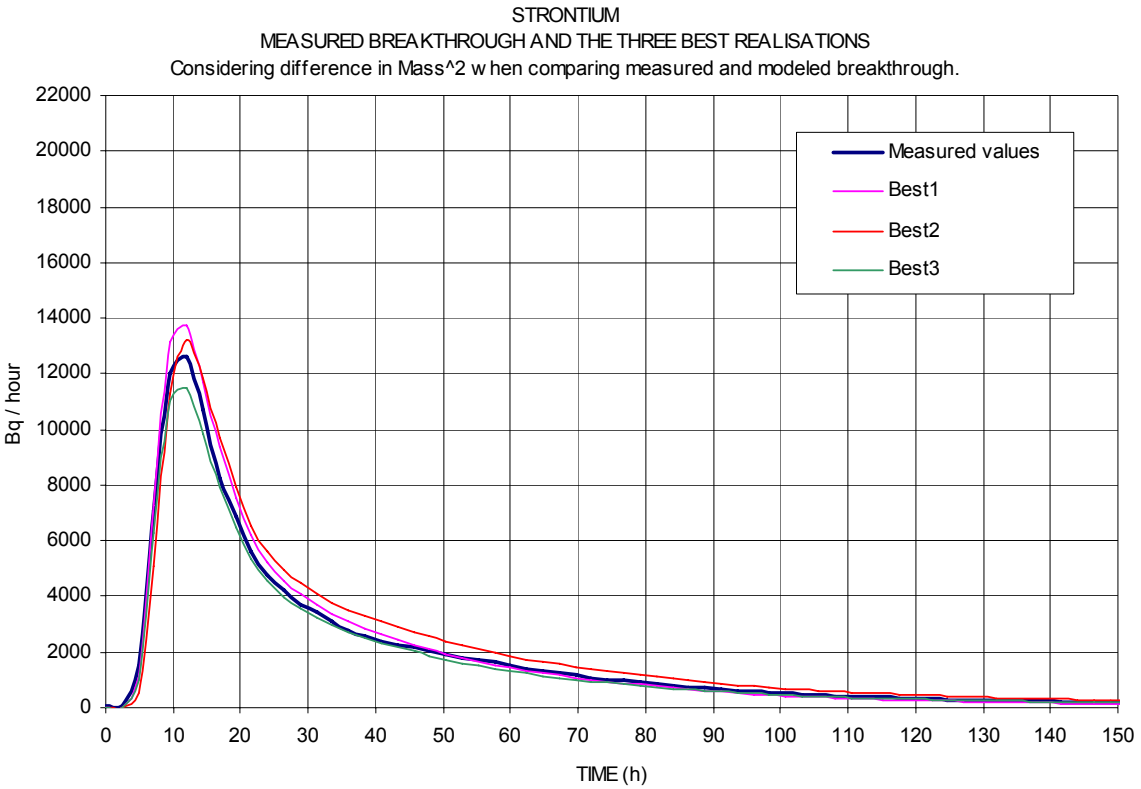

Figure 5-2 *Strontium. Measured breakthrough and the modelled breakthrough for the three best realisations.*

5.5 Assessment of the constraining power of the Strontium tracer test (reactive tracer)

In the figures below (Figure 5-3 through Figure 5-10) we present the given parameter distributions and the constrained distributions, as produced by the simulated Strontium tracer test. The constraining power, or the lack of it, is summarised in Table 5-5, below.

5.5.1 Basic parameters

We conclude:

A general conclusion, based on the assessment of the constraining power of the Strontium tracer test, is that the use of a tracer that only interacts weakly with the rock mass will not produce a large constraining power. There are however a few parameters for which some constraining power is demonstrated, and there are interesting differences between the results of the reactive and non-reactive tracer.

Diorite and the Mylonite rock are located behind the Fault Gouge, and not in direct contact with the flowing water. No constraining power is demonstrated considering the properties of these two rock types (fraction, thickness and porosity). It is likely that this result is given by the relatively short time-scale of the experiments. The mass exchange with the inner zones is insignificant during such short time.

Fault Gouge is located on the surface of the fracture planes and in direct contact with the flowing water. In the Strontium test no constraining power, was demonstrated as regards the porosity of this material, in comparison the HTO test demonstrated some very weak constraining power for porosity. More constraining power was demonstrated as regards the thickness of the Fault Gouge. In the Strontium test 80 percent of the accepted realisations had a thickness less than 0.20 mm, whereas in the HTO test 80 percent had a thickness less than 0.44 mm. For the Fault Gouge thickness, the ranges of the constrained distributions were the same as in the given distributions, but the constrained distributions demonstrated different probability density function. The range of the Fault Gouge Kd values was defined as very large in the given distribution. The Strontium test demonstrated a distribution with a smaller range and with a minimum value at 1.0e-5 Kg/m^3 (1^{th} percentile) and a maximum at 2.3e-2 Kg/m^3 (99^{th} percentile).

Filling material (the Infill) is specified inside the open space of the fracture studied, this material is in direct contact with the flowing water. For the HTO tracer a constraining power was demonstrated for the porosity of the Infill, but primarily as regards the probability distribution and not as regards the range of accepted values. The Strontium test demonstrates however no constraining power for the Infill porosity. The range of the Infill Kd values was defined as very large in the given distribution. The Strontium test demonstrated a distribution with a smaller range and with a minimum value at 1.0e-5 Kg/m^3 (1^{th} percentile) and a maximum at 2.5e-2 Kg/m^3 (99^{th} percentile), close to the same range as for the Fault Gouge.

Zones of stagnant water are specified inside the fracture. The amount of such stagnant water (fraction) and the rate with which this water interacts with the flowing water is also analysed. Constraining power was demonstrated as regards the Stagnant Zone Fraction and Stagnant Zone Rate. For both the Fraction and the Rate, the ranges of the constrained distributions were the same as in the given distributions, but the constrained distributions demonstrated a different probability density function. Hence, some constraining power were demonstrated for these properties. For the Stagnant Zone Fraction, 80% of the accepted realisations demonstrated a Fraction larger than 0.77. Hence, most of the accepted simulations had a large amount of stagnant zones, but a few simulations with very small amount of stagnant zone was also accepted. These results are different compared to the results of the HTO tracer test, the HTO tracer demonstrated a large amount of accepted realisations with a small stagnant zone. Considering the Stagnant Zone Rate, 90% of the accepted realisations had a Rate less than 0.15. Hence, most of the accepted simulations had a small values of the Rate, but a few simulations with large values of Rate was also accepted. These results are different to the results of the HTO tracer test, for the HTO tracer the constraining power as regards the Rate was much weaker, and most of the accepted realisations had rates larger than those of the accepted Strontium realisations.

Dispersivity of the flow domain was also analysed and the results demonstrated a weak constraining power for this parameter. The accepted realisations of the Strontium test demonstrate results that are a mirror image of the results derived from the HTO test.

Considering the Strontium test, the accepted realisations demonstrated a constrained distribution with a lower limit of the dispersivity close to a 0.25 mm (1^{th} percentile), while the given distribution had a lower limit at 0.1 mm. The 20^{th} percentile of the constrained distribution is 0.50 mm and in the given distribution the 20^{th} percentile is 0.28 mm. The upper parts of the distributions are very much the same.

Flow wetted surface area (or the wet area) is the area on the fracture plane, along which the transport takes place. The area is calculated as the sum of the areas on the upper and the lower planes. A distribution of possible areas was derived from the modelling of the flow field, this distribution was transferred to the transport model and defined as the given distribution of the flow wetted surface. The transport model reduces the size of the area where the flow takes place, by introducing the stagnant zones. Hence, there are two different concept of flow wetted surface area: (i) Flow wetted surface area including the stagnant zones and (ii) Flow wetted surface area without the stagnant zones. We have studied both concepts. Considering the first concept (including stagnant zones in the flow wetted surface area), the transport modelling demonstrated no constraining power; the constrained distribution produced is very close to the given distribution. However, for the second concept (excluding the stagnant zones from the flow wetted surface area), the transport modelling demonstrates a significant constraining power for this parameter. Considering all realisations the 90^{th} percentile and the median of the produced values of the flow wetted area were 0.96 m^2 and 0.44 m^2, respectively; but for the accepted realisations the 90^{th} percentile and the median of the produced values of the flow wetted area were 0.45 m^2 and 0.04 m^2, respectively. Hence, the flow wetted surface areas (without stagnant zones) of the accepted realisations are significantly smaller than those of all realisations; the small values of flow wetted surface areas follows from the large amounts of stagnant zones among the accepted realisations.

5.5.2 Combined parameters

For a situation with a simplified flow geometry e.g. flow through channels of a known size, the parameters controlling matrix diffusion may be expressed as the product of a parameter characterising the flow, generally called the F-parameter, and a group of parameters including the distribution coefficients (Kd-values), diffusion coefficients and matrix porosity. The F-parameter may be expresses in several different ways; we have used the formulation given in Equ. 4-2

Considering the Strontium test, we have calculated (i) the distribution of the F-parameter for all realisations (given parameter distributions) and (ii) the distribution of the F-parameter for the selected realisations (constrained parameter distributions). We have used both concepts of flow wetted surface area, as discussed above in Sec. 5.5.1. Considering the first concept (including stagnant zones in the flow wetted area), the transport modelling demonstrated no constraining power. Considering the second concept (excluding the stagnant zones from the flow wetted area), the transport modelling demonstrates a significant constraining power for the F-parameter. The most consistent method is to calculate the F-parameter by use of the second concept–using a flow wetted surface area without the stagnant zones. The results of such calculations are given in Figure 5-10. Considering all realisations (given parameter distribution), the 90^{th} percentile and the median of the produced values of the F-parameter were

179 800 s/m and 52 400 s/m, respectively; but for the accepted realisations (constrained parameter distribution) the 90th percentile and the median of the produced values of the F-parameter were 98 200 s/m and 6 500 s/m, respectively. Hence, the F-parameters of the accepted realisations are significantly smaller than those of all realisations.

Another combined parameter, closely related to the F-parameter, or another way of defining the F-parameter, is the flow wetted surface area over flow, as defined by Equ. 4-3. This formulation does not include the porosity of the Infill material, which is included in Equ. 4-2. We have calculated the probability distributions for the F-parameter, as defined in Equ. 4-3, for all and for the selected realisations. As the flow at the injection point is the same in all realisations, the constraining power will be the same as for the flow wetted surface area.

For a situation in which the partitioning of a contaminant (tracer) can be adequately described by a fast reversible adsorption with a linear isotherm, the retardation of the front of the migrating contaminant, relative the movement of the bulk mass of water, can be described by the following relation, commonly known as the retardation equation (Freeze and Cherry, 1979):

Equ. 5-2

$$\frac{v}{v_c} = 1 + \frac{\rho_b}{n} K_d$$

v = *average linear velocity of the groundwater [length / time].*

v_c = *velocity of the $C / C_0 = 0.5$ theoretical point on the concentration profile of the retarded constituent [length / time].*

ρ_b = *Bulk density of the rock mass [mass / volume].*

n = *Porosity [-].*

K_d = *Partition coefficient [volume / mass].*

The right hand side of the retardation equation is known as the retardation factor and the left hand side is known as the relative velocity. Hence, the retardation factor can be expressed as:

Equ. 5-3

$$R = 1 + \frac{\rho_b}{n} K_d$$

R = Retardation factor [-]

For the Strontium tracer and for the different materials studied (Diorite, Mylonite, Fault Gouge and Infill) and by use of the material properties given in Table 5-1, which is based on data given in the task specifications by Elert and Selroos (2001), and Selroos and Elert (2001), we have calculated plausible ranges of the retardation factor by use of Equ. 5-3. These ranges corresponds to the given parameter distributions. The results are given below in Table 5-4.

Table 5-4 Calculated retardation factors for Strontium based on plausible material properties.

	Altered Diorite	Mylonite	Fault Gouge	Infill	Unit
K_d, min	4.70E-08	2.60E-07	2.60E-10	2.60E-10	m3/kg
K_d, max	9.40E-05	2.50E-04	2.50E-02	2.50E-02	-
n, min	1.00E-03	5.00E-04	0.1	0.1	-
n, max	4.00E-03	5.00E-03	0.2	1.0	-
ρ_b	2.70E+03	2.50E+03	2.50E+03	2.10E+03	kg/m3
Retard. Factor: Minimum	1.0	1.1	1.0	1.0	-
Retard. Factor: Maximum	255	1251	626	526	-

As can be seen from the table above, the range of plausible values of the retardation factor is very large, the minimum value is 1.0 (no retardation) and the maximum value is about 1200. The retardation factors of the given parameter distributions are presented in Figure 5-11.

It follows from Equ. 5-3 that if constraining power is obtained for the Kd-value and/or for the porosity, constraining power will also be obtained for the retardation factor. This is demonstrated in Figure 5-11, the figure presents the given and constrained parameter distributions of the retardation factors, considering Strontium tracer and the following materials: Diorite, Mylonite, Fault Gouge and Infill. Constraining power is not demonstrated for Diorite and Mylonite, but it is for the Fault Gouge and the Infill. For both the Fault Gouge and the Infill, the accepted realisations (constrained parameter distribution) demonstrate much smaller values of the retardation factor than the retardation factors produced by analysing all realisations (given parameter distributions). The largest constraining power is demonstrated for the retardation factor of the Fault Gouge.

Considering all realisations (given parameter distributions), the median of the retardation factor is 216 for the Fault Gouge and 49 for the Infill.

Considering the accepted realisations (constrained parameter distributions), the median of the retardation factor is 49 for the Fault Gouge and 25 for the Infill.

Table 5-5 Summary of the constraining power of the Strontium tracer test(a reactive tracer).

CONSTRAINING POWER OF STRONTIUM TRACER TEST				
PARAMETER		CONSTRAINING POWER (1)	GIVEN DISTRIBUTION PERCENTILES 20^{th} , 50^{th} , 80^{th}	CONSTRAINED DISTRIBUTION PERCENTILES 20^{th} , 50^{th} , 80^{th}
ALTERED DIORITE	Fraction	No		
	Thickness	No		
	Porosity	No		
	Kd - value	No		
	Retardation F.	No		
MYLONITE	Fraction	No		
	Thickness	No		
	Porosity	No		
	Kd - value	No		
	Retardation F.	No		
FAULT GOUGE	Thickness *(mm)*	YES1	0.10 , 0.25 , 0.40	0.01 , 0.04 , 0.20
	Porosity *(-)*	No		
	Kd–value *(m3/Kg)*	YES2	5.2e-3 , 1.3e-2 , 2.1e-2	6.3e-4 , 2.5e-3 , 1.1e-2
	Retardation F.	YES1	89 , 216 , 348	10 , 49 , 158
INFILL (fillling material)	Porosity, *(-)*	No		
	Kd–value *(m3/Kg)*	YES2	5.2e-3 , 1.3e-2 , 2.1e-2	1.1e-3 , 6.0e-3 , 1.4e-2
	Retardation F.	YES1	11 , 49 , 102	2 , 25 , 74
STAGNANT ZONE	Fraction *(-)*	YES1	0.20 , 0.50 , 0.80	0.77 , 0.95 , 0.98
	Rate *(1/m)*	YES1	0.20 , 0.50 , 0.80	0.03 , 0.06 , 0.11
DISPERSIVITY	*(m)*	YES2	0.28 , 0.55 , 0.82	0.49 , 0.70 , 0.88
FLOW WETTED SURFACE AREA	Excluding stagnant zones *(m2)*	YES2	0.169 , 0.441 , 0.768	0.019 , 0.037 , 0.190
F_1-PARAMETER	*(s/m)*	YES2	19 700 , 52 400 , 114 900	2 100 , 6 500 , 29 600

(1)

No = The constrained distribution is very similar to the given distribution. No constraining power is demonstrated.

YES1 = The range of the constrained distribution is similar to that of the given distribution, but the constrained distribution demonstrates a new probability density function. Hence, some constraining power is demonstrated.

YES2 = The range of the constrained distribution is different from the given distribution. The probability density function is also different. Real constraining power is demonstrated.

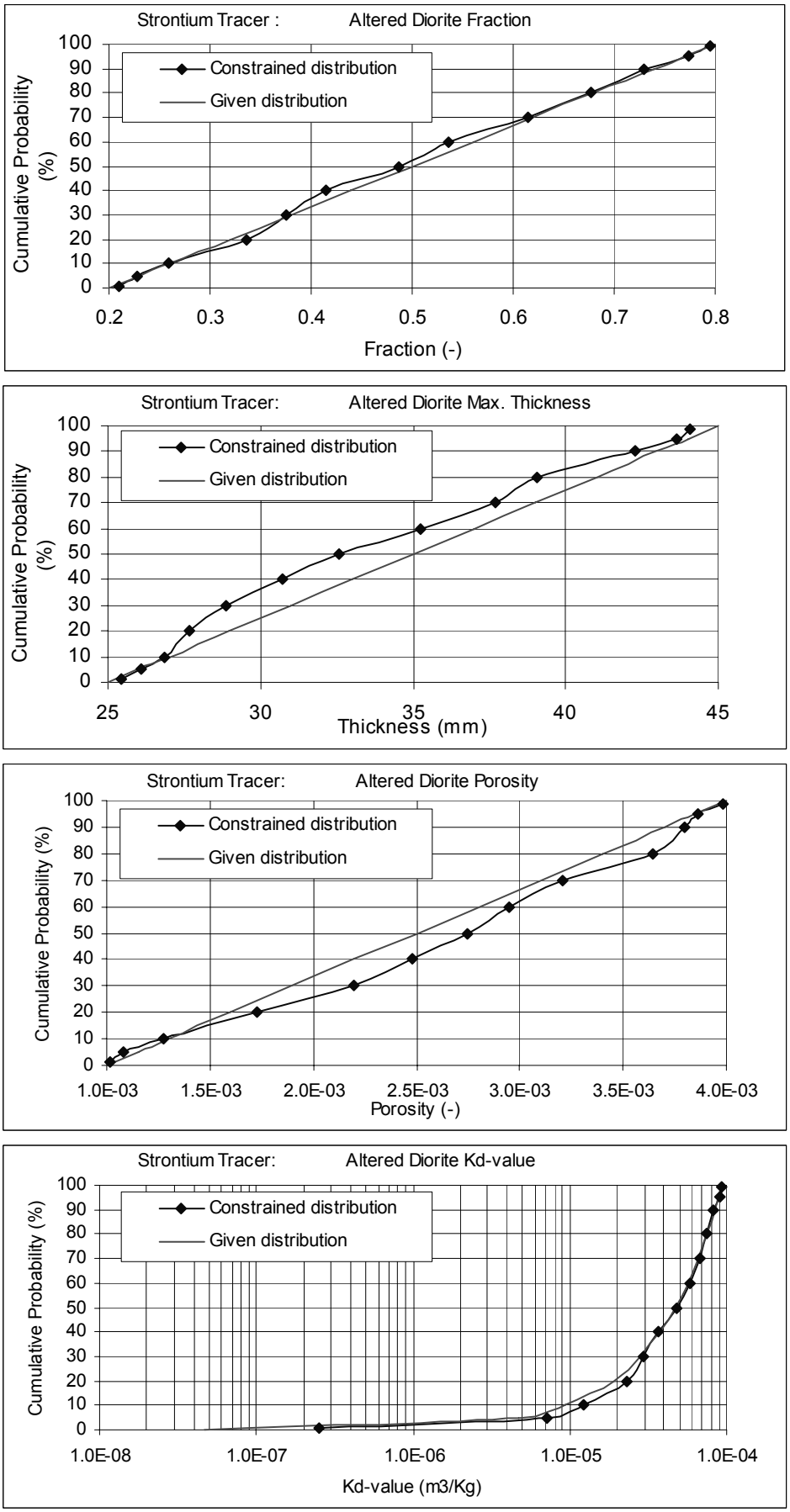

Figure 5-3 *Diorite Parameters*

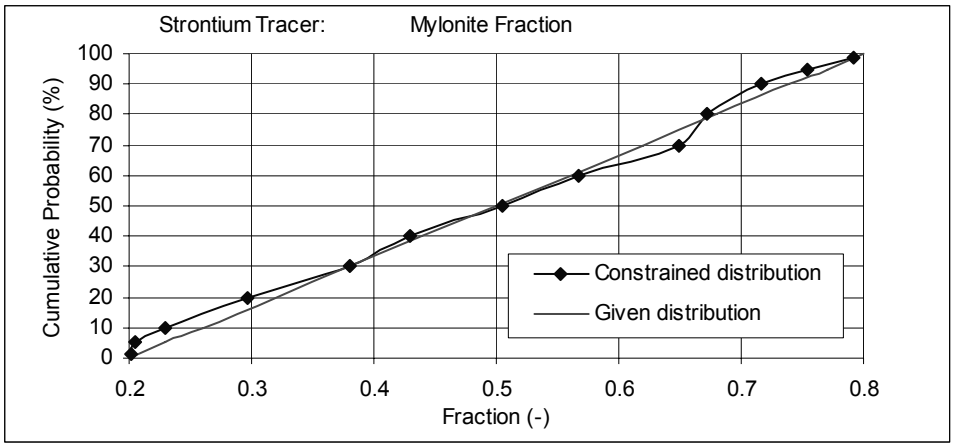

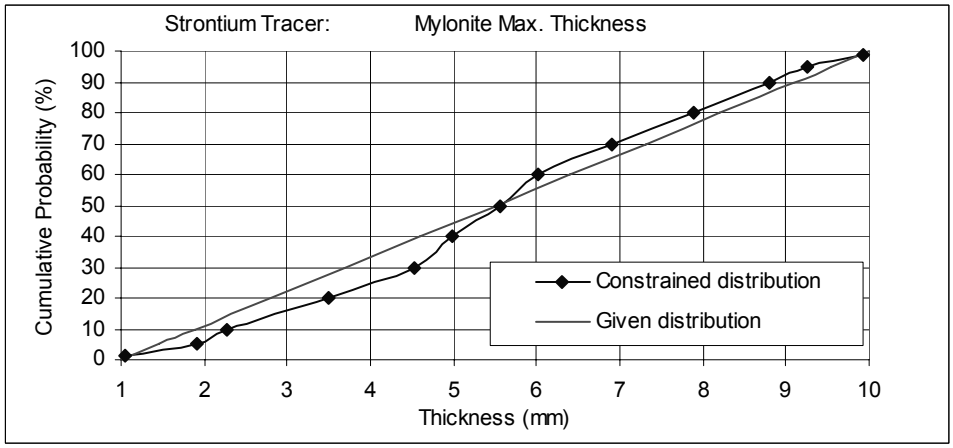

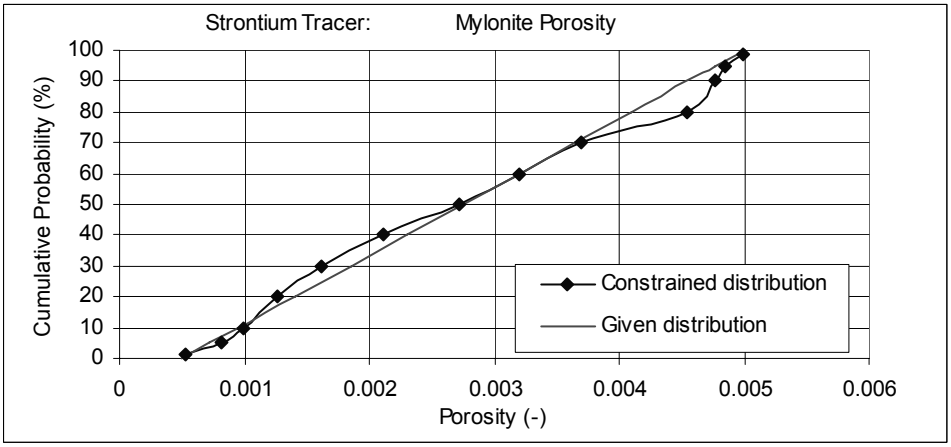

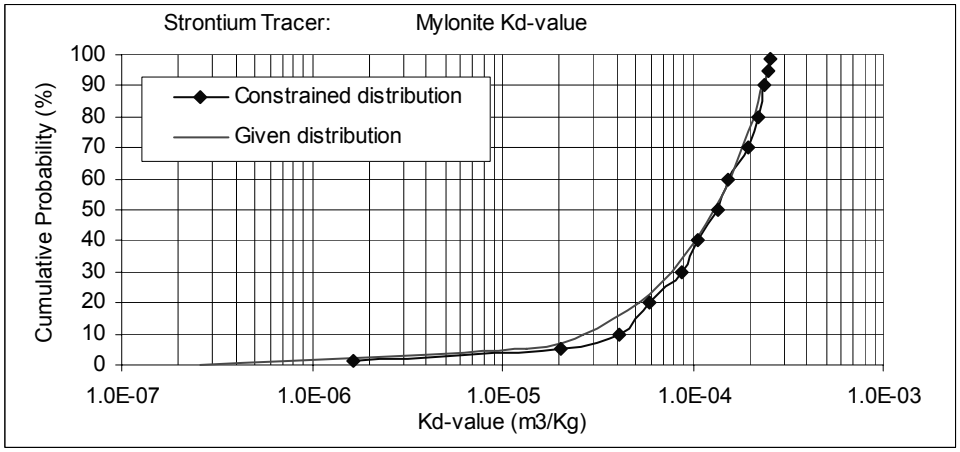

Figure 5-4 *Mylonite Parameters*

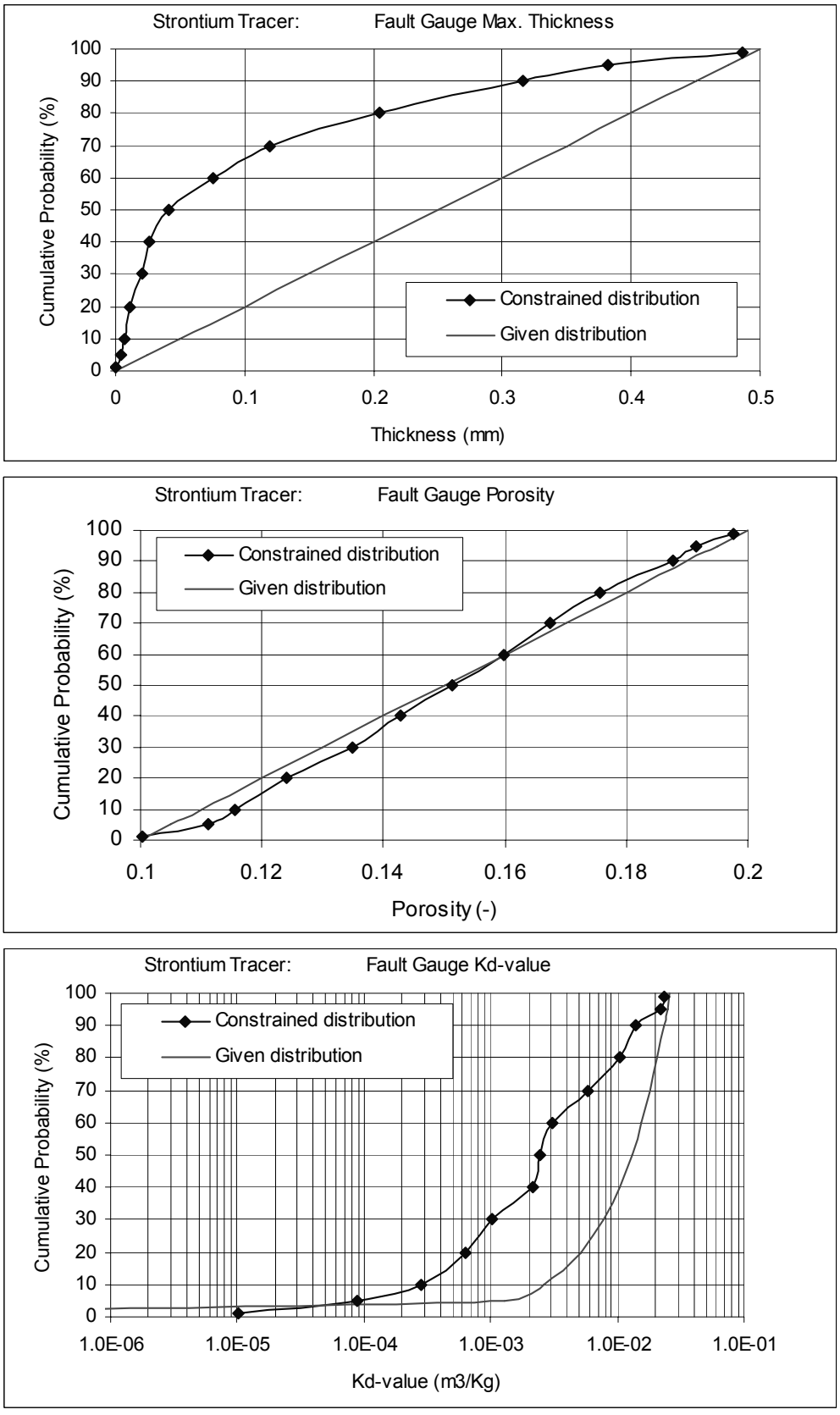

Figure 5-5 *Fault Gouge Parameters*

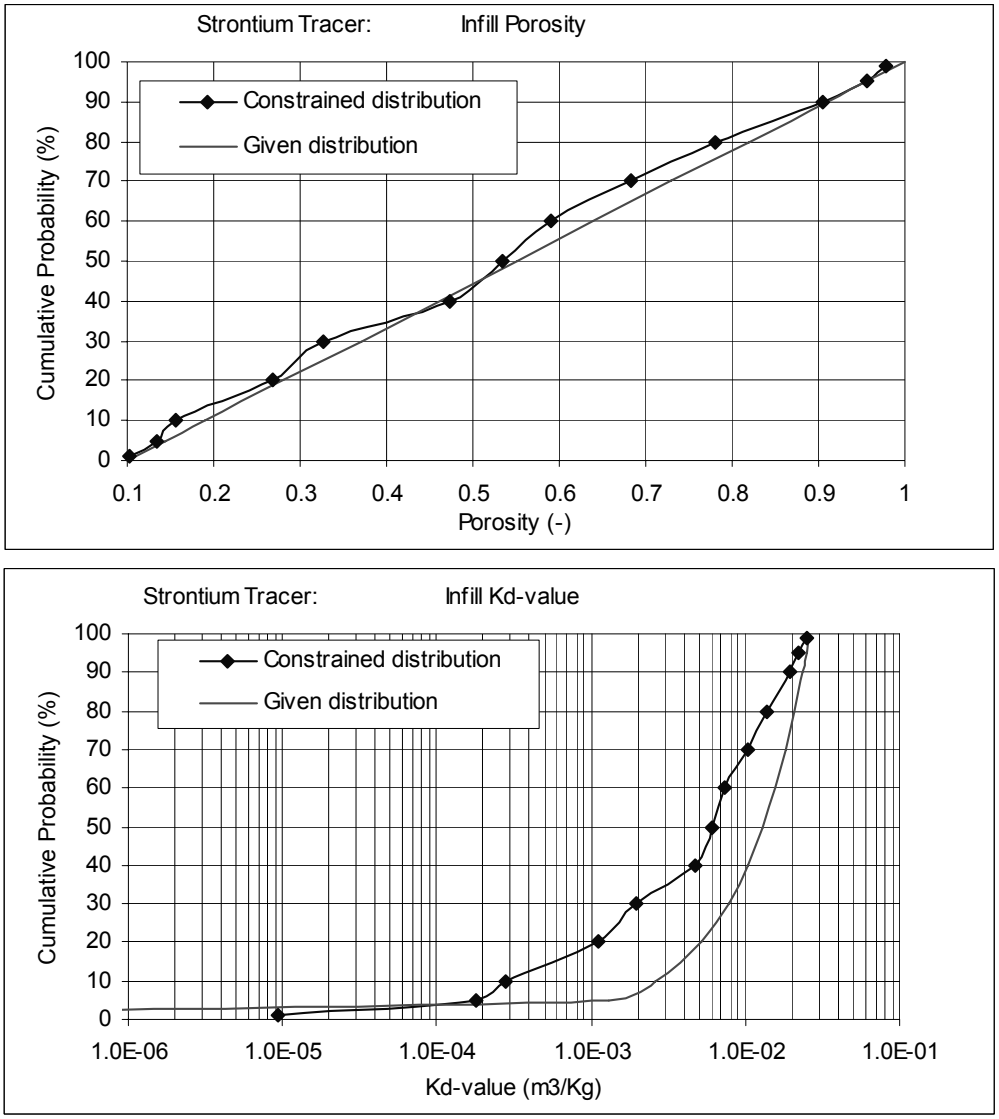

Figure 5-6 *Infill Parameters*

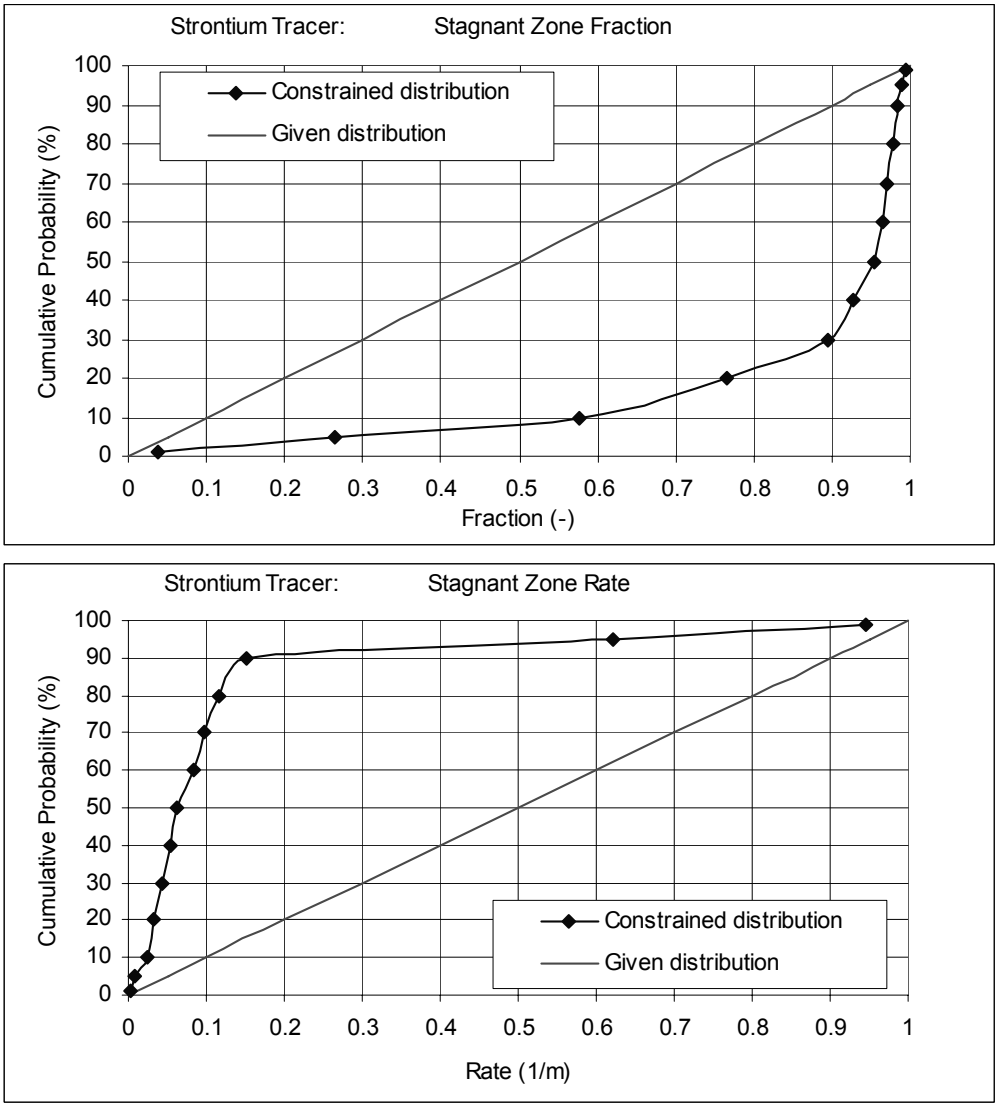

Figure 5-7 *Stagnant Zone Parameters*

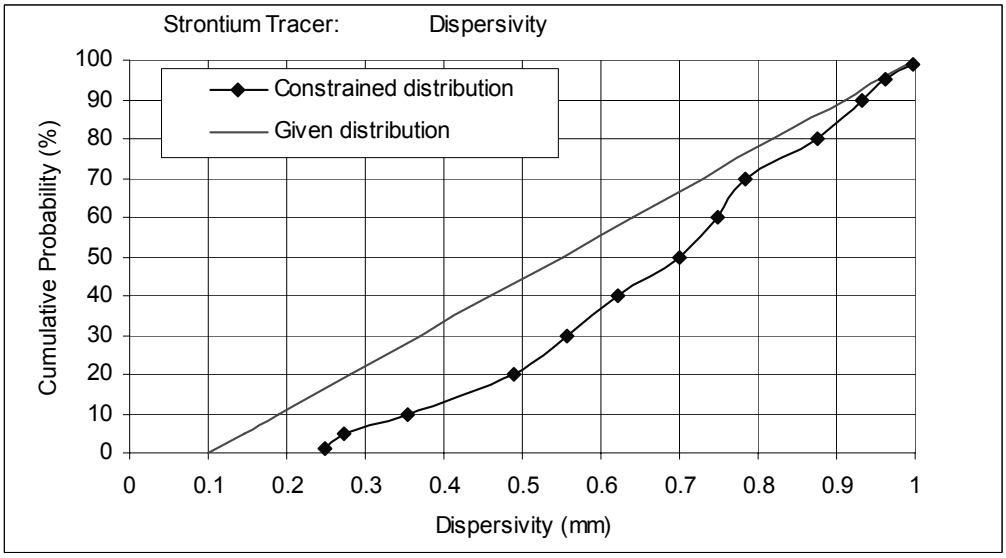

Figure 5-8 *Dispersivity Parameter*

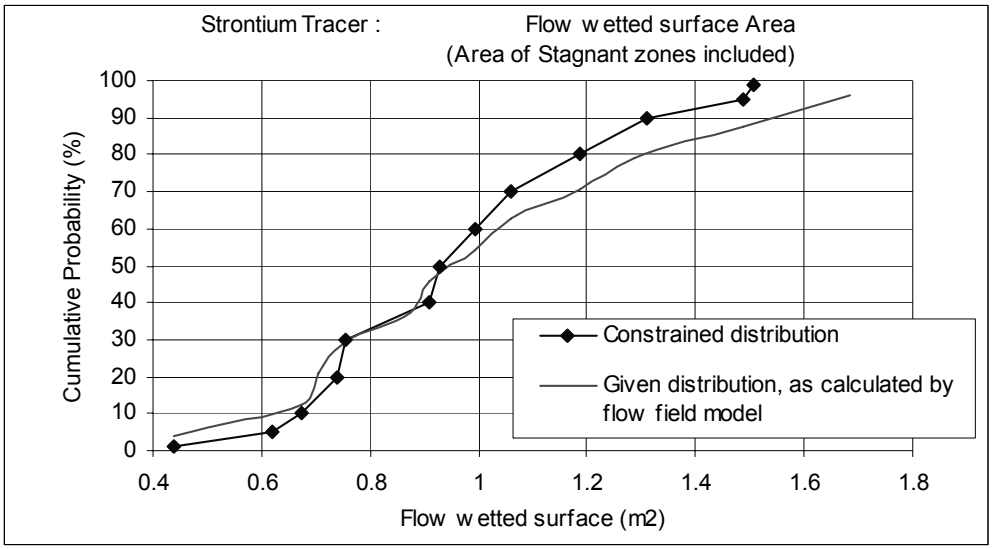

(i)

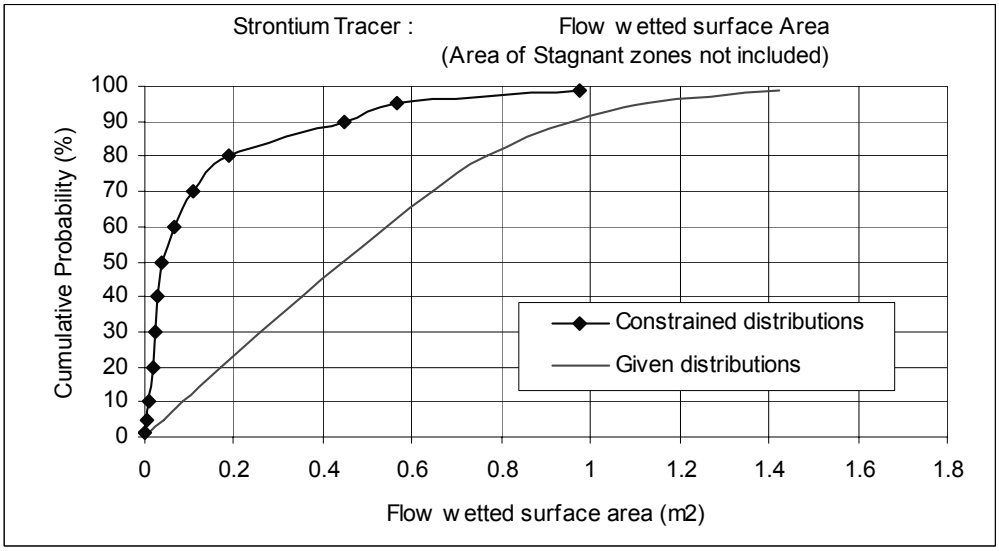

(ii)

Figure 5-9 *Flow wetted surface area, with and without inclusion of the stagnant zones.*

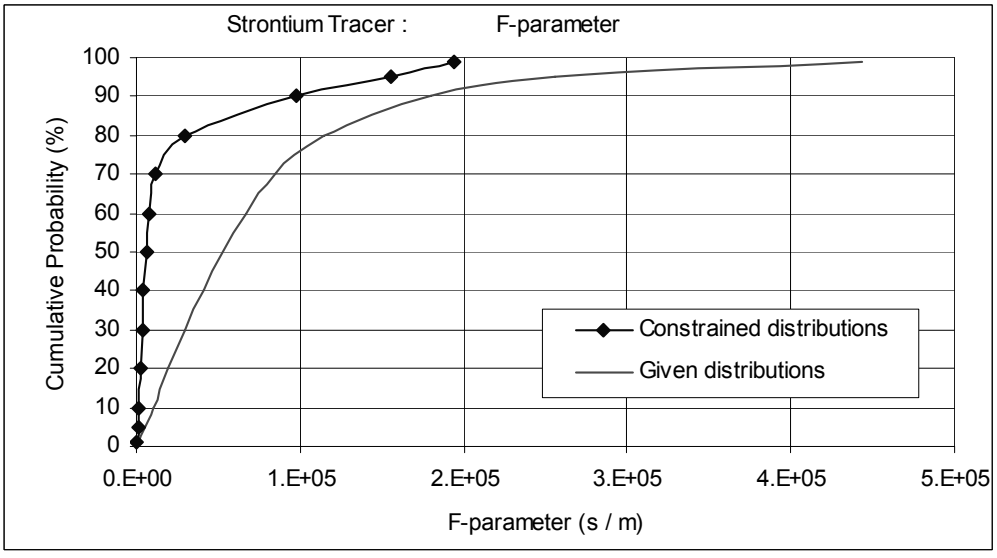

Figure 5-10 *The F-parameter.*

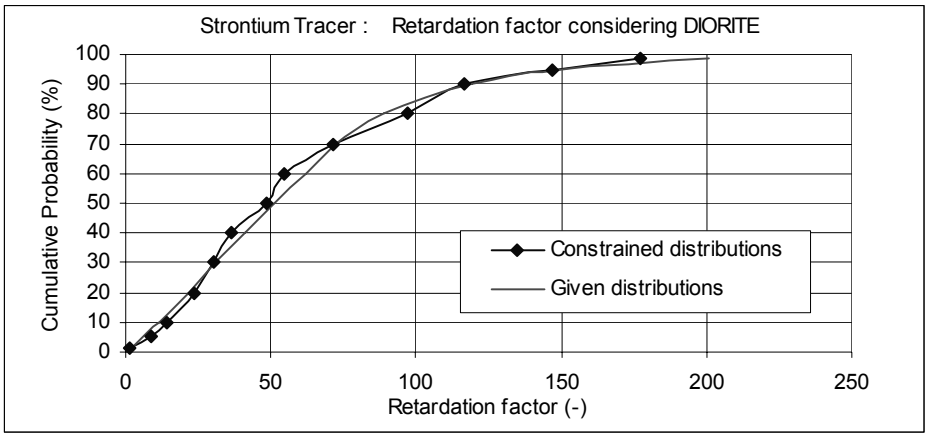

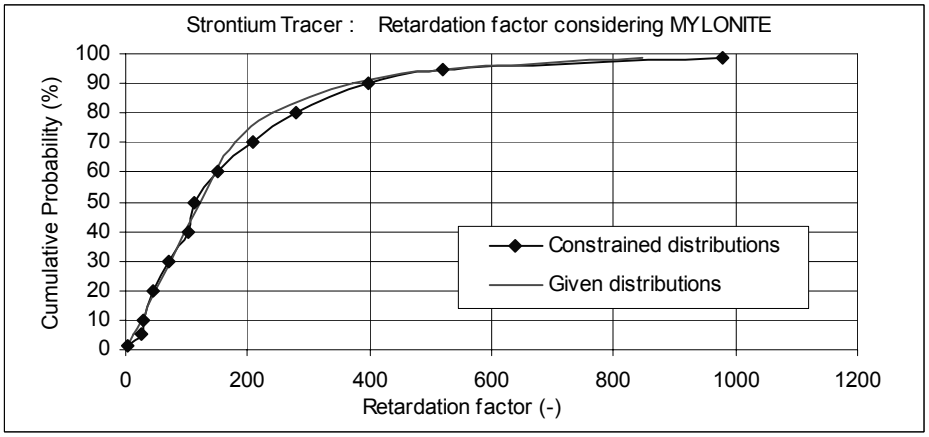

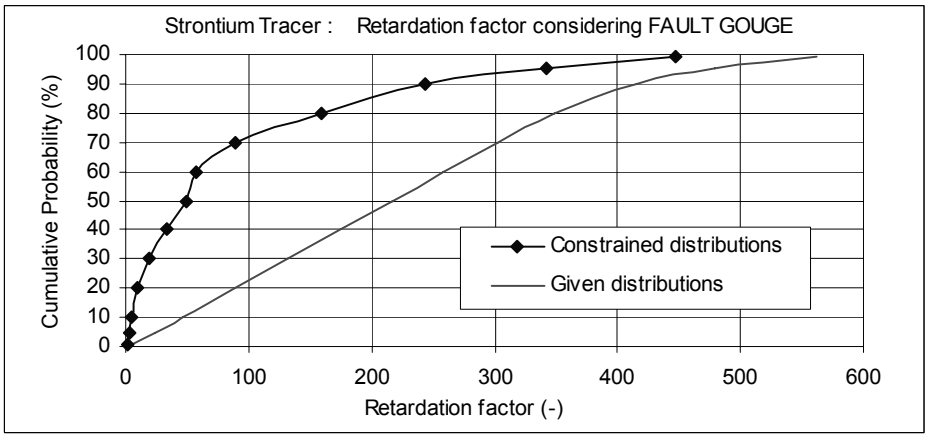

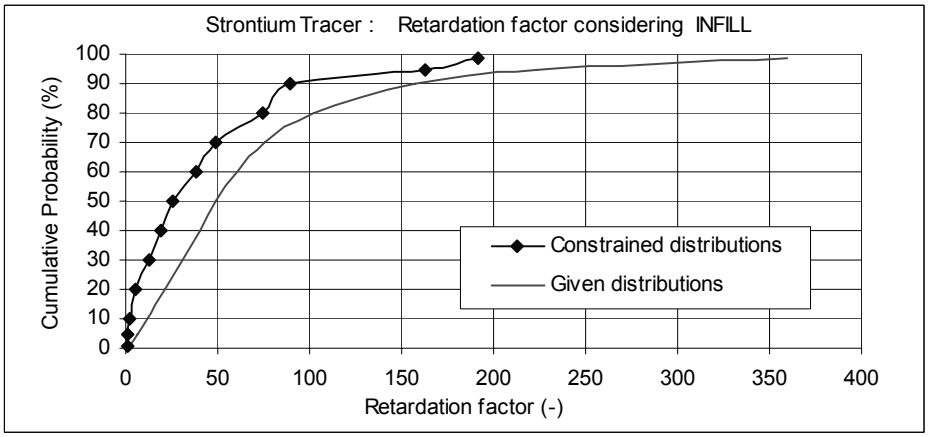

Figure 5-11 *Retardation factors for Diorite, Mylonite, Fault Gouge and Infill material.*

5.6 Analysis of possible correlation between parameters of the constrained distribution

The constrained parameter distributions are based on the 89 realisations that produced breakthrough curves for Strontium with an acceptable match to the measured breakthrough. For these 89 realisations, we have analysed the correlation between the parameters for which constraining power was demonstrated, as well as for other parameters, the studied combinations are given below. The number of studied combinations is 24 (in total there are 136 possible combinations). Scatter plots presenting the results are given in Appendix A.

- Stagnant zone fraction VERSUS:
  - Stagnant zone rate
  - Dispersivity
  - Fault Gouge thickness
  - Fault Gouge Kd-value
  - Fault Gouge porosity
  - Infill Kd-value
  - Infill porosity
  - Flow wetted surface area

- Stagnant zone rate VERSUS:
  - Dispersivity
  - Fault Gouge thickness
  - Fault Gouge Kd-value
  - Fault Gouge porosity
  - Infill Kd-value
  - Infill porosity
  - Flow wetted surface area

- Infill porosity VERSUS:
  - Infill Kd-value
  - Dispersivity
  - Fault Gouge porosity
  - Fault Gouge thickness
  - Fault Gouge Kd-value
  - Flow wetted surface area

- Fault Gouge porosity VERSUS:
  - Fault Gouge Kd-value
  - Fault Gouge thickness
  - Infill Kd-value

No obvious and linear correlation was observed for any of the studied combinations, there are however some interesting relationships, that corresponds to the demonstrated constraining power, e.g:

- Stagnant zone fraction VERSUS Stagnant zone rate (see Figure A-1)
- Stagnant zone fraction VERSUS Dispersivity (see Figure A-2)
- Stagnant zone fraction VERSUS Fault Gouge Kd-value (see Figure A-4)
- Stagnant zone fraction VERSUS Fault Gouge thickness (see Figure A-5)
- Stagnant zone fraction VERSUS Infill Kd-value (see Figure A-7)

6 TASK 6A – Simultaneous simulation of a reactive (strontium) and conservative tracer (HTO)

6.1 Criteria for acceptance of a realisation

For the combined simulation of the breakthrough curves of HTO and Strontium, an accepted realisations must produce breakthrough curves that are close to the measured breakthrough, considering both HTO and Strontium. In the previous simulations the tracers were studied separately; i.e. when we analysed the breakthrough curve of the HTO we did not include the Strontium breakthrough curve in the analyse, and vice versa.

Only the realisations that produces a breakthrough curves close to the measured breakthroughs were accepted for further analyses. The accepted realisations must demonstrate a deviation from the measured breakthrough curves that is less than plus/minus 50% of the measured values; the test is applied between time equal to 4.8 hours and 70 hours. We have simulated and analysed 300 000 realisations, only 33 of these realisations passed the combined test (as defined by the specified boundaries).

6.2 Envelope of accepted realisations

The envelope of the breakthrough curves of the accepted realisations are given below in Figure 6-1. The upper figure presents the envelope of the HTO simulations and the lower figure that of the Strontium simulations; both envelopes (HTO and Strontium) are produced by the same ensemble of accepted realisations.

The green curve is the upper envelope of all accepted realisations; it is not given by a single realisation, but by all accepted realisations; the purple curve is the lower envelope of all accepted realisations.

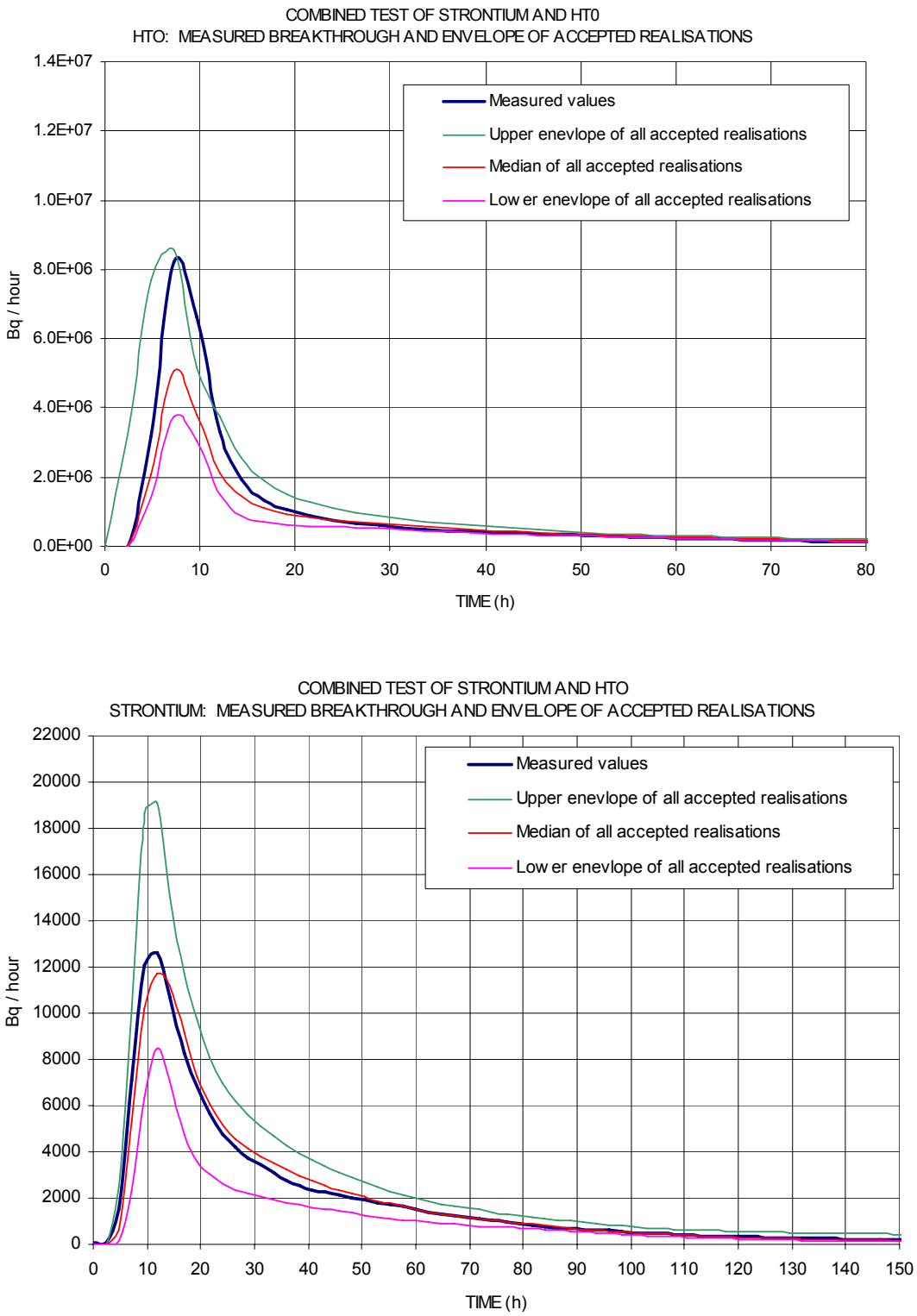

Figure 6-1 *Combined test Strontium and HTO. Measured breakthrough and the envelope of the accepted realisations, considering HTO (upper) and Strontium (lower).*

6.3 Assessment of the constraining power of the combined test of Strontium and HTO tracers

In the figures below (Figure 6-2 through Figure 6-8) we present the given parameter distributions and the constrained distributions, as produced by the simulated combined HTO and Strontium tracer test. When analysing these figures it is necessary to keep in mind that only 33 realisations passed the combined test. The small number of accepted realisations will produce constrained distributions that are not as smooth as the previously presented constrained distributions (Sections 4.5 and 5.5), which were the results of a much larger number of accepted realisations.

A comparison between the results of:

(i) the Strontium test (Figure 5-3 through Figure 5-9) and

(ii) the combined Strontium / HTO test (Figure 6-2 through Figure 6-8),reveals that the differences are small. The results of the combined Strontium / HTO test are the very much the same as the results of the Strontium test.

Hence, the assessment of the constraining power of the Strontium test is also applicable to the combined Strontium / HTO test. Therefore, when presenting the assessment of the constraining power of the combined test, we refer to the assessment of the constraining power of the Strontium test, which is given in Section 5.5.

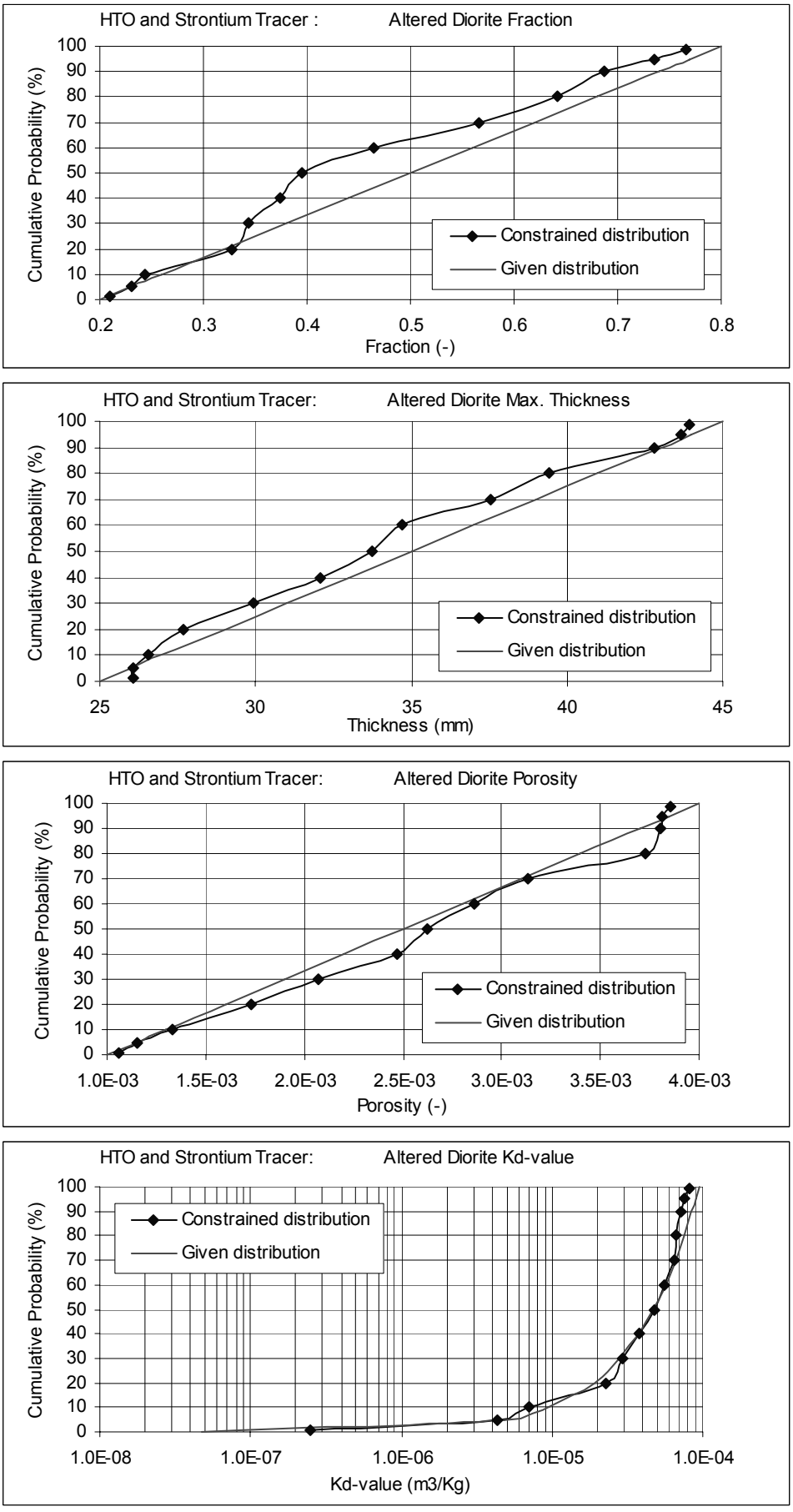

Figure 6-2 *Diorite Parameters*

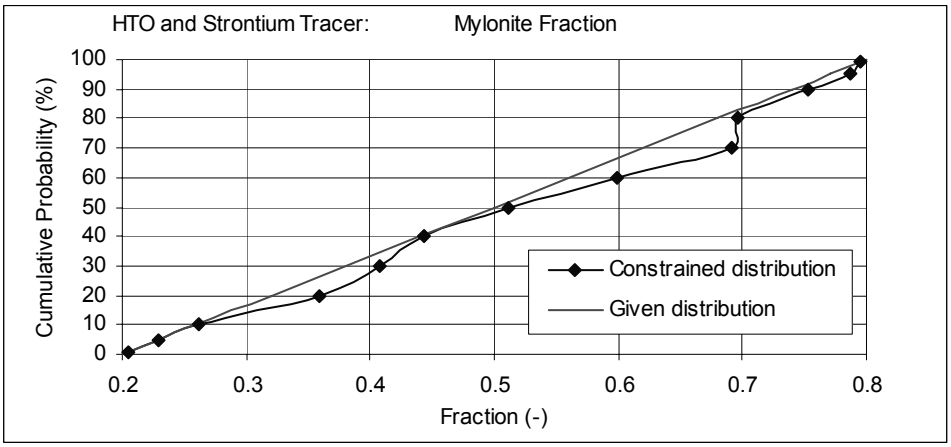

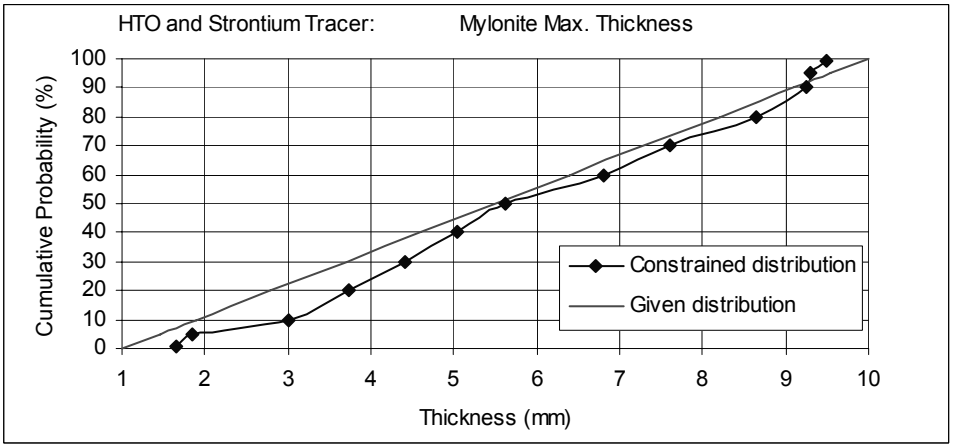

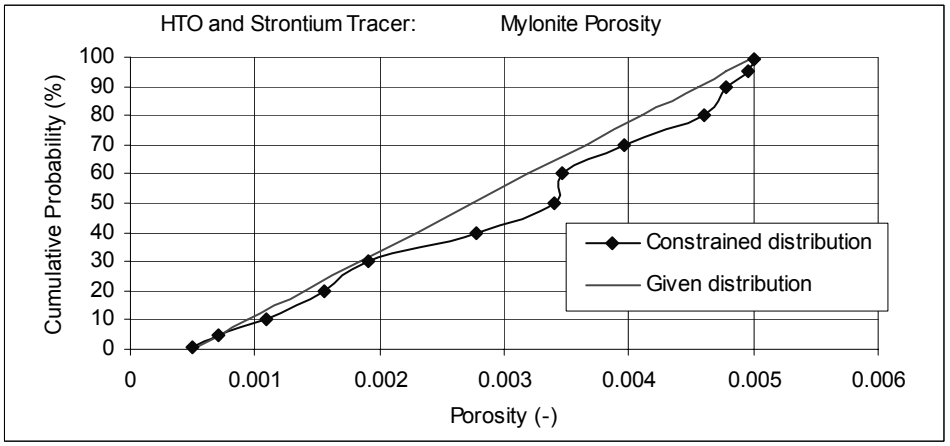

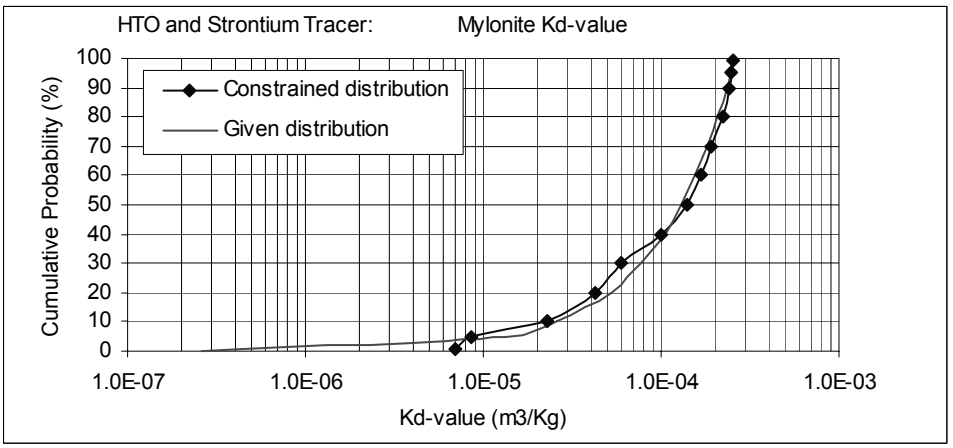

Figure 6-3 *Mylonite Parameters*

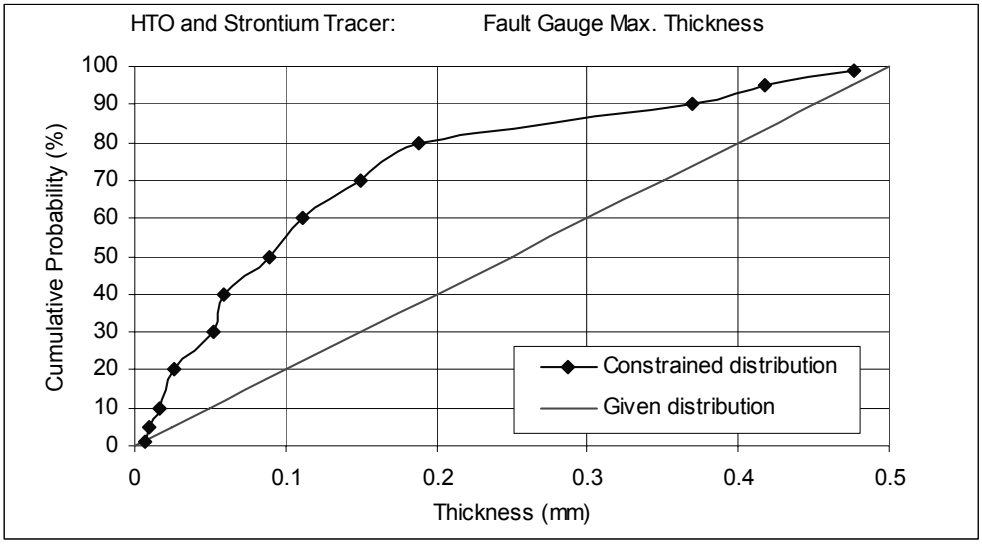

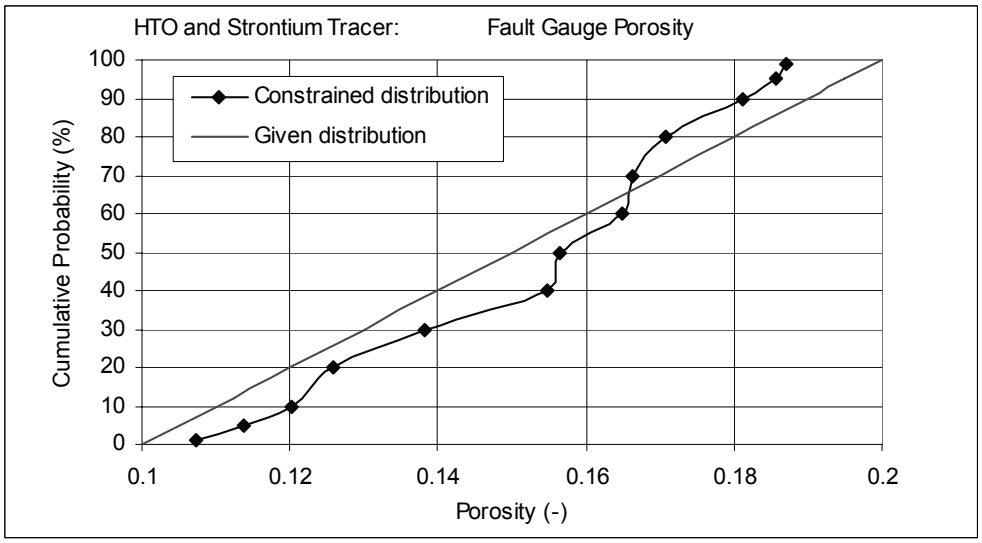

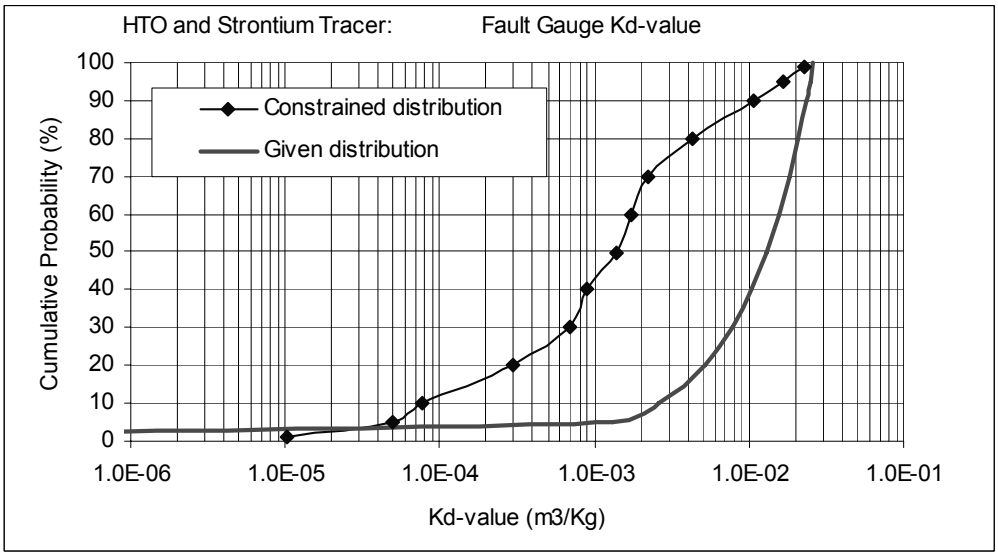

Figure 6-4 *Fault Gouge Parameters*

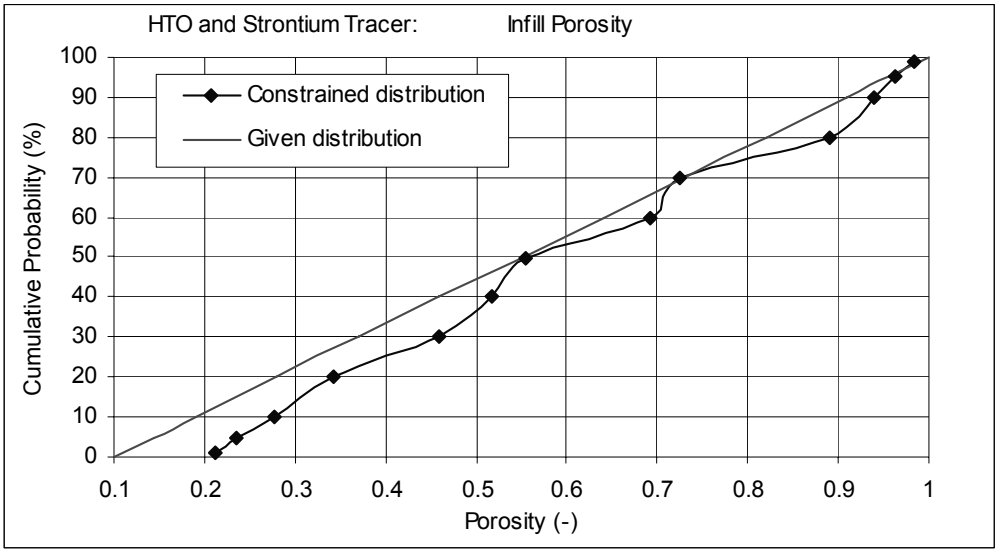

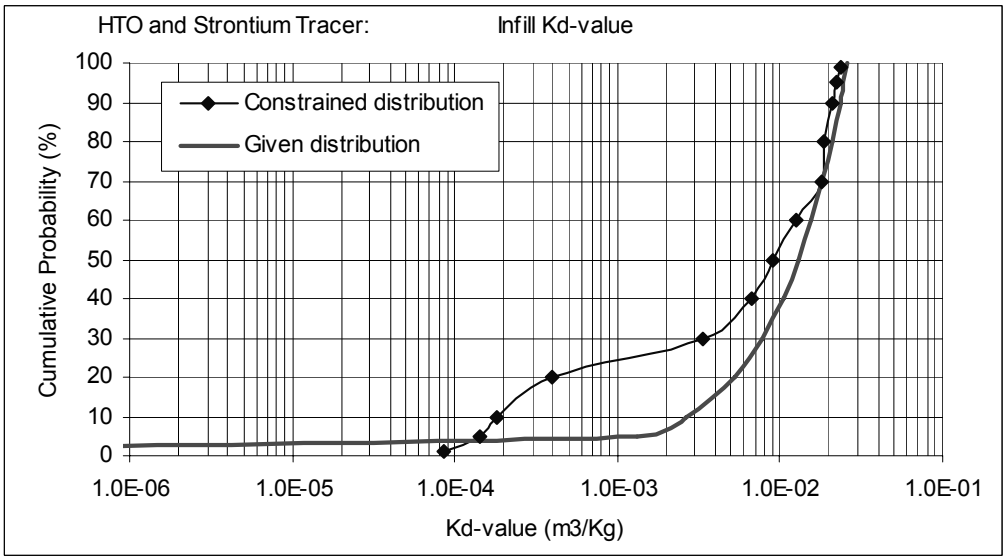

Figure 6-5 *Infill Parameters*

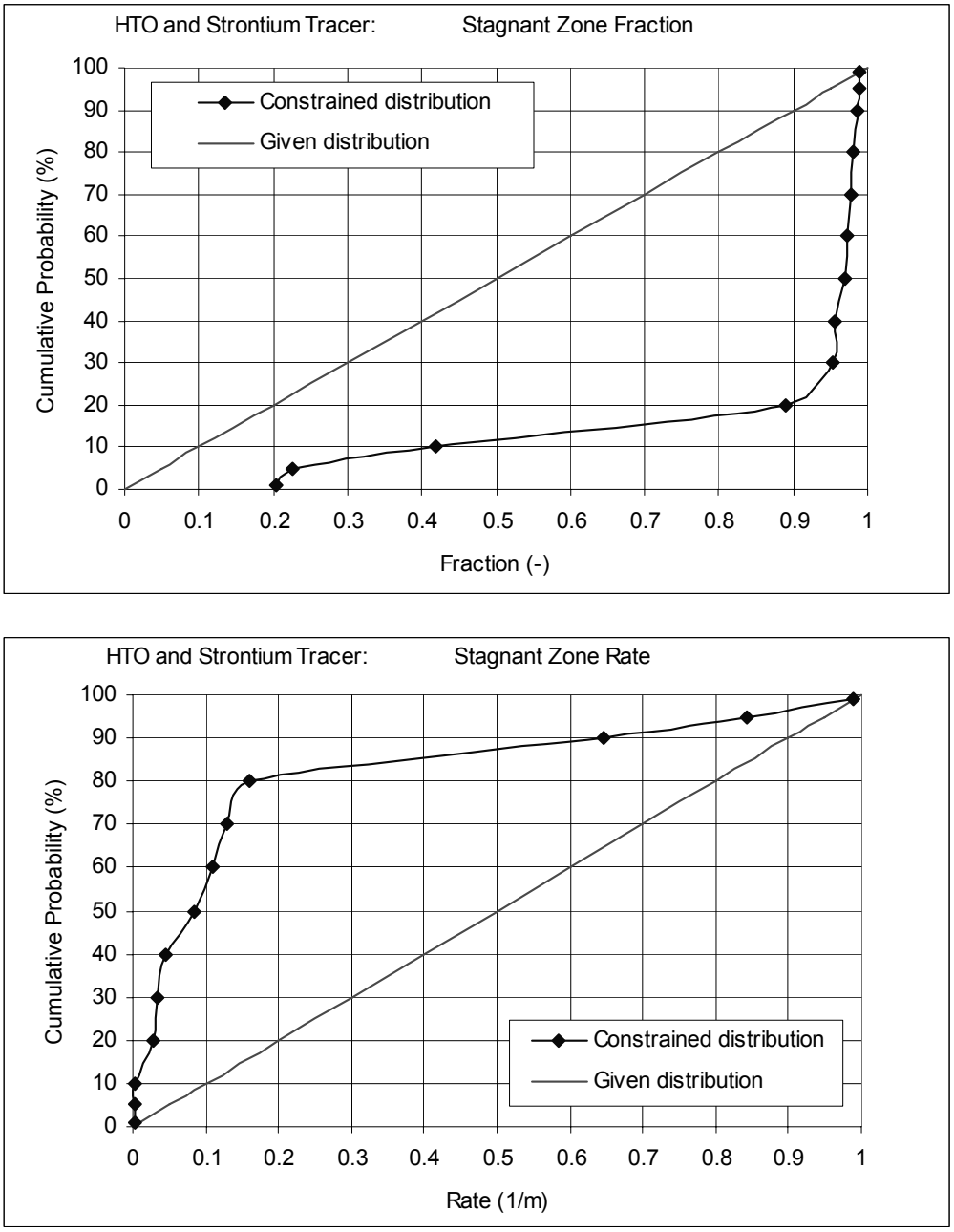

Figure 6-6 *Stagnant Zone Parameters*

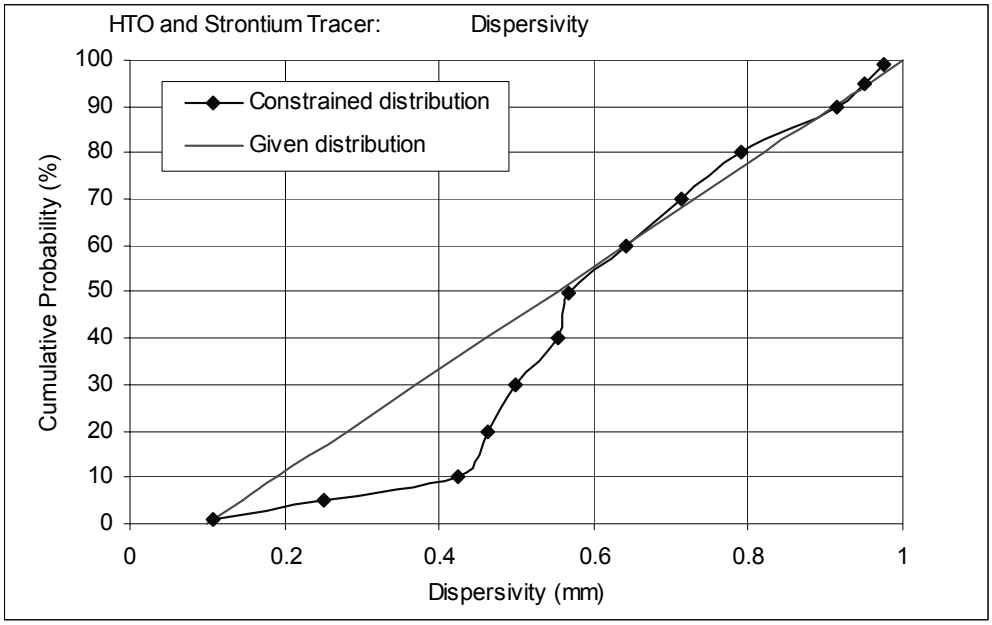

Figure 6-7 *Dispersivity Parameter*

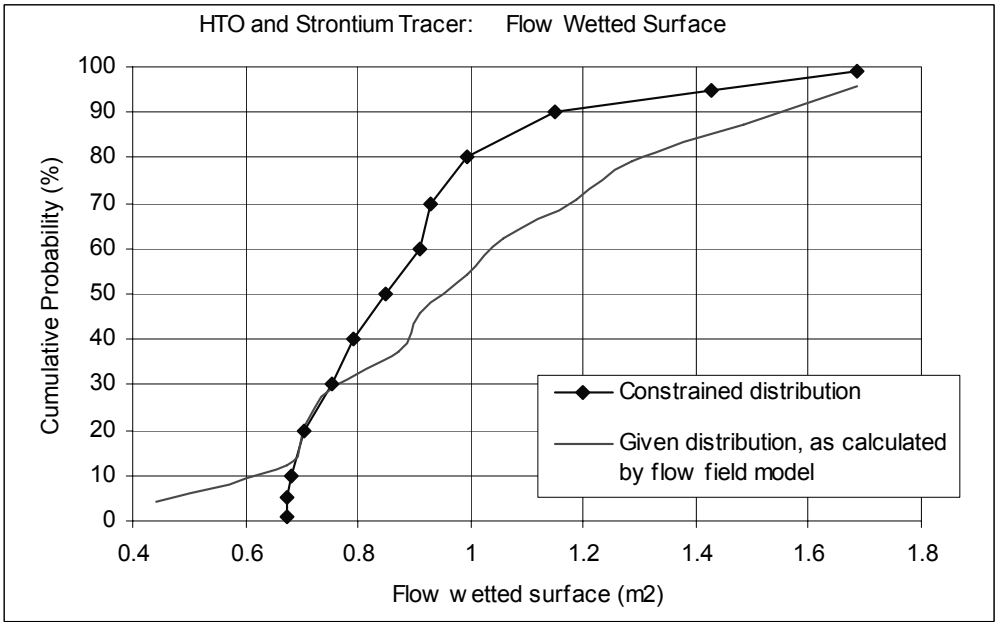

Figure 6-8 *Flow Wetted Surface (wet area).*

7 TASK 6A – Discission and conclusion

The purpose of Task 6A is to model and reproduce selected TRUE-1 trace tests and thereby assess the constraining power of these tests, i. e. the capability to quantify the basic characteristics of the parameters and processes affecting the radionuclide transport in the fractured rock.

The tracer tests were conducted by a simultaneous injection of several radioactive tracers with different characteristics. This study concerns an evaluation of the transport of HTO and Strontium

The following parameters were studied.

-Altered Diorite Rock: Amount along plume, Thickness, Porosity and Kd-value.

-Mylonite Rock: Amount along plume, Thickness, Porosity and Kd-value.

-Fault Gouge: Thickness, Porosity and Kd-value.

-Infill (fracture filling): Porosity and Kd-value.

-Stagnant zones: Amount along plume and exchange Rate.

-Dispersivity.

-Flow wetted surface area.

-Combined parameters: F-parameter and retardation factor.

The tracer tests, with HTO and Strontium were evaluated separately and jointly. The analyses demonstrated that the derived constraining powers were not the same for the three different analyses. The separate HTO analysis demonstrated less constraining power than the separate Strontium analysis. This is also partly reflected by the number of accepted realisations produced by the different tests. Using the same relative criteria for the acceptance of a realisation, the numbers of accepted realisations produced by the different analysis varied substantially. Considering the first analysis i.e. the HTO tracer test, 0.40% of the realisations were accepted. Considering the second analysis i.e. the Strontium tracer test, only 0.03% of the realisations were accepted. Hence, the Strontium test is more discriminating. For the third analysis, i.e. the combined test, the criteria for acceptance were relaxed compared to the separate tests, nevertheless only 0.01% of the realisations were accepted. The results of the third analysis (the combined test) were very close to the results of the separate Strontium analysis. Hence, it is the Strontium tracer that determines the results of the combined test.

It is important to note that even if the constraining powers demonstrated by the evaluation of the different tracers tests differ, there is not necessarily a contradiction between the results. The results reflect different properties of the system studied. The differences occur because the Strontium test is more discriminating; which is demonstrated by the results of the combined test that is very close to the results of the Strontium test.

The analyses of constraining power demonstrates three different types of results:

- The constrained distributions are identical to the given distributions. For such a situation no constraining power is demonstrated considering the parameter studied.
- The constrained distributions have the same range as the given distribution, but demonstrate another probability density function. This is an indication of some constraining power. Because a probabilistic simulation is dependent on both the range and type of probability density function characterising a parameter. (Even if the range is the same for the constrained and given distributions, there is still constraining power; because, if the probabilistic approach is continued to predictive simulations, and if the constrained distributions are used as input data for such simulations, the resulting predictions will depend not only of the range of the input data but on the probability density function of the input data.)
- The constrained distribution has a different range as the given distribution, and demonstrates a different probability density function. This is an indication of genuine constraining power.

A general conclusion, based on the assessment of the constraining power of the HTO and Strontium tracer tests, is that the tracer tests will not produce a large constraining power as regards any of the parameters studied.

The Diorite and the Mylonite rock is located behind the Fault Gouge, and not in direct contact with the flowing water. No constraining power is demonstrated considering the properties of these two rock types (amount, thickness and porosity). It is likely that this result is given by the relatively short time-scale of the experiments. The mass exchange with the inner zones is insignificant during such short time.

The Fault Gouge is located on the surface of the fracture planes and in direct contact with the flowing water. In the Strontium test no constraining power, was demonstrated as regards the porosity of this material, in comparison the HTO test demonstrated some very weak constraining power regarding the porosity. More constraining power was demonstrated as regards the thickness of the Fault Gouge. For the Fault Gouge thickness, the ranges of the constrained distributions were the same as in the given distributions, but the constrained distributions demonstrated very different probability density functions. The range of the Fault Gouge Kd values was defined as very large in the given distribution. The Strontium test demonstrated a distribution with a smaller range.

A filling material (the Infill) is specified inside the open space of the fracture studied, this material is in direct contact with the flowing water. For the HTO tracer a constraining power was demonstrated for the porosity of the Infill, but primarily as regards the probability density function and not as regards the range of accepted values. In contrast, the Strontium test demonstrates no constraining power for the Infill porosity. The range of the Infill Kd values was defined as very large in the given distribution. The Strontium test demonstrated a distribution with a smaller range. The constrained distribution of Kd-values were approximately the same for both the infill and the Fault Gouge.

Zones of stagnant water are specified inside the fracture. The amount of such stagnant water (fraction) and the rate with which this water interacts with the flowing water is also analysed. Constraining power was demonstrated as regards the Stagnant Zone Fraction and Stagnant Zone Rate. For both the Fraction and the Rate, the ranges of the constrained distributions were the same as in the given distributions, but the constrained distributions demonstrated a different probability density function. Hence, some constraining power was demonstrated for these properties.

- Considering the Strontium test and the Stagnant Zone Fraction, 80% of the accepted realisations demonstrated a Fraction larger than 0.77. Hence, most of the accepted simulations had a large amount of stagnant zones, but a few simulations with very small amount of stagnant zone were also accepted. These results are different compared to the results of the HTO tracer test; the HTO tracer demonstrated a large amount of accepted realisations with a small stagnant zone.

- Considering the Strontium test and the Stagnant Zone Rate, 90% of the accepted realisations had a Rate less than 0.15. Hence, most of the accepted simulations had small values of the Rate, but a few simulations with large values of Rate were also accepted. These results are different to the results of the HTO tracer test, for the HTO tracer the constraining power as regards the Rate was much weaker, and most of the accepted realisations had rates larger than those of the accepted Strontium realisations.

Comparing the constrained and given parameter distributions, the differences in the probability density functions of the stagnant zone parameters are larger than for any other parameters, and this is an indication of some constraining power. But, the ranges of the constrained parameter distributions for the stagnant zones are identical to the ranges of the given distributions; hence acceptable fits to measured values were found for all different values of the stagnant zone parameters (but not for all combinations). In addition, the probability density functions derived with the HTO tracer are very different (close to a mirror image) from the probability density functions derived with the Strontium tracer. Together this indicates that the concept of a stagnant zone is a very useful concept when modelling and matching breakthrough curves, but its ability to represent the actual processes and properties that occur along the fracture plane should be considered with care.

The dispersivity of the flow domain was also analysed and the results demonstrated a weak constraining power for this parameter. The accepted realisations of the Strontium test demonstrate results that are a mirror image of the results derived from the HTO test.

The flow wetted surface area (or the wet area) is the area on the fracture plane, along which the transport takes place. The area is defined as the sum of the areas on the upper and the lower planes. A distribution of possible areas was derived from the modelling of the flow field (flow modelling); this distribution was transferred to the transport model and defined as the given distribution of the flow wetted surface. The transport model reduces the size of the cross-sectional area where the flow takes place, by introducing the stagnant zones. Hence, there are two different concept of flow wetted surface area: (i) Flow wetted surface area including the stagnant zones and (ii) Flow wetted surface area without the stagnant zones. We have studied both concepts. Considering the first concept (including stagnant zones in the flow wetted surface area), the transport modelling demonstrated no constraining power by use of the Strontium tracer.

However, for the second concept (excluding the stagnant zones from the flow wetted surface area), the transport modelling demonstrates a significant constraining power for this parameter.

The F-parameter is a combined parameter characterising some aspects of the flow, it is defined as the product of several different parameters (see Equ. 4-2). The transport modelling demonstrated a significant constraining power as regards the F-parameter.

The retardation factor is a combined parameter that represents the retardation of the front of a migrating contaminant, relative the movement of the bulk mass of water, assuming that the retardation is caused by a fast reversible adsorption with a linear isotherm (see Equ. 5-3). The transport modelling demonstrated a significant constraining power considering the retardation factors of the materials in direct contact with the flowing water (Infill and Fault Gouge), but no constraining power for the materials not in direct contact with the flowing water (Mylonite and Diorite).

A summary of the constraining power of the tests is given in Table 4-4 and Table 5-5.

Considering all realisations established with the given parameter distributions, together these realisations demonstrate a large variation in simulated breakthrough curves. The lower envelope of all simulated breakthrough curves is very close to zero (extremely retarded realisations) and the upper envelope is much higher than that of the measured breakthrough. The median (50^{th} percentile) breakthrough curve is very low and has a much later arrival time of the peak, than the measured breakthrough. This indicates that only a small fraction of all the simulated breakthrough curves will match the measured breakthroughs. The given parameter distributions (see Sections 4.1 and 5.1), are based on data that is considered as reasonable, however these distributions will, with a very large probability, produce breakthrough curves that are far from the measured breakthroughs.

Compared to all simulated breakthrough curves, the accepted breakthrough curves are characterized by earlier arrival times and a higher peak (mass flow). More than 99.9% of the simulated breakthrough curves have a slower breakthrough and a smaller peak (compared to the accepted curves). By studying the properties of the constrained distributions it is possible to see how the match to the measured breakthrough curves was obtained (i.e. faster breakthroughs, higer peaks as well as the shape of the tail).

In the constrained parameter distributions for Strontium, the stagnant zone fraction is preferred as large and the stagnant zone rate is preferred as small. Fraction is the cross sectional area occupied by stagnant zones, and rate is the exchange velocity from mobile zone to the stagnant zone. The stagnant zones will: (i) cause a delay of the breakthrough (of mass and peak in mass flow) as they will accumulate and release tracer mass, but (ii) a large stagnant zone will also produce a small cross sectional area available for the main advective transport (the mobile water), which caused a larger advective flow velocity and a faster tracer transport and earlier breakthrough.

In the constrained distributions for Strontium, the thickness of the Fault Gouge is preferred as small. The flowing tracer mass will interact with the Fault Gouge volume (thickness and porosity) by means of diffusion. A small thickness implies a small storage capacity, which will result in a rapid saturation of the storage volume and a faster breakthrough than would have been the case for large values of thickness.

In the constrained parameter distributions for Strontium, the distribution of Kd-values of Fault Gouge and Infill are smaller (smaller range and higher probability of small Kd-values) than in the corresponding given parameter distributions. Two types of linear retardation processes will take place in the model. (i) Equilibrium partitioning between the fluid in the pathway and an infill material; and (ii) equilibrium partitioning between the fluid in the pathway and a coating medium, i.e. the Fault Gouge. The partitioning processes are (in the model) simulated by means of the equilibrium-partitioning concept. Small Kd-values will produce a breakthrough curve with a higher peak and less emphasised tail, than a breakthrough curve produced with larger Kd-values. As mentioned in Section 5.6, there is an interesting relationship between the Stagnant zone fraction and the Infill Kd-value (also between the Stagnant zone fraction and the Fault Gouge Kd), in the constrained parameter distributions.

In the constrained parameter distributions for Strontium, the distribution of Dispersivity values is somewhat larger (smaller range and higher probability of larger values) than in the corresponding given parameter distributions. Dispersion is the tendency for a solute (tracer), dissolved in the groundwater, to spread out from the path that it would be expected to follow according to the advective hydraulics of the flow system. Diffusion and mechanical mixing during fluid advection cause dispersion. In the transport model the effect of mechanical mixing during fluid advection is controlled by a parameter called dispersivity. A large value of dispersivity will produce an early breakthrough, a wide breakthrough curve and a lower peak, compared to a breakthrough curve produced with small value of dispersivity.

The weak constraining power of the tracer tests studied (as demonstrated by the presented analyses), and the good match to measured values that was obtained with the parameter distributions studied, this situation reveals that a good match to measured values can be obtained for a very large spectrum of parameter values, and that the key to finding the good match is to understand how the parameter values should be combined.

We have divided the parameter distributions into three different sets that will be used in the Task 6B2 modelling.

- The given parameter distributions are the input data for the Task 6A modelling. The distributions are based on data given Task 6A and 6B specifications, by Selroos and Elert (2001) and Elert and Selroos (2001). In the given parameter distributions we presume that all parameters are independent.

- The constrained parameter distributions are the results of Task 6A. Based on the analyses of breakthrough curves, as produced by use of the Strontium tracer, we have derived the constrained parameter distributions. The constrained parameter distributions are based on the 89 realisations that produced breakthrough curves for Strontium with an acceptable match to the measured breakthrough (of Strontium). In the constrained parameter distributions we presume that all parameters are independent.

- The constrained coupled parameter distributions are also results of Task 6A, they consists of the ensemble of coupled parameter values as defined by the 89 accepted realisations. The difference compared to the constrained parameter distributions is that in the constrained coupled parameter distributions the individual parameter values are combined, according to the combinations of parameter values that resulted in the 89 accepted realisations. In the constrained coupled parameter distributions the parameters are combined in accordance to the accepted realisations and are not considered as independent. The probability distribution of the parameter values that takes place within the 89 accepted realisations are the same in: (i) the constrained parameter distributions and in (ii) the constrained coupled parameter distributions; the difference is in the way these values are combined.

8 TASK 6B2 – Modelling of flow field and flow paths

8.1 Introduction

This chapter presents the simulation of the flow field and of flow paths (flow modelling) inside Feature A. The flow modelling is based on several assumptions regarding the properties of the system studied these assumptions are presented below. Based on the results of the flow modelling, we have derived a probabilistic description of the shape of the plume of contaminated water (tracers) inside Feature A. The shape of the plume was propagated to the transport modelling.

8.2 Conceptual model

The tracer tests studied in Task 6A took place in a fractured rock mass, the part of the rock mass in which the tracers moved with the groundwater and interacted with the rock mass is called Feature A. For the simulation of tracers in Task 6B2, the same type of flow medium as in Task 6A is to be used. Feature A could be a single fracture or a system of fractures. We have assumed that Feature A is a single fracture that can be represented by a fracture plane with varying flow properties inside the fracture plane. The fracture is defined as a two dimensional plane. The heterogeneity in the flow properties along the fracture plane (the variation in flow properties) was represented by use of the stochastic continuum approach. The general conceptual model was based on the description given in "Task 6B2 Modeling task specification" (T6B2MTS) by Elert and Selroos (2001).

8.3 Computer code used

We have modelled the flow in Feature A by use of the GEOAN computer program. GEOAN is a computer program for simulation of groundwater flow and transport; the code is based on the finite difference approach, see Holmén (1992) and Holmén (1997).

8.4 Mesh and Conductivity

The fracture was defined as a quadrate of size 15 x 15 m, in line with the description given in the modelling specification (T6B2MTS, Elert and Selroos, 2001) The finite difference grid along the fracture plane was defined with the same properties as in Task 6A; hence, with a cell size of 0.2 m x 0.2 m and with a heterogeneous conductivity (see Figure 8-1). The heterogeneity in the flow properties along the fracture plane was defined as in Task6A. The heterogeneity was represented by a stochastic continuum. The conductivity field was defined as a Log-Normal distribution, with a geometric mean of 2.8E-4 m/s. The hydraulic aperture was set to 1 mm. The K-field was defined as not correlated. The standard deviation of the Log-Normal distribution of the K-values is a measure of the heterogeneity of the K-field. A standard deviation (STD) of

zero produces a homogeneous flow field in which all cells have a K-value equal to the geometric mean (2.8E-4 m/s). Larger values of the STD will create a heterogeneous flow field. Based on the results of Task 6A, the standard deviation was set to 1.0 in 10Log space.

We have also established a homogeneous flow model, presented in several figures and tables e.g. Figure 8-2 and Figure 8-8. It should be noted that the purpose of the homogeneous flow model is to demonstrate the flow field of a homogeneous flow medium. The homogeneous model is not used in the modelling of the transport processes.

8.5 Boundary conditions

For the established model we have used specified head boundary conditions along two opposing sides and the no-flow boundary condition along the other two sides (see Figure 8-1). The gradient between the upper and lower specified head boundaries was set to 0.001 (as specified in: T6B2MTS, Elert and Selroos, 2001). The simulation of the flow field was continued until steady state conditions were reached.

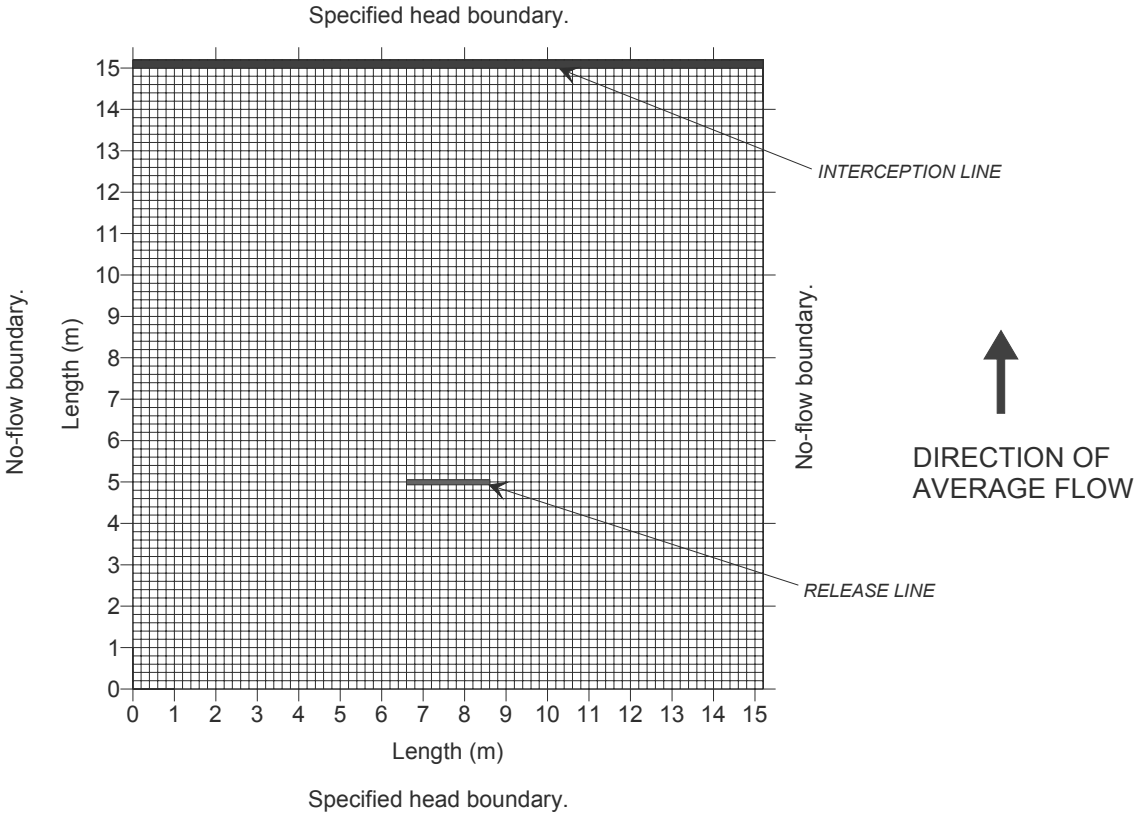

Figure 8-1 *Layout and boundary conditions of the flow model used in Task 6B2. Cell size is 0.2 m x 0.2 m. The tracers are injected along the release line and recovered along the interception line.*

8.6 Simulated flow situation

The simulated situation is specified in T6B2MTS (Selroos and Elert , 2001). The gradient between the upper and lower specified head boundaries is set to 0.001. The flow situation studied is a steady state situation; hence no changes in flow will take place with time. Because of the heterogeneous properties of the flow domain (the heterogeneous conductivity values), the flow along the fracture plane will vary from point to point, both as regards direction and size.

As specified in T6B2MTS (Selroos and Elert , 2001), the purpose of Task 6B2 is to simulate the transport of tracers in a fracture plane, the tracers are injected along a release line and recovered along a interception line. The length of the release line is 2 m and the distance between the release line and the interception line is 10 m. The position of the release and interception lines, as defined in the established model is given in Figure 8-1 (above).

The shortest straight line between the two specified head boundaries gives the average direction of flow, but the average length of a flow path will be somewhat longer than the length given by the shortest straight line, as flow paths in a heterogeneous flow medium will demonstrate a tortuous pattern.

In the model, the heterogeneous flow domain is represented by a two-dimensional stochastic continuum, it follows that the average size of flow will be given by the gradient between the two boundaries and the geometric mean of the conductivity values of the flow domain (and the hydraulic aperture), because for the average (equivalent or effective) conductivity of a two-dimensional heterogeneous stochastic continuum there are no scale effects that needs to be considered, see Matheron (1967) (or Holmén (1997) for numerical calculations), and the average (equivalent or effective) conductivity is given by the geometric mean conductivity of the conductivity field.

In the presented model, the geometric mean of the conductivity (K) is 2.8E-4 m/s and the hydraulic gradient (I) is 0.001, assuming a homogeneous flow domain these properties will produce a specific flow (q) equal to 2.83E-7 m/s, as given by the equation below:

Equ. 8-1

$$q = K\ I$$

The introduction of a length (L) along which the flow takes place and the concept of effective porosity (η_{eff}) makes it possible to calculate a groundwater transport time for a representative homogeneous flow medium, as given by the equation below:

Equ. 8-2

$$t = \frac{L}{\frac{1}{\eta_{eff}} K\ I}$$

By use of the equation above and considering a section of length 10 m, a specific flow equal to 2.83E-7 m/s and an effective porosity of 0.5, the resulting transport time will be 2.3 years, and with an effective porosity of 0.1 the resulting transport time will be 0.5 years. The distance between the release and interception lines is 10 m; hence by assuming a representative homogeneous flow medium, we estimate the average transportation time for the groundwater between these lines to 2.3 years or 0.5 years dependent on the effective porosity.

In a heterogeneous flow medium, much larger velocities than the velocity of a homogeneous flow medium will take place along routes of large conductive and much slower velocities along parts with a small conductivity. Hence, for a heterogeneous flow medium, much shorter transportation times may take place for some of the water and much larger transportation times for other water.

Compared to Task 6A, the groundwater flow velocities of Task 6B2 are much slower. In Task 6A the HTO tracer demonstrated a measured peak at the extraction well after about 7 hours, the distance between the injection well and the extraction well is 5 metres. In Task 6B2, the distance between the release line and interception line is 10 metres, and the advective transportation time between release line and interception line are probably within a few months. Hence, the flow velocity of Task 6A is approx. 100 times faster than that of Task 6B2.

8.7 Method for simulation of flow paths

After steady state conditions were reached in the simulations a tracer was injected along the release line (see Figure 8-1). The tracer was simulated by use of virtual particles that followed the flow field along the fracture plane towards the interception line. The flow paths were determined by use of an analytic solution (Pollock, 1989). Only advection was simulated, no hydromechanical dispersion and no chemical diffusion etc were included in the simulations of flow paths.

For each realisation of the flow field, and along the injection line, and inside each one of the 10 cells that takes place along the injection line, 100 flow paths were released. Hence, the total number of flow paths along the release line becomes 1000 for each realisation, as there are 10 cells along the release line. Examples of the resulting flow paths are given in Figure 8-2 through Figure 8-7.

8.8 Methodology of the stochastic approach

A large number of different realisations of the conductivity field were created. The flow fields of these realisations were calculated by use of the boundary conditions discussed above. Flow paths were released in the flow fields of the different realisations. The paths released along the release line create a plume that describes the flow between the release line and the interception line. The properties of the plumes of the different realisations were analysed.

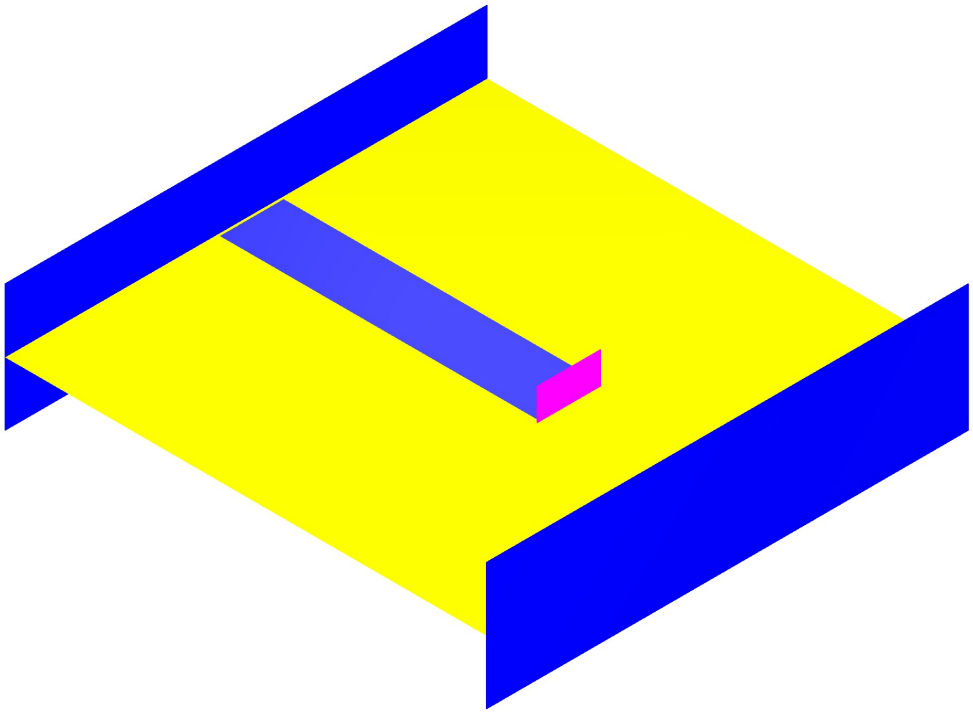

Figure 8-2 *Velocity field and flow paths for a situation with a homogeneous flow domain (three-dimensional view). As the flow is uniform the velocity is the same everywhere and the flow paths are straight lines. The flow paths are marked with blue colour on the yellow fracture plane. The release line is marked with a purple bar. The flow paths are marked with blue colour. The homogeneous model is not used in the transport modelling.*

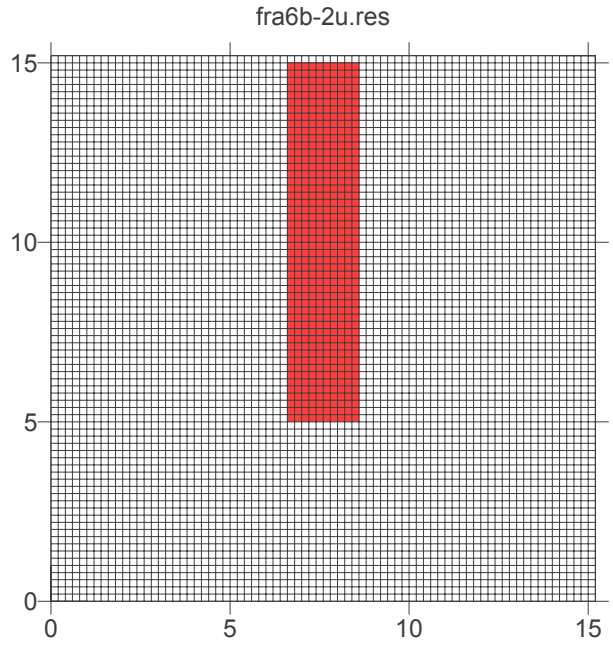

Figure 8-3 *Finite difference mesh and flow paths for a situation with a homogeneous flow domain.*

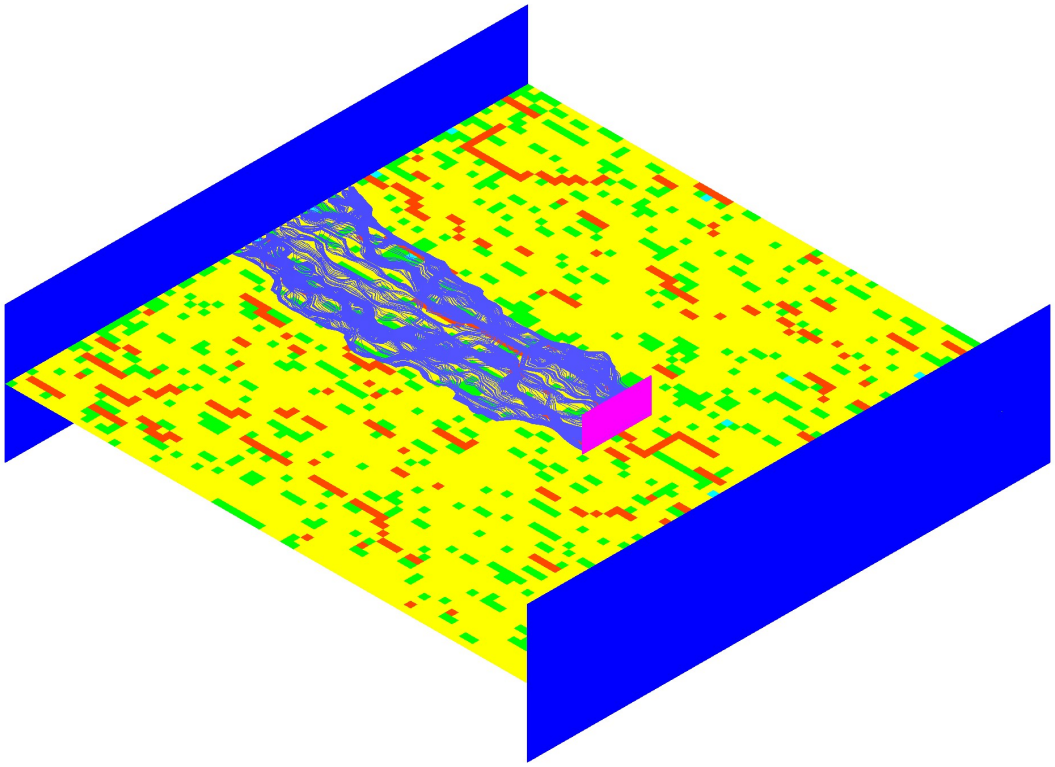

Figure 8-4 *Velocity field and flow paths for a situation with a heterogeneous flow domain (three-dimensional view). Size and direction of flow varies along the fracture plane. Areas with large flow velocity are marked with red colour, areas with smaller flow velocity are marked with yellow and areas with the smallest flow velocity are marked with green. The release line is marked with a purple bar. The flow paths are marked with blue colour. The presented realisation produces the largest plume of all studied realisations.*

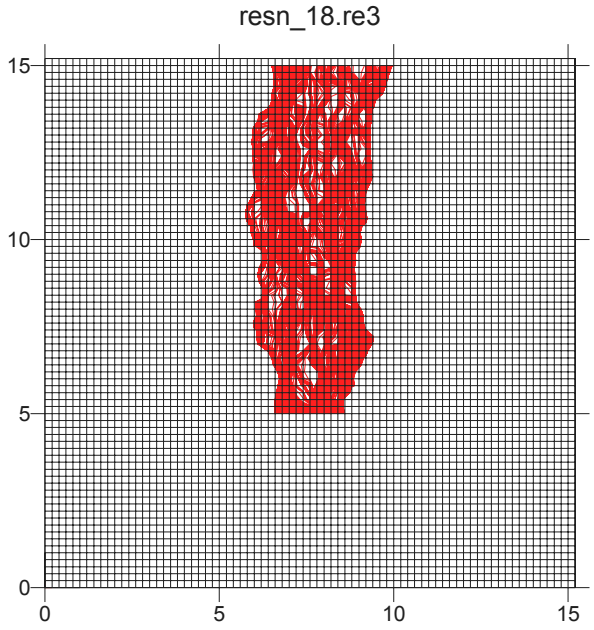

Figure 8-5 *Finite difference mesh and flow paths for a situation with a heterogeneous flow domain. The presented realisation produces the largest plume of all studied realisations.*

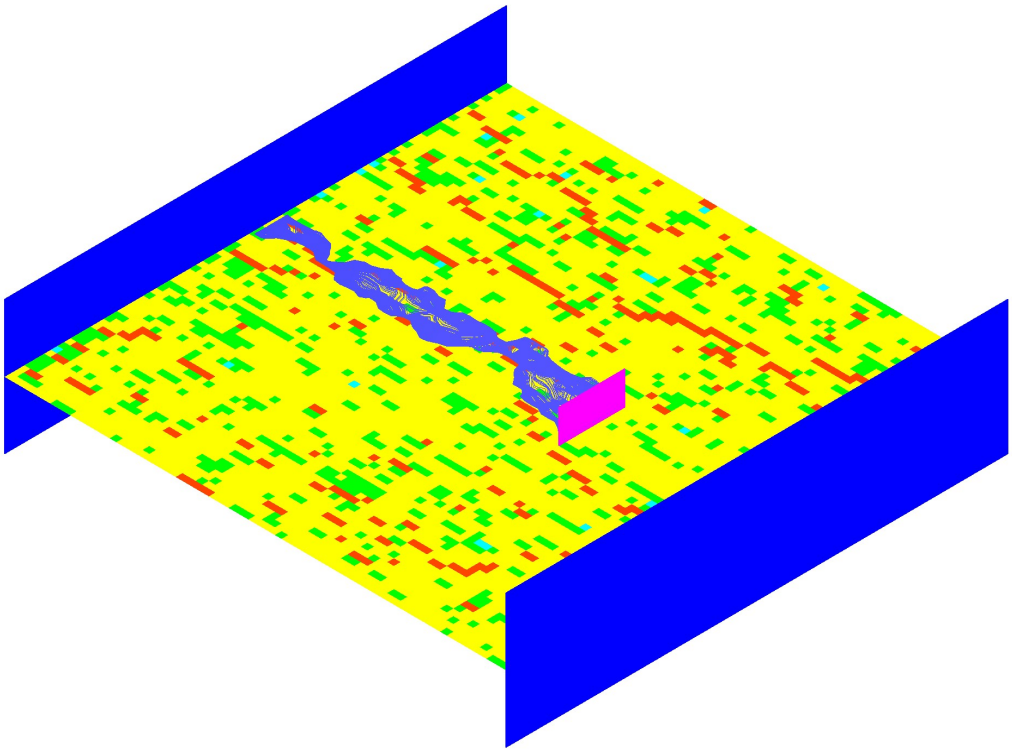

Figure 8-6 *Velocity field and flow paths for a situation with a heterogeneous flow domain (three-dimensional view). Size and direction of flow varies along the fracture plane. Areas with large flow velocity are marked with red colour, areas with smaller flow velocity are marked with yellow and areas with the smallest flow velocity are marked with green. The release line is marked with a purple bar. The flow paths are marked with blue colour. The presented realisation produces the smallest plume of all studied realisations.*

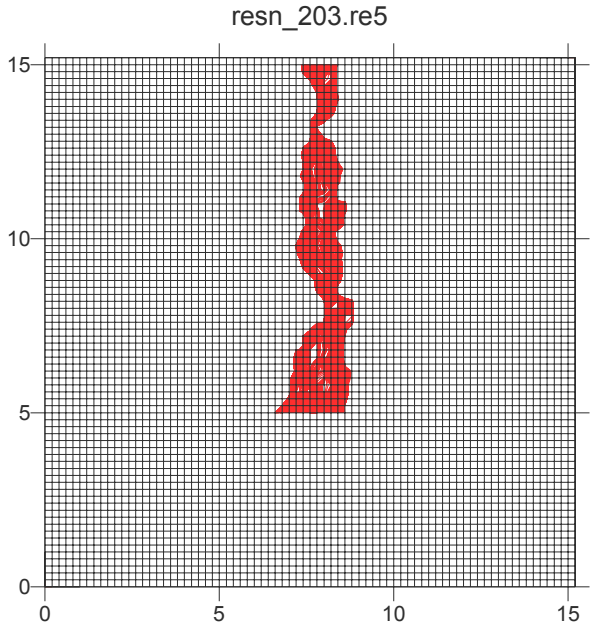

Figure 8-7 *Finite difference mesh and flow paths for a situation with a heterogeneous flow domain. The presented realisation produces the smallest plume of all studied realisations.*

8.9 Results considering the entire plume

In this section we will present the results of the analyses of the entire plume.

8.9.1 Probability distribution of flow along the release line

The flow that passes the release line is also the flow that takes place inside the plume. The groundwater flow along the release line varies from section to section (cell to cell), as the flow domain is heterogeneous. Also the total flow taken over the whole of the release line varies from realisation to realisation. Figure 8-8 below presents the probability distribution of the total flow along the release line, for a model with a heterogeneous flow medium and a model with a homogeneous flow medium. Considering a heterogeneous flow medium, the flow along the release line is 17.2 Litre/hour for the 10^{th} percentile and 28.3 Litre/hour for the 90^{th} percentile, for a homogeneous flow medium the flow is 17.8 Litre/hour.

The median (the 50^{th} percentile) of the flow along the release line of the heterogeneous flow medium is larger than the flow of the homogeneous flow medium. This may at first look erroneous as we have in a previous section stated that the average flow of the heterogeneous flow medium should be given by the geometric mean conductivity. However, that statement is only applicable for the whole of the modelled domain: The lateral boundaries of the whole of the modelled domain are no-flow boundaries. The release line takes place inside the modelled domain and its lateral boundaries are not no-flow boundaries. When the conductivity along the release line is large, flow from the surroundings will converge towards the release line, and thereby create a larger flow along the line than if the boundaries of the line had been no-flow boundaries.

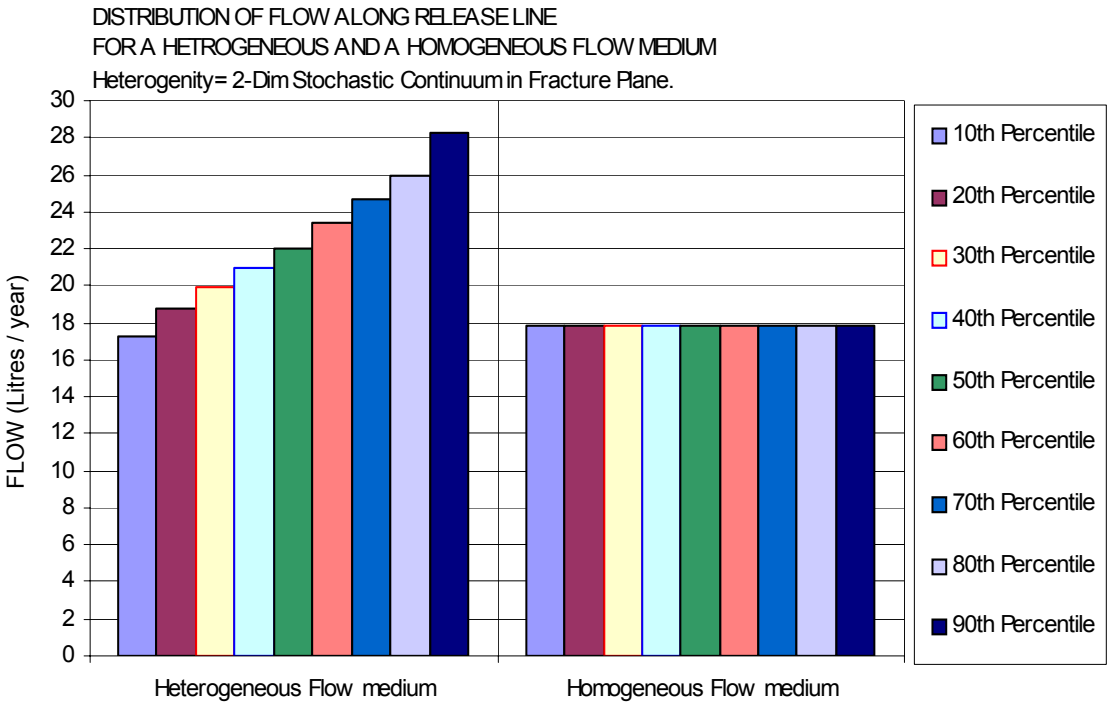

Figure 8-8 *Probability distribution of flow along the release line.*

8.9.2 Probability distribution of flow wetted surface area

By analysing the distribution of flow paths from the injection line–the plume–it is possible to estimate the flow wetted surface area (wet area). In this study the flow wetted surface area is defined as two times the extension of the plume (the area on the upper fracture plane and the area on the lower fracture plane).

Figure 8-9 below presents the probability distribution of the flow wetted surface area, for a model with a heterogeneous flow medium and a model with a homogeneous flow medium. Considering a heterogeneous flow medium, it is well demonstrated by the figure that the size of the flow wetted surface area changes substantially between different realisations of the flow field; the flow wetted surface area is 30.9 m^2 for the 10^{th} percentile and 50.2 m^2 for the 90^{th} percentile. For a homogeneous flow medium, the flow wetted surface area is 40 m^2.

The flow wetted surface area of the plume is given by flow paths released along the whole length of the release line. The flow properties along the release line vary; therefore some of the paths may converge while other may spread out over a large area. The probability that all flow paths should converge into a small channel is extremely small; hence the probability for having a flow wetted surface area smaller than 30 m^2 is small (less then 10%). It is also very unlikely that all flow paths should spread out over large areas; hence the probability for having a flow wetted surface area larger than 50 m^2 is also small (less then 10%).

An interesting result is that the calculated median (the 50^{th} percentile) of the flow wetted surface area of the heterogeneous flow medium is very close to the flow wetted surface area of the homogeneous flow medium.

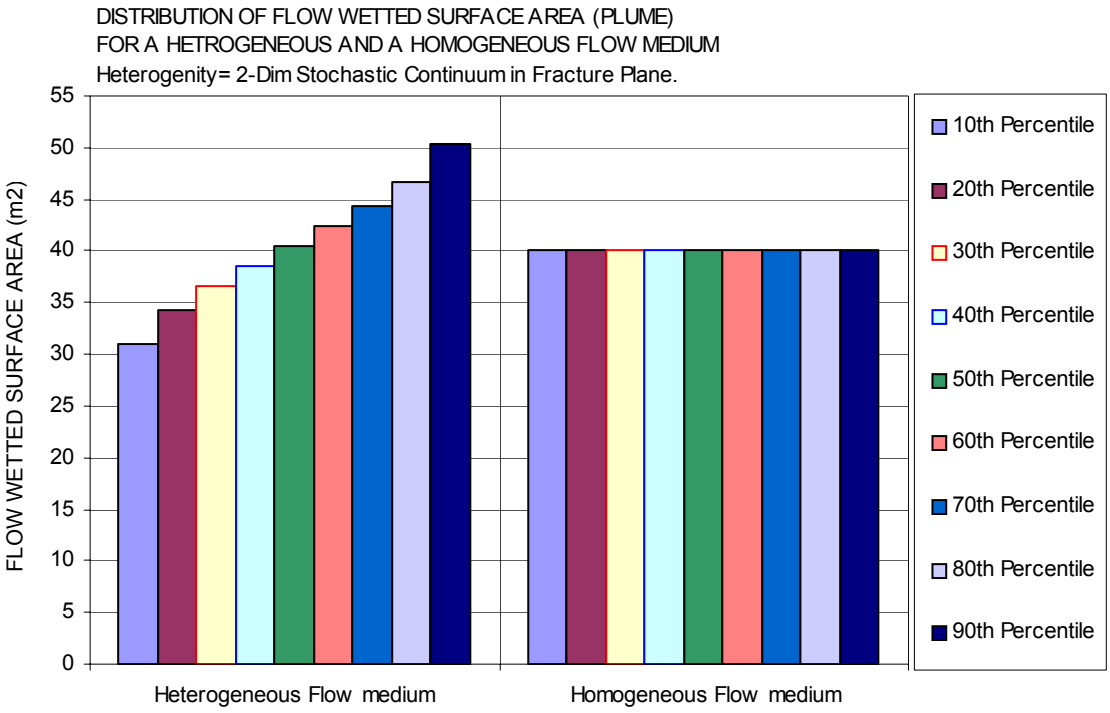

Figure 8-9 *Probability distribution of flow wetted surface area of the plume.*

8.9.3 Probability distribution of shape of flow wetted surface area

In a flow medium with heterogeneous properties, the plume has a non-uniform shape and size. The shape and size of the plume varies between different realisations. At the release line however, the plume has the same width in all realisations, but only a metre or so from the release line the shape and size of the plume varies a lot between different realisations.

A few metres from the release line, the variation in width of plume is the same as at larger distances from the release line. Starting a metre or so from the release line, the variation in size of plume is the same for sections of equal length taken along the average flow direction. This is because at a certain distance from the boundaries, the probability distributions of direction and size of flow is the same (everywhere in the model). Therefore the variation in plume size and shape will be the same. In Task 6B2, the average flow field is not converging as in Task 6A, there is no average trend in size of plume with distance form release line (except for the first metre or so). This is different from Task 6A, because in 6A the flow field was converging towards the extraction well.

The probability distributions of the sizes of different sections along the plume are given in Figure 8-10. The plume is separated into seven separate sections of equal length along the average flow direction. The first section is closest to the release line; and the last section is closest to the interception line. It is demonstrated by Figure 8-10 that the probability distribution of the size of the plume is approximately the same regardless of distance form release line (except for the first metre or so).

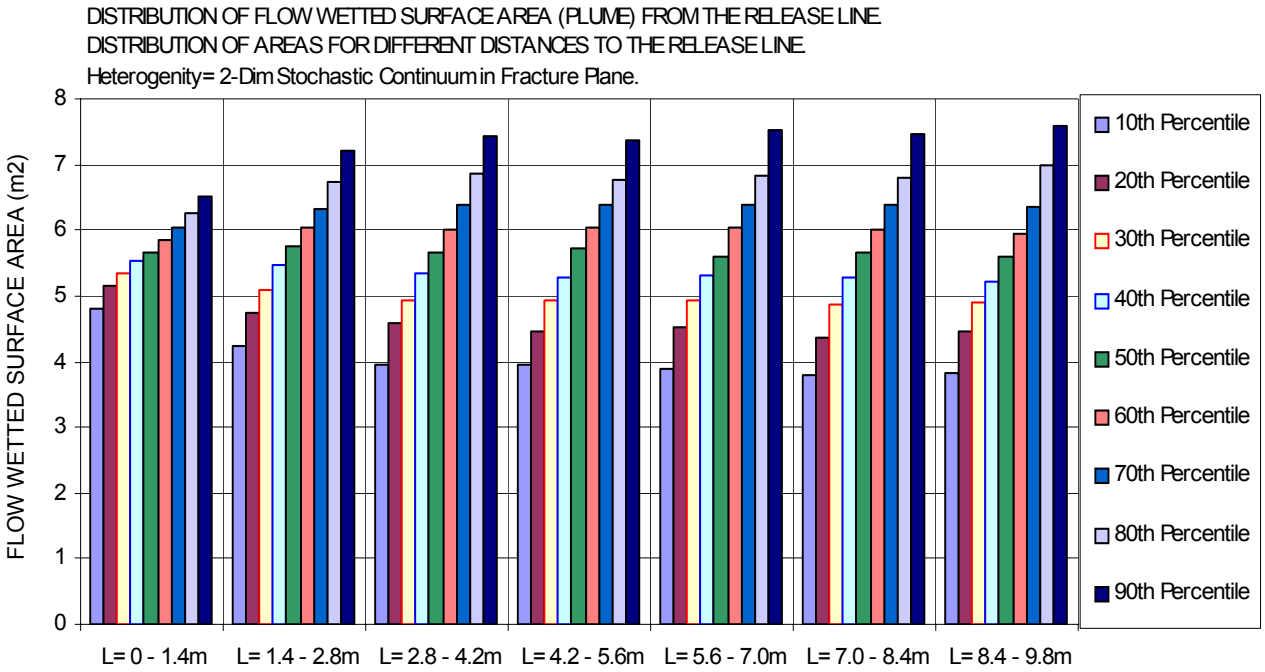

Figure 8-10 *Probability distribution of shape of flow wetted surface area of the plume.*

8.9.4 Probability distribution of length of flow paths inside plume

In a homogeneous flow medium, the shortest line between the two specified head boundaries gives the length of the flow paths.

In a heterogeneous flow medium, the shortest line between the two specified head boundaries gives the average direction of flow, but the average length of a flow path will be somewhat longer than the length given by the shortest line, as flow paths in a heterogeneous flow medium will demonstrate a tortuous pattern.

Figure 8-11 below presents the probability distribution of the length of the flow paths inside of the plume, for a model with a heterogeneous flow medium and a model with a homogeneous flow medium. No flow path can be shorter than 10 m, as this is the distance between the release line and the interception line.

Considering a heterogeneous flow medium, the variation in flow path length is not large, compared to the average length of the flow paths; the length is 10.79 m for the 10^{th} percentile and 11.56 m for the 90^{th} percentile. For a homogeneous flow medium, the length is 10 m.

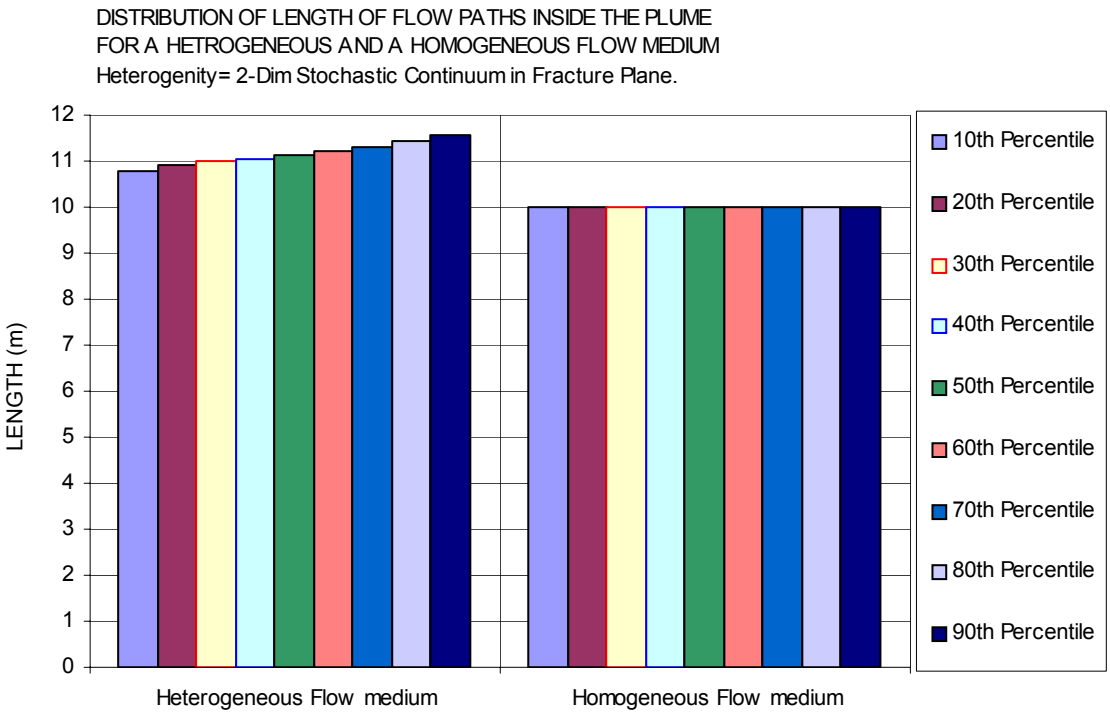

Figure 8-11 *Probability distribution of length of flow paths inside the plume.*

8.9.5 Correlation between flow wetted surface area and flow inside plume

In a heterogeneous flow medium both the size of the plume and the flow inside the plume varies between different realisations. There is however a correlation between the size of the plume (the flow wetted surface area) and the flow inside the plume (release flow). The correlation is presented below in Figure 8-12 (a scatter plot based on 700 different realisations). The following conclusion can be made based on Figure 8-12. Size of plume and size of flow demonstrates a strong positive correlation; hence it is very likely that if the flow is large along the release line, also the flow wetted surface area of the plume will be large.

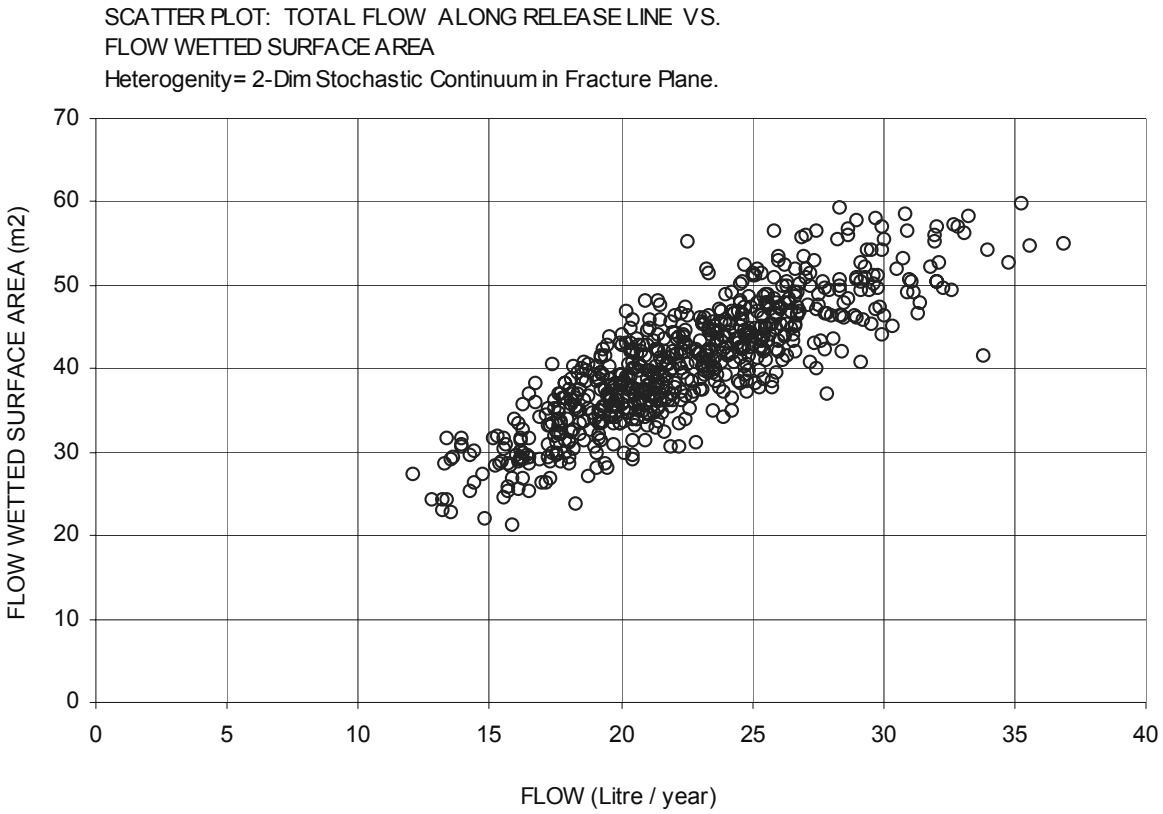

Figure 8-12 *Correlation between flow wetted surface area and flow inside the plume.*

8.9.6 Correlation between length of flow paths and flow inside plume

In a heterogeneous flow medium both the size of the plume and the flow inside the plume varies between different realisations. In general the flow paths inside a plume demonstrates a tortuous pattern.

Is there a correlation between the mean flow path length of a plume and the flow inside the plume? To answer that question we produced Figure 8-13. The figure is a scatter plot based on 700 different realisations that presents mean flow path length versus the flow inside the plume (the release flow). As can be seen from the figure there is no correlation (or a very weak correlation) between the studied parameters.

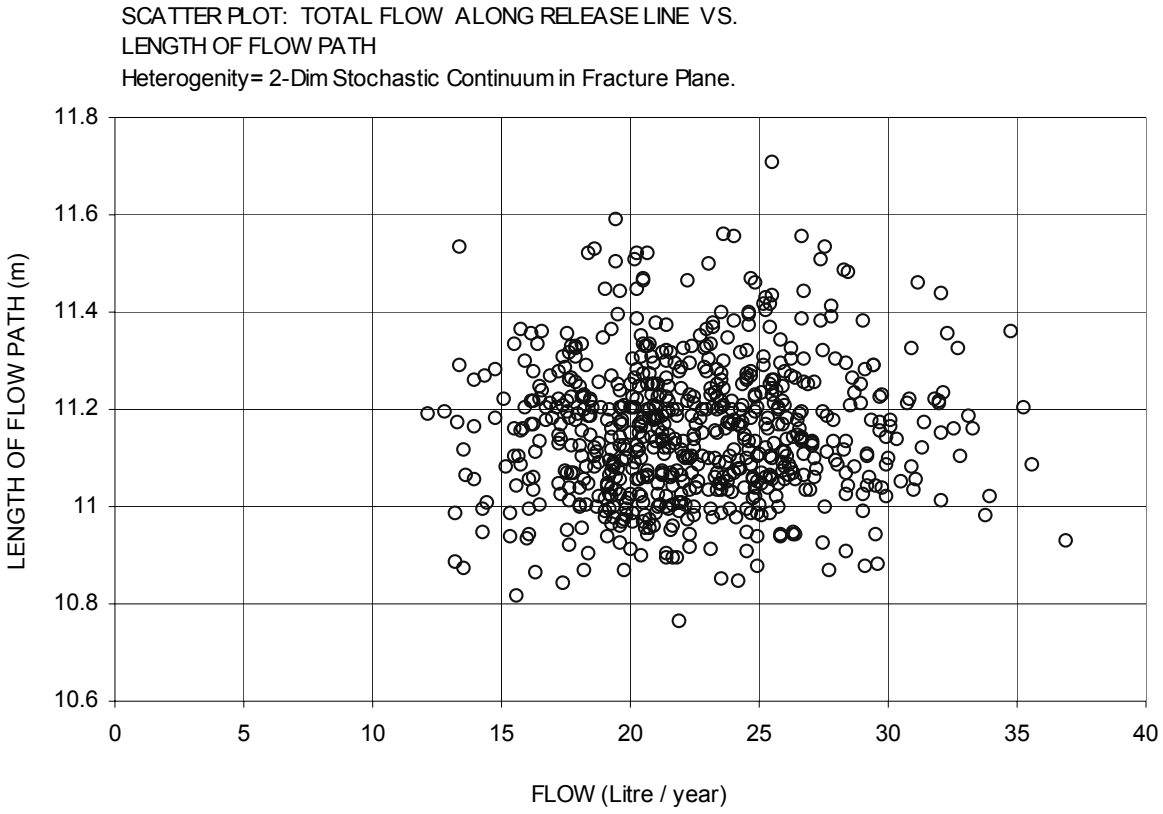

Figure 8-13 *Correlation between mean length of flow paths and flow inside the plume.*

8.10 Results considering sub-plumes

8.10.1 Definition of a sub-plume

In this second part of the analysis of the flow field and the plume, the plume is divided into 10 sections (sub-plumes) that starts along the release line. At the release line, each section (sub-plume) has the same width–equal to 0.2 m–that is given by the cell size of the stochastic continuum mesh. Because of the heterogeneous properties of the flow medium, the width and size of these sub-plumes varies a lot along the flow direction from the release line and to the interception line. The reason for dividing the plume into 10 sub-plumes is that we want to include, in the transport model, the flow and velocity distribution inside of the plume. In the figure below (Figure 8-14) the different sub-plumes are marked with different colours, the different sizes of the sub-plumes are well demonstrated.

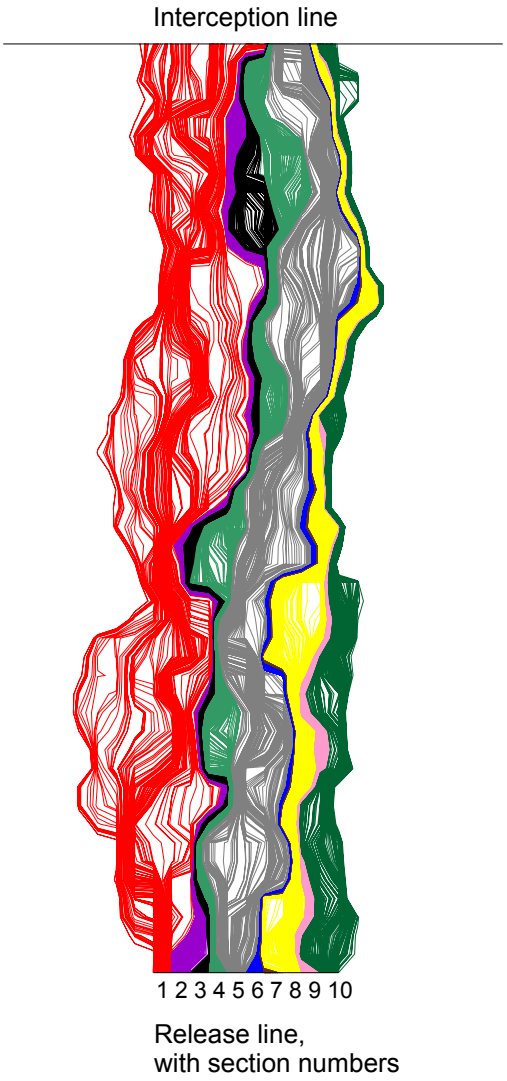

Figure 8-14 *An example of a plume and its sub-plumes. Each sub-plume (denoted by different colours) starts along the release line, and has a width along the release line equal to 0.2 m. Because of the heterogeneous properties of the flow medium, the width (and size) of the sub-plumes varies a lot between the release line and the interception line.*

An example of a very large sub-plume is given below in Figure 8-15; and a very small sub-plume is given in Figure 8-16.

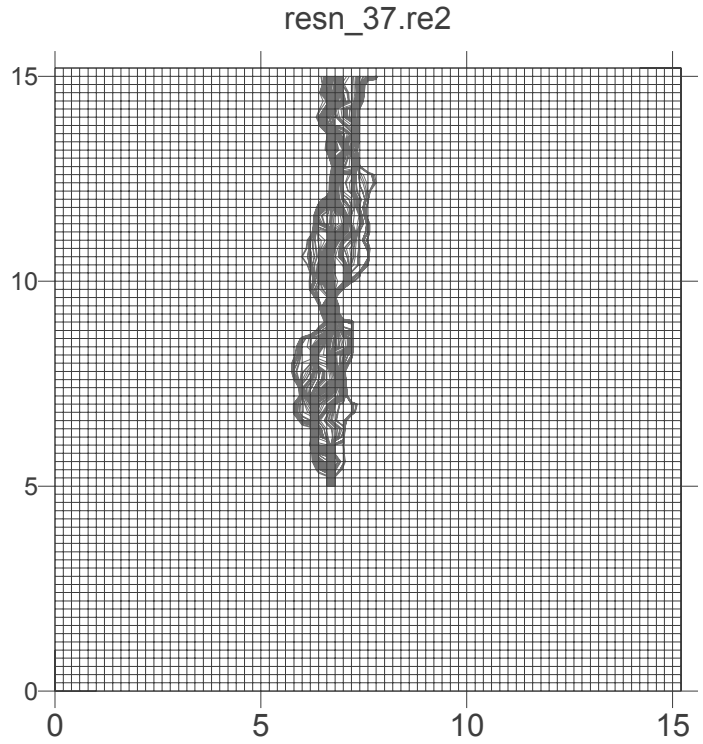

Figure 8-15 *Example of a very large sub-plume.*

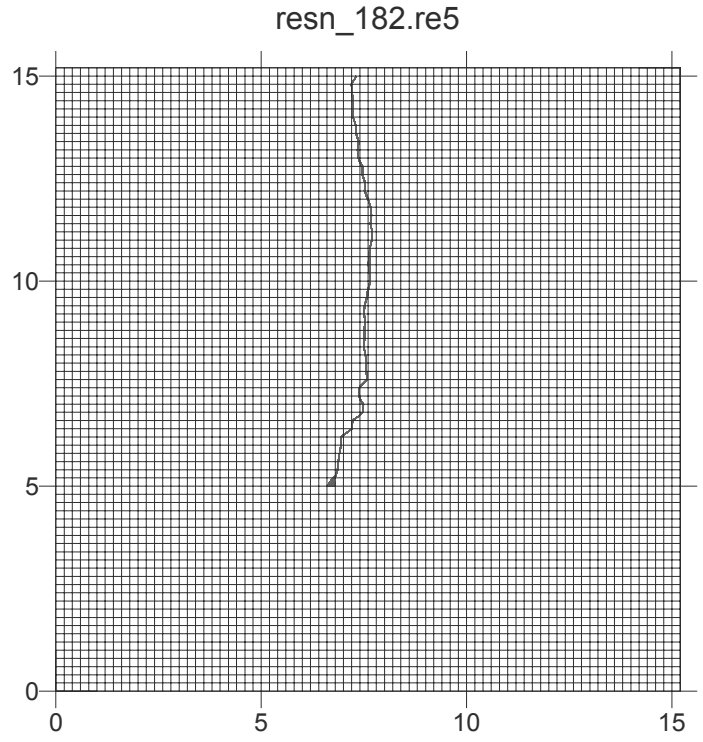

Figure 8-16 *Example of a very small sub-plume.*

Below we will present the results of the statistical evaluation of one of the sub-plumes (the first of the ten different sub-plumes); the statistical analyses demonstrate the same statistical results for all sub-plumes.

8.10.2 Probability distribution of flow along one section of the release line – flow of a sub-plume

The groundwater flow along one section (cell) of the release line produces the flow of the sub-plume of that cell. This flow will vary between different realisations, as the flow domain is heterogeneous. Figure 8-17 below presents the probability distribution of the flow along one section of the release line (flow of a sub-plume), for a model with a heterogeneous flow medium (700 realisations) and the corresponding flow of a model with a homogeneous flow medium. Considering a heterogeneous flow medium, the flow along the release line is 0.25 Litre/hour for the 10^{th} percentile and 4.7 Litre/hour for the 90^{th} percentile, for a homogeneous flow medium the flow is 1.78 Litre/hour.

Considering the heterogeneous flow medium, the probability distribution of the flow of a sub-plume is a distribution with a biased shape (see Figure 8-17); the shape reflects the log-normal distribution of the conductivity values of the cells.

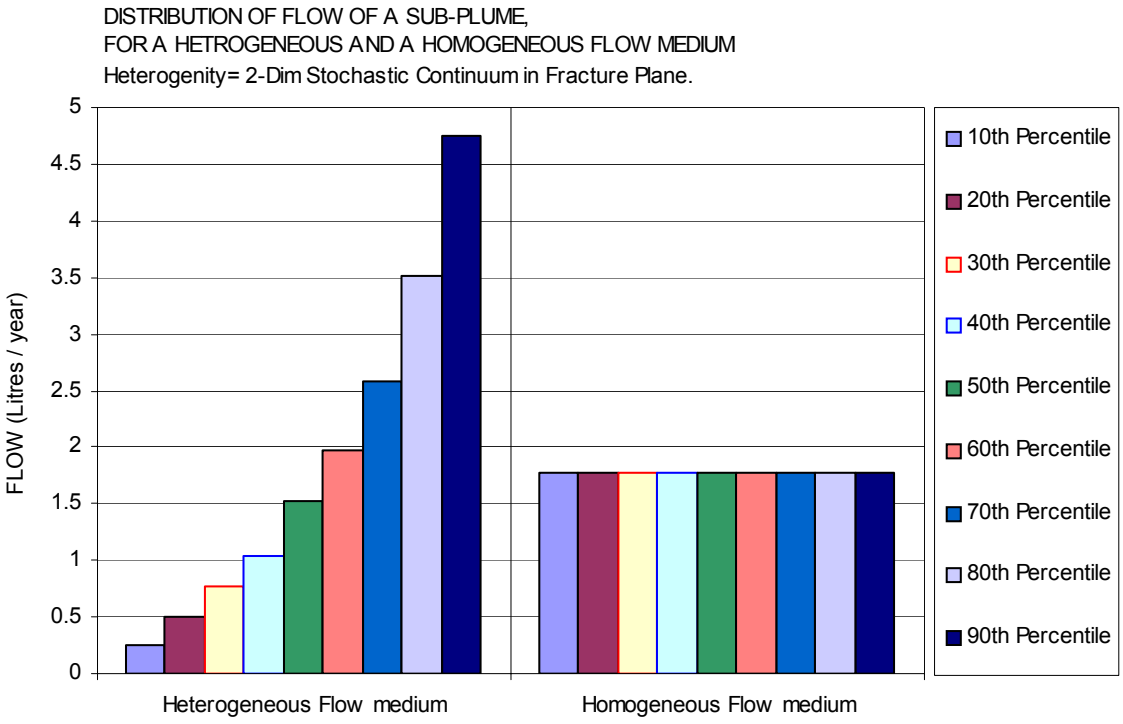

Figure 8-17 *Probability distribution of flow along one section of the release line (the flow inside a sub plume).*

8.10.3 Probability distribution of flow wetted surface area of a sub-plume

By analysing the distribution of flow paths from one section of the injection line it is possible to estimate the flow wetted surface area (wet area) of a sub-plume. (In this study the flow wetted surface is defined as two times the extension of the plume, the area on the upper fracture plane and the area on the lower fracture plane).

Figure 8-18 below presents the probability distribution of the flow wetted surface area of a sub-plume, for a model with a heterogeneous flow medium (700 realisations) and a model with a homogeneous flow medium. Considering a heterogeneous flow medium, it is well demonstrated by the figure that the size of the flow wetted surface area changes substantially between different realisations of the flow field; the flow wetted surface area is 1.1 m^2 for the 10^{th} percentile and 8.9 m^2 for the 90^{th} percentile. A comparison between the probability distributions of the plume and a sub-plume, demonstrates that, the variance is larger (in relation to the mean of the distributions) for the distribution representing the sub-plume. For a homogeneous flow medium, the flow wetted surface area of a sub-plume is 4 m^2.

Considering the whole plume (see Sec.8.9.2), the flow wetted surface area is given by flow paths released along the whole length of the release line. The flow properties along the release line vary; therefore some of the paths may converge while other may spread out over a large area. For a sub-plume however, the flow wetted surface area is given by flow paths released along one section of the release line, and inside that section the flow properties are constant. Therefore all flow paths released from one section may converge towards a very small channel or spread out over a large area. It follows that the variance in flow wetted surface area is much larger for a sub-plume than for the plume, and that the flow wetted surface area of a sub-plume could be very small.

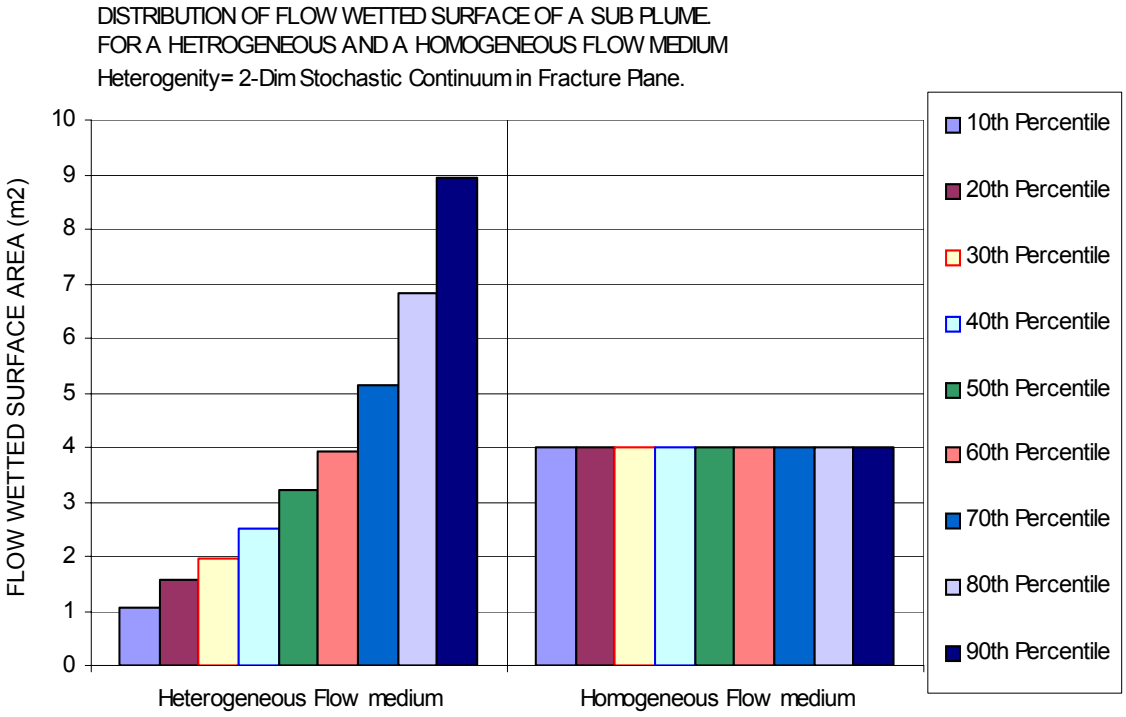

Figure 8-18 *Probability distribution of flow wetted surface area of a sub-plume.*

8.10.4 Probability distribution of shape of flow wetted surface area of a sub-plume

The analysis of the shape of a sub-plume produces the same principal results as the analysis of the shape of the plume (see Sec.8.9.3). The analysis of the shape of a sub-plume demonstrates that a few metres from the release line, the variation in width of plume is the same as at larger distances from the release line. Starting a metre or so from the release line, the variation in size of plume is the same for sections of equal length taken along the average flow direction. This is because at a certain distance from the boundaries, the probability distributions of direction and size of flow is the same (everywhere in the model). Therefore the variation in plume size and shape will be the same. In Task 6B2, the average flow field is not converging, there is no average trend in size of plume with distance form release line (except for the first metre or so). This is different from Task 6A, because in 6A the flow field was converging towards the pumping well.

The probability distributions of the sizes of different sections along the plume are given in Figure 8-19. The plume is separated into seven separate sections of equal length along the average flow direction. The first section is closest to the release line; and the last section is closest to the interception line. It is demonstrated by Figure 8-19 that the probability distribution of the size of the plume is approximately the same regardless of distance form release line (except for the first metre or so).

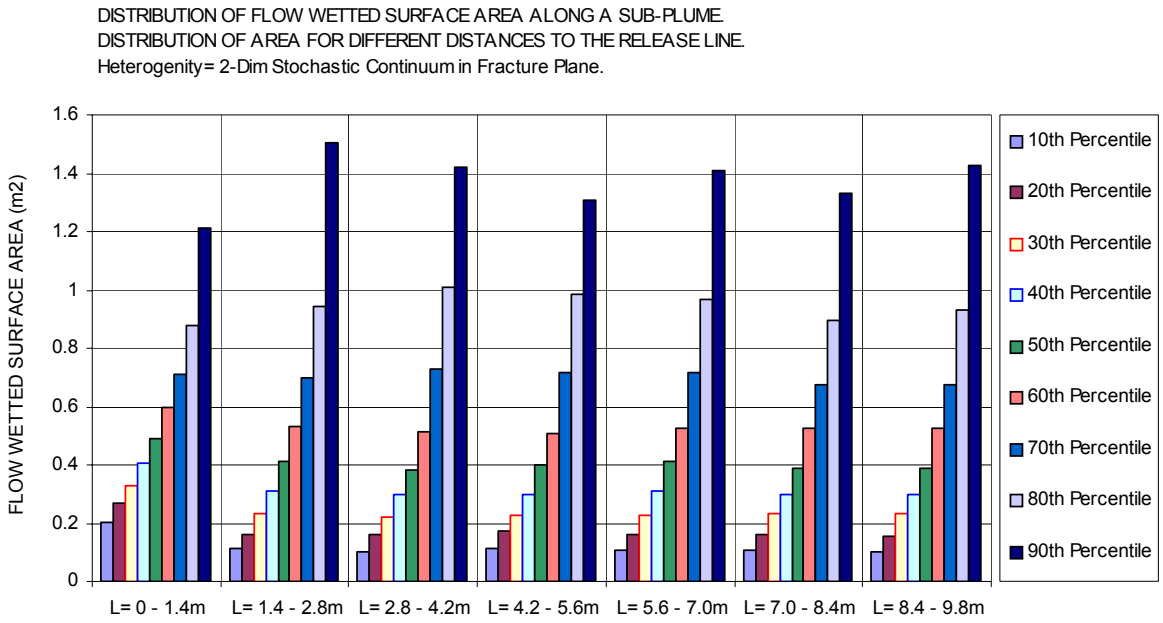

Figure 8-19 *Probability distribution of shape of flow wetted surface area of a sub-plume.*

8.10.5 Correlation between flow wetted surface area and flow inside a sub-plume

In a heterogeneous flow medium both the size of the plume and the flow inside the plume varies between different realisations. There is however a correlation between the size of the plume (the flow wetted surface area) and the flow inside the plume (release flow).

Considering a sub-plume, the correlation is presented below in Figure 8-20 (a scatter plot based on 700 different realisations). The following conclusion can be made based on Figure 8-20. Size of plume and size of flow demonstrates a strong positive correlation; hence it is very likely that if the flow is large along the release line, also the flow wetted surface area of the plume will be large, and that if the flow is small the flow wetted surface area is small as well. The positive correlation between flow and flow-wetted area is stronger for a sub-plume than for the whole of the plume.

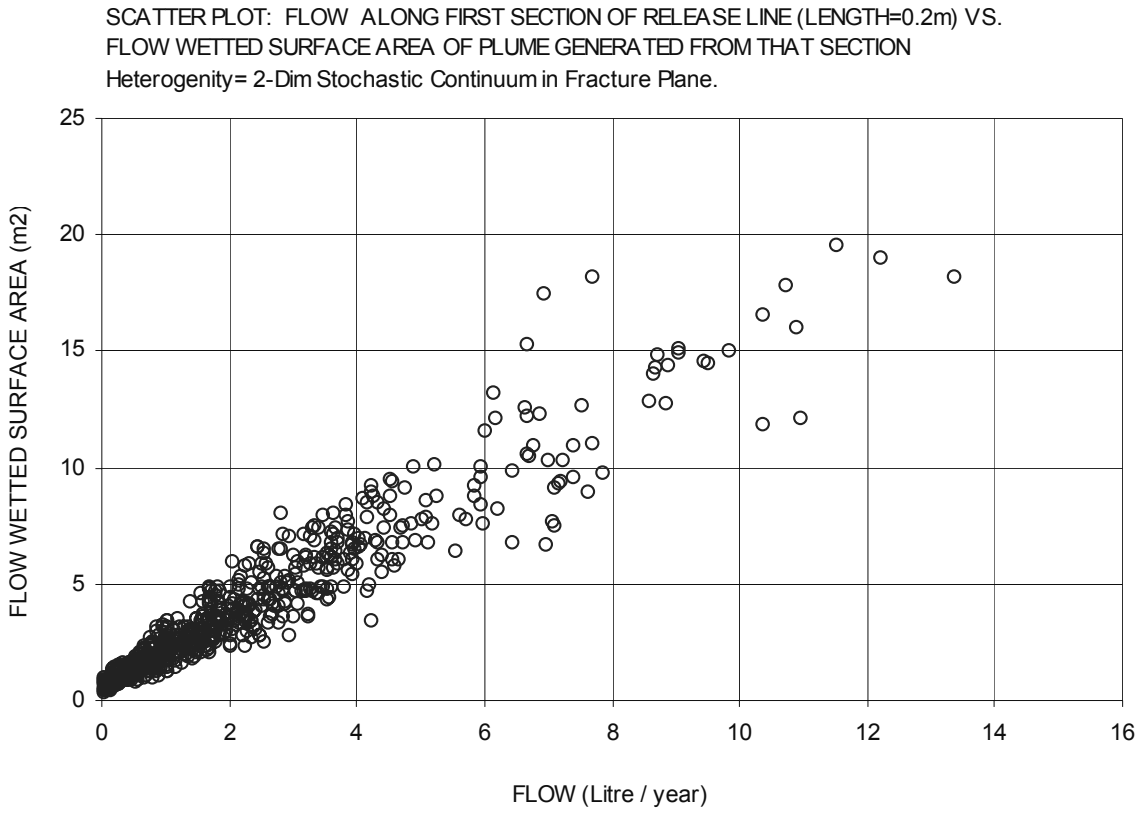

Figure 8-20 *Correlation between flow wetted surface area and flow inside a sub-plume.*

8.10.6 Correlation between flow path lengths and flow inside a sub-plume

In a heterogeneous flow medium both the size of the plume and the flow inside the plume varies between different realisations. In general the flow paths inside a plume demonstrates a tortuous pattern.

The correlation between the mean flow path length of a sub-plume and the flow inside the sub-plume is given below in Figure 8-21. The figure is a scatter plot based on 700 different realisations, and it presents mean flow path length versus the flow inside the sub-plume. As can be seen from the figure there is no correlation (or a very weak correlation) between the studied parameters. The figure demonstrates however that the variance of the probability distribution of mean flow path length decreases with size of flow inside the sub-plume. Or with other words, consider sub-plumes with small flows, for such plumes the mean length of the flow paths inside the plume may vary a lot between different plumes (realisations); but for sub-plumes with large flows, the mean length of the flow paths inside the plume is approximately the same for different plumes (realisations).

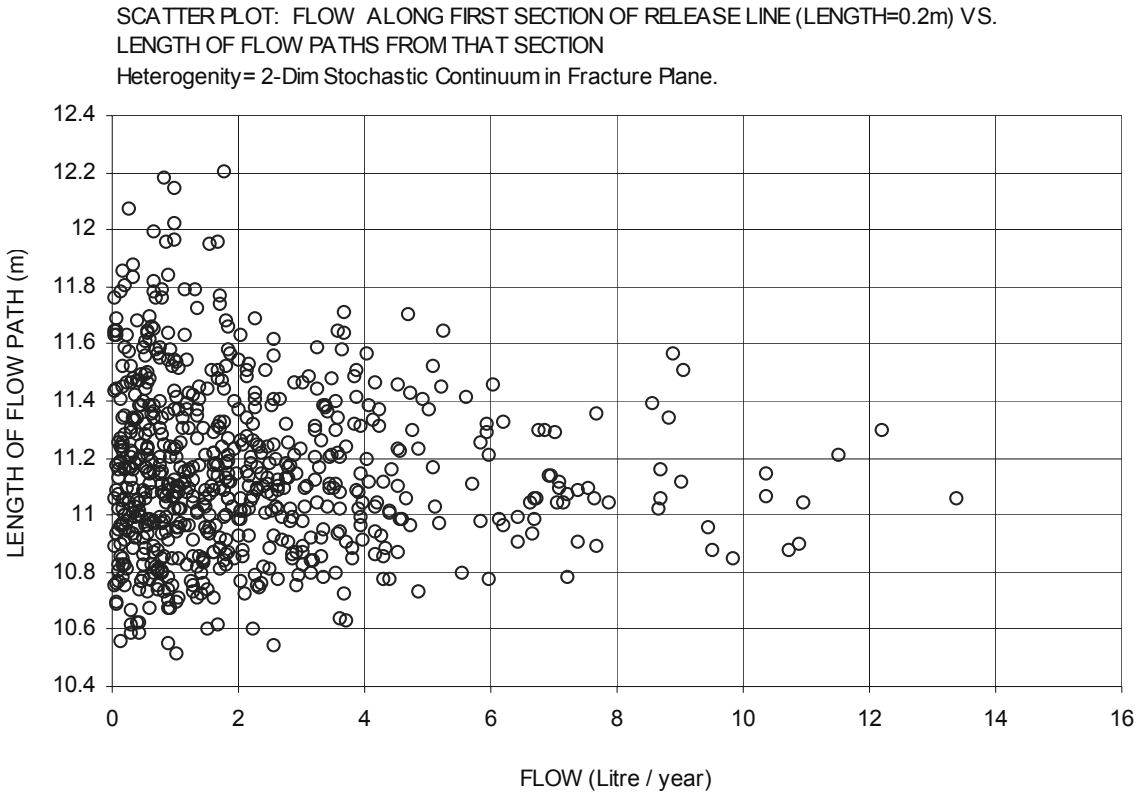

Figure 8-21 *Correlation between mean length of flow paths and flow inside a sub-plume.*

8.11 Data transferred to the transport model

By use of stochastic continuum modelling of the flow in the studied fracture, the shapes and flows of simulated plumes were calculated. The shapes and flows of these plumes (from release line to interception line) were transferred to the transport model.

The plume analysed in the flow modelling is divided into 10 sub-plumes, as discussed in the previous section. In the GoldSim transport model, a GoldSim pipe represents each one of the sub-plumes.

The properties that are transferred to the pipes of the transport model are the following: flow in a sub-plume (m^3/year), length of a sub-plume (m) and flow wetted surface area of a sub-plume (m^2). These properties are coupled to each other in a complicated way, e.g. it is likely that a sub-plume with a large flow also has a large flow wetted surface area (see previous section). Therefore, we have used a bootstrapping method in which the properties of the GoldSim pipes of different realisation of the transport model are directly given by the properties of the sub-plumes of the different realisations of the flow model. By use of this method the correlation between the flow, length and flow wetted surface area, is preserved in the transport modelling.

9 TASK 6B2 – Transport model - Methodology

9.1 Computer code used

Modelling of the solute transport processes was conducted by using the GoldSim computer program. The transport model was constructed by utilising the standard elements of the GoldSim Radionuclide Transport (RT) Module.

9.2 Modelling approach – General methodology

The transport modelling for Task 6B2 is based on the GoldSim Transport Module. The modelling was carried out as a probabilistic analysis. Hence, the uncertainties in the parameters of the system studied were described with ranges within which the parameters may vary–the parameters were defined by statistical distributions. A large number of different realisations of the parameters was created, i.e. 10 000 different realisations of a transport model with different properties. For each realisation (transport model), a prescribed injection rate, as well as a Dirac pulse, was used as a boundary condition. In this way the transport models simulates the injection of tracers. The resulting breakthrough curves, as simulated by the GoldSim computer code, are presented and discussed in this chapter.

The probability distributions of the transport parameters are separated into three sets, the transport modelling was carried out for all three sets:

(i) *Given parameter distributions* which reflects the assumed likely ranges of transport parameter values. The properties of these distributions are based on the data given in the Task 6A and 6B specification, by Selroos and Elert (2001) and Elert and Selroos (2001). These parameter distributions were also used as input data to the Task 6A model. In the given parameter distributions we presume that all parameters are independent.

(ii) *Constrained parameter distributions.* The constrained distributions were derived in Task 6A, they are based on the given parameter distributions and the results of a sensitivity analysis of a well test. The constrained parameter distributions are based on the analyses of breakthrough curves, as produced by use of the Strontium tracer, the 89 realisations that produced breakthrough curves for Strontium with an acceptable match to the measured breakthrough (of Strontium). In the constrained parameter distributions we presume that all parameters are independent.

(iii) *The constrained coupled parameter distributions* are also results of Task 6A, they consists of the ensemble of coupled parameter values as defined by the 89 accepted realisations. The difference compared to the constrained parameter distributions is that in the constrained coupled parameter distributions the individual parameter values are combined, according to the combinations of parameter values that resulted in the 89 accepted realisations. In the constrained coupled parameter distributions the parameters are combined in accordance to the accepted realisations and are not considered as independent. The probability

distribution of the parameter values that takes place within the 89 accepted realisations are the same in: (i) the constrained parameter distributions and in (ii) the constrained coupled parameter distributions; the difference is in the way these values are combined.

9.3 Represented transport processes

The transport processes that are represented by the GoldSim RT Module are: (i) advection, (ii) dispersion, (iii) retardation, (iv) decay and ingrowth [not included inthis study], and (v) exchanges with immobile storage zones (e.g. matrix diffusion). The retardation processes are represented by equilibrium partitioning between: (i) the fluid in the pathway and a user defined infill medium, and (ii) the fluid in the pathway and a user specified coating medium as well as a skin zone (around the perimeter of the pathway/fracture), and (iii) the diffusing fluid and the rock matrix. The hydraulic interchanges with immobile storage zones along the main transport pathway are governed by (i) matrix diffusion into immobile zones in which the transfer rate into and out of the zone is proportional to the concentration gradient and the diffusive properties of the zone, and (ii) a "stagnant" dispersive zone, in which the interchange is proportional to the concentration difference and a transfer rate. As defined in the task specifications by Selroos and Elert (2001) and Elert and Selroos (2001), radioactive decay and ingrowth is not considered in the modelling. The geometry and transport processes are illustrated in the cross-section of Figure 3-2.

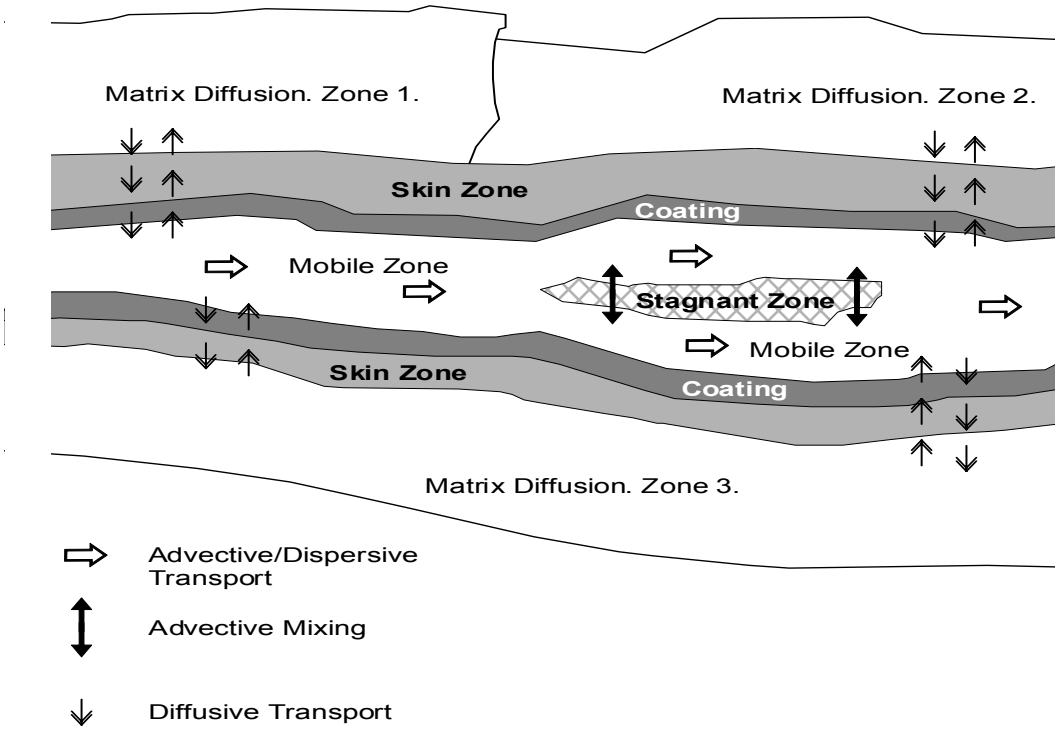

Figure 9-1 *A schematic cross-section along a pathway, showing examples of the features and processes that can be represented in the GoldSim RT Module.*

9.4 Geometry and flow of transport model

The idealised geometry of the fracture zone is presented below in Figure 3-3 in terms of a vertical cross section along the transport path. The open fracture and the stagnant zones contain a highly porous infill material with a stochastic porosity in the range 0.1–1, i.e. for some cases these zones are merely filled with streaming water. The fracture wall is covered with a coating (Fault Gouge) along the entire wetted perimeter. Behind the coating, there are two immobile zones in parallel; Altered Diorite and Mylonite.

The solute transport model consists of ten "GoldSim pipes" in parallel, representing ten parallel sections along the plume from the injection line (release line) to the interception line. The pipes represent the part of the fracture studied (Feature A) that is affected by the plume, between the injection line and the interception line. The defined length and width of the pipes were based on the results of the stochastic continuum modelling of the flow field and of the plume (see previous chapters). An illustration of the methodology of the horizontal layout of the transport model is given in Figure 9-3.

The GoldSim transport model consists of ten GoldSim pipes with different properties; some of the properties of the pipes are given by the flow modelling (e.g. flow wetted surface area, etc), other properties are stochastically generated by the GoldSim transport model (e.g. Kd-values, etc).

In the analyses of the flow fields and the plumes, carried out as a part of the flow modelling, each plume is divided into ten sub-plumes, as discussed in the previous section. In the GoldSim transport model, a GoldSim pipe represents each of these sub-plumes.

The properties that are given by the flow model (the sub-plumes) are the following: flow in pipe (m^3/year), length of pipe (m) and flow wetted surface area of pipe (m^2). These properties are coupled to each other in a complicated way. Therefore, we have used a bootstrapping method in which the properties of the GoldSim pipes of different realisation of the transport model are directly given by the properties of the sub-plumes of the different realisations of the flow model.

We have generated approx. 700 plumes by use of the flow model. For each realisation of the transport model one of these plumes is randomly selected, the flow properties of the GoldSim pipes are given by the properties of the sub-plumes of the selected plume. By use of this method the correlation between the flow, length and flow wetted surface area, is explicitly accounted for in the transport modelling.

For each of the 10 pipes, flow, length and flow wetted surface area is given by the modelling of the flow field. For a single realisation, the flow properties are different for all 10 pipes of the transport model (the variation is given by the 700 realisations of the plume). The transport properties are stochastically generated by GoldSim and are the same for all ten pipes of a single realisation of the transport model, but vary between different realisations.

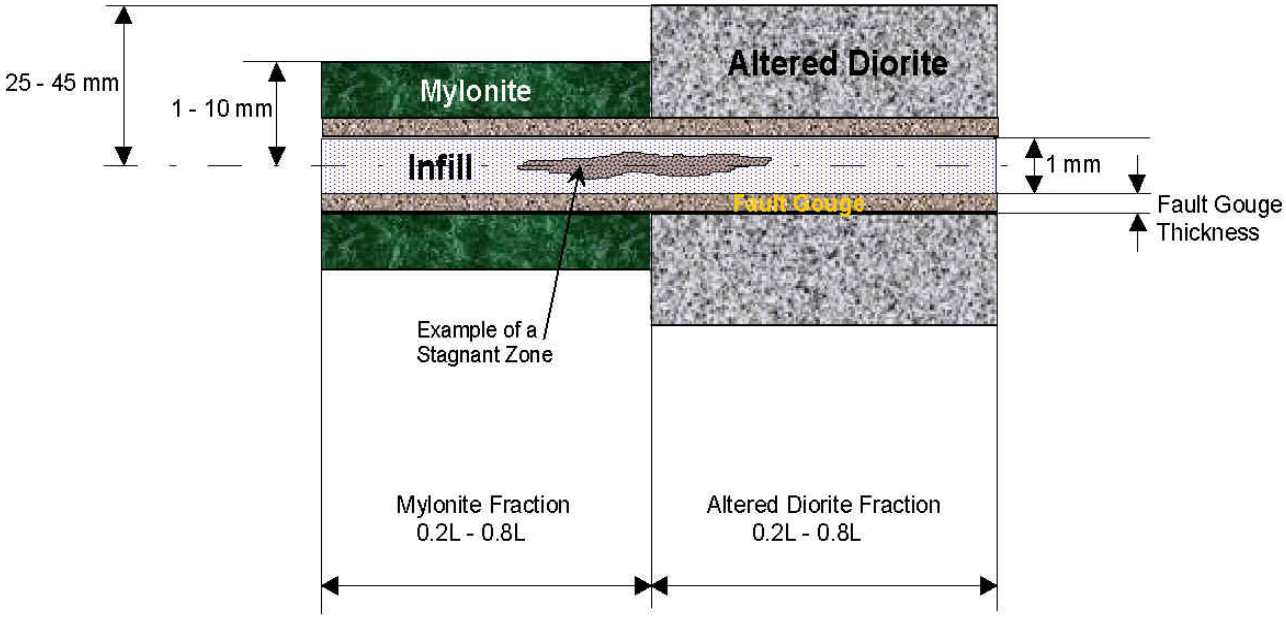

Figure 9-2 *Vertical cross section of an idealised geometry along a GoldSim pipe element. The total length is L. The element thicknesses are not to scale.*

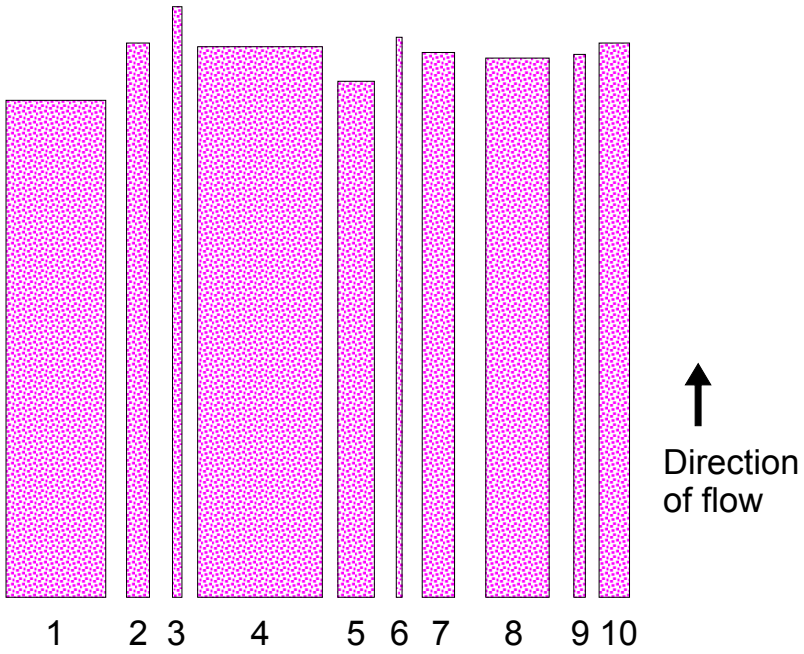

Figure 9-3 *An illustration of the methodology of the horizontal layout of the transport model. In the transport model ten parallel GoldSim pipes represent the plume, the properties of the GoldSim pipes are based on the properties of ten sub-plumes, as calculated by the flow field model.*

9.5 Mass flow and radioactivity

In the actual tracer tests, reproduced in Task 6A, the flow of the tracers studied were measured by use of the radioactivity of the tracers. If the measured radioactivity is corrected for radioactive decay, the measured radioactivity is directly proportional to the mass flow of the radioactive tracer. The measured radioactivity is given in Mega Bequrel per time unit, e.g. MBq / day. We have used the same concept in these simulations; the mass flow of a tracer studied is given as an activity in MBq / time unit.

9.6 Simulated tracers and tracer injection boundary condition

We have studied two tracers, HTO and Strontium. The HTO tracer is considered to be a conservative tracer, i.e. it does not adsorb onto the rock surface. Strontium is a non-conservative tracer (reactive) with relative weak reactive characteristics. As defined in modelling task specification, Elert and Selroos (2001), two types of tracer injection boundary condition was used:

- A constant injection rate of 1MBq/year.
- A Dirac pulse injection (a unit input = 1MBq).

In the transport model at the injection line, an equal amount of activity (tracer mass) was injected in each GoldSim pipe, regardless of flow in pipe.

9.7 Stagnant zones and the hydraulic gradient

The importance of the stagnant zones was demonstrated in the modelling of Task 6A. In the GoldSim RT Module the stagnant zones are inside the fracture plane and represents areas where the water is stagnant or the flow velocity is very small compared to the flow velocity of the mobile water.

In Task 6A (a pump test) the overall hydraulic gradient was large compared to a natural flow situation; in task 6B2 the overall hydraulic gradient is small and represents a natural gradient. Different hydraulic gradients may influence the amount of stagnant zones. Comparing the velocity of the water in the mobile zones and the velocity of the water in the low velocity areas “the stagnant” zones, we note that for a flow situation with a small gradient (as in Task 6B2) the differences in velocities are much smaller than during a pump test. Hence, areas in which the flow may be described as nearly stagnant during a pump test may not necessarily be described as stagnant under natural gradients. It follows that the amount of stagnant zones may change as the hydraulic gradient change.

The distributions of parameter values analysed in Task 6B2 includes a large variation in amounts of stagnant zones, both for the given parameter distributions and for the constrained and constrained coupled parameter distributions, we have therefore not changed the amount of stagnant zones when transferring the parameter distributions from the flow situation of Task 6A to that of Task 6B2.

9.8 Given parameter distributions

The tables below presents the given parameter distributions. These parameter distributions are the same as the given data used in Task 6A. The properties of these distributions are based on the data given in the Task 6A and 6B specification, by Selroos and Elert (2001) and Elert and Selroos (2001). Based on the given parameter distributions a large number of different realisations (10 000 realisations for each scenario) of the transport properties were established. These realisations were established under the prerequisite that all material and transport parameters of the given distributions are independent (not correlated). The number of parameters is 17.

Table 9-1 Given parameter distributions for HTO (a conservative tracer). Material properties.

	Min value	Max value	Distribution	Unit
Altered Diorite Poros	1e-3	4e-3	Uniform	-
Altered Diorite Kd	0	0	Discrete	m3/kg
Mylonite Poros	5e-4	5e-3	Uniform	-
Mylonite Kd	0	0	Discrete	m3/kg
Fault Gouge Poros	0.1	0.2	Uniform	-
Fault Gouge Kd	0	0	Discrete	m3/kg
Infill Poros	0.1	1	Uniform	-
Infill Kd	0	0	Discrete	m3/kg

Table 9-2 Given parameter distributions for Strontium (a reactive tracer). Material properties.

	Min value	Max value	Distribution	Unit
Altered Diorite Poros	1e-3	4e-3	Uniform	-
Altered Diorite Kd	4.7e-8	9.4e-5	Uniform	m3/kg
Mylonite Poros	5e-4	5e-3	Uniform	-
Mylonite Kd	2.6e-7	2.5e-4	Uniform	m3/kg
Fault Gouge Poros	0.1	0.2	Uniform	-
Fault Gouge Kd	2.6e-10	2.5e-2	Uniform	m3/kg
Infill Poros	0.1	1	Uniform	-
Infill Kd	2.6e-10	2.5e-2	Uniform	m3/kg

Table 9-3 Given parameter distributions for HTO and Strontium. Transport geometry properties.

	Range	Distribution	Unit
Altered Diorite Fraction	0.2-0.8	Uniform	-
Altered Diorite Max Thickness	25 – 45	Uniform	mm
Mylonite Fraction	0.2-0.8	Uniform	-
Mylonite Max Thickness	1 – 10	Uniform	mm
Fault Gouge Fraction	1	Discrete	-
Fault Gouge Max Thickness	0 – 0.5	Uniform	mm
Dispersivity	0.01 – 1	Uniform	m
Stagnant Zone Fraction (1)	0 – 1	Uniform	-
Stagnant zones Rate (1)	0 – 1	Uniform	1/m
(1) Stagnant zone fraction is the cross sectional area occupied by stagnant zones, and Stagnant zone rate is the exchange velocity from mobile zone to the stagnant zone.			

9.9 Constrained parameter distributions

In Table 9-4 below, the constrained parameter distributions are presented. The constrained parameter distributions are equal to the given distributions, except for differences that take place within the following distributions:

- Stagnant zones, rate and fraction
- Fault Gouge thickness.
- Kd-values of Fault Gouge and Infill.
- Dispersivity.
- Flow wetted surface area,
- Combined parameters: F-parameter and Retardation factor.

Table 9-4 Summary of the constraining power of the Strontium tracer test (a reactive tracer).

CONSTRAINING POWER OF STRONTIUM TRACER TEST				
PARAMETER		CONSTRAINING POWER (1)	GIVEN DISTRIBUTION PERCENTILES 20^{th} , 50^{th} , 80^{th}	CONSTRAINED DISTRIBUTION PERCENTILES 20^{th} , 50^{th} , 80^{th}
ALTERED DIORITE	Fraction	No		
	Thickness	No		
	Porosity	No		
	Kd - value	No		
	Retardation F.	No		
MYLONITE	Fraction	No		
	Thickness	No		
	Porosity	No		
	Kd - value	No		
	Retardation F.	No		
FAULT GOUGE	Thickness *(mm)*	YES1	0.10 , 0.25 , 0.40	0.01 , 0.04 , 0.20
	Porosity *(-)*	No		
	Kd–value *(m3/Kg)*	YES2	5.2e-3 , 1.3e-2 , 2.1e-2	6.3e-4 , 2.5e-3 , 1.1e-2
	Retardation F.	YES1	89 , 216 , 348	10 , 49 , 158
INFILL (fillling material)	Porosity, *(-)*	No		
	Kd–value *(m3/Kg)*	YES2	5.2e-3 , 1.3e-2 , 2.1e-2	1.1e-3 , 6.0e-3 , 1.4e-2
	Retardation F.	YES1	11 , 49 , 102	2 , 25 , 74
STAGNANT ZONE	Fraction *(-)*	YES1	0.20 , 0.50 , 0.80	0.77 , 0.95 , 0.98
	Rate *(1/m)*	YES1	0.20 , 0.50 , 0.80	0.03 , 0.06 , 0.11
DISPERSIVITY	*(m)*	YES2	0.28 , 0.55 , 0.82	0.49 , 0.70 , 0.88
FLOW WETTED SURFACE AREA	Excluding stagnant zones *(m2)*	YES2	0.169 , 0.441 , 0.768	0.019 , 0.037 , 0.190
F_1-PARAMETER	*(s/m)*	YES2	19 700 , 52 400 , 114 900	2 100 , 6 500 , 29 600

(1)

No = The constrained distribution is very similar to the given distribution. No constraining power is demonstrated.

YES1 = The range of the constrained distribution is similar to that of the given distribution, but the constrained distribution demonstrates a new probability density function. Hence, some constraining power is demonstrated.

YES2 = The range of the constrained distribution is different from the given distribution. The probability density function is also different. Real constraining power is demonstrated.

The constrained parameter distributions are the results of the Task 6A analysis of the breakthrough of Strontium tracer. For a more complete presentation of the constrained parameter distributions, including combined parameters, we refer to the Section 5.5. Based on the constrained parameter distributions a large number of different realisations (10 000 realisations for each studied scenario) of the transport properties were established. These realisations were established under the prerequisite that all material and transport parameters of the constrained distributions are independent (not correlated).

9.10 Constrained coupled parameter distributions

The constrained parameter distributions are the results of Task 6A; they were derived based on the analyses of breakthrough curves, as produced by use of the Strontium tracer and the transport model of Task 6A. The constrained parameter distributions are based on the 89 realisations that produced breakthrough curves for Strontium with an acceptable match to the measured breakthrough (of Strontium), see Section 5.5 and Appendix A.

The constrained coupled parameter distributions consists of the ensemble of coupled parameter values as defined by the 89 accepted realisations. The difference compared to the constrained parameter distributions is that in the constrained coupled parameter distributions the individual parameter values are combined according to combinations of parameter values that took place in the 89 accepted realisations.

The realisations established with the given and constrained parameter distributions were established under the prerequisite that all parameters of the distributions are independent (not correlated).

The realisations established with the constrained coupled parameter distributions are established in a different way. For the realisations established with the coupled distributions, the transport model selects randomly one of the 89 accepted combinations of material and transport parameter values, and combines it with one of the 700 plumes (the plumes are discussed in previous sections, see Sections 8.9, 8.10 and 9.4).

The probability distribution of parameter values that takes place within the 89 accepted realisations are the same in: (i) the constrained parameter distributions and in (ii) the constrained coupled parameter distributions; the difference is in the way these values are combined.

10 TASK 6B2 – Constant injection rate

10.1 General

For these simulations a constant injection rate of the tracers studied was prescribed at the release line. The constant injection rate was set to 1 MBq/year, for both the HTO tracer and the Strontium tracer. The two tracers were simulated separately, but with identical stochastic procedures. At the interception line, 10 m from the release line, the flow of tracer was calculated. The mass flow at the interception line will increase with time, from zero and up to a mass flow equal to the constant injection rate, i.e. when equilibrium state is reached. Simulations were carried out for both the HTO and the Strontium tracer, and by use of both the given parameter distributions and the constrained parameter distributions.

10.2 Examples of breakthrough curves

10.2.1 HTO – tracer

Considering the HTO tracer, a few examples of breakthrough curves are given in Figure 10-1, Figure 10-2 and Figure 10-3. The curves given in Figure 10-1 were calculated with the given parameter distributions, while the curves in Figure 10-2 were calculated with the constrained parameter distributions, and finally the curves given in Figure 10-3 were calculated with the use of the constrained coupled parameter distributions.

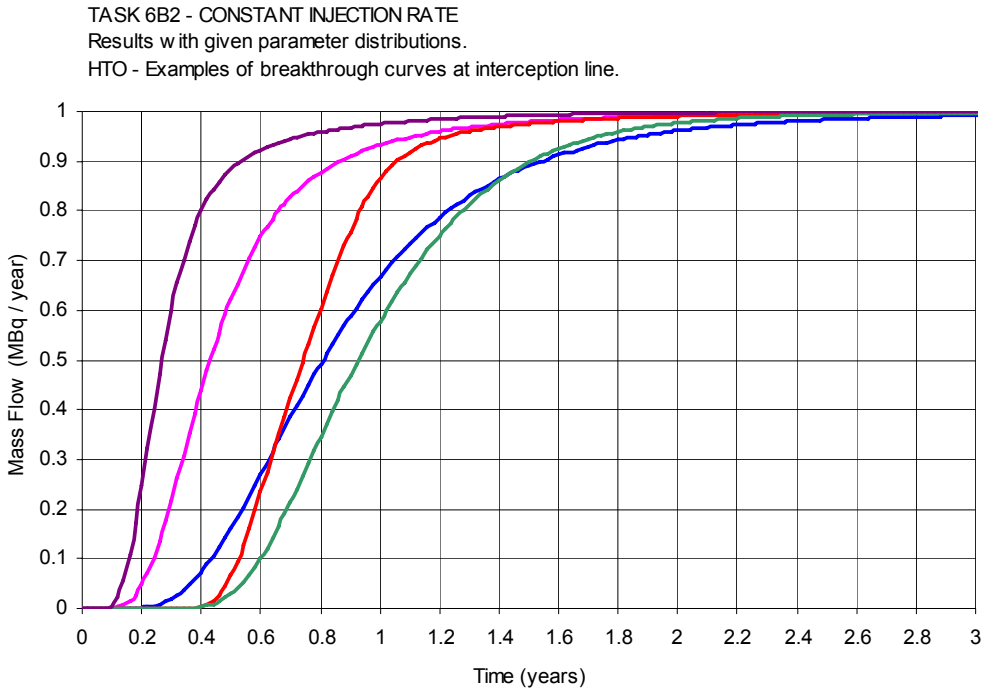

Figure 10-1 *HTO – Examples of breakthrough curves calculated by use of the given parameter distributions*

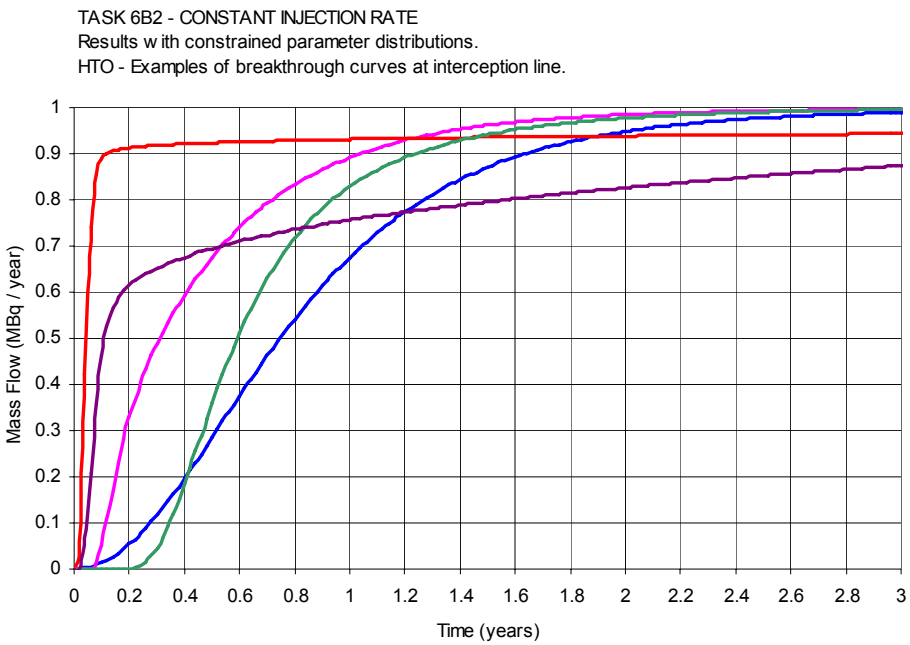

Figure 10-2 *HTO – Examples of breakthrough curves calculated by use of the constrained parameter distributions.*

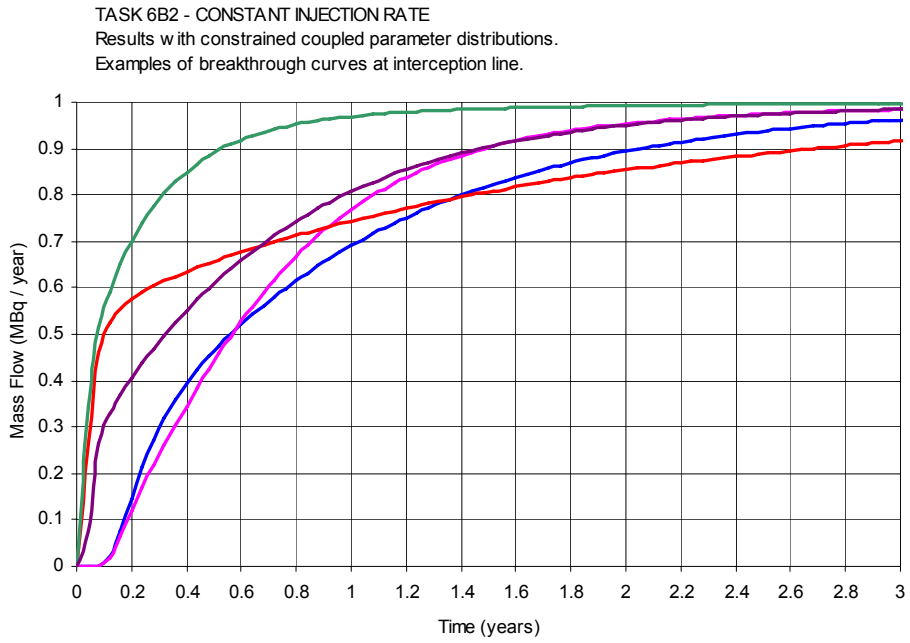

Figure 10-3 *HTO – Examples of breakthrough curves calculated by use of the constrained coupled parameter distributions.*

10.2.2 Strontium – tracer

Considering the Strontium tracer, a few examples of breakthrough curves are given in Figure 10-4, Figure 10-5 and Figure 10-6. The curves given in Figure 10-4 were calculated with the given parameter distributions, while the curves in Figure 10-5 were calculated with the constrained parameter distributions, and finally the curves given in Figure 10-6 were calculated with the use of the constrained coupled parameter distributions.

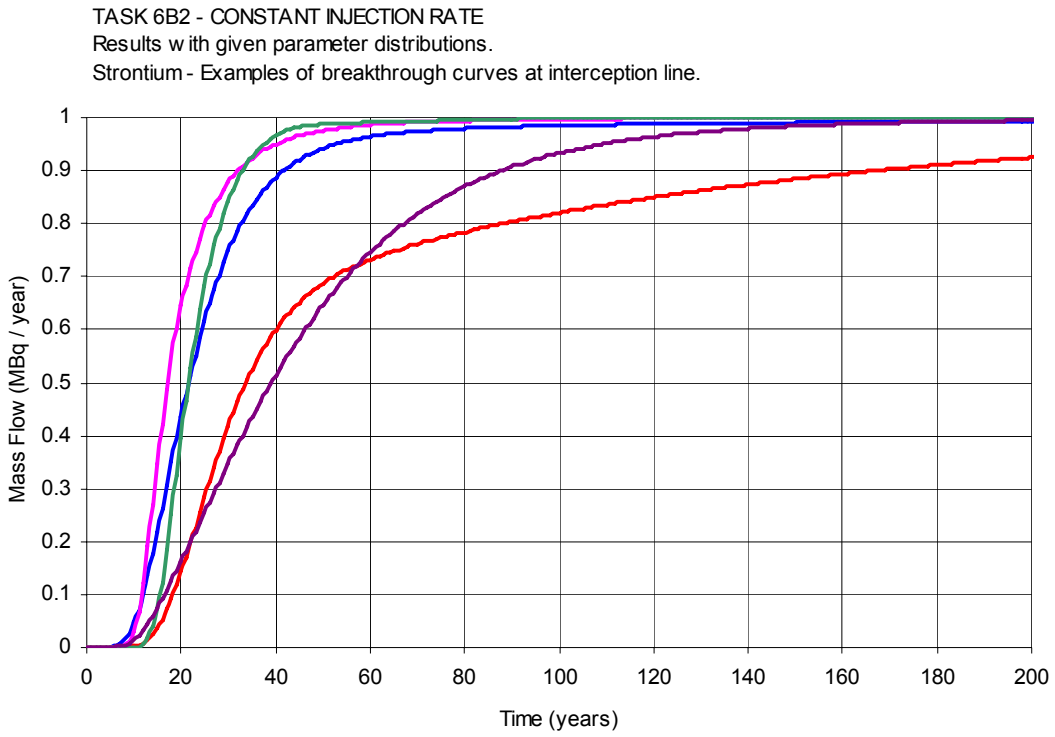

Figure 10-4 *Strontium – Examples of breakthrough curves calculated by use of the given parameter distributions.*

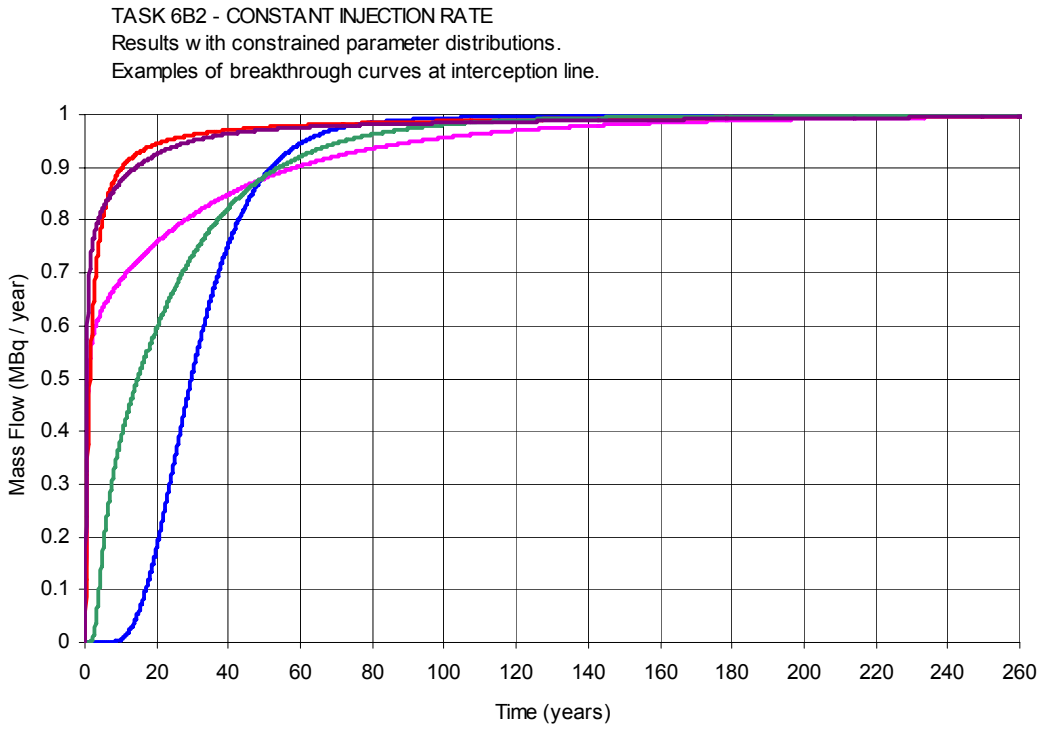

Figure 10-5 *Strontium – Examples of breakthrough curves calculated by use of the constrained parameter distributions.*

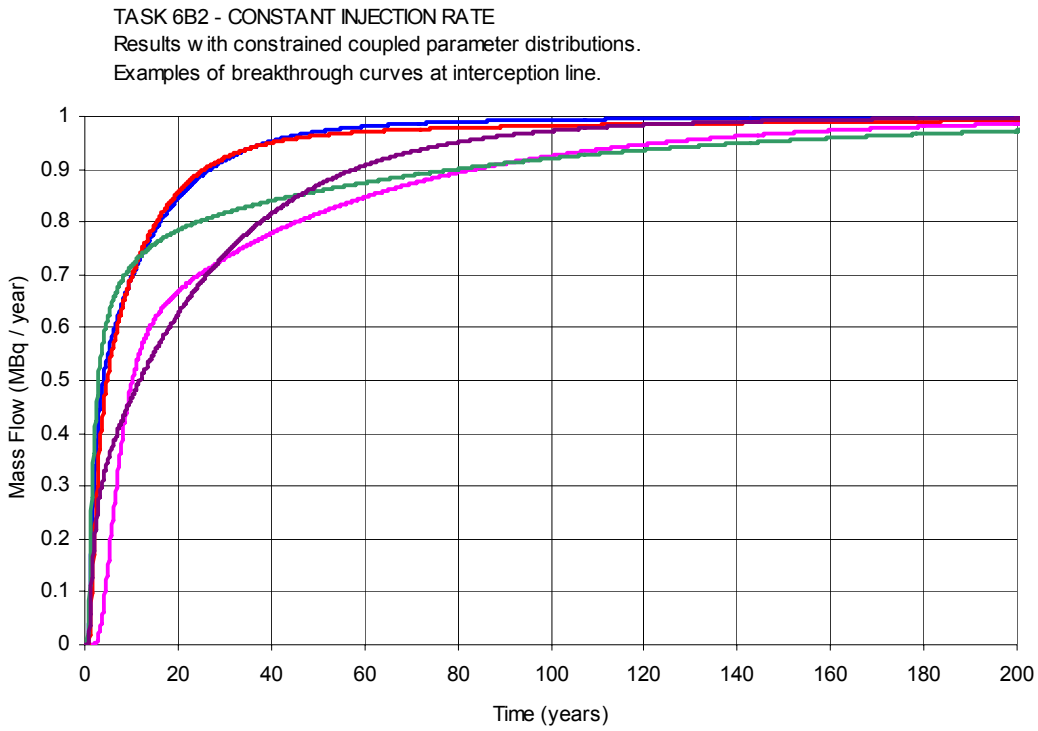

Figure 10-6 *Strontium – Examples of breakthrough curves calculated by use of the constrained coupled parameter distributions.*

10.3 Probability distribution of mass flow versus time

At each time step of the simulation, the probability distribution of mass flow at the interception line (breakthrough of mass) is calculated. (There is one probability distribution for each timestep of the simulation.) The probability distributions are characterised by percentiles. The results are given in figures presenting the probability for different amounts of mass flow, versus time.

Considering HTO and a constant injection rate, the probability distributions of mass flow at the interception line versus time, is given in Figure 10-7 and Figure 10-8.

Considering Strontium and a constant injection rate, the probability distributions of mass flow at the interception line versus time, is given in Figure 10-9 and Figure 10-10.

10.4 Probability distribution of breakthrough times for recovery of mass flow

The tracer mass flow (not cumulative mass) at the interception line is called the recovered mass flow (it is not the recovered mass, but the recovered mass flow). The recovered mass flow is calculated as a percentage of the released mass flow (i.e. a percentage of the constant injection rate). For different amounts of recovered mass flow, i.e 5%, 50% and 95%, we have calculated the probability distribution of the corresponding breakthrough times. Hence, the probability distribution of the breakthrough times for 5, 50 and 95 percent of recovered mass flow.

Considering HTO and a constant injection rate, the probability distributions of breakthrough time for recovery of mass flow at the interception line, is given in Figure 10-11 and Figure 10-12, below.

Considering Strontium and a constant injection rate, the probability distributions of breakthrough time for recovery of mass flow at the interception line, is given in Figure 10-13 and Figure 10-14, below.

10.5 Summary of results – constant injection rate

10.5.1 HTO- tracer

We summarize the following results for the HTO tracer, considering a constant injection rate of 1 MBq/year, 10 metres upstream of the interception line. The mass flow at the interception line will be close to the constant injection rate within less than 4 years.

For the HTO tracer at the interception line:

For the Given parameter distributions:

With a probability of 90%

The mass flow is 5% of the injection rate within 0.44 years.

The mass flow is 50% of the injection rate within 0.92 years.

The mass flow is 95% of the injection rate within 2.35 years.

For the Constrained parameter distributions:

With a probability of 90%

The mass flow is 5% of the injection rate within 0.17 years.

The mass flow is 50% of the injection rate within 0.58 years.

The mass flow is 95% of the injection rate within 4.10 years.

For the Constrained coupled parameter distributions:

With a probability of 90%

The mass flow is 5% of the injection rate after within 0.14 years.

The mass flow is 50% of the injection rate after within 0.52 years.

The mass flow is 95% of the injection rate after within 3.77 years.

For a given percentage of recovered mass flow, the length of the period between the 95th and the 5th percentiles of the breakthrough time (for recovery of mass flow) is a measure of the uncertainty in the predictions of the breakthrough curves. Considering a small amount of recovered mass, the period represents the uncertainty in predictions of the first part of the breakthrough curves. Considering a large amount of recovered mass, the period represents the uncertainty in predictions of the last part of the breakthrough curves.

Considering the HTO tracer and the length of period between the 95th and 5th percentile of breakthrough time:

Considering recovery of 5% of the mass flow and the:

Given parameter distributions, the length of the period is 0.43 years

Constrained parameter distributions, the length of the period is 0.24 years

Constrained coupled parameter distributions, the length of the period is 0.19 years.

Considering recovery of 50% of the mass flow and the:

Given parameter distributions, the length of the period is 0.80 years

Constrained parameter distributions, the length of the period is 0.65 years

Constrained coupled parameter distributions, the length of the period is 0.54 years.

Considering recovery of 95% of the mass flow and the:

Given parameter distributions, the length of the period is 2.0 years

Constrained parameter distributions, the length of the period is 4.0 years

Constrained coupled parameter distributions, the length of the period is 3.2 years

10.5.2 Strontium tracer

We conclude the following results for the Strontium tracer, considering a constant injection rate of 1 MBq/year, ten metres upstream of the interception line. The mass flow at the interception line will be close to the constant injection rate within less than 190 years.

For the Strontium tracer at the interception line:

For the Given parameter distributions:

With a probability of 90%

The mass flow is 5% of the injection rate within 37 years.

The mass flow is 50% of the injection rate within 72 years.

The mass flow is 95% of the injection rate within 175 years.

For the Constrained parameter distributions:

With a probability of 90%

The mass flow is 5% of the injection rate within 9.2 years.

The mass flow is 50% of the injection rate within 29 years.

The mass flow is 95% of the injection rate within 205 years.

For the Constrained coupled parameter distributions:

With a probability of 90%

The mass flow is 5% of the injection rate within 3.9 years.

The mass flow is 50% of the injection rate within 21 years.

The mass flow is 95% of the injection rate within 187 years.

For a given percentage of recovered mass flow, the length of the period between the 95^{th} and the 5^{th} percentiles of the breakthrough time (for recovery of mass flow) is a measure of the uncertainty in the predictions of the breakthrough curves. Considering a small amount of recovered mass, the period represents the uncertainty in predictions of the first part of the breakthrough curves. Considering a large amount of recovered mass, the period represents the uncertainty in predictions of the last part of the breakthrough curves.

Considering the Strontium tracer and the length of period between the 95th and 5th percentile of breakthrough time:

Considering recovery of 5% of the mass flow and the:

Given parameter distributions, the length of the period is 38.2 years

Constrained parameter distributions, the length of the period is 13.2 years

Constrained coupled parameter distributions, the length of the period is 4.7 years.

Considering recovery of 50% of the mass flow and the:

Given parameter distributions, the length of the period is 70.3 years

Constrained parameter distributions, the length of the period is 36.4 years

Constrained coupled parameter distributions, the length of the period is 23.6 years.

Considering recovery of 95% of the mass flow and the:

Given parameter distributions, the length of the period is 164.4 years

Constrained parameter distributions, the length of the period is 237.0 years

Constrained coupled parameter distributions, the length of the period is 211.1 years.

For the HTO as well as for the Strontium, it is likely that the constrained parameter distributions, and the constrained coupled parameter distribution, will produce an earlier arrival of small and median mass flows, but for the final increase in mass flow, e.g. from 90% and up to 100% of the injection rate, may take a somewhat longer time with the constrained distributions than with the given distributions.

For a given percentage of recovered mass flow, the length of the period between the 95th and the 5th percentiles of the breakthrough time (for recovery of mass flow) is a measure of the uncertainty in the predictions of the breakthrough curves. The results above (concerning this time period) demonstrate that the smallest uncertainty is produced by use of the constrained coupled parameter distributions, especially for the predictions of the first part of the breakthrough curves. For the first part of the breakthrough curves (recovery of 5% of the mass flow), the uncertainty produced by the constrained coupled parameter distributions is nearly an order of magnitude smaller than that produced by the given parameter distributions (both for HTO and Strontium), this demonstrates the constraining power of the tracer test analysed in Task 6A. However, considering the last part of the breakthrough curves (recovery of 95% of the mass flow), the uncertainty in the result produced by the constrained coupled parameter distributions is larger than the results produced by the given parameter distributions.

This illustrates the importance of transport processes that had no large influence on the tracer test studied in Task 6A, for example interaction (e.g. matrix diffusion and adsorption) with materials (Diorite and Mylonite) that are not in direct contact with the flowing water, may be very important at the time scales of the recovery of 95% of injected mass in Task 6B2. Hence, as the tracer test studied in Task 6A demonstrated no constraining power for these transport properties (matrix diffusion), the uncertainty in the result produced by the constrained coupled parameter distributions is of the same size (or larger) than the uncertainty in the results produced with the given parameter distributions, at these large time scales (large time scales in comparison to the time scale of the tracer test).

HTO

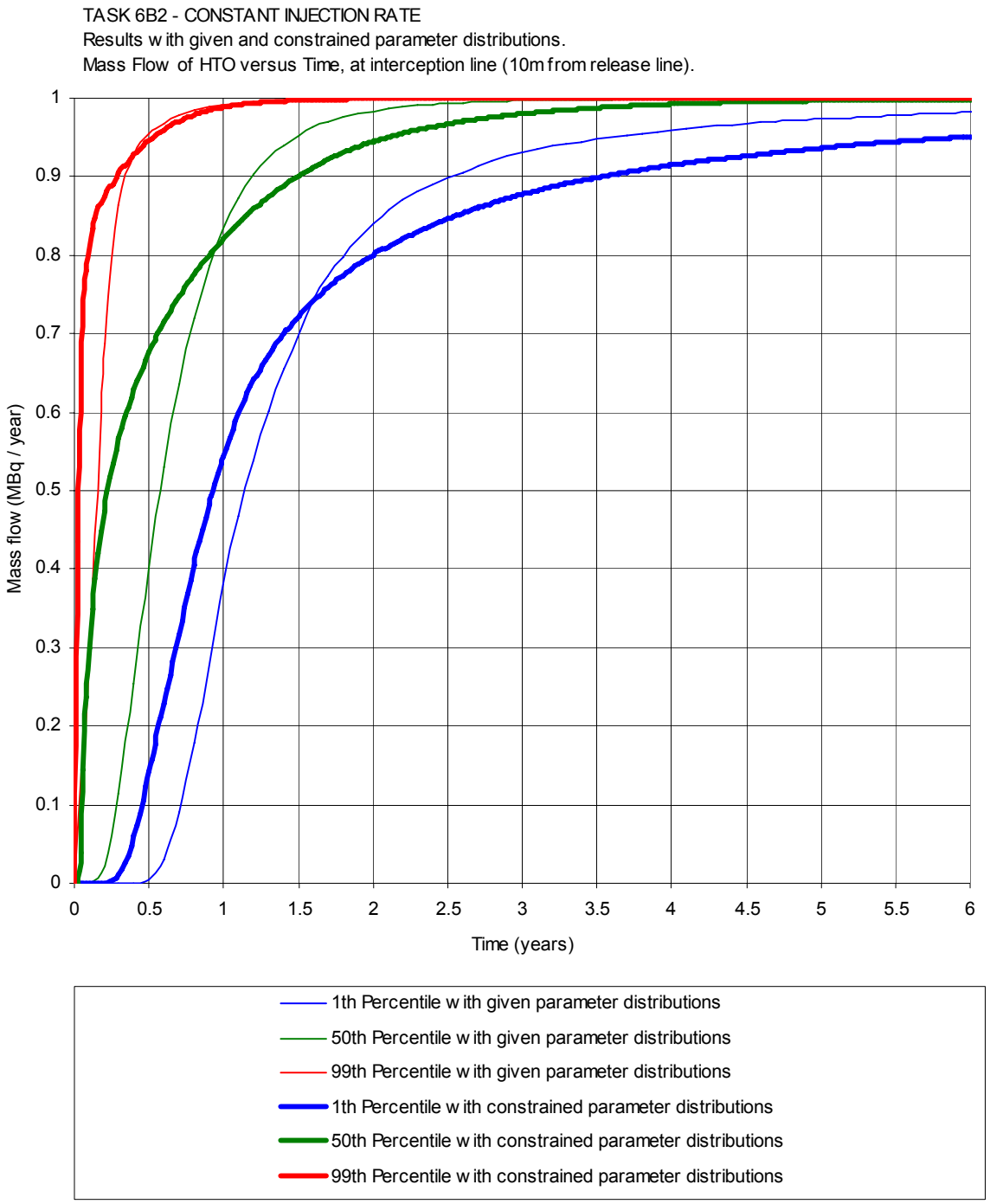

Figure 10-7 *HTO – Constant injection rate. Probability distributions of mass flow versus time, at the interception line. Results with given and constrained parameter distributions.*

HTO

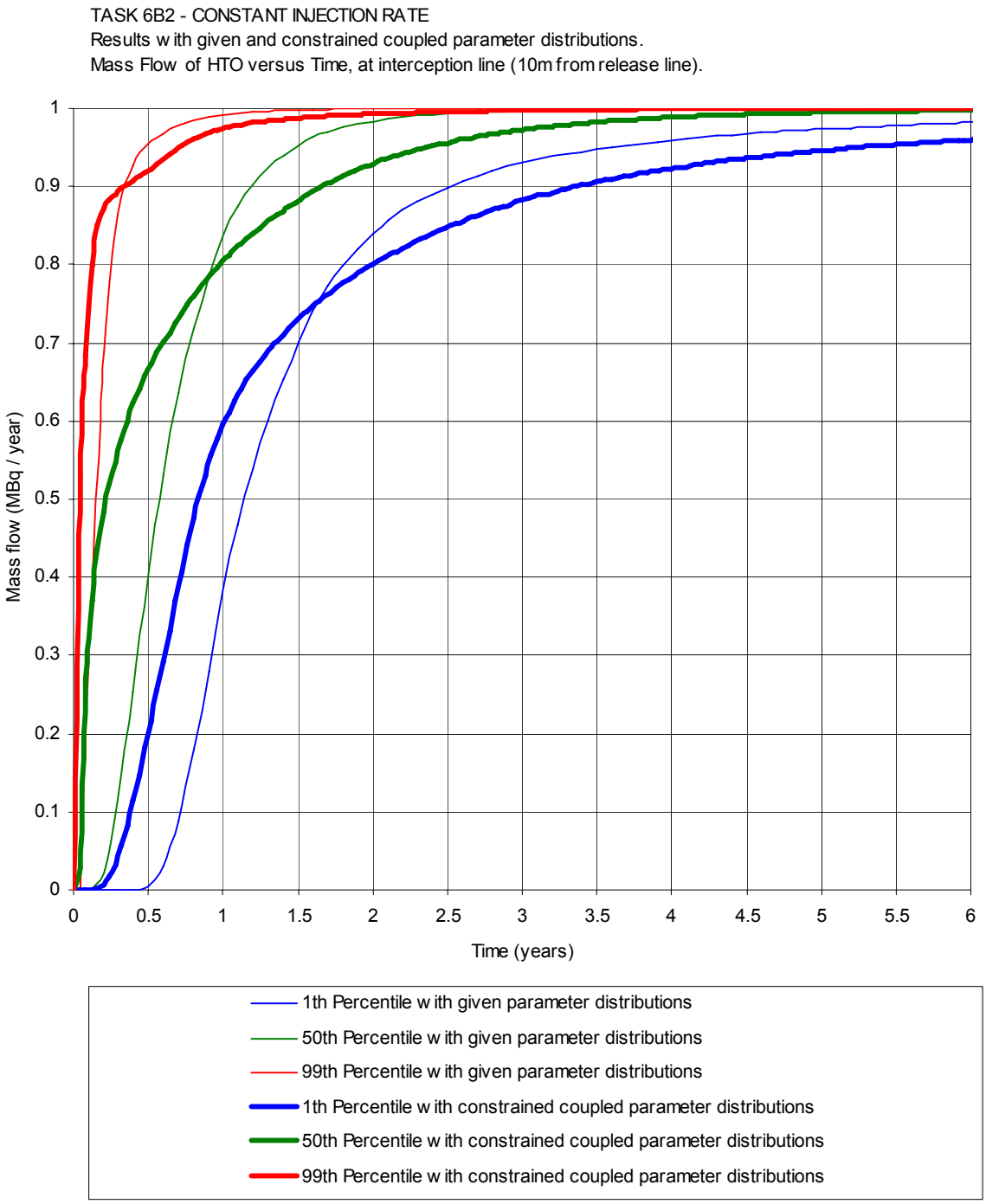

Figure 10-8 *HTO – Constant injection rate. Probability distributions of mass flow versus time, at the interception line. Results with given and constrained coupled parameter distributions.*

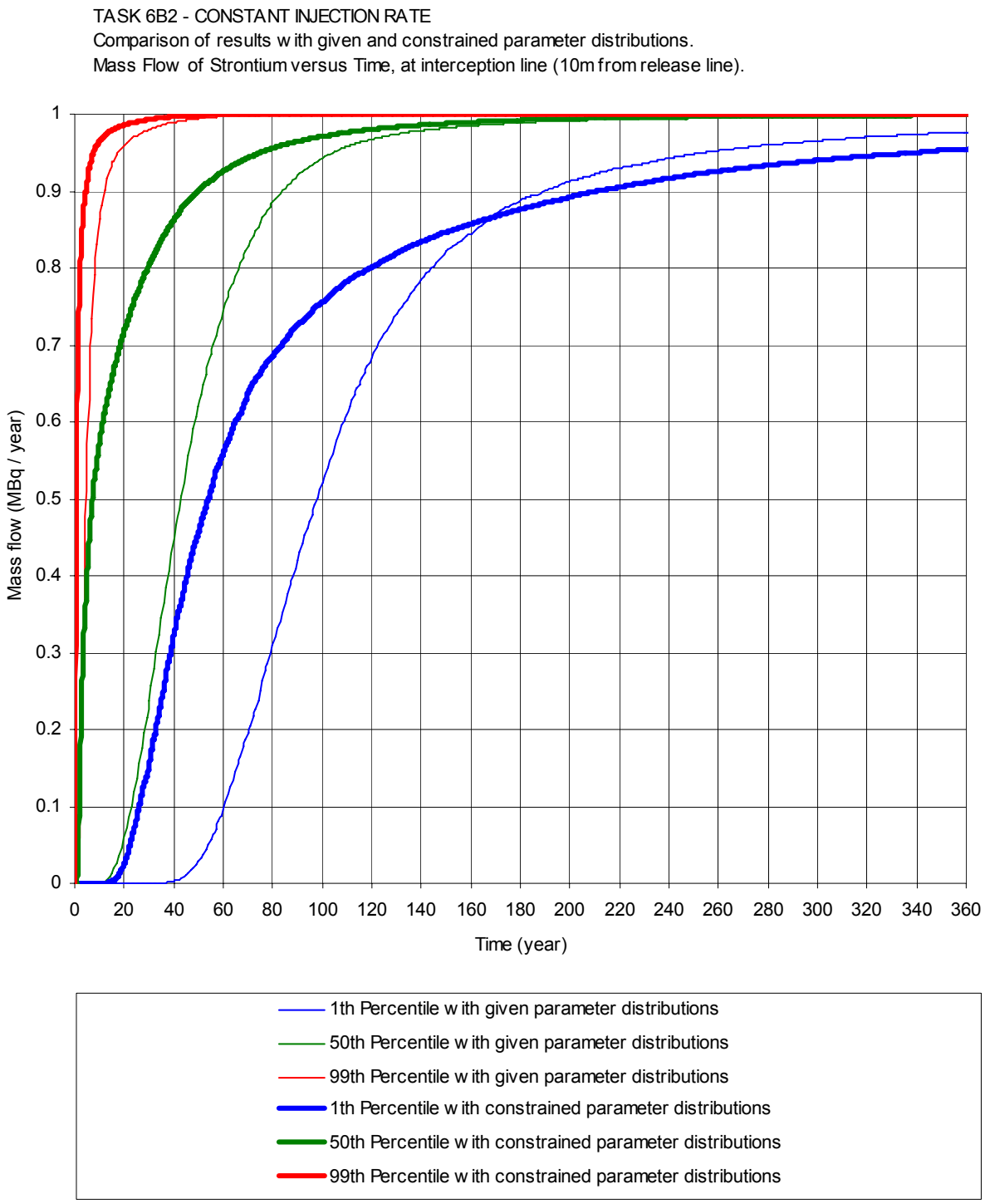

Figure 10-9 *Strontium – Constant injection rate. Probability distributions of mass flow versus time, at the interception line. Results with given and constrained parameter distributions.*

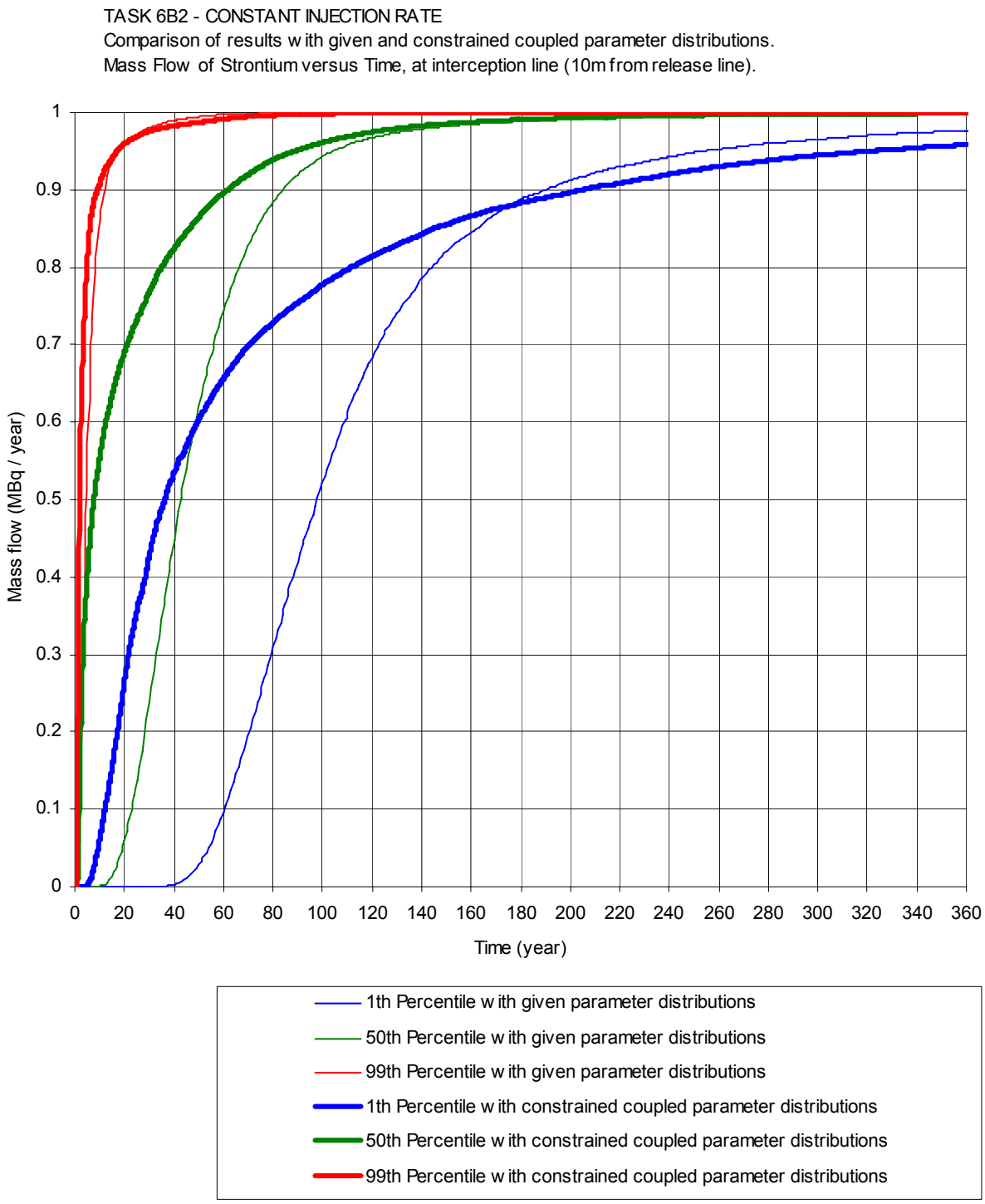

Figure 10-10 *Strontium – Constant injection rate. Probability distributions of mass flow versus time, at the interception line. Results with given and constrained coupled parameter distributions.*

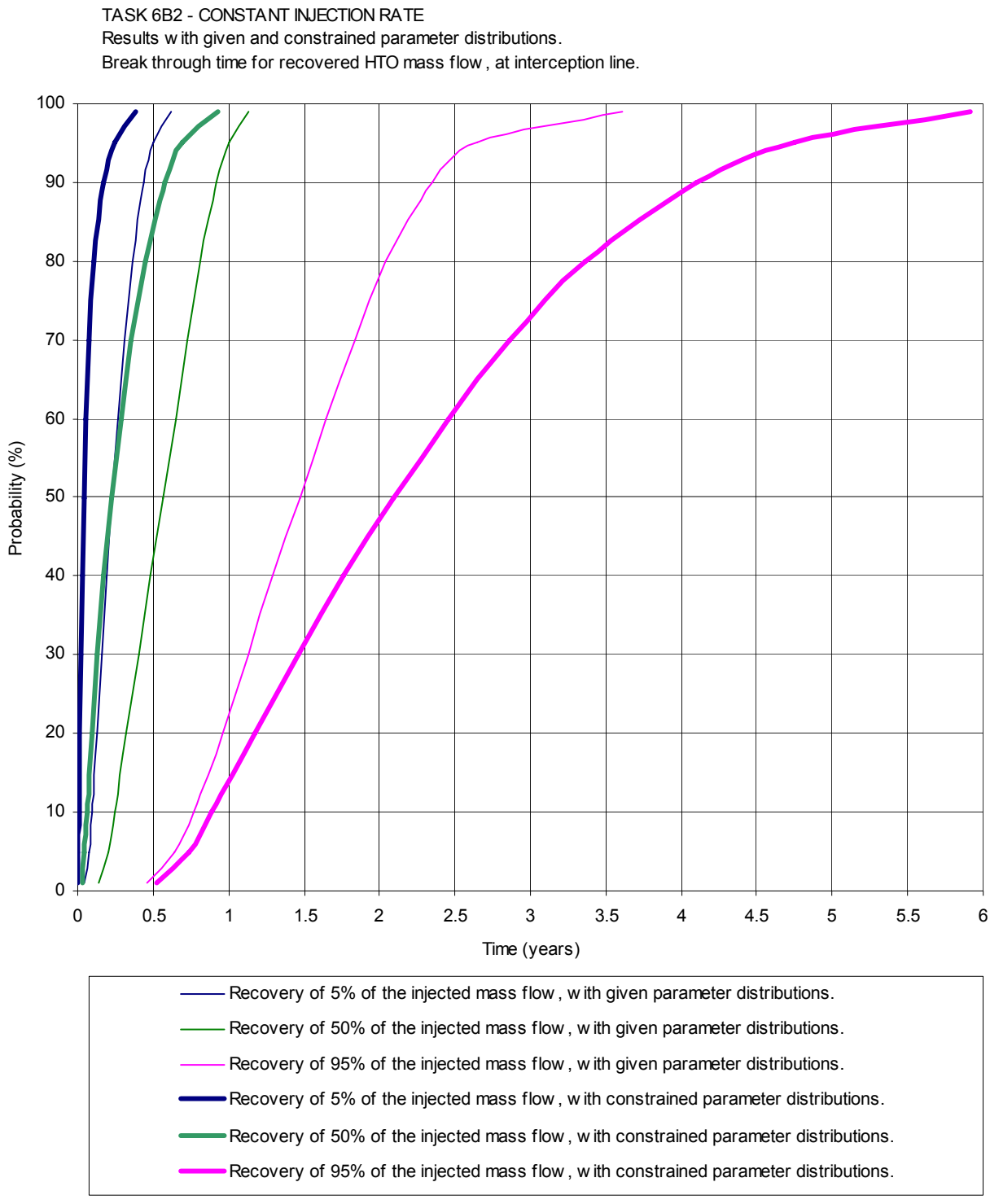

Figure 10-11 *HTO – Constant injection rate. Probability distributions of breakthrough times for recovery of injected mass flow. Results with given and constrained parameter distributions.*

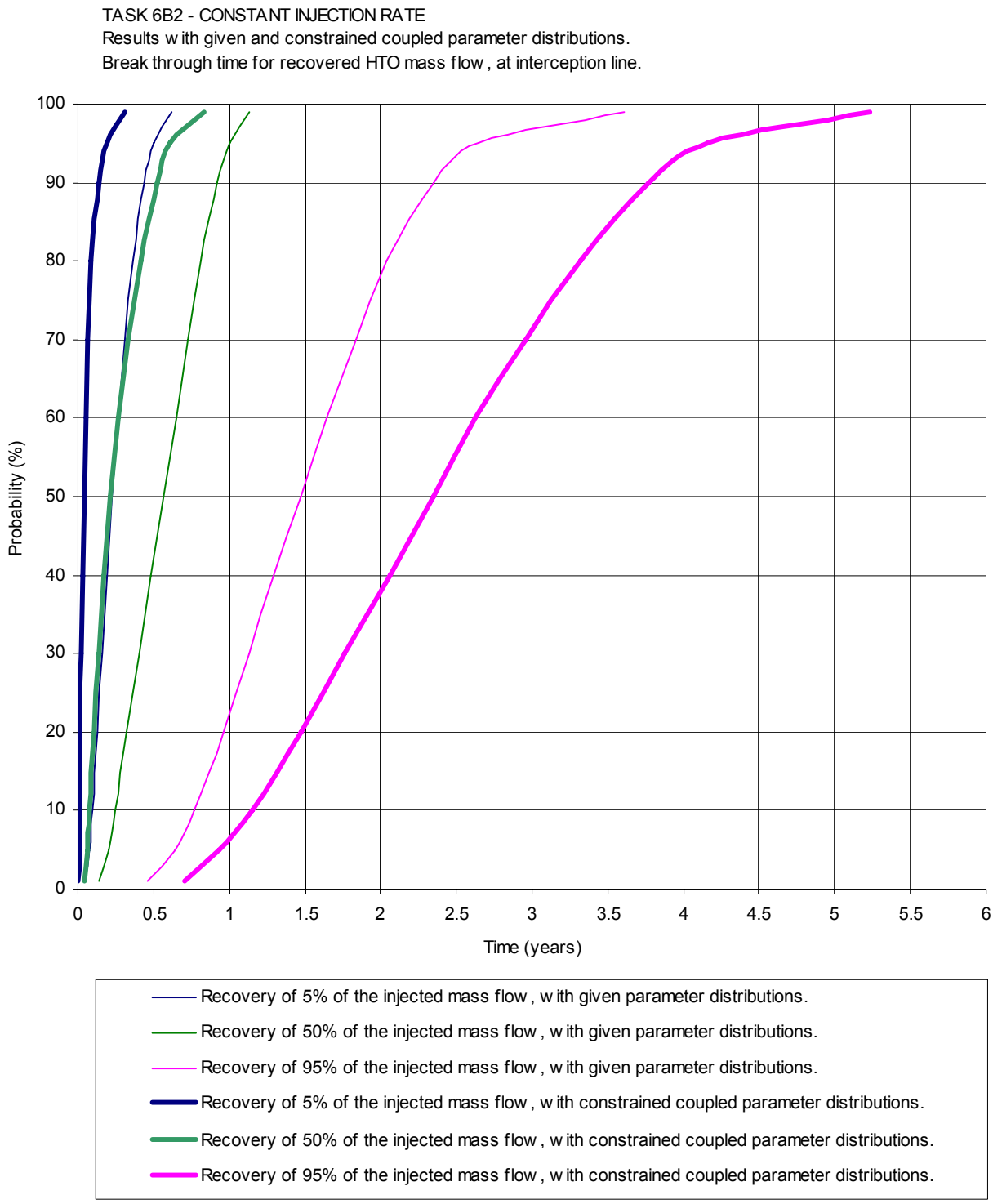

Figure 10-12 *HTO – Constant injection rate. Probability distributions of breakthrough times for recovery of injected mass flow. Results with given and constrained coupled parameter distributions.*

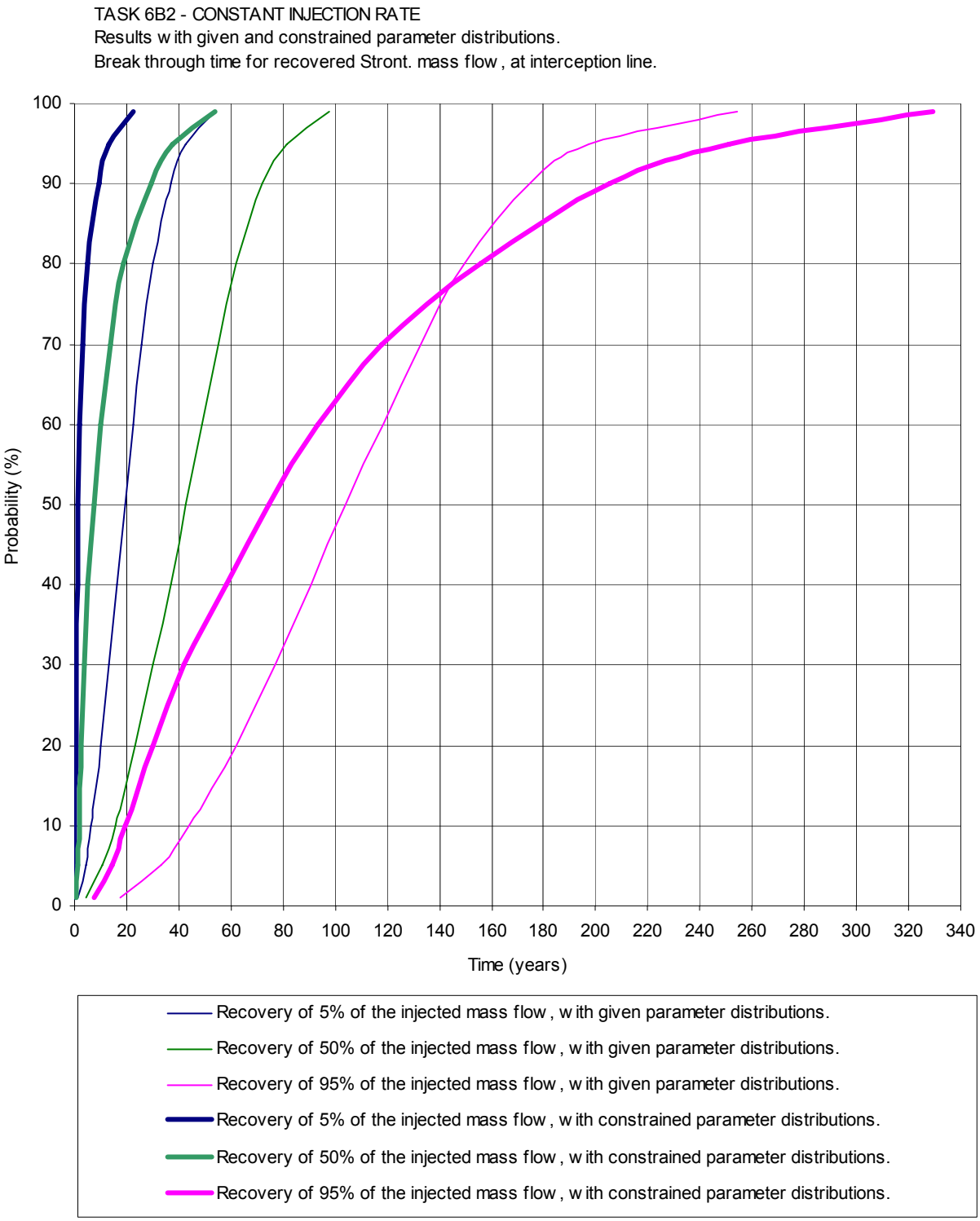

Figure 10-13 *Strontium – Constant injection rate. Probability distributions of breakthrough times for recovery of injected mass flow. Results with given and constrained parameter distributions.*

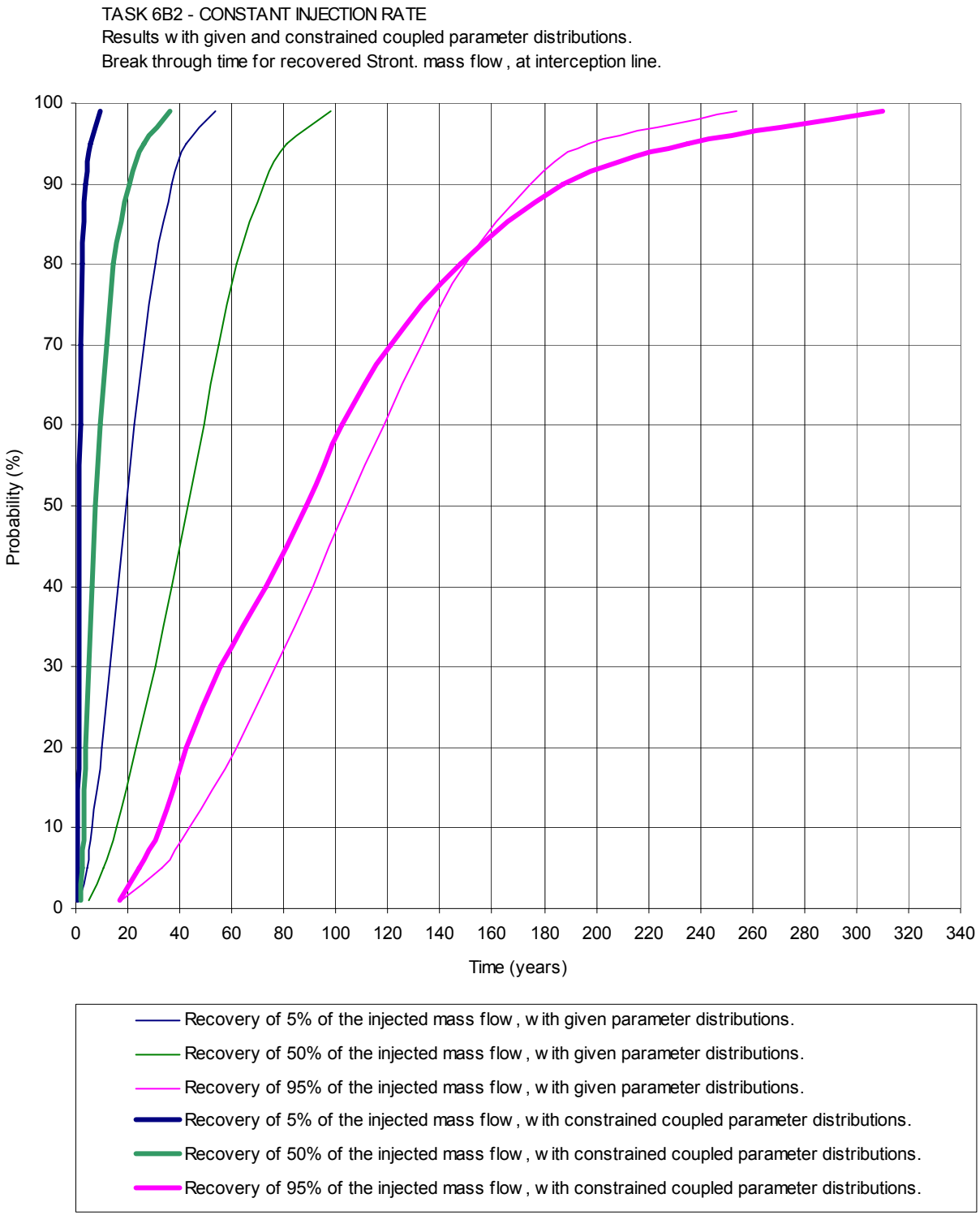

Figure 10-14 *Strontium – Constant injection rate. Probability distributions of breakthrough times for recovery of injected mass flow. Results with given and constrained coupled parameter distributions.*

11 TASK 6B2 – Dirac pulse injection

11.1 General

For these simulations a Dirac pulse injection of the tracers studied was prescribed at the release line. The injected amount of tracer corresponds to 1 MBq, for the HTO tracer and the same amount for the Strontium tracer. At the interception line, ten metres from the release line, the flow of tracer was calculated. With time the flow of mass at the interception line will increase from zero, and after a short period form a single or multiple, week or strong, local maximums in mass flow (peaks), and after some further time, the mass flow will decline towards zero. Simulations were carried out for both the HTO and the Strontium tracer, and by use of both the given parameter distribution and the constrained parameter distribution.

11.2 Examples of breakthrough curves

11.2.1 HTO - tracer

Considering the HTO tracer, a few examples of breakthrough curves are given in Figure 11-1, Figure 11-2, Figure 11-3 and Figure 11-4. The curves given in Figure 11-1 were calculated with the given parameter distributions. Figure 11-2 were calculated with the constrained parameter distributions, while the curves in Figure 11-3 and Figure 11-4 were calculated with the constrained coupled parameter distributions.

11.2.2 Strontium - tracer

Considering the Strontium tracer, a few examples of breakthrough curves are given in Figure 11-5, Figure 11-6, Figure 11-7 and Figure 11-8. The curves given in Figure 11-5 were calculated with the given parameter distributions. Figure 11-6 were calculated with the constrained parameter distributions, while the curves in Figure 11-7 and Figure 11-8 were calculated with the constrained coupled parameter distributions.

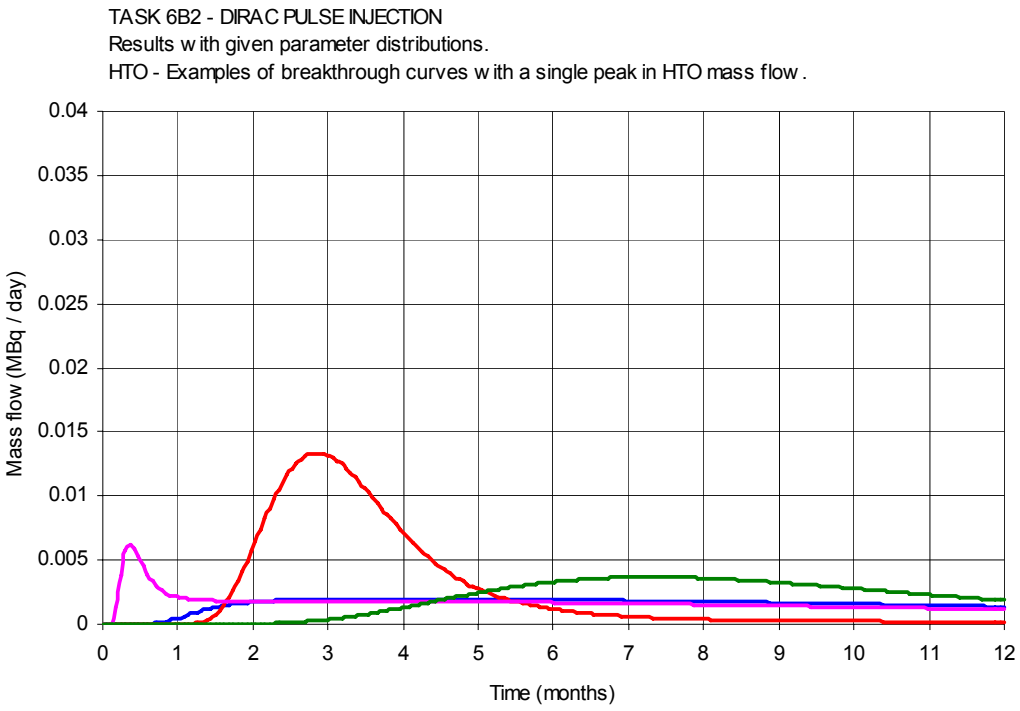

Figure 11-1 *HTO – Examples of breakthrough curves calculated by use of the given parameter distributions.*

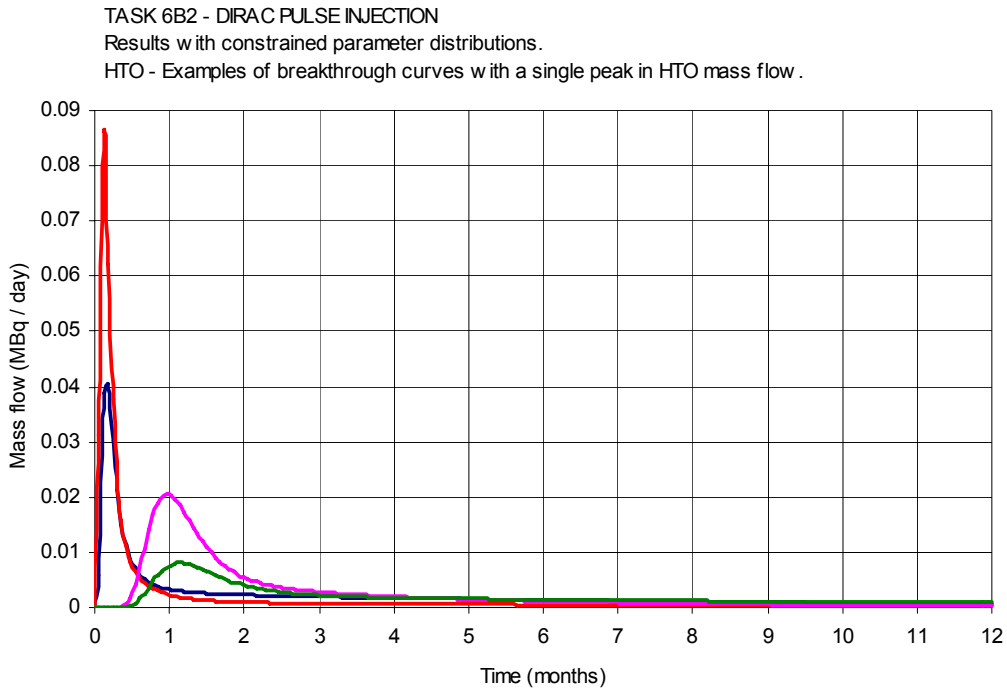

Figure 11-2 *HTO – Examples of breakthrough curves calculated by use of the constrained parameter distributions. Note that the y-scale is different compared to the other HTO figures.*

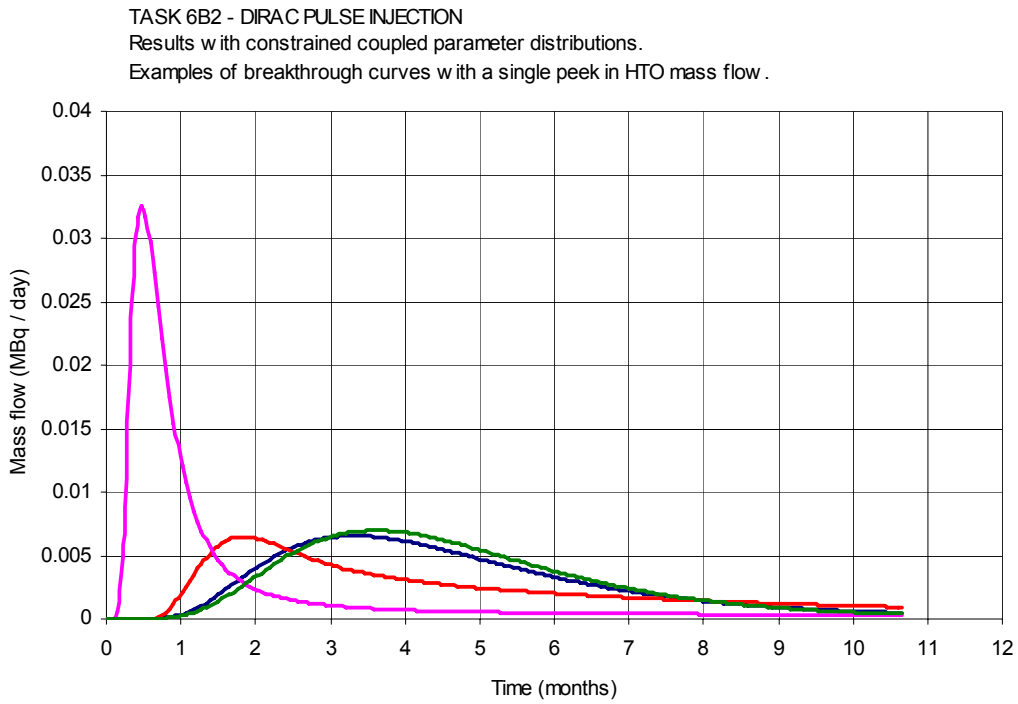

Figure 11-3 *HTO – Examples of breakthrough curves calculated by use of the constrained coupled parameter distributions.*

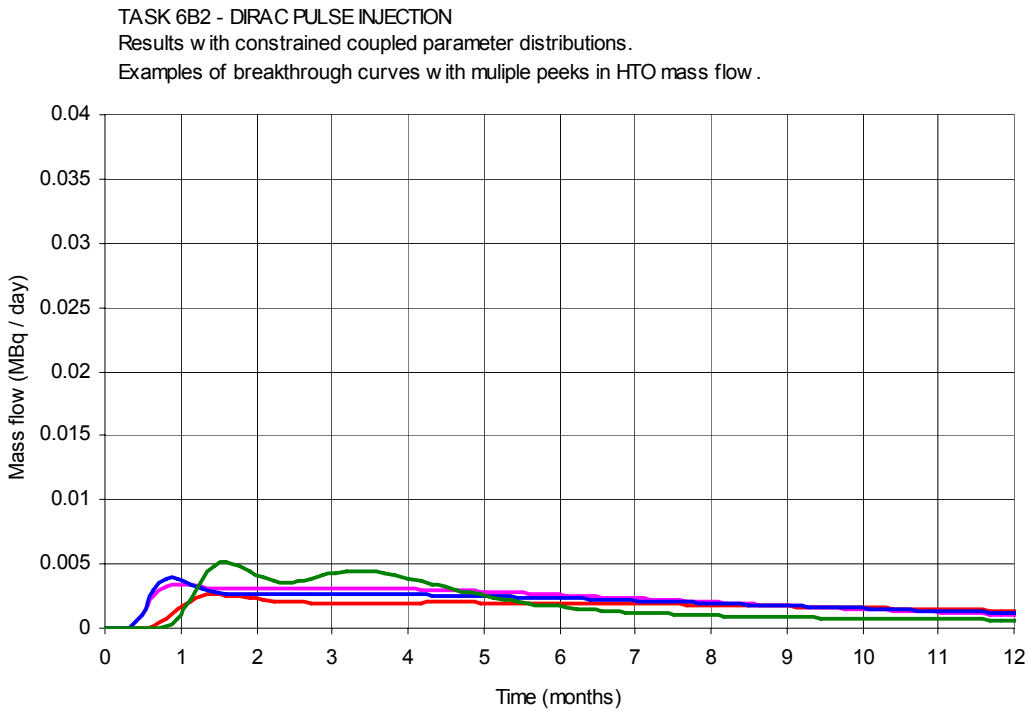

Figure 11-4 *HTO – Examples of breakthrough curves calculated by use of the constrained coupled parameter distributions. The presented breakthrough curves contain multiple peaks in HTO mass flow.*

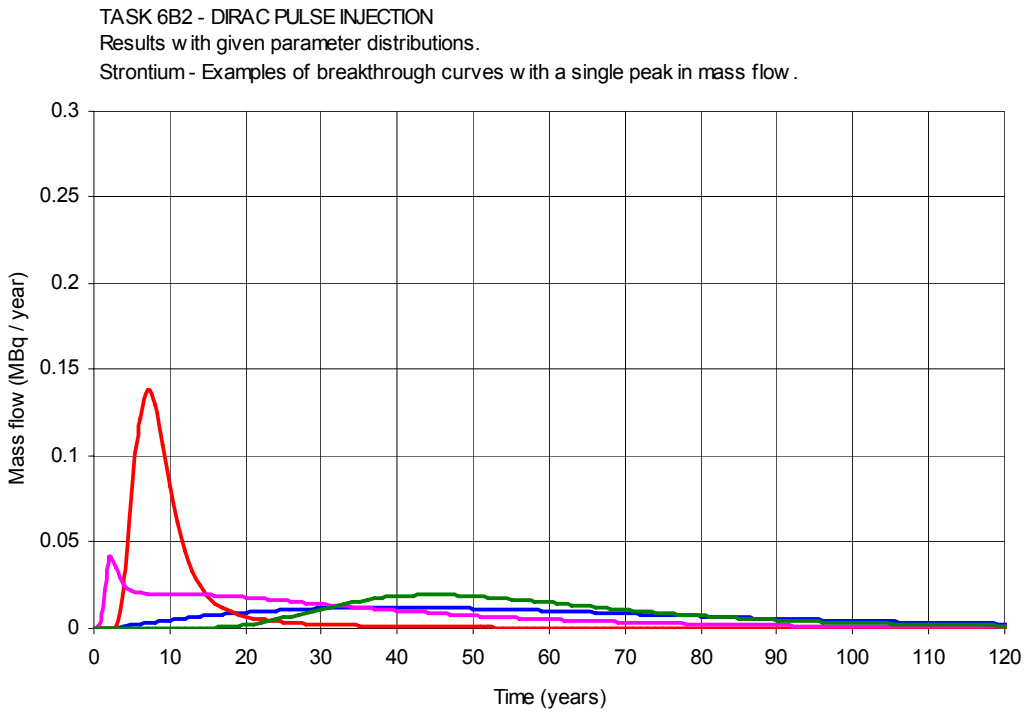

Figure 11-5 *Strontium – Examples of breakthrough curves calculated by use of the given parameter distributions.*

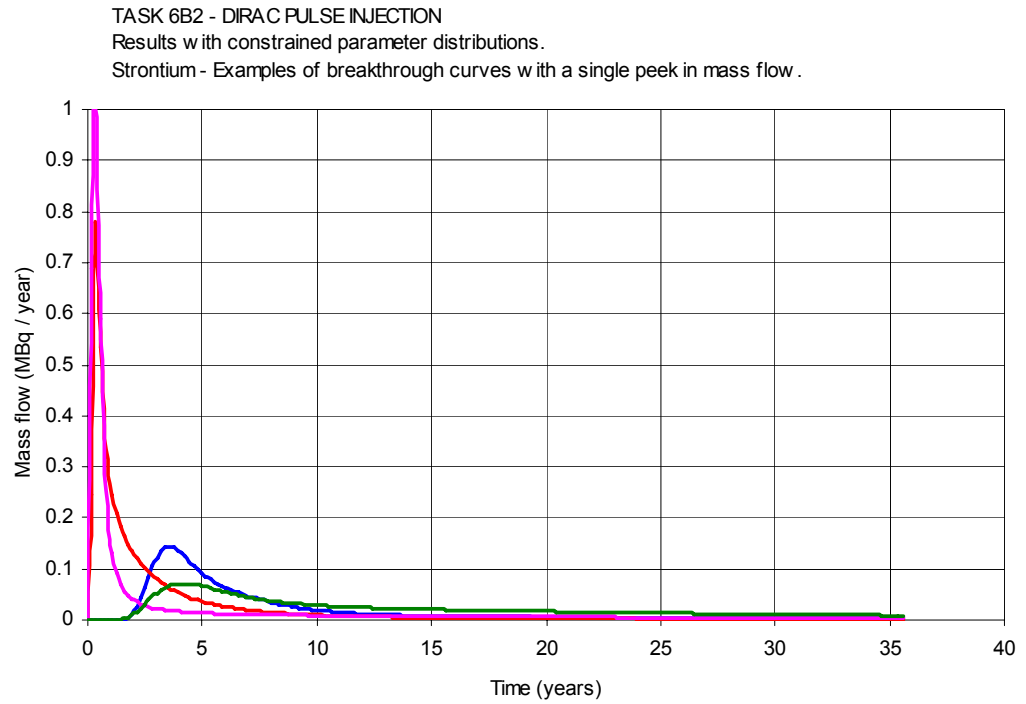

Figure 11-6 *Strontium – Examples of breakthrough curves calculated by use of the constrained parameter distributions. Note that the scale is different in this figure, compared to the other figures with Strontium and a Dirac pulse.*

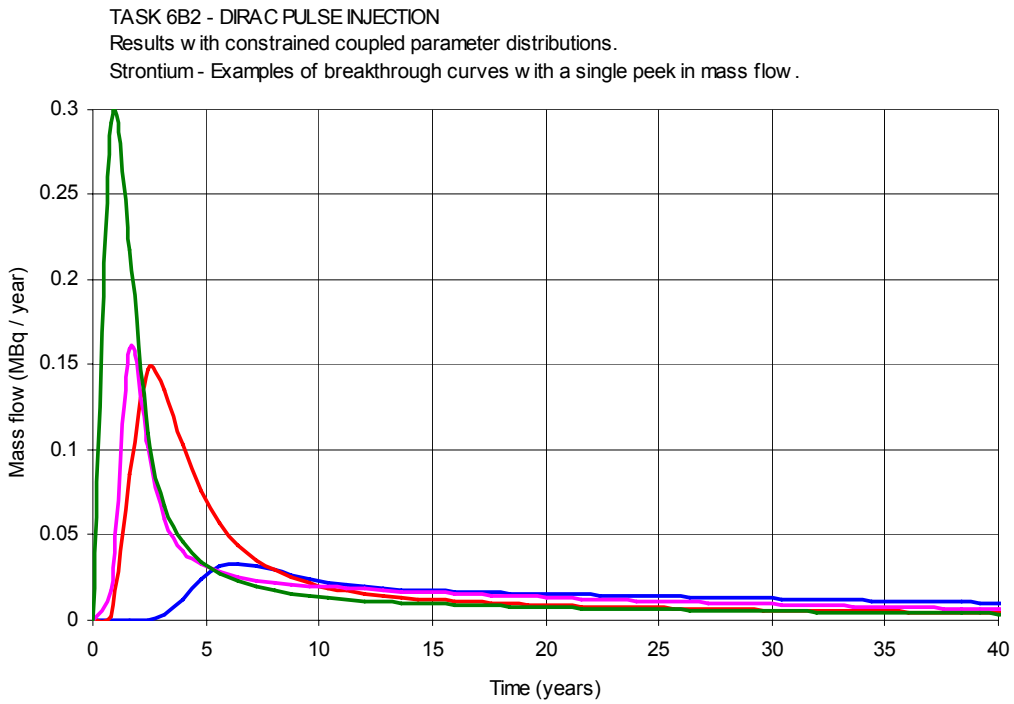

Figure 11-7 *Strontium – Examples of breakthrough curves calculated by use of the constrained coupled parameter distributions.*

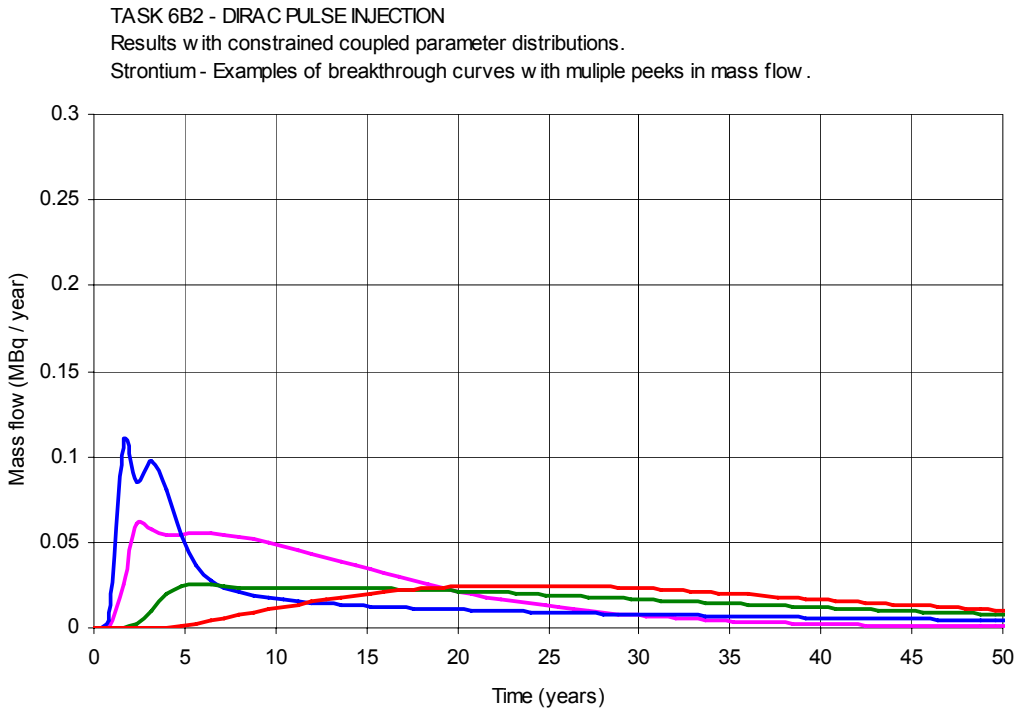

Figure 11-8 *Strontium - Examples of breakthrough curves calculated by use of the constrained coupled parameter distributions. The presented breakthrough curves contain multiple peaks in mass flow. Some curves may have a second distinctive maximum at a late time.*

11.3 Probability distribution of mass flow versus time

At each time step of the simulation, the probability distribution of mass flow at the interception line (breakthrough of mass) is calculated. (There is one probability distribution for each timestep of the simulation.) The probability distributions are characterised by percentiles. The results are given in figures presenting the probability for different amounts of mass flow, versus time.

Considering HTO and a Dirac pulse injection, the probability distributions of mass flow at the interception line versus time, is given in Figure 11-9.

Considering Strontium and a Dirac pulse injection, the probability distributions of mass flow at the interception line versus time, is given in Figure 11-11.

11.4 Probability distribution of breakthrough times for recovery of mass

The total amount of arrived tracer mass (cumulative mass) at the interception line is called the recovery of mass. The recovered mass is calculated as a percentage of the released mass (i.e. the mass contained in the Dirac pulse). For different amounts of recovered mass, i.e 5%, 50% and 95%, we have calculated the probability distribution of the corresponding breakthrough times. Hence, the probability distribution of the breakthrough times for 5, 50 and 95 percent of recovered mass.

The results are given in Figure 11-13 and Figure 11-15 below; these figures present the cumulative probability distributions.

11.5 Analyses of peaks

The velocity distribution within the plume is represented in the transport model by ten parallel GoldSim pipes. The flow properties, e.g. size of flow, are not the same in the ten pipes, but vary from pipe to pipe. Therefore multiple peaks of mass flow may occur at the interception line. The probability of having multiple peaks is however small. We have analysed the variation in mass flow at the interception line with regard to the properties of the peaks in mass flow.

11.5.1 HTO tracer

The probability distributions of arrival time for the largest peak in mass flow are given in Figure 11-17, below. The probability distributions of size of largest peak in mass flow are given in Figure 11-18. The probability of having a multiple peaks is approximately 3.0 percent for both the given parameter distributions and the constrained parameter distributions, and approximately 0.3 percent with the constrained coupled parameter distributions.

11.5.2 Strontium

The probability distributions of arrival time for the largest peak in mass flow are given in Figure 11-21, below. The probability distributions of size of largest peak in mass flow are given in Figure 11-22. The probability of having a multiple peaks is approximately 3 to 4 percent with the given and constrained parameter distributions, and approximately 0.4 percent with the constrained coupled parameter distributions.

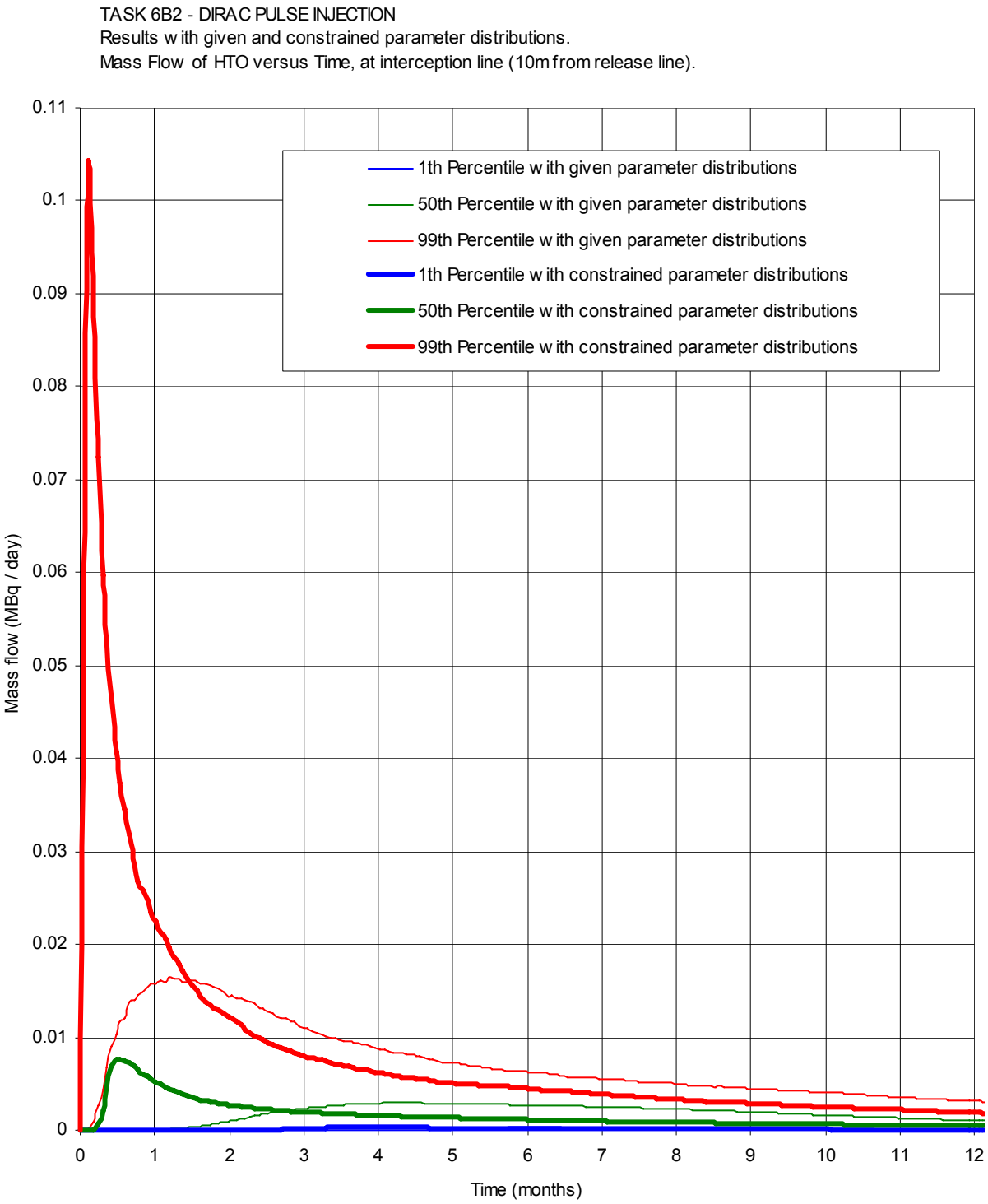

Figure 11-9 *HTO – Dirac pulse injection. Probability distributions of mass flow versus time, at the interception line. Results with given and constrained parameter distribution.*

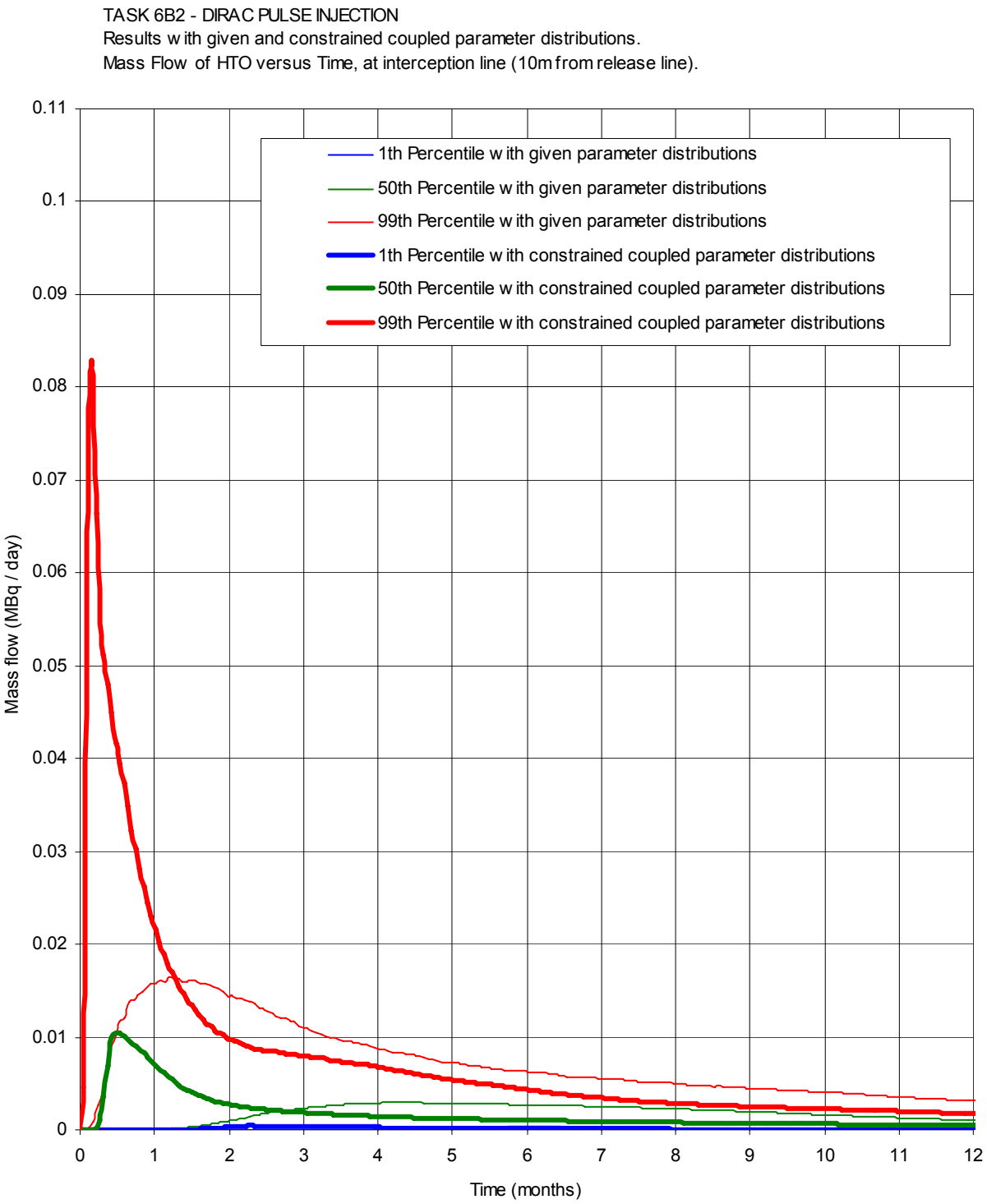

Figure 11-10 *HTO – Dirac pulse injection. Probability distributions of mass flow versus time, at the interception line. Results with given and constrained coupled parameter distributions. Note that the scale is different in this figure compared to that of the previous figure.*

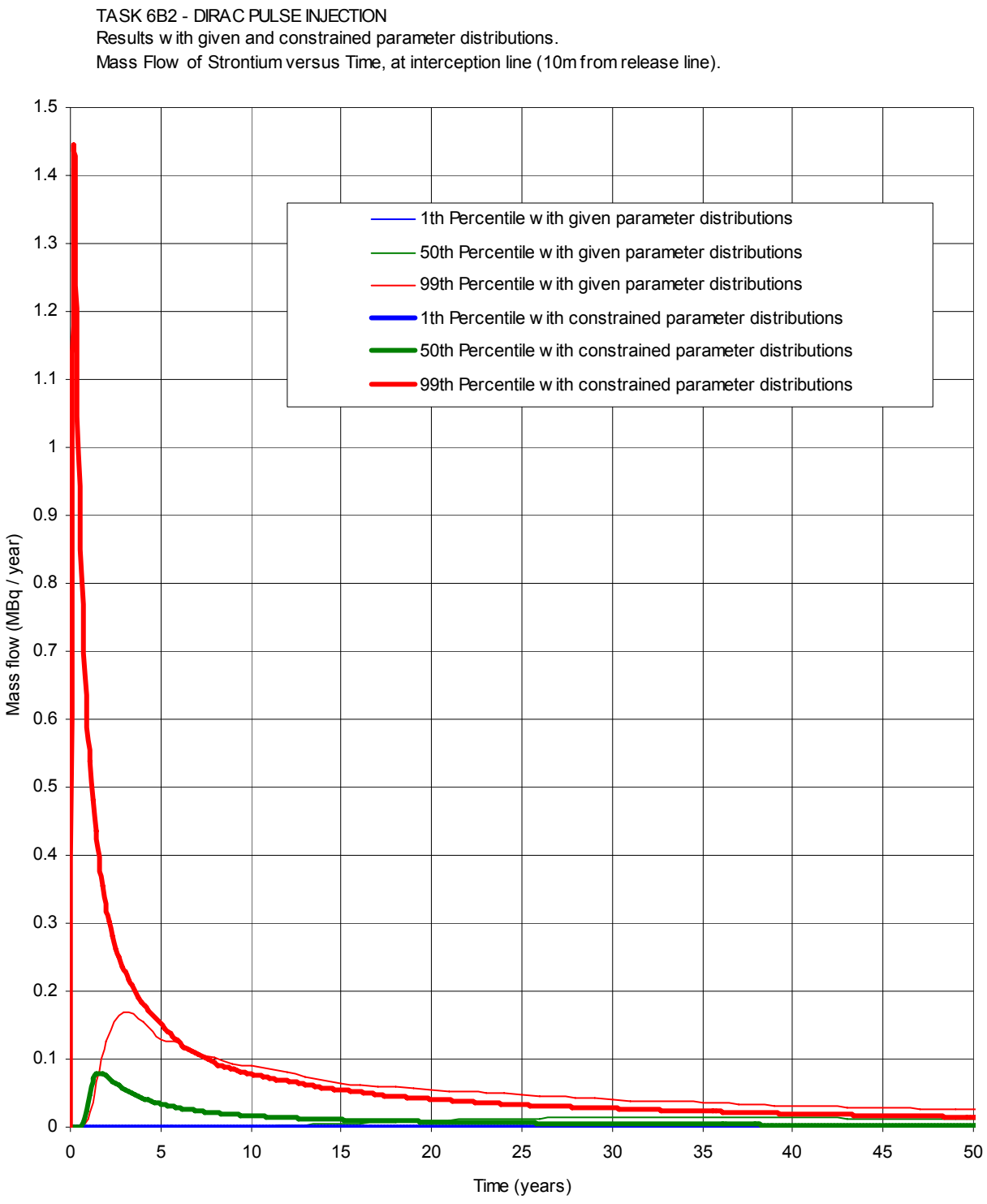

Figure 11-11 *Strontium – Dirac pulse injection. Probability distributions of mass flow versus time at the interception line. Results with given and constrained parameter distributions.*

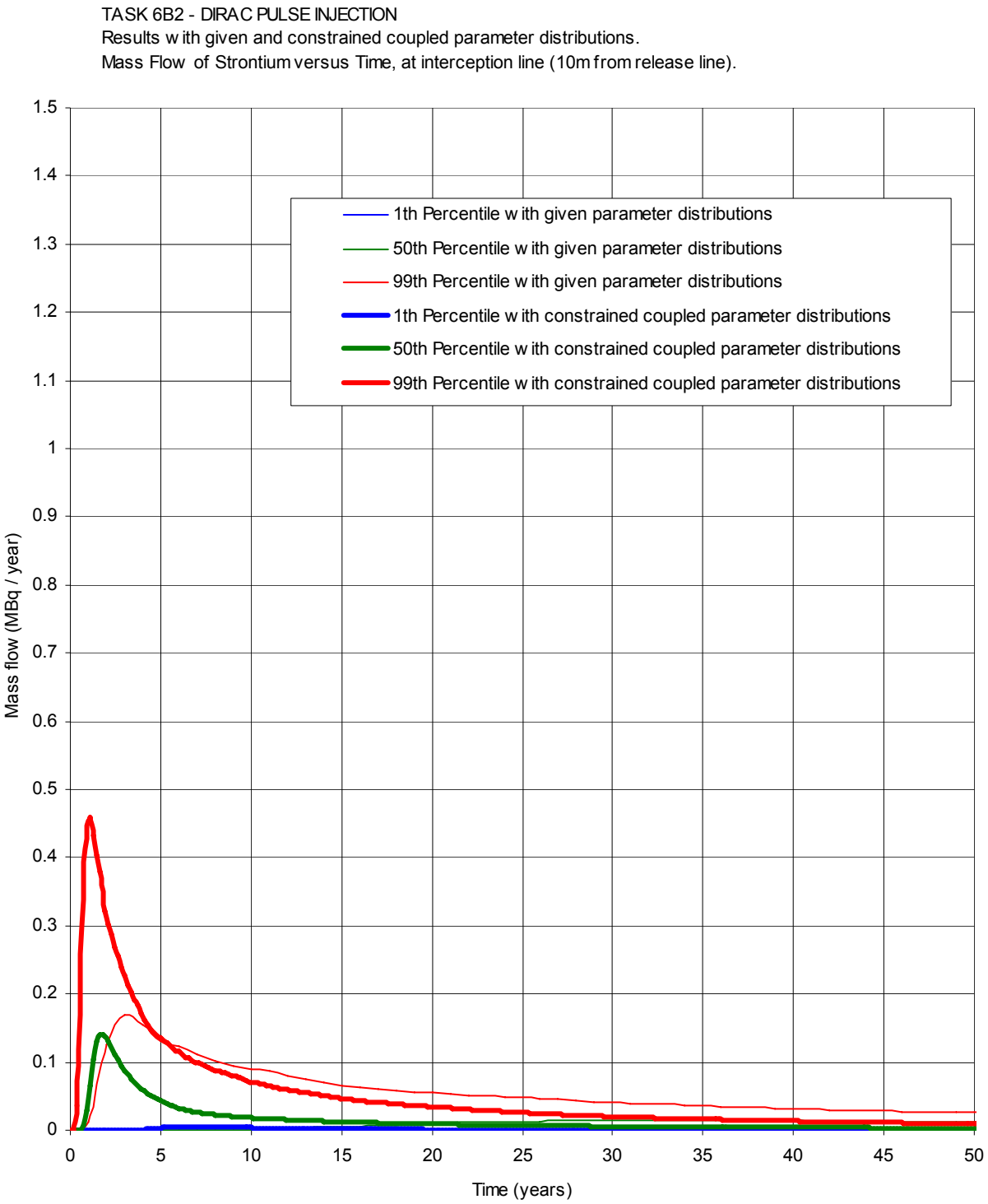

Figure 11-12 *Strontium – Dirac pulse injection. Probability distributions of mass flow versus time at the interception line. Results with given and constrained coupled parameter distributions.*

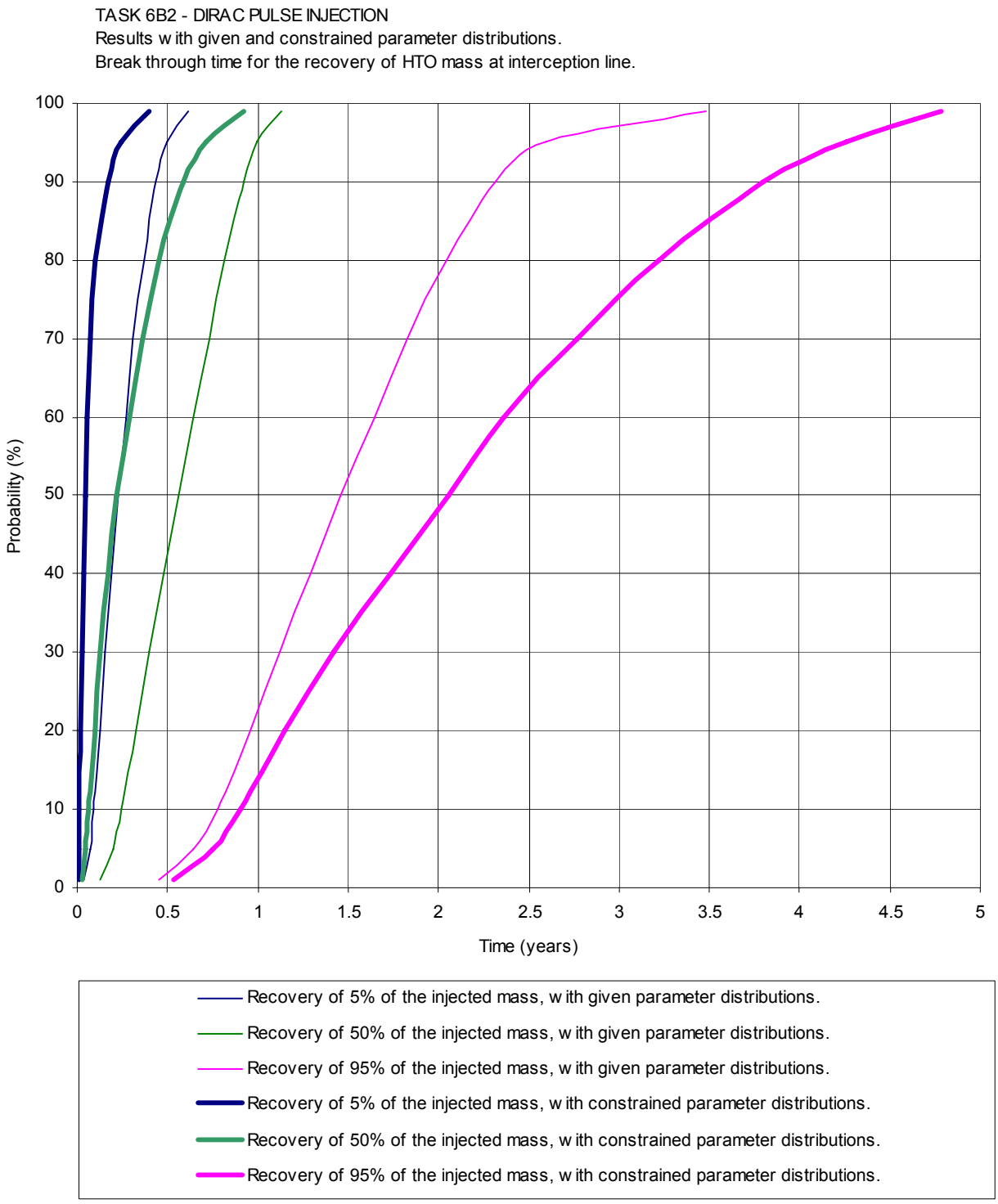

Figure 11-13 *HTO – Dirac pulse injection. Probability distributions of breakthrough times for recovery of injected mass. Results with given and constrained parameter distributions.*

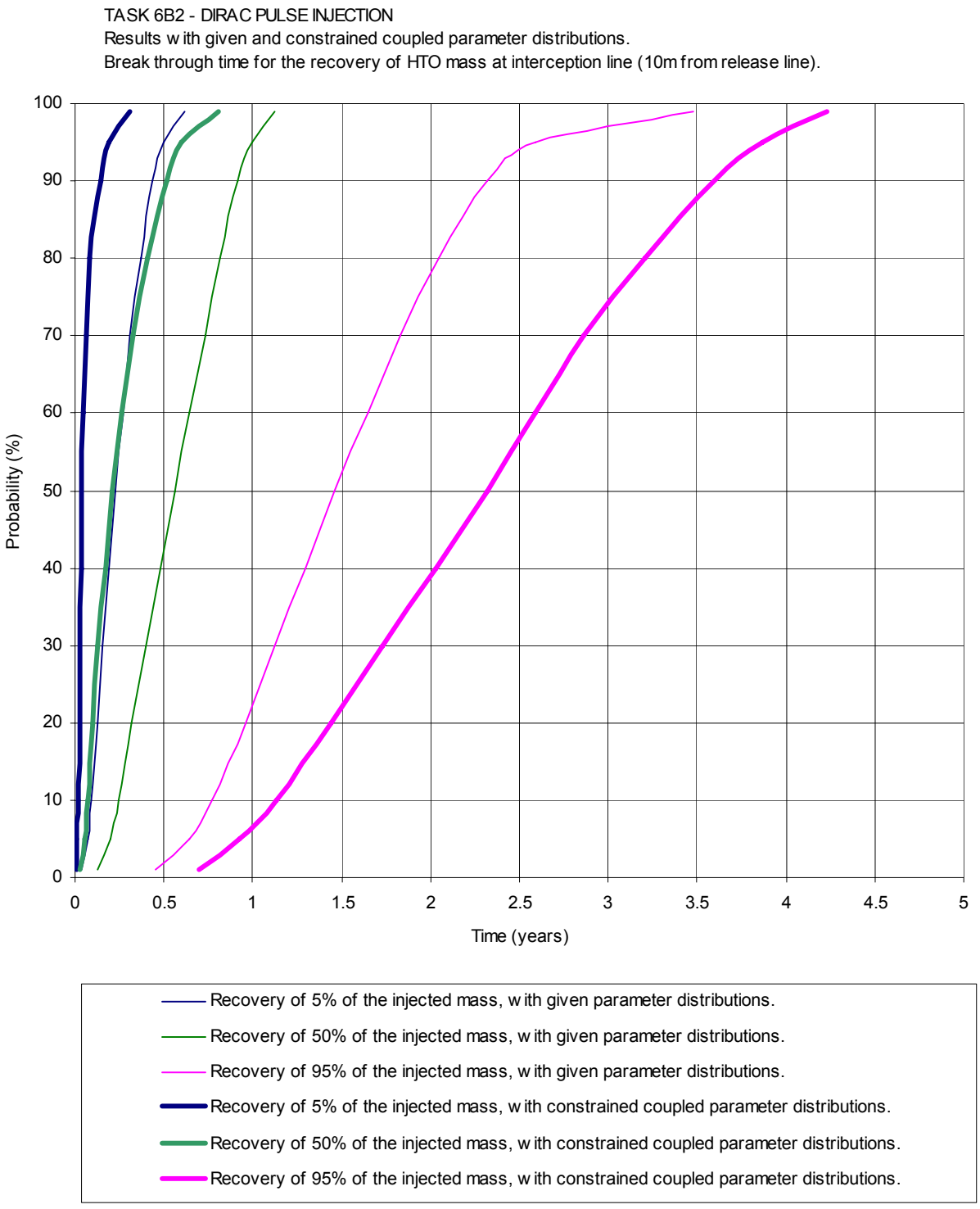

Figure 11-14 *HTO – Dirac pulse injection. Probability distributions of breakthrough times for recovery of injected mass. Results with given and constrained coupled parameter distributions.*

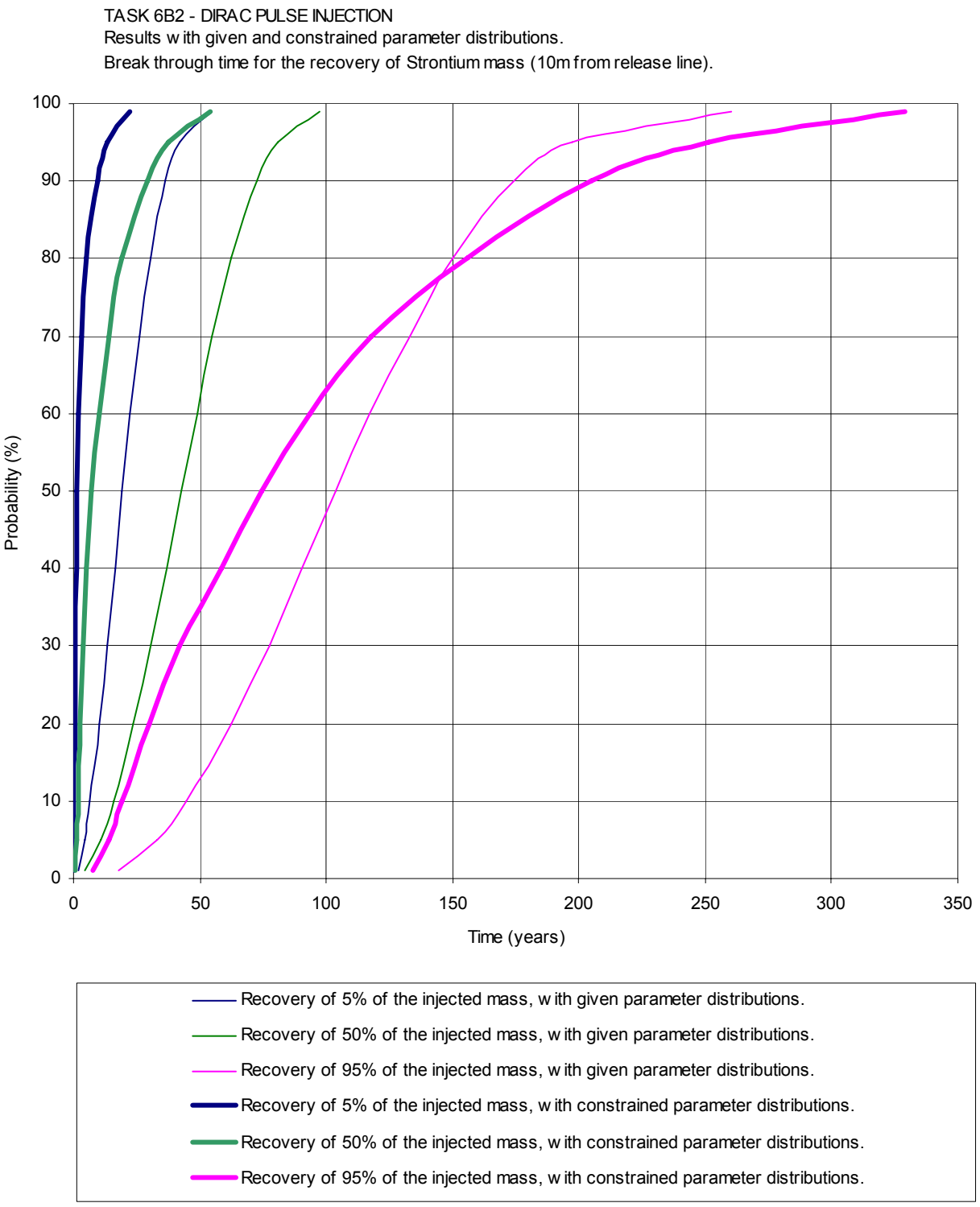

Figure 11-15 *Strontium – Dirac pulse injection. Probability distributions of breakthrough times for recovery of injected mass. Results with given and constrained parameter distributions.*

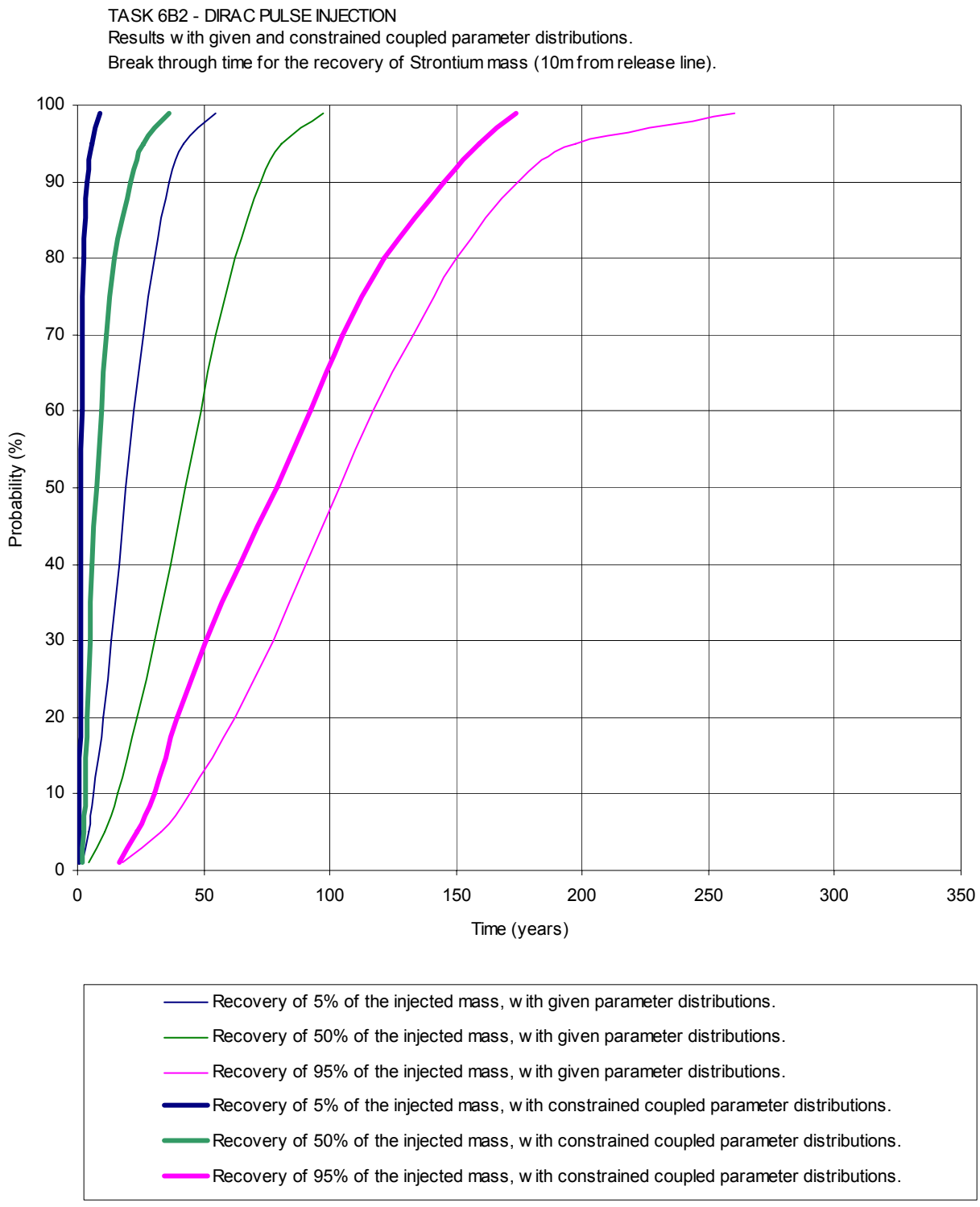

Figure 11-16 *Strontium – Dirac pulse injection. Probability distributions of breakthrough times for recovery of injected mass. Results with given and constrained coupled parameter distributions.*

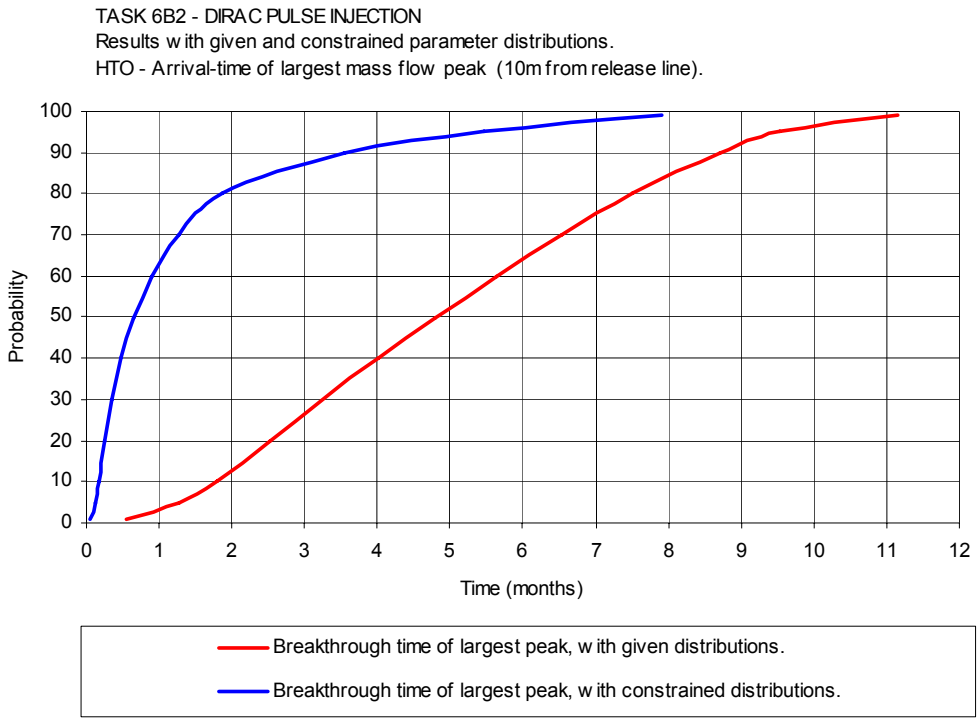

Figure 11-17 *HTO – Dirac pulse injection. Probability distributions of arrival time for the largest peak in mass flow. Results with given and constrained parameter distributions.*

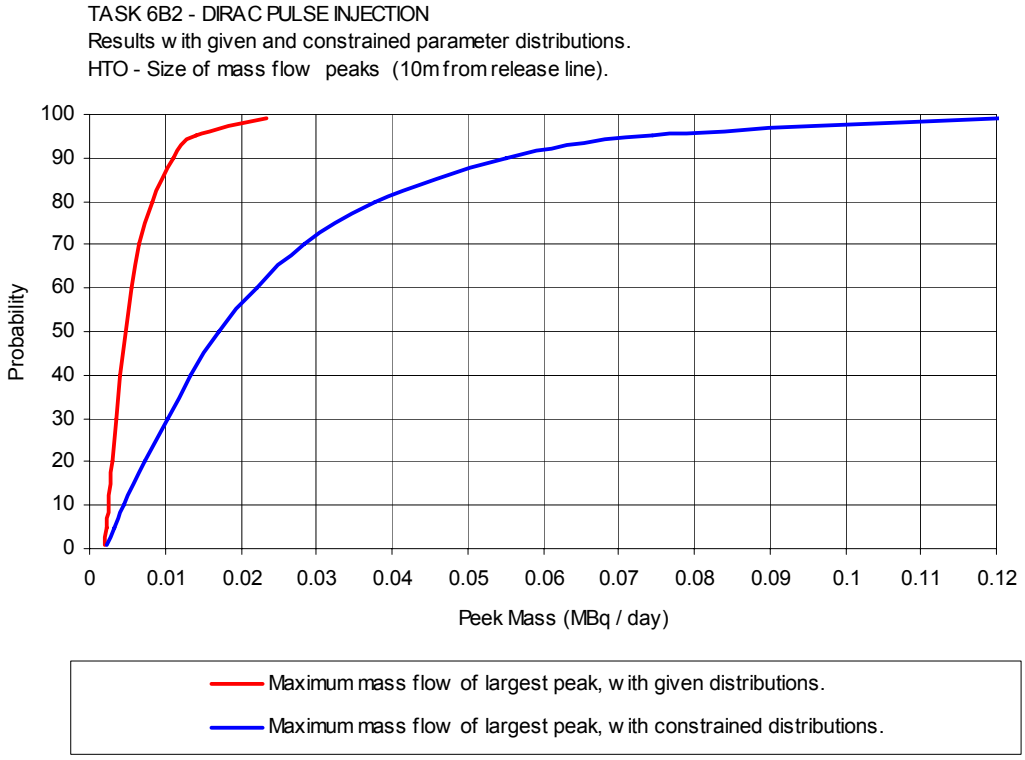

Figure 11-18 *HTO – Dirac pulse injection. Probability distributions of size of largest peak in mass flow. Results with given and constrained parameter distributions.*

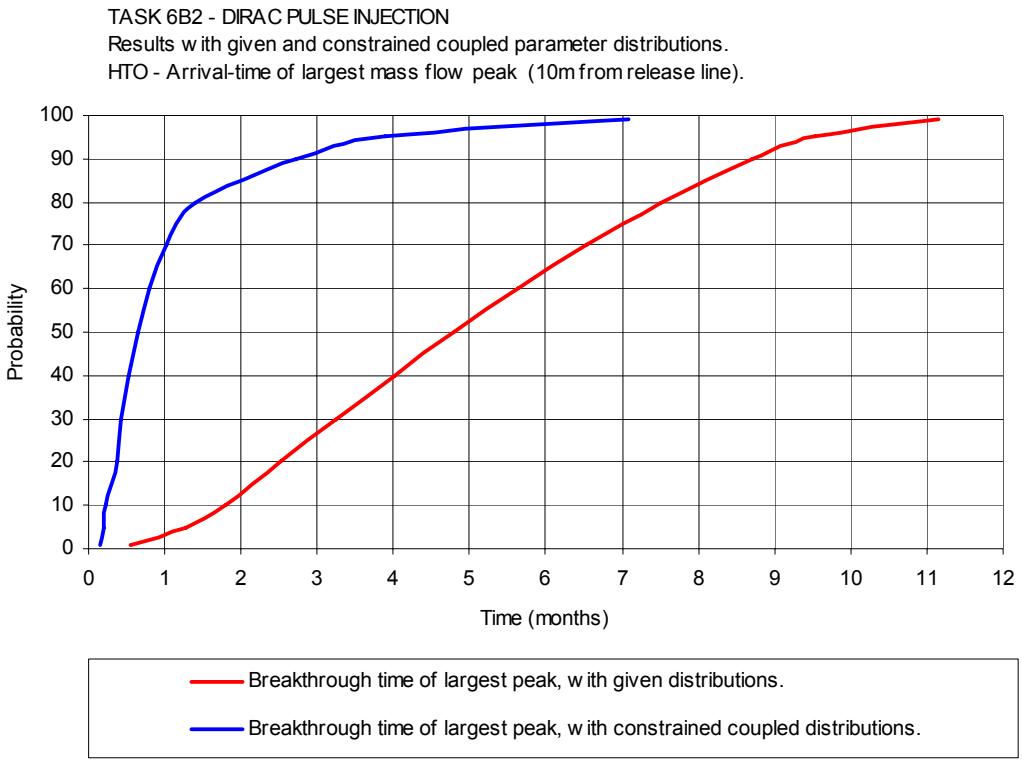

Figure 11-19 *HTO – Dirac pulse injection. Probability distributions of arrival time for the largest peak in mass flow. Results with given and constrained coupled parameter distributions.*

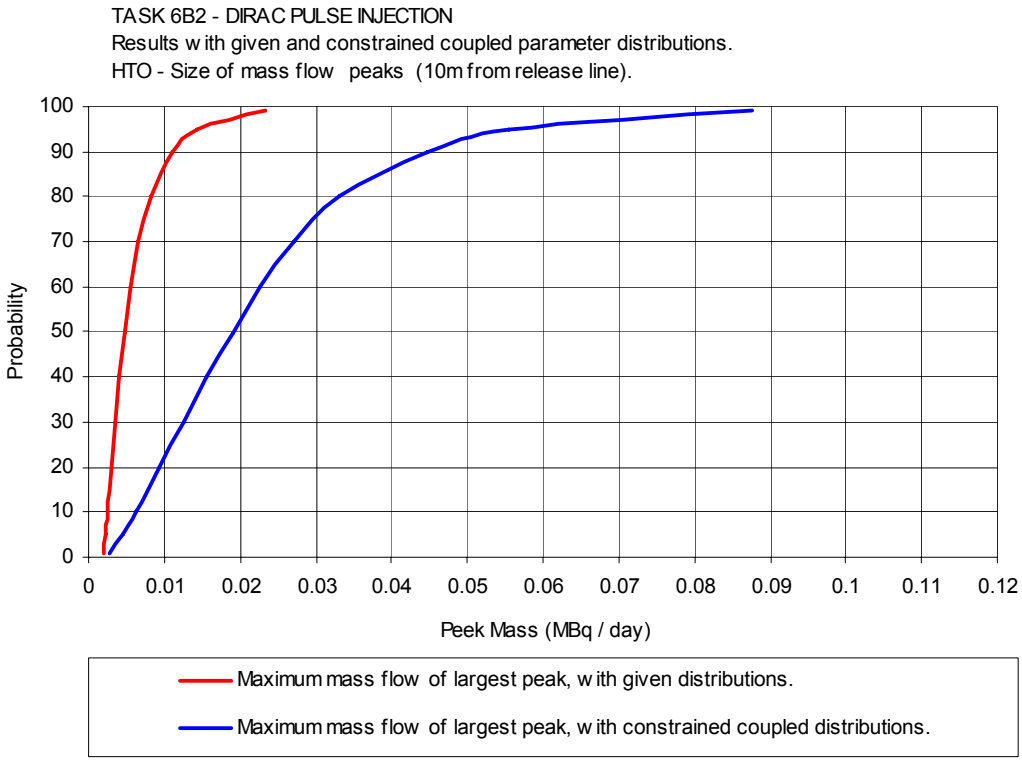

Figure 11-20 *HTO – Dirac pulse injection. Probability distributions of size of largest peak in mass flow. Results with given and constrained coupled parameter distributions*

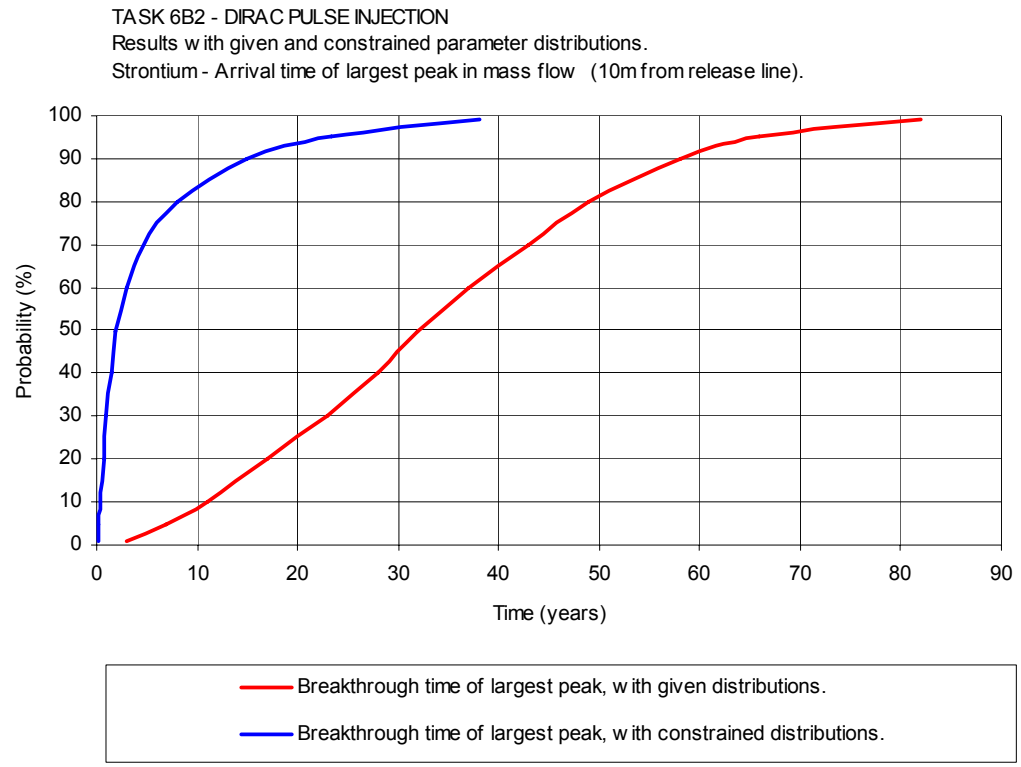

Figure 11-21 *Strontium – Dirac pulse injection. Probability distributions of arrival time for the largest peak in mass flow. Results with given and constrained parameter distributions.*

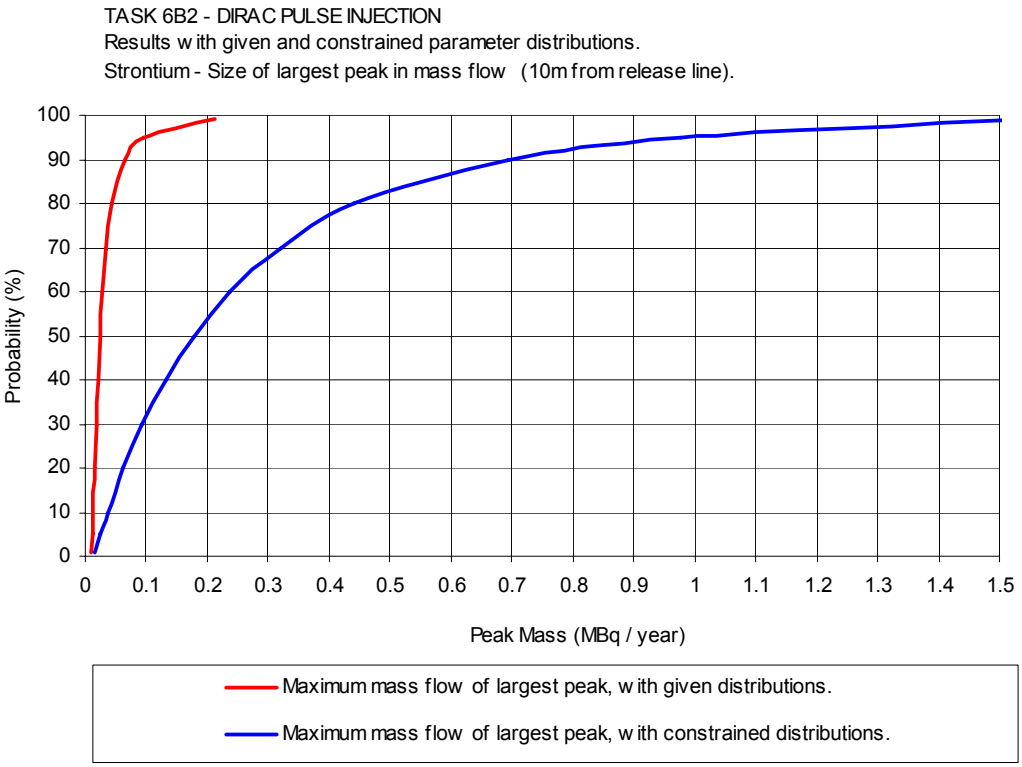

Figure 11-22 *Strontium – Dirac pulse injection. Probability distributions of size of largest peak in mass flow. Results with given and constrained parameter distributions.*

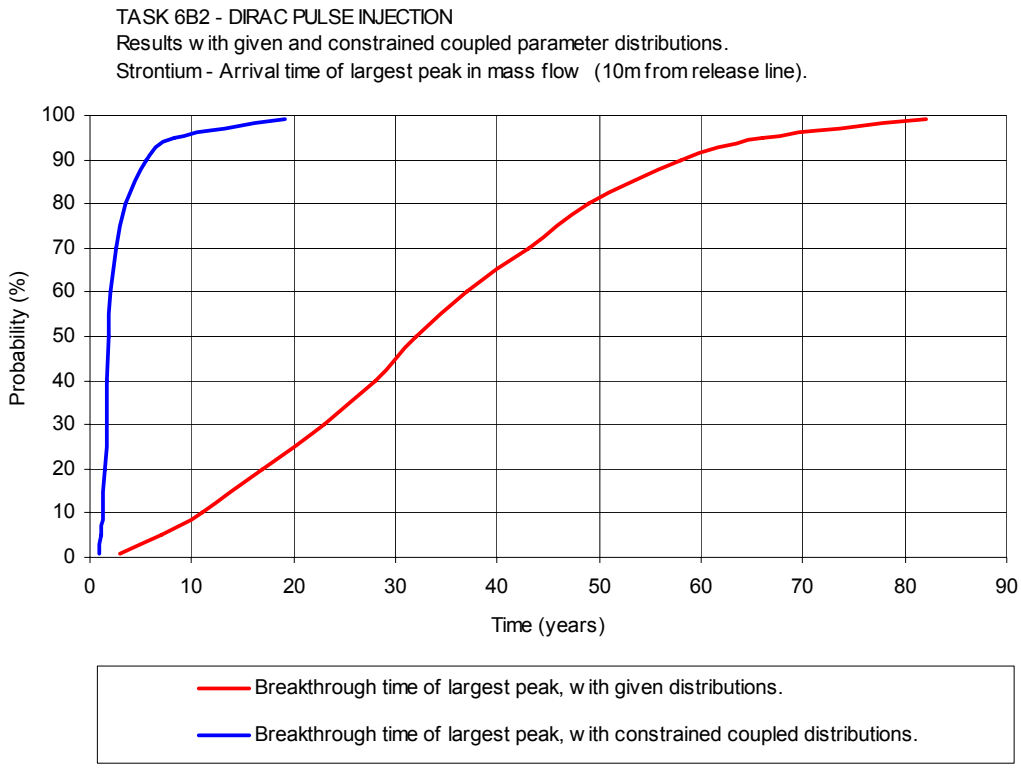

Figure 11-23 *Strontium – Dirac pulse injection. Probability distributions of arrival time for the largest peak in mass flow. Results with given and constrained coupled parameter distributions.*

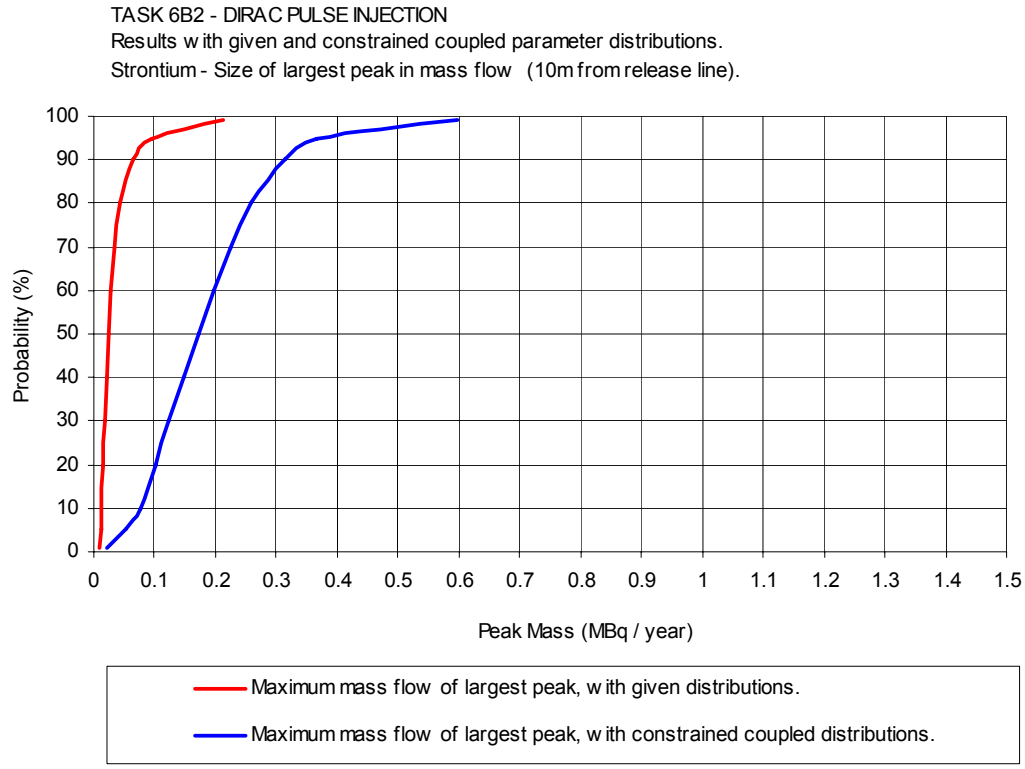

Figure 11-24 *Strontium – Dirac pulse injection. Probability distributions of size of largest peak in mass flow. Results with given and constrained coupled parameter distributions.*

11.6 Summary of results - Dirac pulse injection

11.6.1 HTO tracer

We summarize the following results for the HTO tracer, considering a Dirac pulse injection of 1 MBq, 10 metres upstream of the interception line.

Peak in mass flow – Arrival time

Most realisations demonstrate a single peak in mass flow, but realisations with multiple peaks occur, but with a small probability. The probability of having a multiple peaks is 2.8 percent, considering both the given and constrained parameter distributions, but with the constrained coupled distribution the probability is only 0.3 percent.

It is likely that at the interception line, the maximum mass flow–the largest peak–will occur within less than two and a half months.

For the given parameter distributions:

With a probability of 10%, the peak will occur within 1.8 months
With a probability of 50%, the peak will occur within 4.8 months
With a probability of 90%, the peak will occur within 8.7 months

For the constrained parameter distributions:

With a probability of 10%, the peak will occur within 0.2 months
With a probability of 50%, the peak will occur within 0.7 months
With a probability of 90%, the peak will occur within 3.5 months

For the constrained coupled parameter distributions:

With a probability of 10%, the peak will occur within 0.2 months
With a probability of 50%, the peak will occur within 0.6 months
With a probability of 90%, the peak will occur within 2.6 months

The uncertainty in peak arrival time is described by the length of the period between the arrival times with 90% and 10% probability (other probability-values can also be used).

A comparison of the different parameter distributions gives the following result:

Given parameter distributions: Difference in arrival time is 6.9 months.
Constrained parameter distributions: Difference in arrival time is 3.3 months.
Constrained coupled parameter distributions: Difference in arrival time is 2.4 months

It is demonstrated by the comparison above, that the smallest uncertainty is produced by use of the constrained coupled parameter distributions; expressed as length of a time period, the uncertainty produced with this distribution is 35% of the uncertainty produced with the given parameter distribution. It is likely that the constrained and constrained coupled parameter distributions will produce an earlier peak in mass flow than the peak produced with the given parameter distributions. The uncertainties in peak arrival time are also demonstrated by Figure 11-17 and Figure 11-19.

Peak in mass flow – Size of peak

It is likely that at the interception line, the size of the maximum mass flow (the largest peak) will be less than 0.04 MBq/day.

For the given parameter distributions:

With a probability of 10%, the size of the peak will be less than 0.0026 MBq/day
With a probability of 50%, the size of the peak will be less than 0.0047 MBq/day
With a probability of 90%, the size of the peak will be less than 0.011 MBq/day

For the constrained parameter distributions:

With a probability of 10%, the size of the peak will be less than 0.0046 MBq/day
With a probability of 50%, the size of the peak will be less than 0.017 MBq/day
With a probability of 90%, the size of the peak will be less than 0.055 MBq/day

For the constrained coupled parameter distributions:

With a probability of 10%, the size of the peak will be less than 0.0062 MBq/day
With a probability of 50%, the size of the peak will be less than 0.019 MBq/day
With a probability of 90%, the size of the peak will be less than 0.045 MBq/day

The uncertainty in size of peak is described by the difference between the sizes of peaks with 90% and 10% probability (other probability-values can also be used).

A comparison of the different parameter distributions gives the following result:

Given parameter distributions: Difference in size is 0.0084 MBq/day
Constrained parameter distributions: Difference in size is 0.050 MBq/day
Constrained coupled parameter distributions: Difference in size is 0.039 MBq/day

It is demonstrated by the comparison above, that the smallest uncertainty is produced by use of the given parameter distributions; expressed as a difference in size of peak, the uncertainty produced with this distribution is about 24% of that produced with the constrained coupled parameter distributions. The reason that the given distributions produce the smallest uncertainty in size of peak is that in general the peaks produced with the given distributions are much smaller than those produced by the constrained and constrained couple parameter distributions. The largest uncertainty is produced by the constrained parameter distributions. The uncertainties in size of peak are also demonstrated by Figure 11-18 and Figure 11-20.

Recovery of mass

The recovered mass at the interception line is calculated as a percentage of the released mass (i.e. the mass contained in the Dirac pulse). For different amounts of recovered mass, i.e 5%, 50% and 95%, we have calculated the probability distribution of the corresponding breakthrough times.

For the given parameter distributions:

With a probability of 90%

5% of the mass will be recovered within 0.44 years.
50% of the mass will be recovered within 0.92 years.
95% of the mass will be recovered within 2.32 years.

For the constrained parameter distributions:

With a probability of 90%

5% of the mass will be recovered within 0.17 years.

50% of the mass will be recovered within 0.59 years.

95% of the mass will be recovered within 3.80 years.

For the constrained coupled parameter distributions:

With a probability of 90%

5% of the mass will be recovered within 0.14 years.

50% of the mass will be recovered within 0.52 years.

95% of the mass will be recovered within 3.60 years.

The constrained and the constrained coupled parameter distributions will produce an earlier arrival of the peak, and therefore the recovery of the first 5% and 50% of mass will take place earlier with these parameter distributions than with the given parameter distributions. However, the constrained and constrained coupled parameter distributions will also produce a somewhat more persistent and long-lived tail than that produced by the given parameter distributions; and therefore the recovery of 95% of mass will take place later with the constrained parameter distributions and the constrained coupled parameter distributions than with the given parameter distributions.

For a given percentage of recovered mass, the length of the period between the 95^{th} and the 5^{th} percentiles of the breakthrough time (for recovery of mass) is a measure of the uncertainty in the predictions of the breakthrough curves. Considering a small amount of recovered mass, the period represents the uncertainty in predictions of the first part of the breakthrough curves. Considering a large amount of recovered mass, the period represents the uncertainty in predictions of the last part of the breakthrough curves.

Considering the HTO tracer and the length of the period between the 95^{th} and 5^{th} percentile of breakthrough time:

Considering recovery of 5% of the mass and the:

Given parameter distributions, the length of the period is 0.43 years

Constrained parameter distributions, the length of the period is 0.23 years

Constrained coupled parameter distributions, the length of the period is 0.18 years.

Considering recovery of 50% of the mass and the:

Given parameter distributions, the length of the period is 0.80 years

Constrained parameter distributions, the length of the period is 0.68 years

Constrained coupled parameter distributions, the length of the period is 0.54 years.

Considering recovery of 95% of the mass and the:

Given parameter distributions, the length of the period is 1.96 years

Constrained parameter distributions, the length of the period is 3.51 years

Constrained coupled parameter distributions, the length of the period is 2.94 years.

The results above demonstrate that for the first part of the Dirac pulse–as described by the recovery of 5% and 50% of the mass–the smallest uncertainty is produced by use of the constrained coupled parameter distributions, this demonstrates the constraining

power of the tracer test analysed in Task 6A. However, considering the last part of the breakthrough curves (recovery of 95% of the mass), the uncertainty in the result produced by the constrained coupled parameter distributions is larger than the uncertainty in the results produced by the given parameter distributions (but smaller than the uncertainty produced by the constrained distribution).

This illustrates the importance of transport processes that had no large influence on the tracer test studied in Task 6A, for example interaction (e.g. matrix diffusion and adsorption) with materials (Diorite and Mylonite) that are not in direct contact with the flowing water, may be very important at the time scales of the recovery of 95% of injected mass in Task 6B2. Hence, as the tracer test demonstrated no constraining power for these transport properties (matrix diffusion), the uncertainty in the result produced by the constrained coupled parameter distributions is of the same size (or larger) than the uncertainty in the results produced with the given parameter distributions, at these large time scales (large time scales in comparison to the time scale of the tracer test).

An interesting result is that the uncertainty discussed above, as described by the length of a time period, is very much the same both for the constant injection and for the Dirac pulse (see Sec.10.5.1).

11.6.2 Strontium tracer

We conclude the following results for the Strontium tracer, considering a Dirac pulse injection of 1 MBq, ten metres upstream of the interception line.

Peak in mass flow – Arrival time

Most realisations demonstrate a single peak in mass flow, but realisations with multiple peaks occur, but with a small probability. The probability of having a multiple peaks is between 3 and 4 percent for both the given and constrained parameter distributions, and about 0.4 percent for the constrained coupled parameter distributions

It is likely that at the interception line, the maximum mass flow–the largest peak–will occur within less than six years.

For the given parameter distributions:

With a probability of 10%, the peak will occur within 11 years.
With a probability of 50%, the peak will occur within 32 years.
With a probability of 90%, the peak will occur within 58 years.

For the constrained parameter distributions:

With a probability of 10%, the peak will occur within 0.4 years.
With a probability of 50%, the peak will occur within 2.0 years.
With a probability of 90%, the peak will occur within 15 years.

For the constrained coupled parameter distributions:

With a probability of 10%, the peak will occur within 1.2 years.
With a probability of 50%, the peak will occur within 1.8 years.
With a probability of 90%, the peak will occur within 5.5 years.

The uncertainty in peak arrival time is described by the length of the period between the arrival times with 90% and 10% probability (other probability-values can also be used).

A comparison of the different parameter distributions gives the following result:

Given parameter distributions: Difference in arrival time is 47 years.

Constrained parameter distributions: Difference in arrival time is 15 years.

Constrained coupled parameter distributions: Difference in arrival time is 4.3 years.

It is demonstrated by the comparison above, that the smallest uncertainty is produced by use of the constrained coupled parameter distributions; expressed as length of a time period, the uncertainty produced with this distribution is 9% of the uncertainty produced with the given parameter distribution, and 29% of the uncertainty produced with the constrained parameter distribution. The constrained and constrained coupled parameter distributions will produce a much earlier peak in mass flow than the peak produced with the given parameter distributions. The uncertainties in peak arrival time are also demonstrated by Figure 11-21 and Figure 11-23

Peak in mass flow – Size of peak

It is likely that at the interception line, the size of the maximum mass flow (the largest peak) will be less than 0.3 MBq/year.

For the given parameter distributions:

With a probability of 10%, the size of the peak will be less than 0.013 MBq/year

With a probability of 50%, the size of the peak will be less than 0.024 MBq/year

With a probability of 90%, the size of the peak will be less than 0.066 MBq/year

For the constrained parameter distributions:

With a probability of 10%, the size of the peak will be less than 0.037 MBq/year

With a probability of 50%, the size of the peak will be less than 0.177 MBq/year

With a probability of 90%, the size of the peak will be less than 0.693 MBq/year

For the constrained parameter distributions:

With a probability of 10%, the size of the peak will be less than 0.076 MBq/year

With a probability of 50%, the size of the peak will be less than 0.171 MBq/year

With a probability of 90%, the size of the peak will be less than 0.313 MBq/year

The uncertainty in size of peak is described by the difference between the sizes of peaks with 90% and 10% probability (other probability-values can also be used).

A comparison of the different parameter distributions gives the following result:

Given parameter distributions: Difference in size is 0.053 MBq/year.

Constrained parameter distributions: Difference in size is 0.65 MBq/ year.

Constrained coupled parameter distributions: Difference in size is 0.24 MBq/ year.

It is demonstrated by the comparison above that the smallest uncertainty is produced by use of the given parameter distributions; expressed as a difference in magnitude of peak, the uncertainty produced with this distribution is about 22% of that produced with the constrained coupled parameter distributions. The reason that the given distributions produce the smallest uncertainty in size of peak is that in general the peaks produced

with the given distributions are much smaller than those produced by the constrained and constrained couple parameter distributions. The probability of having large peaks is the highest with the constrained parameter distributions. The uncertainties in size of peak are also demonstrated by Figure 11-22 and Figure 11-24

Recovery of mass

The recovered mass at the interception line is calculated as a percentage of the released mass (i.e. the mass contained in the Dirac pulse). For different amounts of recovered mass, i.e 5%, 50% and 95%, we have calculated the probability distribution of the corresponding breakthrough times.

For the given parameter distributions:

With a probability of 90%

5% of the mass will be recovered within 36.5 years.

50% of the mass will be recovered within 72.7 years.

95% of the mass will be recovered within 174.6 years.

For the constrained parameter distributions:

With a probability of 90%

5% of the mass will be recovered within 9.2 years.

50% of the mass will be recovered within 29.2 years.

95% of the mass will be recovered within 205.2 years.

For the constrained coupled parameter distributions:

With a probability of 90%

5% of the mass will be recovered within 3.9 years.

50% of the mass will be recovered within 20.7 years.

95% of the mass will be recovered within 145.3 years.

The constrained and the constrained coupled parameter distributions will produce an earlier arrival time of the peak than the arrival time produced with the given parameter distributions. Recovery of the first 5%, 50%and 95% of injected mass will take place earlier with the constrained coupled parameter distributions than with the other two distributions.

For a given percentage of recovered mass flow, the length of the period between the 95^{th} and the 5^{th} percentiles of the breakthrough time (for recovery of mass flow) is a measure of the uncertainty in the predictions of the breakthrough curves. Considering a small amount of recovered mass, the period represents the uncertainty in predictions of the first part of the breakthrough curves. Considering a large amount of recovered mass, the period represents the uncertainty in predictions of the last part of the breakthrough curves.

Considering the Strontium tracer and the length of period between the 95^{th} and 5^{th} percentile of breakthrough time:

Considering recovery of 5% of the mass flow and the:

Given parameter distributions, the length of the period is 38.0 years

Constrained parameter distributions, the length of the period is 13.2 years

Constrained coupled parameter distributions, the length of the period is 4.6 years.

Considering recovery of 50% of the mass flow and the:

Given parameter distributions, the length of the period is 70.3 years

Constrained parameter distributions, the length of the period is 36.4 years

Constrained coupled parameter distributions, the length of the period is 23.4 years.

Considering recovery of 95% of the mass flow and the:

Given parameter distributions, the length of the period is 164.8 years

Constrained parameter distributions, the length of the period is 237.0 years

Constrained coupled parameter distributions, the length of the period is 135.9 years.

The results above demonstrate that for the recovery of 5%, 50% and 95% of the injected mass, the smallest uncertainty is produced by use of the constrained coupled parameter distributions, this demonstrates the constraining power of the tracer test analysed in Task 6A. For the first part of the Dirac pulse, as characterised by recovery of 5% and 50% of injected mass, the uncertainty produced by the constrained coupled parameter distributions is small compared to the uncertainty produced by the given distributions.

For recovery of 5% and 50% of injected mass, the uncertainty produced by the constrained coupled parameter distributions are 12% and 33% (respectively) of the uncertainty produced by the given parameter distributions. Considering the last part of the breakthrough curves (recovery of 95% of the mass), the uncertainty in the result produced by the constrained coupled parameter distributions is not so much smaller than that produced by the given distributions. For recovery of 95% of injected mass, the uncertainty produced by the constrained coupled parameter distributions is 82% of the uncertainty produced by the given parameter distributions.

This illustrates the importance of transport processes that had no large influence on the tracer test studied in Task 6A, for example interaction (e.g. matrix diffusion and adsorption) with materials (Diorite and Mylonite) that are not in direct contact with the flowing water. These processes may be very important at the time scales of the recovery of 95% of injected mass in Task 6B2. Hence, as the tracer test studied in Task 6A demonstrated no constraining power for these transport properties (matrix diffusion), at large time scales (large time scales in comparison to the time scale of the tracer test) the uncertainty in the result produced by the constrained coupled parameter distributions is smaller than the uncertainty in the results produced with the given parameter, but not very much smaller.

An interesting result is that the uncertainty discussed above, as described by the length of a time period, is approximately the same for both the constant injection of tracer and for the Dirac pulse injection (compare with Section 10.5.2). Except for the constrained coupled parameter distribution and 95% of recovered mass, for this situation the uncertainty is much smaller for the Dirac pulse than for the Constant injection rate. Hence, considering the constrained coupled parameter distributions (which produce the best predictions) and the first 50% of recovered mass, the uncertainty is approximately the same when considering a constant injection of mass or a Dirac pulse.

11.7 Comparison of arrival times of HTO and Strontium tracers in Tasks 6A and 6B2 – Retardation factor and delay factor

11.7.1 Retardation factor

For a situation in which the partitioning of a contaminant (tracer) can be adequately described by a fast reversible adsorption with a linear isotherm, the retardation of the front of the migrating contaminant, relative the movement of the bulk mass of water, can be described by a relation, commonly known as the retardation equation, presented as Equ. 5-2. The retardation factor is defined in Equ. 5-3.

The retardation factor, as defined in Equ. 5-3, depends on the density of the material in which the flow takes place and the porosity of the material, as well as of the partitioning coefficient (Kd-value) of the studied contaminant (tracer) and the material. All these parameters are the same in Task 6A and in Task 6B2, therefore the retardation factors for the given and constrained parameter distributions, as calculated and presented for Task 6A (see Figure 5-11), are also applicable to the analysis of Task 6B2.

In Task 6A, considering the Strontium tracer and the retardation factor, constraining power was demonstrated for the Fault Gouge and for the Infill material. Considering the given parameter distributions, the median of the retardation factor is 216 for the Fault Gouge and 49 for the Infill. Considering the constrained parameter distributions, the median of the retardation factor is 49 for the Fault Gouge and 25 for the Infill. No constraining power was demonstrated for the Mylonite and Diorite, considering the given and the constrained parameter distributions, the median of the retardation factor is 121 for the Mylonite and 51 for the Diorite.

For the constrained and constrained coupled parameter distributions, and considering the materials in direct contact with the flowing water (Infill and Fault Gouge), the medians of the distributions of retardation factors indicate a retardation factor in the range between 25 and 49. Considering the materials behind the Fault Gouge (Mylonite and Dirite), the medians of the distributions of retardation factors indicates a retardation factor between 51 and 121. Hence, we estimate a retardation factor equal to approximately 50, as a rough estimate of a median value of retardation applicable to the whole system of different materials.

11.7.2 Delay factor

The measured (and reproduced) breakthrough curves of Task 6A demonstrates that the peak in mass flow of the HTO tracer took place approximately 7 hours from the start of the injection, and the peak in mass flow of the Strontium tracer took place approximately 12 hours from the start of the injection. Hence, in Task 6A, the arrival time of the peak of the Strontium tracer was 1.7 times longer than that of the HTO tracer.

The delay of the Strontium traces is caused by the reactive properties of the Strontium tracer and its interaction with surrounding materials, i.e. adsorption on Infill and Fault Gouge materials, and in the long time perspective also adsorption on the Diorite and Mylonite rock that takes place in the matrix diffusion zone, behind the Fault Gouge. The flow velocities are large in Task 6A, therefore the delay caused by the reactive transport processes will not be very significant. The capability of the reactive transport processes to slow down the transport of a reactive tracer is not well demonstrated in Task 6A.

The HTO tracer is considered to be a conservative tracer, i.e. it does not adsorb onto the rock surface, but it will interact with stagnant zones etc. A delay factor (see Equ. 11-1) can be defined based on the difference in breakthrough time between the HTO and the Strontium tracer. The delay factor is a measure of the effects of reactive transport processes.

Equ. 11-1

$$D_{Sr} = \frac{t_{Sr}}{t_{HTO}}$$

D_{Sr} = *Delay factor for Strontium*

t_{Sr} = *Breakthrough or Arrival time for Strontium (a reactive tracer)*

t_{HTO} = *Breakthrough or Arrival time for HTO (a conservative tracer)*

Considering the pump test of Task 6A, the following delay factors are obtained for peak arrival time, as well as for recovery of 5%, 50% and 95% of injected mass, see Table 11-1, below. It is demonstrated by the table that the delay factors varies with time and amount of recovered mass, it increases with amount of recovered mass, as long as the recovered mass is not as large as approximately 95%.

Table 11-1 Tracer test of Task 6A, measured delay factors for Strontium

	Considering the tracer test studied in Task 6A (measured data)		
Type of Breakthrough	**HTO Time in Hours**	**STRONTIUM Time in Hours**	**Delay Factor for Strontium**
PEAK	7	12	1.7
5% recovery of injected mass.	5.2	7.9	1.5
50% recovery of injected mass.	11.1	24.4	2.2
95% recovery of injected mass.	77.0	165.6	2.1

In Task 6B2, the flow and flow velocities are small (at least compared to those of Task 6A) and the effects of the delaying transport processes will be larger than in Task 6A, even for a relative weakly interacting tracer as Strontium.

Considering the simulated arrival time of tracer mass of a Dirac pulse, the modelled results of Task 6B2 will produce the delay factors given in Table 11-2 through Table 11-5.

Table 11-2 Task 6B2. Delay factors for Strontium, considering peak arrival time.

	Task 6B2: Dirac pulse and Peak Arrival Time			
Parameter Distribution	**Percentile of Arrival time**	**HTO Time in Years**	**STRONTIUM Time in Years**	**Delay Factor For Strontium**
GIVEN	50^{th} (median)	0.40	32	80
	90^{th}	0.72	58	80
CONSTRAINED	50^{th} (median)	0.058	2.0	34
	90^{th}	0.29	15	52
CONSTRAINED COUPLED	50^{th} (median)	0.061	1.78	**29**
	90^{th}	0.23	5.51	**24**

Table 11-3 Task 6B2. Delay factors for Strontium, considering breakthrough time for recovery of 5% of injected mass.

	Task 6B2: Dirac pulse and breakthrough time for recovery of 5% of injected mass			
Parameter Distribution	**Percentile of Breakthrough time**	**HTO Time in Years**	**STRONTIUM Time in Years**	**Delay Factor for Strontium**
GIVEN	50^{th} (median)	0.226	19.3	86
	90^{th}	0.438	36.5	83
CONSTRAINED	50^{th} (median)	0.043	1.54	36
	90^{th}	0.174	9.46	54
CONSTRAINED COUPLED	50^{th} (median)	0.041	1.45	**35**
	90^{th}	0.142	3.89	**27**

Table 11-4 Task 6B2. Delay factors for Strontium, considering breakthrough time for recovery of 50% of injected mass.

	Task 6B2: Dirac pulse and breakthrough time for recovery of 50% of injected mass			
Parameter Distribution	**Percentile of Breakthrough time**	**HTO Time in Years**	**STRONTIUM Time in Years**	**Delay Factor for Strontium**
GIVEN	50^{th} (median)	0.56	42.8	76
	90^{th}	0.91	72.7	80
CONSTRAINED	50^{th} (median)	0.22	7.4	34
	90^{th}	0.59	29.4	50
CONSTRAINED COUPLED	50^{th} (median)	0.212	7.76	**37**
	90^{th}	0.517	20.71	**40**

Table 11-5 Task 6B2. Delay factors for Strontium, considering breakthrough time for recovery of 95% of injected mass.

	Task 6B2: Dirac pulse and breakthrough time for recovery of 95% of injected mass			
Parameter Distribution	**Percentile of Breakthrough time**	**HTO Time in Years**	**STRONTIUM Time in Years**	**Delay Factor for Strontium**
GIVEN	50^{th} (median)	1.46	104	71
	90^{th}	2.32	175	75
CONSTRAINED	50^{th} (median)	2.05	75	36
	90^{th}	3.80	209	55
CONSTRAINED COUPLED	50^{th} (median)	2.31	78.7	34
	90^{th}	3.60	145.3	40

As demonstrated in the tables above, the delay factor is much larger in Task 6B2 than in Task 6A.

In Task 6B2, considering the constrained coupled parameter distribution (which produce the best estimate) and the peak arrival time, the delay factor is 29 (for the median of the peak arrival time), which is 17 times larger the corresponding delay factor of Task 6A (delay fac.=1.7).

In Task 6B2, considering the constrained coupled parameter distribution and the recovery of 5%, 50% and 95% of injected mass, the delay factor is close to 36 for all three amounts of recovered mass, when considering the median of the breakthrough times. A delay factor of 36 is 17 times larger than the corresponding delay factor of Task 6A (delay fac.=2.1).

11.7.3 Comparison of calculated retardation factors and delay factors

The retardation factor, as defined in Equ. 5-3 represents the retardation of the front of a migrating contaminant, relative the movement of the bulk mass of water; considering the velocity of the $C / C_0 = 0.5$ theoretical point on the concentration profile of the retarded constituent, assuming that the retardation is caused by a fast reversible adsorption with a linear isotherm. . This concept of retardation factor, calculated separately for each material along the flow route, is not necessarily directly comparable to the delay factor as defined in Equ. 11-1.

Nevertheless, for the modelled transport of Task 6B2 a comparison of the two concepts demonstrated that the difference between the calculated (and estimated) retardation factors and delay factors is not very large.

- In Section 11.7.1, we estimated a retardation factor for Strontium, considering the constrained and constrained coupled parameter distributions equal to approximately 50, as a rough estimate of a median value representing the retardation of the whole system of different materials.

- In Section 11.7.2, we calculated a delay factors for Strontium, considering breakthrough time for recovery of 50% of injected mass, the results are presented in Table 11-4. For the constrained coupled parameter distribution and the 50^{th} percentile the delay factor is equal to 37, for the 90^{th} percentile the delay factor is equal to 40.

Considering Task 6A, a comparison of: (i) the estimated median value of the retardation factors, and (ii) the measured delay factors directly obtained from the tracer test studied in Task 6A (measured data), will not produce a good agreement. The measured delay factor for the breakthrough time of the recovery of 50% of injected mass is equal to 2.2 (see Table 11-1); the estimated median retardation factor is equal to 50. The main reason why the estimated delay caused by the reactive transport processes is overestimated, is because the total time scale of the experiment of Task 6A is small.

12 Task 6B2 – Discussion and conclusion

The purpose of Task 6B2 is to model selected flow and transport cases at the TRUE-1 site with Performance Assessment (PA) relevant (long-term) boundary conditions and temporal scales. Compared to Task 6A, the temporal scale of Task 6B2 is much larger and reflects a PA-situation and not the flow of a standard tracer test, as used in Site Characterisation (SC).

Considering a conservative tracer (HTO), the recovery of 95% of the injected mass took 77 hours in the Task 6A tracer test, but may take 3 years in the flow field of Task 6B2. Hence, the temporal scale of Task 6B2 is several hundreds of times larger. Because of the relative long period studied in Task 6B2, transport processes that are of importance in the longer time perspective of a PA analysis e.g. matrix diffusion, will have an important influence on the transport modelled in Task 6B2.

We have modelled the transport processes based on three different parameter distributions (see Section 9.2):

- Given parameter distributions.
- Constrained parameter distributions.
- Constrained coupled parameter distributions.

The parameter distributions that produce the most representative results for the TRUE-1 site is the Constrained coupled parameter distributions; the parameter properties of this distribution were constrained by the evaluation of the tracer test studied in Task 6A, and these distributions also include the correct combinations of parameter values.

Considering the Given parameter distributions and the HTO tracer:

- For a Dirac pulse the peak in mass flow will take place,
  Within 4.8 months regarding the median (50% probability).
  Within 8,7 months with a probability of 90%.

- For a Dirac pulse, and with a probability of 90%,
  5% of the mass will be recovered within 0.44 years.
  50% of the mass will be recovered within 0.9 years.
  95% of the mass will be recovered within 2.3 years.

Considering the Given parameter distributions and the STRONTIUM tracer:

- For a Dirac pulse the peak in mass flow will take place,
  Within 32 years regarding the median (50% probability).
  Within 58 years with a probability of 90%.

- For a Dirac pulse, and with a probability of 90%,
  5% of the mass will be recovered within 36 years.
  50% of the mass will be recovered within 73 years.
  95% of the mass will be recovered within 175 years.

Considering the Constrained coupled parameter distributions and the HTO tracer:

- For a Dirac pulse the peak in mass flow will take place,
  Within 0.6 months regarding the median (50% probability).
  Within 2,6 months with a probability of 90%.

- For a Dirac pulse, and with a probability of 90%,
  5% of the mass will be recovered within 0.14 years.
  50% of the mass will be recovered within 0.5 years.
  95% of the mass will be recovered within 3.6 years.

Considering the Constrained coupled parameter distributions and the STRONTIUM tracer:

- For a Dirac pulse the peak in mass flow will take place,
  Within 1.8 years regarding the median (50% probability).
  Within 5.5 years with a probability of 90%.

- For a Dirac pulse, and with a probability of 90%,
  5% of the mass will be recovered within 4 years.
  50% of the mass will be recovered within 21 years.
  95% of the mass will be recovered within 145 years.

The Given parameter distributions represent reasonable ranges of parameter values, but these distributions are not constrained by the results of the abovementioned tracer test. And as seen above, the given distributions will generally produce a much later arrival of the mass (except for recovery of 95% of injected HTO mass) than the results produced with the constrained coupled parameter distributions.

The uncertainty in the breakthrough curves of tracer mass can be described by the length of the period between the arrival times with 90% and 10% probability, for a given condition of mass flow e.g. the peak in mass flow or recovery of a certain amount of injected mass. Considering uncertainty expressed in this way, for HTO as well as for Strontium, the smallest uncertainty in prediction was obtained by utilising the Constrained coupled parameter distributions, when simulating: peak arrival time, as well as recovery of 5%, 50% an d95% of injected mass. The only exception is for HTO and recovery of 95% of injected mass, for this situation smallest uncertainty was obtained with the given distributions.

Considering the Strontium tracer and size of uncertainty in prediction of breakthrough curves, the smallest uncertainty is produced by use of the constrained coupled distributions, but the difference in uncertainty (compared to the uncertainty produced by the other parameter distributions) is largest at the first part of the breakthrough curves, when 95% of the injected mass is recovered, the uncertainty in predictions made by the constrained coupled parameter distributions is smaller, but not much smaller, than the uncertainty produced by the given distributions.

The reason for this is that when considering the last part of the breakthrough curves in Task 6B2 (e.g. recovery of 95% of the injected mass), the time scale is much larger than the time scale studied in the Task 6A tracer test. Transport processes that had no large influence on the tracer test studied in Task 6A, for example interaction (e.g. matrix diffusion and adsorption) with materials (Diorite and Mylonite) that are not in direct

contact with the flowing water, may be very important at the time scales of the recovery of 95% of injected mass in Task 6B2. It follows that because the tracer test studied and analysed in Task 6A demonstrated no constraining power for these transport properties (e.g. matrix diffusion), the uncertainty in the result produced by the constrained coupled parameter distributions is not necessarily much smaller, than the uncertainty produced with the given parameter distributions, at these large time scales (large time scales in comparison to the time scale of the tracer test).

An interesting result is that the uncertainty discussed above, as described by the length of a time period, is approximately the same for both the constant injection of tracer and for the Dirac pulse injection. Except for the constrained coupled parameter distribution and 95% of recovered mass, for this situation the uncertainty is smaller for the Dirac pulse than for the Constant injection rate. Hence, considering the constrained coupled parameter distributions (which produce the best predictions) and the first 50% of recovered mass, the uncertainty is approximately the same when considering a constant injection of mass or a Dirac pulse.

The measured (and reproduced) breakthrough curves of the tracer test studied in Task 6A, demonstrated that the peak in mass flow of HTO occurred approximately 7 hours after the start of injection, while the peak in mass flow of Strontium occurred after approximately 12 hours. Hence, in Task 6A, the peak arrival time of Strontium was 1.7 times longer than that of HTO. HTO is considered to be a conservative tracer, i.e. it does not adsorb onto the rock surface, but it will interact with stagnant zones etc. A delay factor may be defined (see Equ. 5-1) by means of the difference in breakthrough time between HTO and Strontium. The delay factor is a measure of the effects (retardation) of reactive transport processes. Considering the arrival time of the Strontium peak, the delay factor observed in the tracer test of Task 6A is 1.7. Considering the recovery of 5%, 50% and 95% of injected mass, the delay factor for Strontium in Task 6A (the STT-1b experiment) is, 1.5, 2.1 and 2.2, respectively.

In Task 6B2, the flow and flow velocities are relatively small (compared to those of Task 6A) and the effects of the delaying transport processes will be larger than in Task 6A, even for a relative weakly interacting tracer as Strontium. Considering Task 6B2, a Dirac pulse and the constrained coupled parameter distributions, we summarise the following results:

- The simulated arrival times of the peaks in HTO and Strontium mass flow give rise to a delay factor for Strontium equal to approximately 27.
- The simulated breakthrough times of the recovery of 5%, 50% and 95% of injected HTO and Strontium mass will produce a delay factor for Strontium close to 36, for all three amounts of recovered mass, when considering the median breakthrough time (50% probability).

As demonstrated above, the delay factor is much larger in Task 6B2 than in Task 6A. In Task 6B2, considering the constrained coupled parameter distribution (which produce the best estimate) and the peak arrival time, the delay factor is 29 (for the median of the peak arrival time), which is 17 times larger than the corresponding delay factor of Task 6A

In Task 6B2, considering the constrained coupled parameter distribution and the recovery of 5%, 50% and 95% of injected mass, the delay factor is close to 36 for all three amounts of recovered mass, when considering the median of the breakthrough times. A delay factor of 36 is 17 times larger than the corresponding delay factor of Task 6A.

The retardation factor (see Equ. 5-3) represents the retardation of the front of a migrating contaminant, relative the movement of the bulk mass of water, assuming that the retardation is caused by a fast reversible adsorption with a linear isotherm. This concept of retardation factor, calculated separately for each material along the flow route, is not necessarily directly comparable to the delay factor (as defined in Equ. 11-1). Nevertheless, for the modelled transport of Task 6B2 a comparison of the two concepts demonstrated that the difference between the calculated (and estimated) retardation factors and the calculated delay factors is not very large. Considering the Strontium tracer and the constrained coupled parameter distributions, a rough estimate of a median retardation value representing the retardation of the whole system of different materials is approximately equal to 50 (see Section 11.7.1). We have calculated a delay factor, considering the Strontium tracer and the breakthrough time for recovery of 50% of injected mass. For the constrained coupled parameter distribution and the 50^{th} percentile, the delay factor is equal to 37, for the 90^{th} percentile the delay factor is equal to 40.

Considering Task 6A, a comparison of: (i) the estimated median value of the retardation factors, and (ii) the measured delay factors directly obtained from the tracer test studied in Task 6A (measured data), will not produce a good agreement. The measured delay factor for the breakthrough time of the recovery of 50% of injected mass is equal to 2.2 (see Table 11-1); the estimated median retardation factor is equal to 50. The main reason why the estimated delay caused by the reactive transport processes is overestimated, is because the total time scale of the experiment of Task 6A is small.

The interaction of the tracers with rock masses not in direct contact with the flowing water is an important process at PA-time scales, e.g. reactive processes and matrix diffusion. And the properties that control these processes are not well constrained by a standard tracer test. Disregarding these processes at PA time scales will cause substantial underestimations of transport times.

13 Implications of the applied methodology, considering performance assessment modelling based on site characterisation data

This study may be characterised as a probabilistic performance assessment modelling, based on site characterisation data. Task 6A is a site characterisation (SC) modelling, and Task 6B2 is a performance assessment (PA) modelling.

Traditionally when using SC data for deriving plausible ranges of parameter values, the objective is to derive probability distributions of the parameters studied. It is also often assumed that these distributions are independent and not correlated to each other, or some uncertain correlation is introduced between a few parameters.

The basic problem is that flow and transport models incorporate a large number of parameters, and credible fits to test results can be achieved with many different combinations of those parameters. Thus, testing can not be expected to produce definitive values of the parameters, or even useful probability distributions for them. The probability distributions are not very useful because it is the specific *combinations* of parameter values that succeed or fail to match tests. In other words, the analysis of the tests will result in extremely complex combined probability functions for the entire suite of parameters.

The approach we have used in this study recognises that it would not be possible to extract conventional probability distributions for individual parameters, and their correlations, for the complex non-linear system that we are studying.

By generating random realisations, based on a set of plausible (given) parameter distributions, and keeping only the realisations that produce an acceptable match to the field-test data set (the tracer test), we have done an informal Bayesian approach to map the entire joint probability density space and convert from prior to updated probabilities. In this way we have derived the constrained parameter distributions. The constrained distributions are, however, not necessarily very useful (as discussed above). Therefore we have established the constrained coupled parameter distributions.

The constrained coupled parameter distributions consist of the ensemble of coupled parameter values as defined by the accepted realisations. The difference compared to the constrained (uncoupled) parameter distributions is that in the constrained coupled parameter distributions the individual parameter values are combined, according to the parameter combinations that resulted in the accepted realisations.

The use of the constrained coupled parameter distributions for the PA modelling will produce better predictions with smaller uncertainties than the use of the constrained parameter distribution, because the constrained coupled parameter distributions will include the correct correlation between the parameters studied; and this is an important improvement compared to an assumption of independent parameters or the inclusion of some uncertain and limited correlation between a few parameters.

This might have important implications for how PA analyses should be carried out. The approach, in which one tries to establish independent distributions for each parameter, possibly with some correlations, is not necessarily the best approach, as it may be nearly impossible to integrate the knowledge gained from different field-tests into such distributions.

Instead, we propose the following approach, which is an approach used in this study:

I. Use as much general data as possible to develop the given parameter distributions (with possible correlations).

II. Use the given parameter distributions as input data for SC modelling. Only realisations that produce an acceptable match to field-test data sets, considering one or several tests, will be propagated to the PA-modelling. To improve the efficiency of the process of finding the acceptable realisations, constrained parameter distributions can be derived and these distributions can be used, instead of the given distributions, as input data for the SC modelling. In a wider perspective, a more complex modelling can be carried out; and the field-test data, against which the modelling results are matched, may not only come from tracer tests, but could also be taken from other tests and analyses, e.g. pump tests, laboratory analyses of chemical properties etc.

III. PA modelling for the specific combinations of parameter values that passed all tests against field data (the constrained coupled parameter distributions).

References

ANDRA (2001). "General Technical Specification, Äspö Modelling Task Force Task 6, 2002-2004", Provided by ANDRA in their call for tenders.

Benabderrahmane, Dershowits, Selroos, Uchida and Winberg (2000). "Task 6: Performance Assesement Modelling Using Site Characterisation Data" Provided by ANDRA in their call for tenders.

Elert and Selroost (2001). "Task 6B". Modelling task specification. Ver 1.0", Provided by ANDRA in their call for tenders.

Freeze R. A. and Cherry J. A. (1979). "Groundwater" Prentic-Hall, Inc., Englewood Cliffs, N.J. ISBN 0-13-365312-9

Holmén J.G. (1992). "A three-dimensional finite difference model for calculation of flow in the saturated zone", Department of quaternary geology, Uppsala University, Uppsala, Sweden, ISBN 91-7376-119-2, ISSN 0348-2979.

Holmén J.G. (1997)."On the flow of groundwater in closed tunnels. Generic hydrogeological modelling of nuclear waste repository, SFL 3-5", Technical Report No. 97-10, Swedish Nuclear Fuel and Waste Management Corporation, Stockholm.

Matheron G. (1967). "Elements pour unr théorie des milieux poreux.", Masson, Paris, France. 1967.

Selroos and Elert (2001) "Task 6A & 6B. Modelling task specification. Ver 1.0", Provided by ANDRA in their call for tenders.

Winberg A., Andersson P., Hermanson j., Byegård J., Cvetkovic V. and Birgerson L. (2000). "Äspö HRL. Final report of the first stage of the tracer retention understanding experiments" SKB TR-00-07, Swedish Nuclear Fuel Co, Box 5864, SE-102 40 Stockholm, Sweden.

Appendix A

Relationship between parameters

Based on the analyses of breakthrough curves, as produced by use of the Strontium tracer and the transport model, we have derived the constrained parameter distributions; this was done in Task 6A. The constrained parameter distributions are based on the 89 realisations that produced breakthrough curves for Strontium with an acceptable match to the measured breakthrough (of Strontium). For these 89 realisations, we have analysed the correlation between the parameters for which constraining power was demonstrated, as well as for other parameters, the studied combinations are given below. The number of studied combinations is 24 (in total there are 136 possible combinations).

- Stagnant zone fraction VERSUS:
  - Stagnant zone rate
  - Dispersivity
  - Flow wetted surface area
  - Fault Gouge Kd-value
  - Fault Gouge thickness
  - Fault Gouge porosity
  - Infill Kd-value
  - Infill porosity
- Stagnant zone rate VERSUS:
  - Dispersivity
  - Flow wetted surface area
  - Fault Gouge Kd-value
  - Fault Gouge thickness
  - Fault Gouge porosity
  - Infill Kd-value
  - Infill porosity
- Infill porosity VERSUS:
  - Infill Kd-value
  - Flow wetted surface area
  - Dispersivity
  - Fault Gouge porosity
  - Fault Gouge thickness
  - Fault Gouge Kd-value
- Fault Gouge porosity VERSUS:
  - Fault Gouge Kd-value
  - Fault Gouge thickness
  - Infill Kd-value

No obvious and linear correlation was observed for any of the studied combinations, there are however some interesting relationships, that corresponds to the demonstrated constraining power, e.g:

- Stagnant zone fraction	VERSUS	Stagnant zone rat	(see Figure A-1)
- Stagnant zone fraction	VERSUS	Dispersivity	(see Figure A-2)
- Stagnant zone fraction	VERSUS	Fault Gouge Kd-value	(see Figure A-4)
- Stagnant zone fraction	VERSUS	Fault Gouge thickness	(see Figure A-5)
- Stagnant zone fraction	VERSUS	Infill Kd-value	(see Figure A-7)

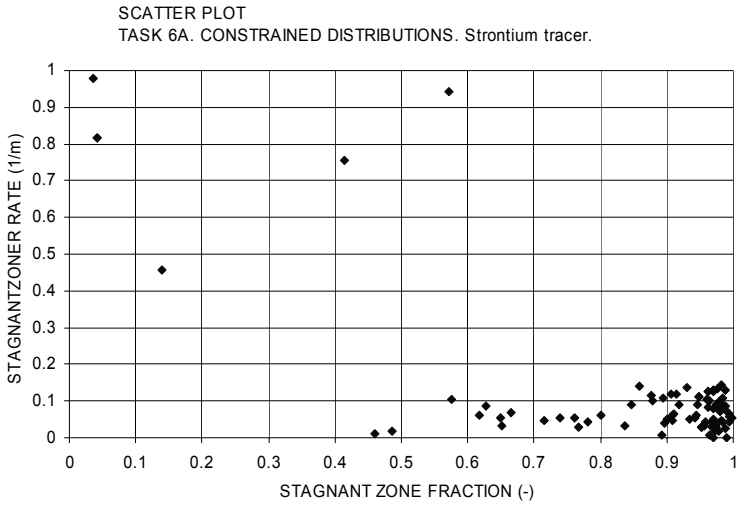

Figure A-1 *Stagnant zone fraction versus Stagnant zone rate.*

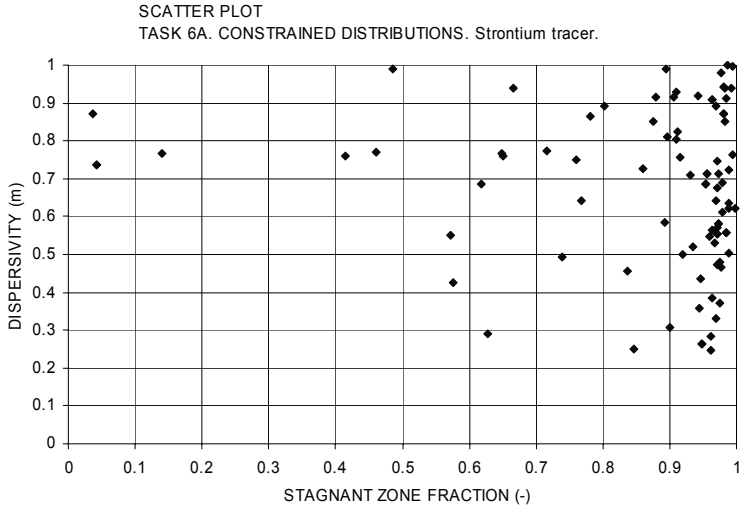

Figure A-2 *Stagnant zone fraction versus Dispersivity.*

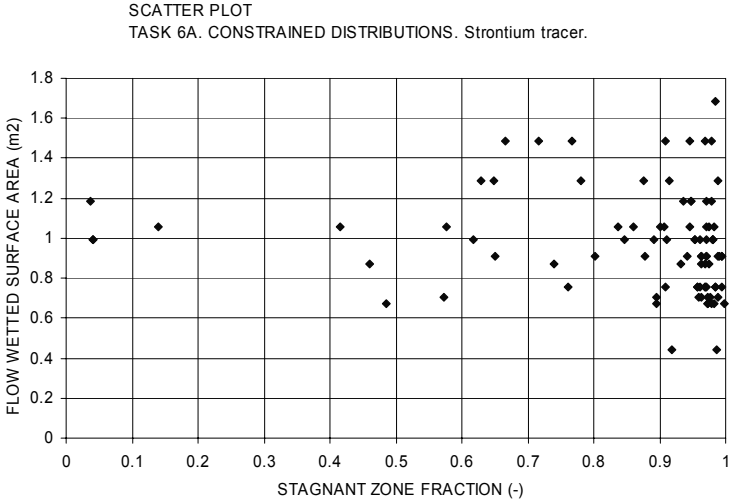

Figure A-3 *Stagnant zone fraction versus Flow wetted surface area.*

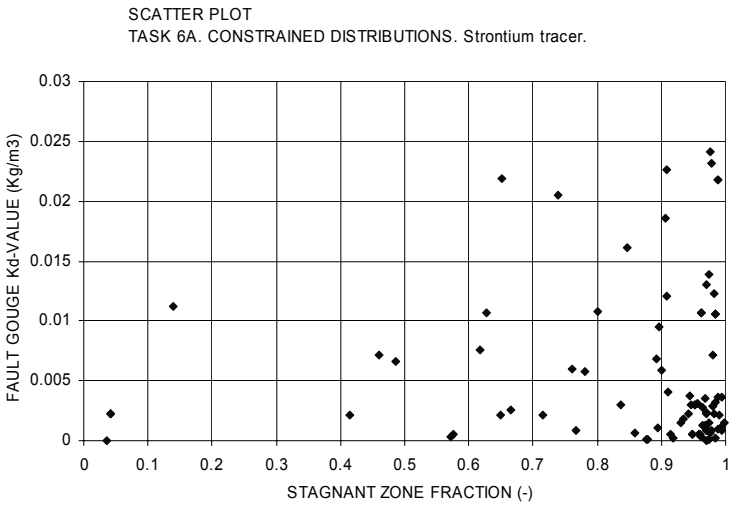

Figure A-4 *Stagnant zone fraction versus Fault Gouge Kd-value.*

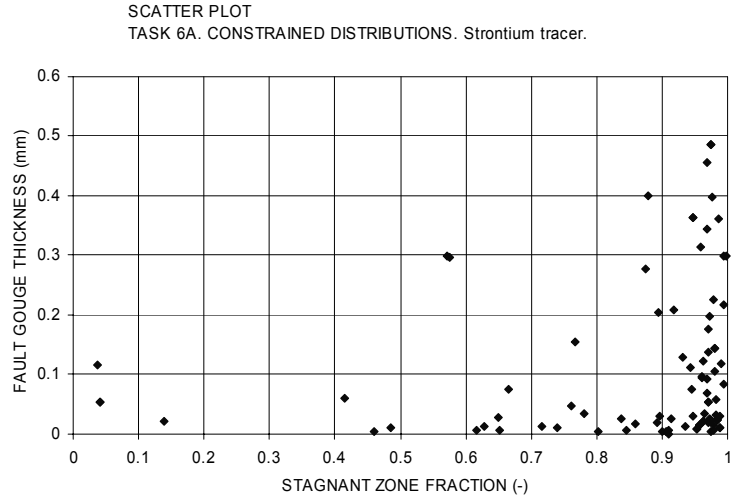

Figure A-5 *Stagnant zone fraction versus Fault Gouge thickness.*

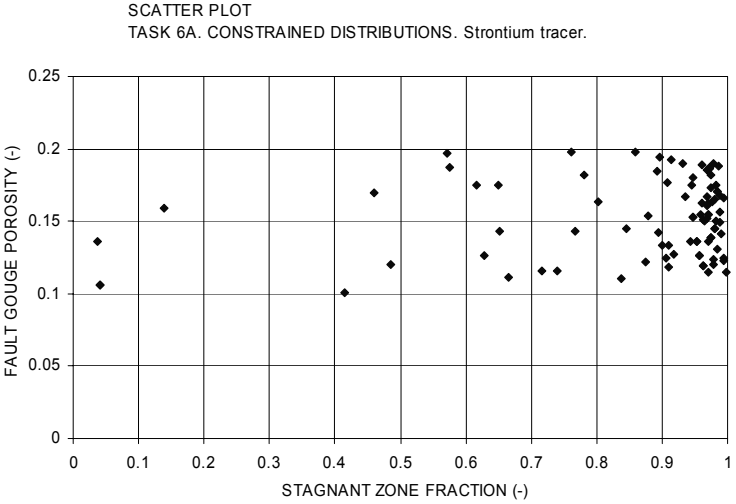

Figure A-6 *Stagnant zone fraction versus Fault Gouge porosity.*

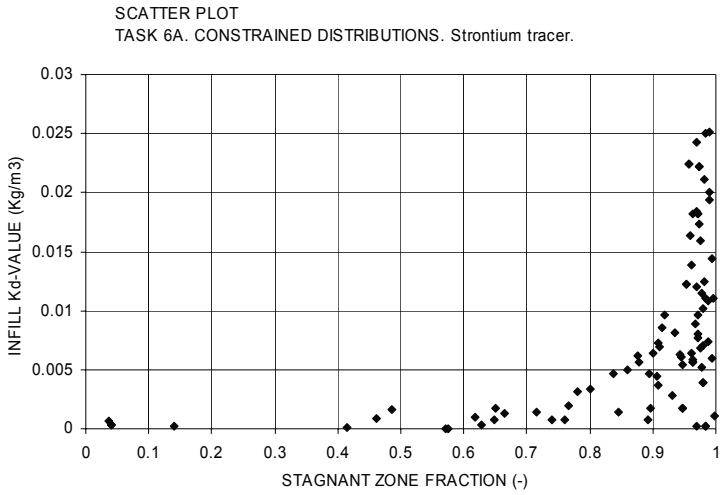

Figure A-7 *Stagnant zone fraction versus Infill Kd-value.*

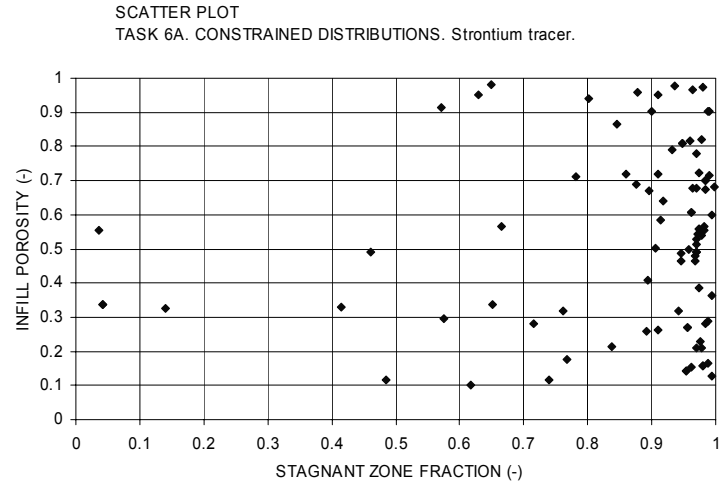

Figure A-8 *Stagnant zone fraction versus Infill porosity.*

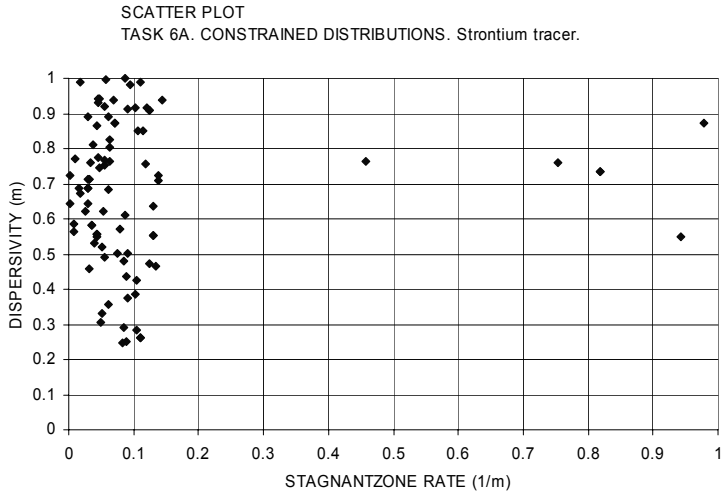

Figure A-9 *Stagnant zone rate versus Dispersivity.*

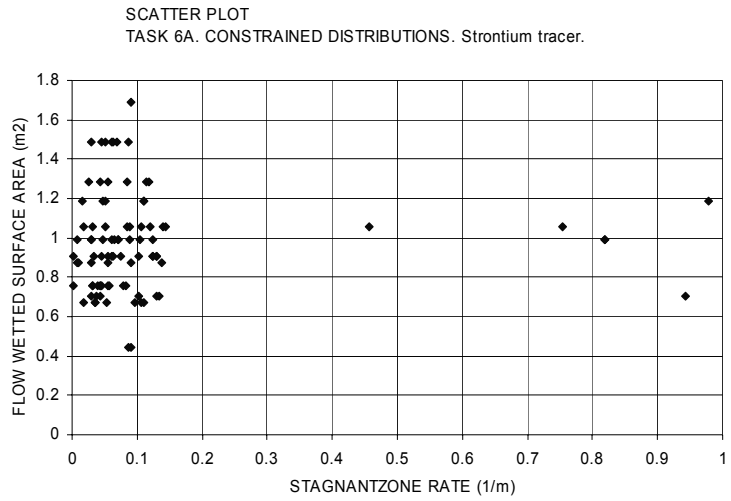

Figure A-10 *Stagnant zone rate versus Flow wetted surface area.*

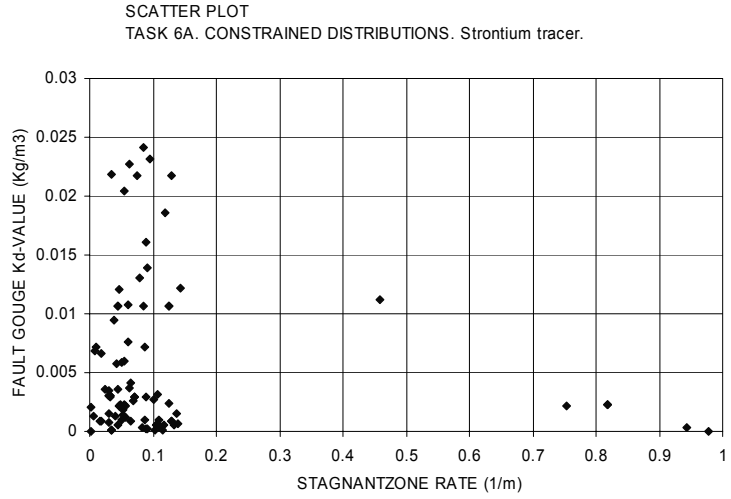

Figure A-11 *Stagnant zone rate versus Fault Gouge Kd-value.*

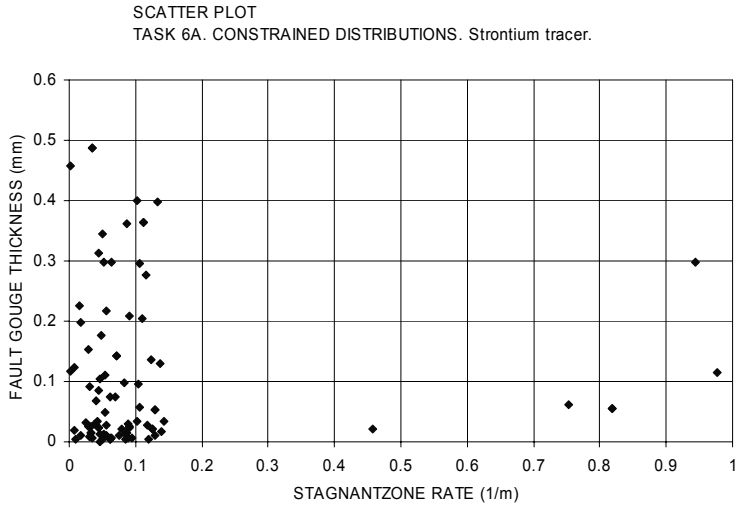

Figure A-12 *Stagnant zone rate versus Fault Gouge thickness.*

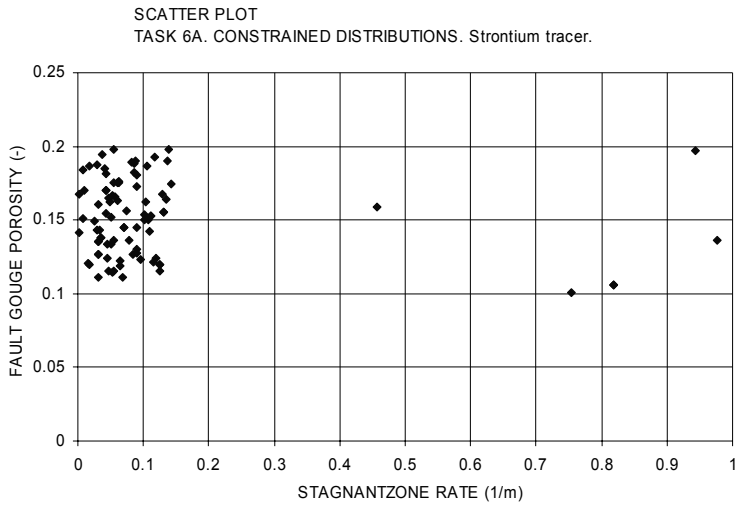

Figure A-13 *Stagnant zone rate versus Fault Gouge porosity.*

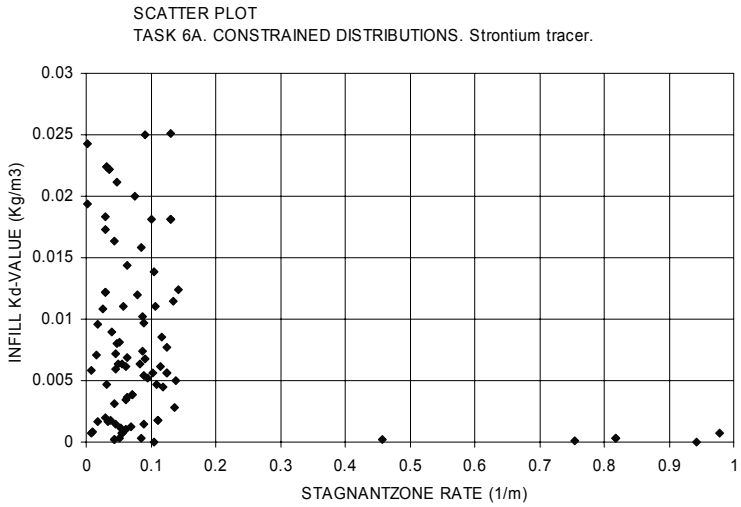

Figure A-14 *Stagnant zone rate versus Infill Kd-value.*

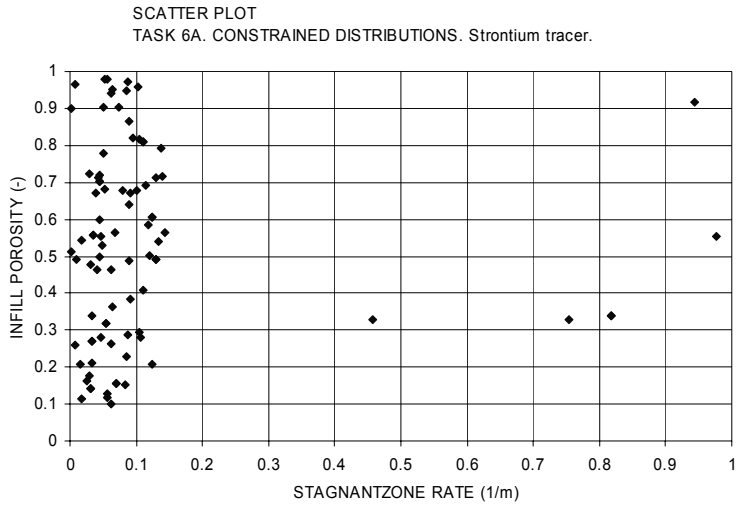

Figure A-15 *Stagnant zone rate versus Infill porosity.*

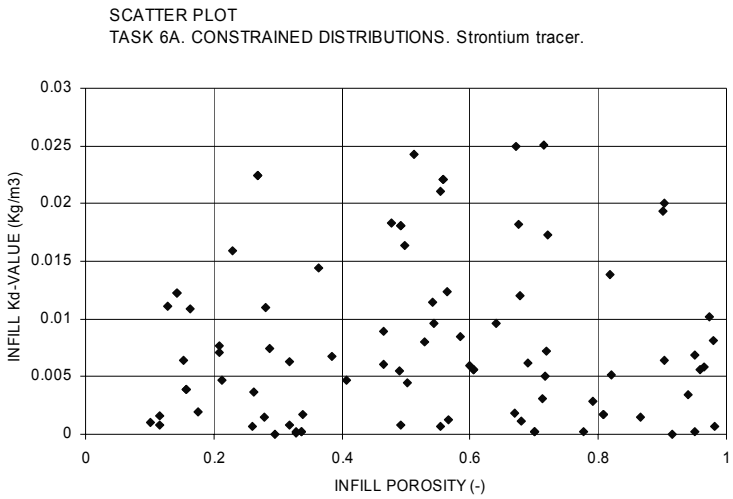

Figure A-16 *Infill porosity versus Infill Kd-value.*

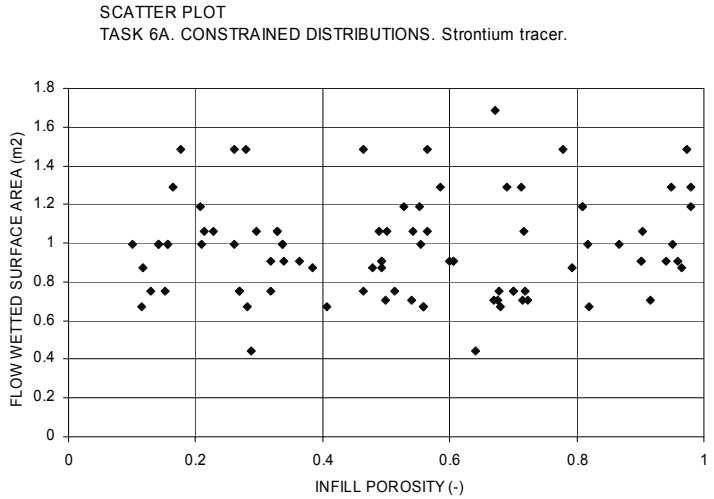

Figure A-17 *Infill porosity versus Infill Flow wetted surface area.*

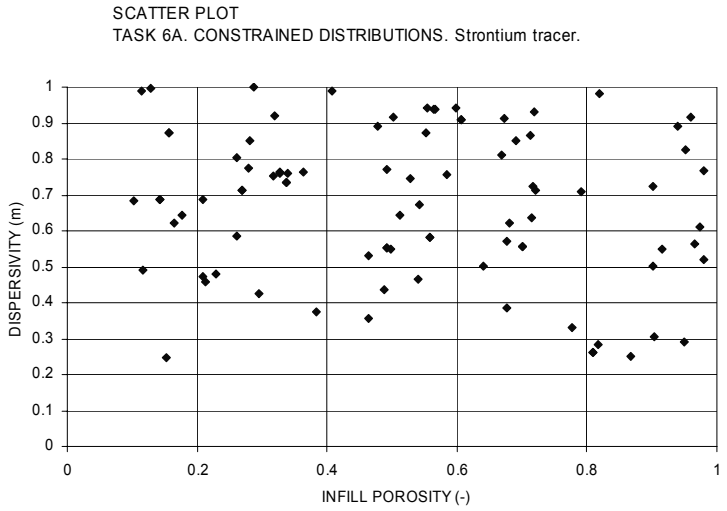

Figure A-18 *Infill porosity versus Dispersivity.*

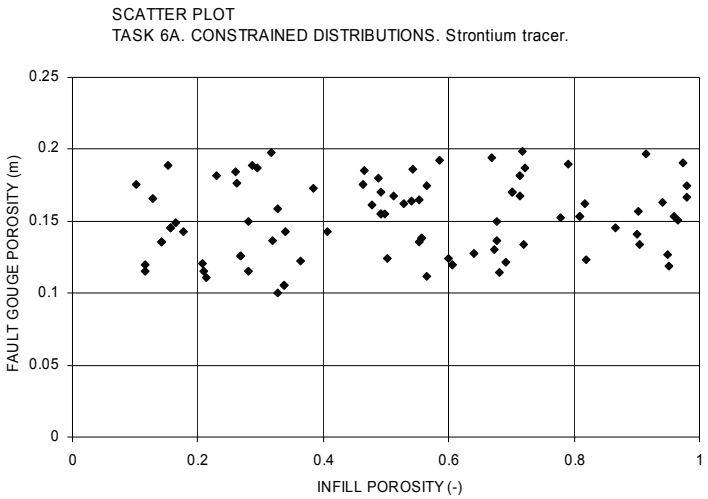

Figure A-19 *Infill porosity versus Fault Gouge porosity.*

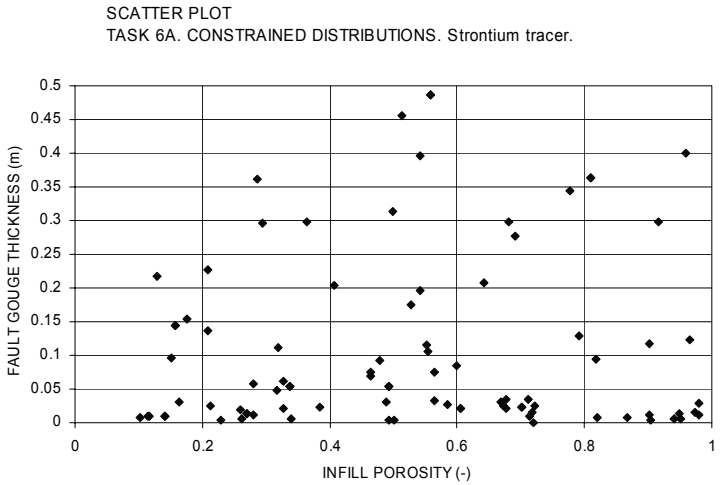

Figure A-20 *Infill porosity versus Fault Gouge thickness.*

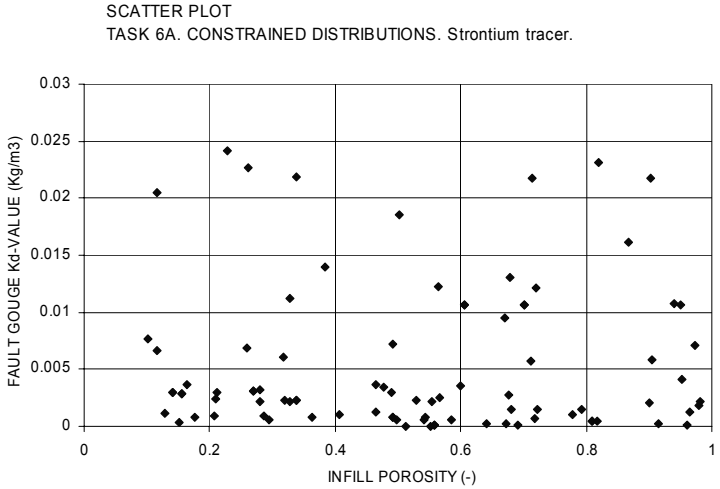

Figure A-21 *Infill porosity versus Fault Gouge Kd-value.*

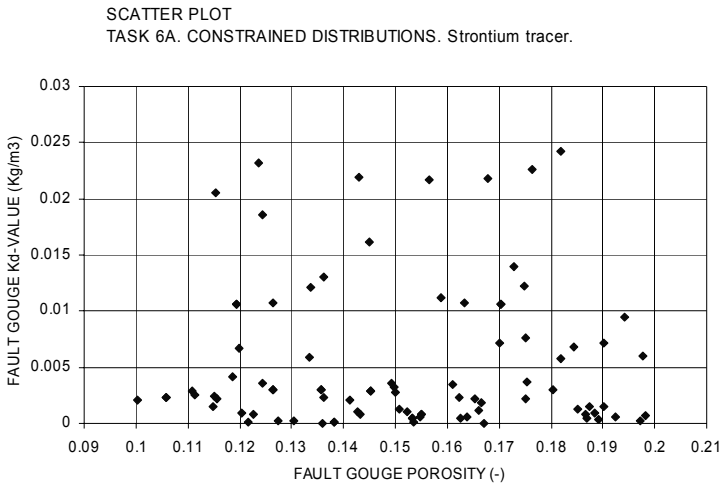

Figure A-22 *Fault Gouge porosity versus Fault Gouge Kd-value.*

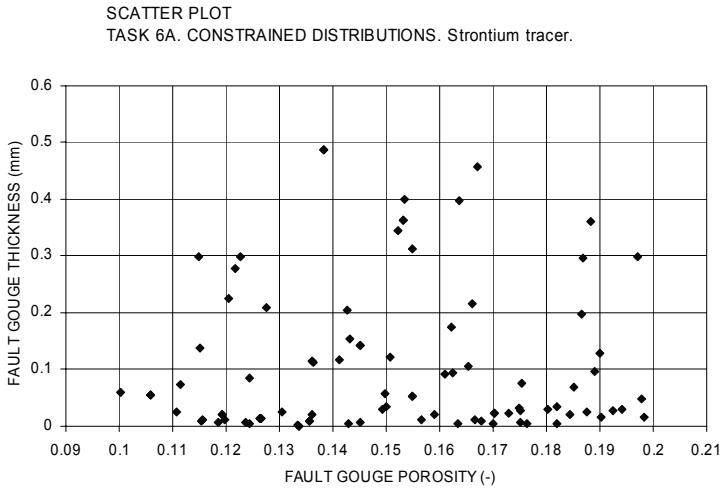

Figure A-23 *Fault Gouge porosity versus Fault Gouge thickness.*

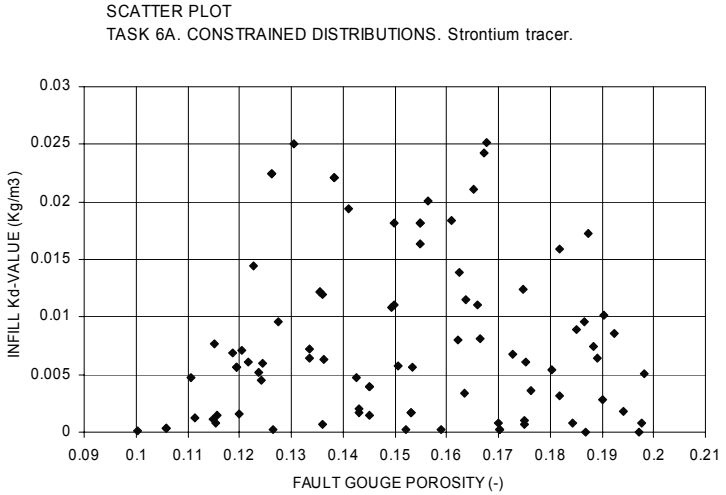

Figure A-24 *Fault Gouge porosity versus Infill Kd-values.*

Appendix B

TASK 6B2. Probability distributions of mass flow versus time

Calculated mass at the interception line. Results for:

- Given parameter distributions.

- Constrained coupled parameter distributions.

The figures presents the probability distributions of mass flow versus time by use of a Log-Log scale.

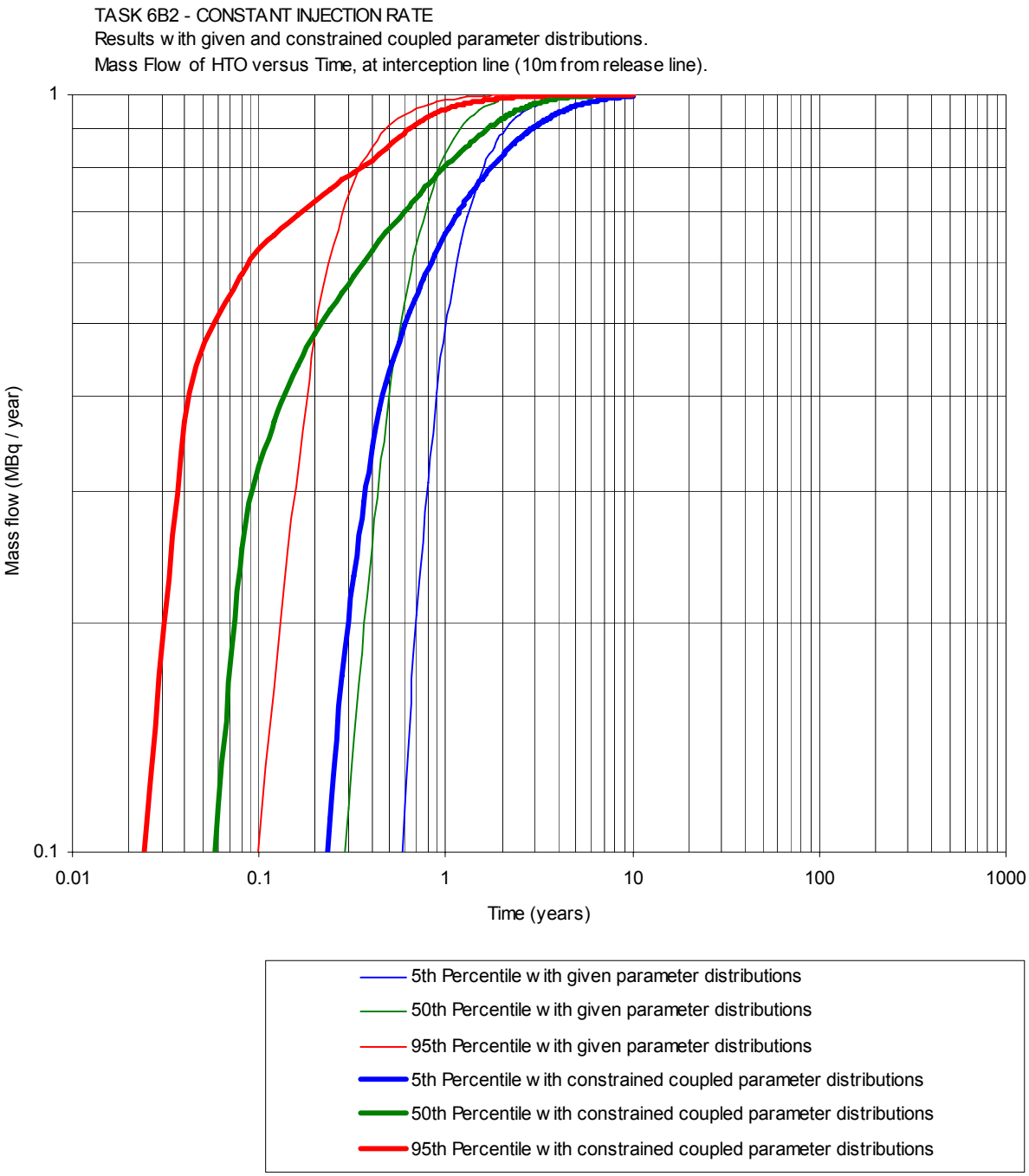

Figure B-1

TASK 6B2 – HTO – Constant injection rate. Probability distributions of mass flow versus time, at the interception line. Results with given and constrained coupled parameter distributions.

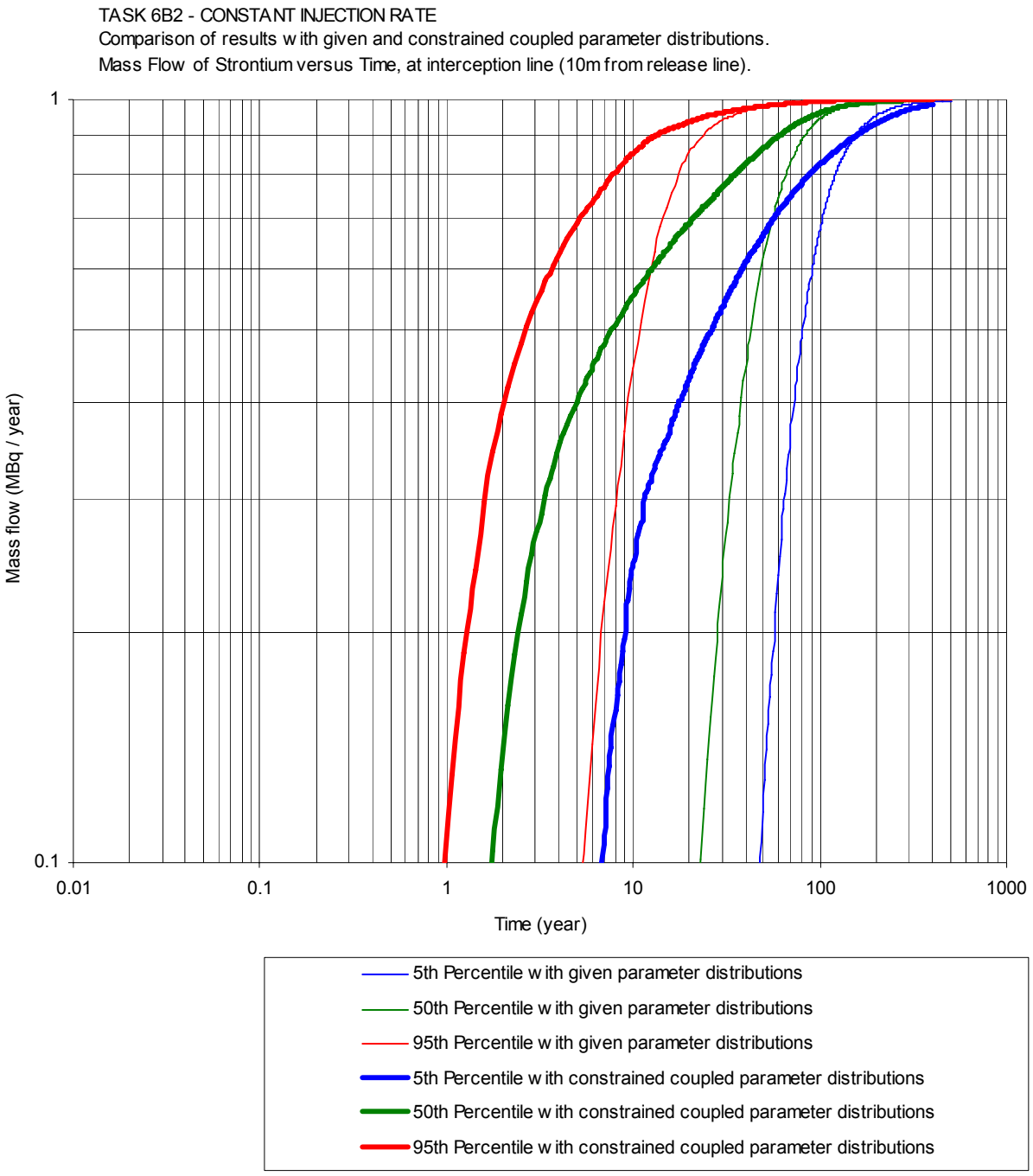

Figure B-2

TASK 6B2 – STRONTIUM – Constant injection rate. Probability distributions of mass flow versus time, at the interception line. Results with given and constrained coupled parameter distributions.

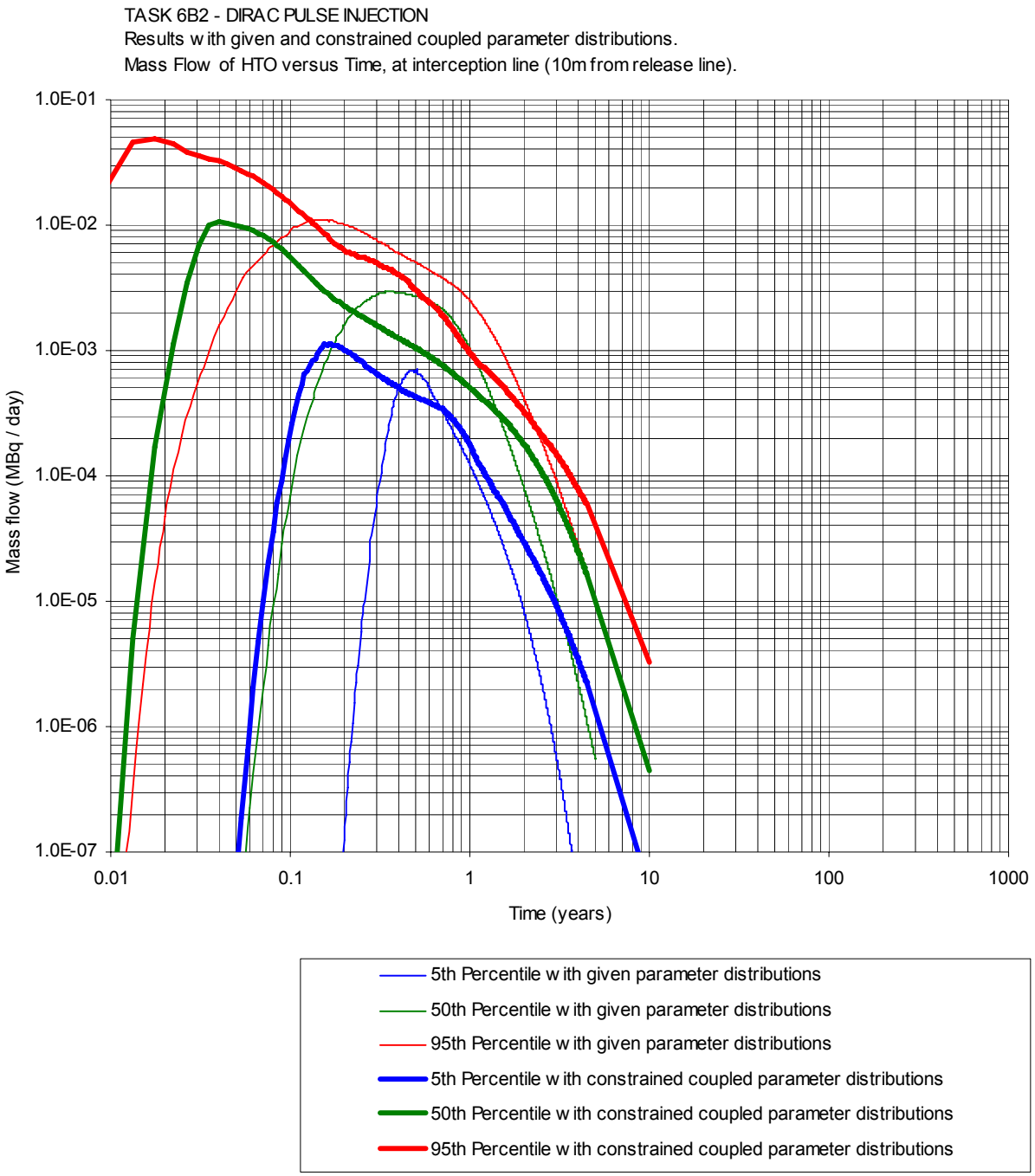

Figure B-3

TASK 6B2 – HTO – Dirac pulse. Probability distributions of mass flow versus time, at the interception line. Results with given and constrained coupled parameter distributions.

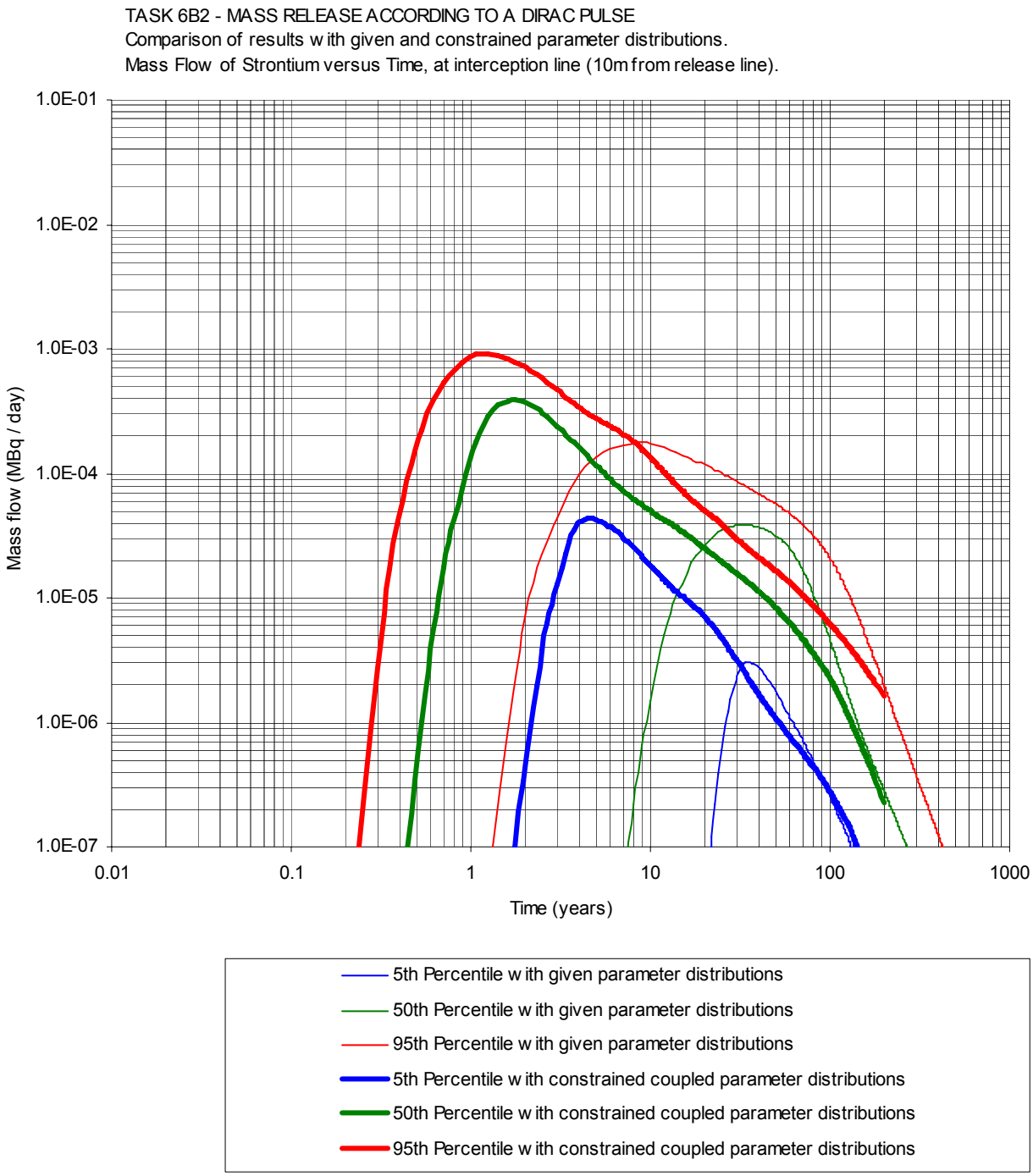

Figure B-4

TASK 6B2 – STRONTIUM – Dirac pulse. Probability distributions of mass flow versus time, at the interception line. Results with given and constrained coupled parameter distributions.